Electrochemical Society

GET YOUR FREE COPY OF THIS INFORMATIVE, ILLUSTRATED BROCHURE

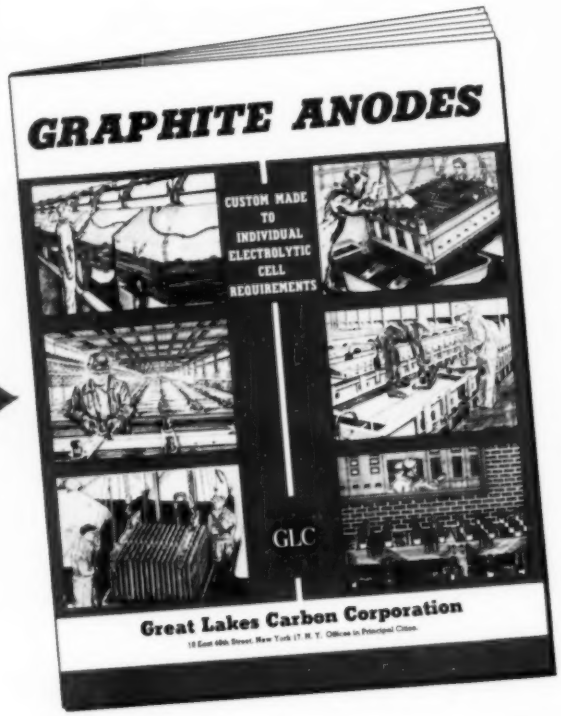

Everyone connected with electrolytic cell operations should have a copy of our new brochure GRAPHITE ANODES. It contains a wealth of useful information.

Here you will find tables of standard sizes and grades of square and rectangular anodes for diaphragm and mercury cells...reasons why anodes custom made to individual cell requirements are more economical and efficient...a brief review of our special anode production and machining facilities...and an explanation of our technical exchange program which has helped our customers lower cell operating costs.

Write us for a copy of GRAPHITE ANODES— it is yours for the asking.

PRODUCTS ELECTRODE GLC DIVISION YOU CAN TRUST ®

GREAT LAKES CARBON CORPORATION

18 EAST 48TH STREET, NEW YORK 17, N. Y.

EDITORIAL STAFF

H. H. Uhlig, Chairman, Publication Committee

Cecil V. King, Editor

Norman Hackerman, Technical Editor

Ruth G. Sterns, Managing Editor

U. B. Thomas, News Editor

H. W. Salzberg, Book Review Editor

Natalie Michalski, Assistant Editor

DIVISIONAL EDITORS

W. C. Vosburgh, Battery

Milton Stern, Corrosion, I

R. T. Foley, Corrosion, II

T. D. Callinan, Electric Insulation

Seymour Senderoff, Electrodeposition

H. C. Froelich, Electronics

Ernest Peskell, Electronics—Semiconductors

Sherlock Swann, Jr., Electro-Organic, I

Stanley Wawzonek, Electro-Organic, II

John M. Blocher, Jr., Electrothermics and Metallurgy, I

A. U. Seybolt, Electrothermics and Metallurgy, II

N. J. Johnson, Industrial Electrolytic

C. W. Tobias, Theoretical Electrochemistry, I

A. J. deBethune, Theoretical Electrochemistry, II

ADVERTISING OFFICE

ECS
1860 Broadway, New York 23, N. Y

ECS OFFICERS

W. C. Gardiner, President
Olin Mathieson Chemical Corp., Niagara Falls, N. Y.

R. A. Schaefer, Vice-President
The Bunting Brass and Bronze Co., Toledo, Ohio

Henry B. Linford, Vice-President
Columbia University, New York, N. Y.

F. L. LaQue, Vice-President
International Nickel Co., Inc., New York, N. Y.

Lyle I. Gilbertson, Treasurer
Air Reduction Co., Murray Hill, N. J.

I. E. Campbell, Secretary
National Steel Corp., Weirton, W. Va.

Robert K. Shannon, Executive Secretary
National Headquarters, The ECS, 1860 Broadway, New York 23, N. Y.

Manuscripts submitted to the Journal should be sent, in triplicate, to the Editorial Office at 1860 Broadway, New York 23, N. Y. They should conform to the Instructions to Authors, last published in the April 1960 issue, pp. 100C-101C. Manuscripts so submitted become the property of The Electrochemical Society and may not be published elsewhere, in whole or in part, unless permission is requested of and granted by the Editor.

Inquiries re positive microfilm copies for volumes should be addressed to University Microfilms, Inc., 313 N. First St., Ann Arbor, Mich.

Journal of the

Electrochemical Society

MAY 1960 **VOL. 107 • NO. 5**

CONTENTS

Editorial

100th Anniversary. *A. Fleischer* 116C

Technical Papers

An Investigation of the Discharge Characteristics of Groups VI-VIII Oxides in an Alkaline Electrolyte. *C. K. Morehouse and R. Glicksman* 361

Kinetics of the Dissolution of Copper in Aqueous Solutions of Aliphatic Diamines. *S. C. Sircar and D. R. Wiles* 366

Dissolution of Single Crystals of Copper in Aqueous Ethylenediamine. *L. H. Jenkins* 371

Studies on Cathodic Protection Using the Hull Cell, I. Action of Corrosion Inhibitors. *K. S. Rajagopalan and Y. V. P. Ramachandra Row* 379

Particle Separations by Nonuniform Electric Fields in Liquid Dielectrics, Batch Methods. *H. A. Pohl and J. P. Schwar* 383

Nonuniform Field Effects in Poorly Conducting Media. *H. A. Pohl* 386

Continuous Separations of Suspensions by Nonuniform Electric Fields in Liquid Dielectrics. *H. A. Pohl and C. E. Plymale* 390

Electrodeposition of High-Purity Chromium from Electrolytes Containing Fluoride or Fluosilicate. *N. Ryan* 397

Polarization of Luminescence in ZnS and CdS Single Crystals. *A. Lempicki* 404

Polarization of Fluorescence in CdS and ZnS Single Crystals. *J. L. Birman* 409

Effect of CdS Addition in ZnS:Cu, In and ZnS:Ag, In Phosphors. *E. F. Apple* 418

Growth and Heat Treatment of Zinc Sulfide Single Crystals. *A. Kremheller* 422

Characteristics of the {111} Surfaces of the III-V Intermetallic Compounds. *H. C. Gatos and M. C. Lavine* 427

Etching Behavior of the {110} and {100} Surfaces of InSb. *H. C. Gatos and M. C. Lavine* 433

Polarographic Reductions of Benzyl Halides. *L. W. Marple, L. E. I. Hummelstedt, and L. B. Rogers* 437

Preparation of Boron from Boron Carbide. *D. R. Stern* 441

Contribution to the Theory of Current Distribution in Local Cells. *C. Wagner* 445

Effect of Hydrogen Pressure on the Hydrogen Overvoltage on Bright Rhodium. *S. Schuldiner* 452

Technical Notes

Effect of Oxygen on the Active-Passive Behavior of Stainless Steel. *N. D. Greene* 457

A Controlled Diffusion Process for Indium in N-Type Germanium. *F. Barson, M. J. Dyett, C. Karan, and W. E. Mutter* 459

Technical Feature

The Double Layer in Electrochemistry. *A. N. Frumkin* 461

Brief Communications

Preparation of Solid Electrodes for Hydrogen Overpotential Studies. *A. C. Makrides and M. T. Coltharp* 472

Periodic Phenomena at a Nickel Electrode in Sulfuric Acid. *J. Osterwald and H.-G. Feller* 473

Current Affairs 120C-126C

Published monthly by The Electrochemical Society, Inc., from Manchester, N. H., **Executive Offices, Editorial Office and Circulation Dept., and Advertising Office** at 1860 Broadway, New York 23, N. Y., combining the JOURNAL and TRANSACTIONS OF THE ELECTROCHEMICAL SOCIETY. Statements and opinions given in articles and papers in the JOURNAL OF THE ELECTROCHEMICAL SOCIETY are those of the contributors, and The Electrochemical Society assumes no responsibility for them. Nondeductible subscription to members $5.00; subscription to nonmembers $18.00. Single copies $1.25 to members, $1.75 to nonmembers.

Copyright 1960 by The Electrochemical Society, Inc.

Entered as second-class matter at the Post Office at Manchester, N. H., under the act of August 24, 1912.

One of a series

Catching Up with a Slippery Equation

What goes on when two moving surfaces are separated by a film of oil?

Simple question? Maybe, but engineers and mathematicians have been trying to answer this classic question of lubrication ever since Osborne Reynolds neatly stated the problem in equation form back in 1886.

Unfortunately, analytical methods for solving Professor Reynolds' partial differential equation worked only for unrealistic oil bearings, bearings with widths approaching zero or infinity. And approximate methods were crude, requiring a complete recalculation for each slight change in the bearing.

Recently, mathematicians at the General Motors Research Laboratories came up with the most versatile and efficient method of solution yet made. Their analytical method for solving the two-dimensional Reynolds' equation applies to all finite journal bearings – as well as other hydrodynamic bearings – with *no* assumptions or approximations about boundary locations. The new method uses a long-neglected energy theorem recorded by Sir Horace Lamb instead of the force relationship tried by Reynolds and others.

Besides being a valuable contribution to the theory of lubrication, this work has its practical side: namely, accurate, serviceable design curves for engineers. At GM Research, we believe delving into both the theoretical and applied sides of a problem is important to progress. It is a way of research that helps General Motors fulfill its pledge of "more and better things for more people."

General Motors Research Laboratories

Warren, Michigan

Hydrodynamic analyses have led to specific answers about bearing operation. Shown here are the oil pressure distribution (main illustration) and load-carrying capacity for a non-rotating journal with a reciprocating load.

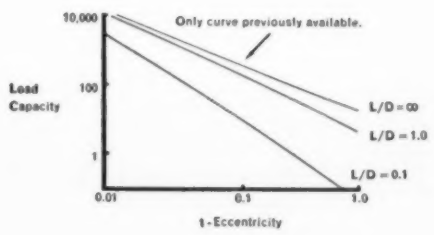

HAROLD S. BLACK, LAMME MEDALIST

A MAN WINS A MEDAL...AND STRENGTHENS A PHILOSOPHY

The search for the "hitherto unattainable" sometimes ends in strange places.

For years Bell Laboratories engineer Harold S. Black pondered a problem: how to rid amplifiers of the distortion which unhappily accumulated as signal-transmission paths were made longer and amplifiers were added. There had been many approaches but all had failed to provide a practical answer.

Then one day in 1927 the answer came—not in a research laboratory, but as he traveled to work on the Lackawanna Ferry. On a newspaper, Mr. Black jotted down those first exciting calculations.

Years later, his *negative feedback principle* had revolutionized the art of signal amplification. It is a principal reason why telephone and TV networks can now blanket the country, the transoceanic cable is a reality, and military radar and missile-control systems are models of precision.

For this pioneer achievement, and for numerous other contributions to communications since then (some 60 U. S. patents are already credited to him), Mr. Black received the 1957 Lamme Medal from the American Institute of Electrical Engineers. He demonstrated that the seemingly "unattainable" often *can* be achieved, and thus strengthened a philosophy that is shared by all true researchers.

He is one of many Bell Telephone Laboratories scientists and engineers who have felt the challenge of telephony and have risen to it, ranging deeply into science and technology. Numerous medals and awards have thus been won. Two of these have been Nobel Prizes, a distinction without equal in any other industrial concern.

Much remains to be done. To create the communication systems of the future, we must probe deeper still for new knowledge of Nature's laws. We must continue to develop new techniques in switching, transmission and instrumentation for every kind of information-bearing signal. As never before, communications offer an inspiring challenge to creative men.

BELL TELEPHONE LABORATORIES

WORLD CENTER OF COMMUNICATIONS RESEARCH AND DEVELOPMENT

Editorial

100th Anniversary

ON March 26, 1860, Gaston Planté described and displayed the first practical storage battery at a meeting of l'Academie des Sciences. Planté's storage battery was assembled with nine cells in cylindrical glass jars, each cell having an element of two spirally wound lead sheets separated by a coarse woven cloth, and having an electrolyte of 10% sulfuric acid. This lead-acid battery, representing a constructive reduction to practice of the ideas and knowledge gained from studies of electrode polarization, must be rated as a pioneering invention whose usefulness and service to mankind deserve applause.

It is fitting and proper that the personnel of science pause to pay tribute to its pioneers and savants, to its great events, and to its spiritual and material fruits. This mode of thinking and acting is appropriate in every way, for scientists are always extraordinarily in debt to the work and ideas developed by their predecessors. The contemporary breadth and depth of knowledge in any single field of science, as for example in electrochemistry, reflect a sophistication that largely conceals the evolutionary path to its present state through experiment and interpretation. It is also a refreshing experience to relive the trials and tribulations of the earlier generation of investigators who attained sound and basic advances in science and technology under conditions that would be considered unacceptable by today's standards. Then, as now, the impetus was man's thirst for an insight and conquest of the unknown.

Gaston Planté was a noted French physicist who made important contributions in studies of electricity at high voltages and of electrical phenomena in the atmosphere. The centenary of his birth in 1834 was celebrated in France at a special convention at which many societies from many countries were represented. This year it is our intention to recall the centenary of Planté's brain child, the storage battery.

The storage battery is available today in many types utilizing diverse electrochemical systems. It plays an important role in everyday life. The storage battery industry is a large industry. Its principal product, the lead-acid storage battery, is manufactured in great numbers. The automotive type alone is produced at the rate of about 35,000,000 batteries per year by the American industry.

In celebration of the 100th anniversary of the invention of the lead-acid storage battery by Gaston Planté, the Battery Division of our Society has planned a symposium on the lead-acid battery at the Fall Meeting in Houston, Texas. The electrochemistry of lead-acid batteries is a challenging subject and an interesting, informative program is planned.

A. FLEISCHER[1]

[1] Thomas A. Edison Research Laboratories, West Orange, N. J.

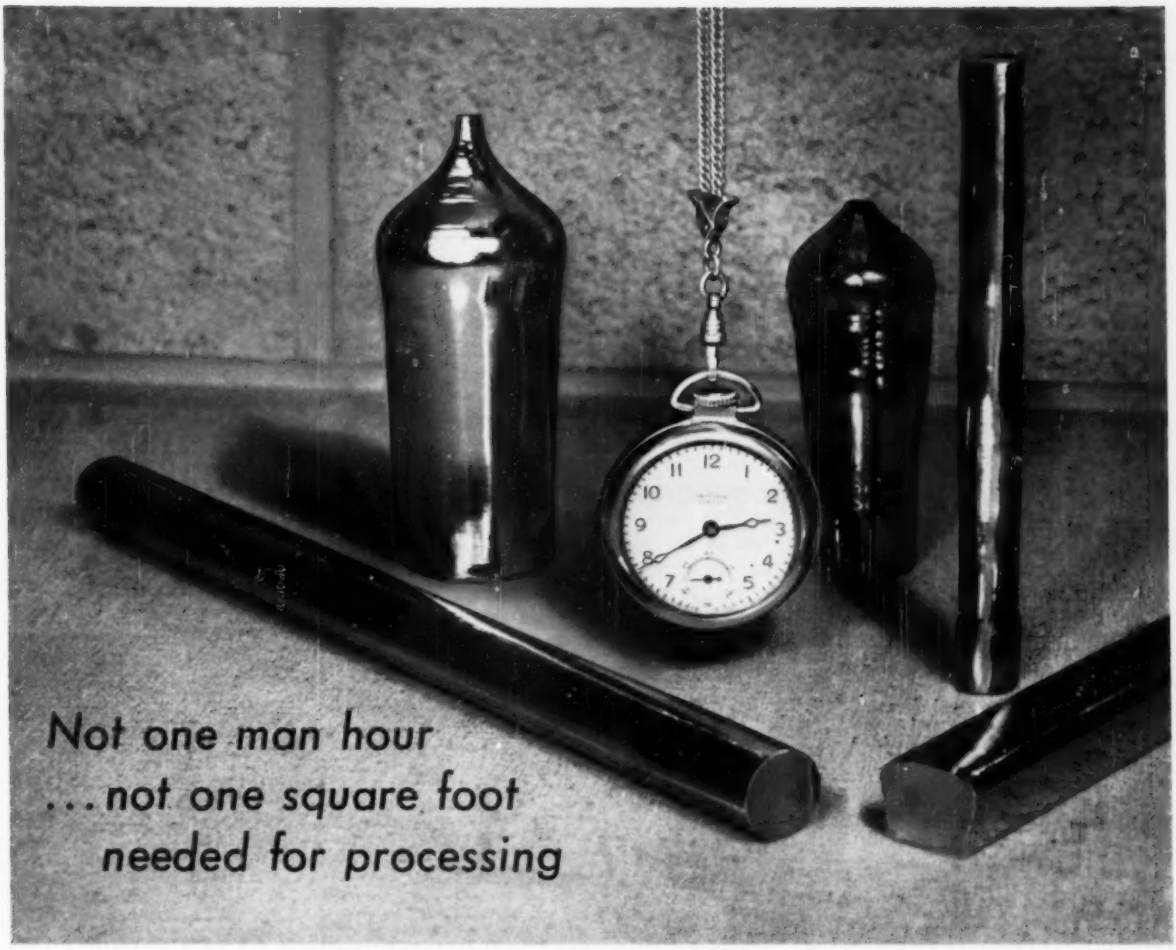

Now Sylvania grows germanium and silicon doped single crystals for you!

Now device makers can concentrate completely on device making! Sylvania grows germanium and silicon single crystals to your most exacting specifications. You not only get a guaranteed quality material ready to use; you're freed of many manpower, space and time problems. You're freed of the cost and trouble of buying and maintaining special equipment, training manpower, and handling scrap. And you can take full advantage of the engineering excellence of the Sylvania staff!

Germanium single crystals are prepared by either the Czochralski or horizontal techniques. Silicon single crystals are produced by both the float zoning and Czochralski methods.

Single crystal slices of either material are also available.

Resistivity, conductivity type, orientation, lifetime, dislocation density, and size are controlled to meet your requirements.

Sylvania know-how makes these crystals available to you at prices that are predictable and attractive. For details, write to the Chemical & Metallurgical Division, Sylvania Electric Products Inc., Towanda, Pennsylvania.

SYLVANIA

Subsidiary of **GENERAL TELEPHONE & ELECTRONICS**

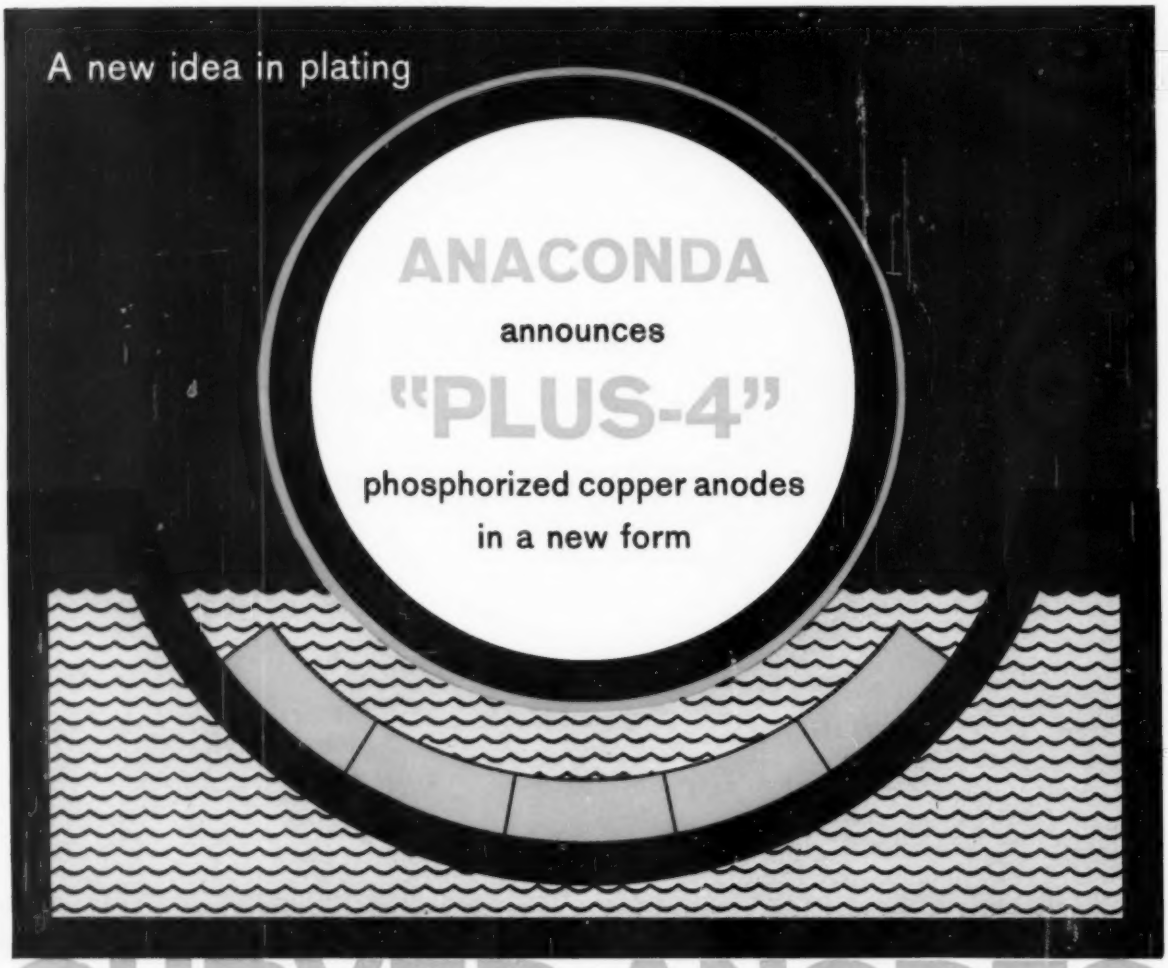

CURVED ANODES

for plating cylinders faster and more uniformly

To make anode surfaces parallel the rotogravure cylinder being plated, and to fit the curve of the current-carrying slings, Anaconda "Plus-4" phosphorized copper anodes are now extruded to precisely curved shapes.

This design gives both cost savings and improved cylinder quality:

1. A more evenly plated cylinder. Because the distance between the cylinder and the anode surface is more uniform, the copper deposit is smoother and more uniform.

2. Finishing operations in most cases are reduced, as much as 50%, because of the uniform copper deposit.

3. Less scrap because anodes corrode more evenly.

4. Improved electrical efficiency and faster plating because of better contact with sling.

For more information, write: The American Brass Company, Waterbury 20, Conn. In Canada: Anaconda American Brass Ltd., New Toronto, Ont. 60107

Note: When you request information, please specify inside radius of anode.

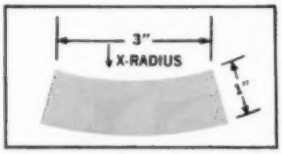

"PLUS-4"® phosphorized copper anodes

ANACONDA®

products made by The American Brass Company

An Investigation of the Discharge Characteristics of Groups VI-VIII Oxides in an Alkaline Electrolyte

C. K. Morehouse and R. Glicksman

Semiconductor and Materials Division, Radio Corporation of America, Somerville, New Jersey

ABSTRACT

Experimental half-cell potential discharge data are given for a number of Groups VI-VIII oxides in strongly alkaline NaOH solution, along with comparisons between these data and their theoretical potentials. In general, the reduction of these oxides at a carbon electrode in alkaline electrolyte is irreversible.

Many of the desirable features of a battery cathode material, such as a high reversible electrode potential and coulombic capacity, stability, and compatibility with other cell components, are found among the metallic oxides. In a previous paper (1) experimental half-cell discharge data were given for a number of Groups Ib-Vb oxides in strongly alkaline NaOH solution along with comparisons between these data and their theoretical potentials. As an extension of this work, half-cell potential discharge data for various Group VI-VIII oxides in NaOH electrolyte are presented in this paper.

Experimental Procedure

Discharge data on the various oxides were obtained by use of a technique previously described by the authors (2). In this technique, a 0.5 g sample of the cathode material mixed with 10% Shawinigan acetylene black was discharged at constant current in a large volume of electrolyte. The change in the cathode potential with time was measured with a L&N Type K potentiometer using a saturated calomel reference electrode. Discharge data were corrected for the *IR* drop associated with the apparatus and electrolyte by means of an oscillographic technique.

The half-cell potentials are all referred to the normal hydrogen electrode and represent the average of two or three measurements. The reproducibility of the data is ±0.01-0.03 v.

In this study, a zinc anode was used with an alkaline electrolyte of 30% by weight NaOH solution which was saturated with ZnO. The solution was 10.7*M* prior to the addition of ZnO. The purpose of the ZnO is to reduce the corrosion of the Zn anode in the strongly alkaline electrolyte. During the discharge, hydroxide ions are formed, but as the solution is strongly alkaline initially, the change in hydroxide ion activity of the solution is negligible.

Potential measurements of the HgO electrode in this electrolyte vs. a S.C.E. give a value of +0.043 v for the HgO half-cell referred to the normal hydrogen electrode. The deviation from the standard potential of the HgO electrode ($E^\circ - E = +0.055$ v) is due to the greater hydroxide ion activity of the electrolyte, as well as to the existence of a liquid junction potential at the alkaline-saturated KCl interface. As these factors are constant for all measurements of the half-cell potentials, +0.055 v can be added to the experimentally determined discharge potentials of the various oxides in order to compare these values with their standard electrode potentials.

Experimental Data and Discussion of Results

Group VIb oxides.—Figure 1 shows half-cell potential discharge curves of CrO_3, Cr_2O_3, MoO_3, and WO_3 obtained when these compounds are discharged at a rate of 0.005 amp/g in the strongly alkaline NaOH electrolyte. As would be expected from standard potential data (3), Cr_2O_3, MoO_3, and WO_3 are reduced with great difficulty and have discharge potentials of −1.10 v or lower. The −1.10 v value is the potential characteristic of the discharge of hydrogen on the carbon electrode in this alkaline solution at that current density. In agreement with these results, Von Stackelberg, *et al.* (4) found that molybdate and tungstate do not produce polarographic waves in neutral or alkaline solution.

Chromic trioxide, which is discharged as a chromate ion in alkaline electrolyte, undergoes a one-step reduction at a potential from −0.35 to −0.40 v in this electrolyte. This value is about 0.2 v more negative than its reversible potential. Hence, the reduction of chromate ion under these conditions of discharge is irreversible. This fact is in general agreement with the polarographic data of Lingane and Kolthoff (5) for the reduction of chromate ion at the dropping mercury electrode. However, their half-wave potential values are from 0.25 to 0.30 v more negative than the cathode potential of CrO_3 given in Fig. 1.

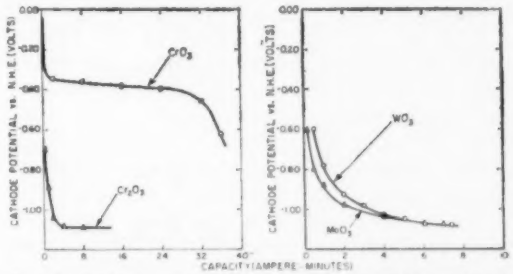

Fig. 1. Cathode potential of various group VIb oxides discharged in 30% NaOH-70% H_2O, saturated with ZnO electrolyte at a rate of 0.005 amp/g.

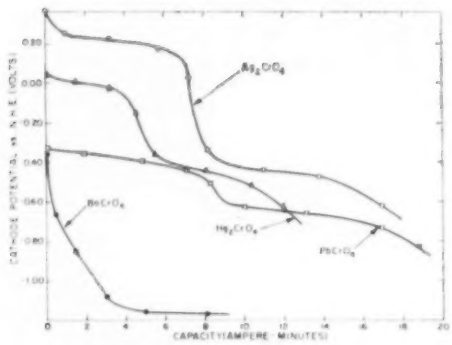

Fig. 2. Cathode potential of various chromates discharged in 30% NaOH-70% H_2O, saturated with ZnO electrolyte at a rate of 0.005 amp/g.

Under the present conditions of discharge, the reduction of CrO_4^- does not proceed farther than the +3 oxidation state because the discharge of hydrogen ions at the carbon cathode takes place at a less negative potential than that required for the reduction of $Cr(OH)_3$ or CrO_2^-. Thus, the reduction of CrO_4^- in alkaline solution can be expressed by the following equation

$$CrO_4^- + 4H_2O + 3e^- = Cr(OH)_3 + 5\ OH^-,\ E^\circ_R = -0.13\ v \quad [1]$$

If a 3 electron change and a −0.60 v end potential are assumed, the CrO_4 electrode operates at an electrode efficiency of 73.5%.

Figure 2 shows half-cell potential discharge curves of $BaCrO_4$ and the metal chromates, Ag_2CrO_4, Hg_2CrO_4, and $PbCrO_4$, all of which contain a reducible cation. The latter three compounds exhibit a two-step potential-time discharge curve with potential steps characteristic of their respective oxides (1), and of the chromate ion. For $PbCrO_4$, the chromate ion is discharged first because its cathode potential is less negative than that of the plumbite ion. With a −0.60 v end potential for Ag_2CrO_4 and Hg_2CrO_4, and an −0.80 v end potential for $PbCrO_4$, and if a 5 electron change is assumed, electrode efficiencies of 69, 74, and 73%, respectively, are obtained from these compounds.

The rapid decrease in cathode potential of the highly insoluble $BaCrO_4$ compound during discharge is believed due to the resultant low concentration of chromate ion available for the electrochemical reaction.

Group VIIb oxides.—Work by Walkley (6-8) on the Mn-Mn^{++} and Mn^{++}-MnO_2 couples has done much to clarify the thermodynamics of the various oxidation states of manganese. According to Latimer (3), it now appears definite that cell measurements on the Mn^{++}-MnO_2 and MnO_2-MnO_4^- couples are reliable and reproducible when the manganese dioxide is in the form of pyrolusite, prepared by heating manganous nitrate. He lists the following alkaline cell reactions which involve manganese dioxide, manganate, and permanganate

$$MnO_4^- + 2H_2O + 3e^- = MnO_2\ (\text{pyrolusite}) + 4\ OH^-,\ E^\circ_R = +0.588\ v \quad [2]$$

$$MnO_4^- + e^- = MnO_4^{=},\ E^\circ = +0.564\ v \quad [3]$$

$$MnO_4^{=} + 2H_2O + 2e^- = MnO_2 + 4\ OH^-,\ E^\circ_R = +0.60\ v \quad [4]$$

The MnO_4^--MnO_2 potential was obtained from direct cell measurements (9), and values for the MnO_4^--$MnO_4^{=}$ and $MnO_4^{=}$-MnO_2 couples were obtained by recalculations of the equilibrium measurements of Schlesinger and Siems (10).

The half-cell potential discharge curves presented in Fig. 3 show that $KMnO_4$ initially operates at a potential from 0.06 to 0.08 v lower than the theoretical potentials of the MnO_4^--$MnO_4^{=}$ and $MnO_4^{=}$-MnO_2 couples, after corrections are made for the pH of the solution and for the liquid junction potential. The two-step potential-time discharge curve of this compound in alkaline electrolyte can be interpreted in terms of a 3 electron reduction to MnO_2, with subsequent reduction to the +3 and +2 oxidation states of manganese. No analytical data, however, are available to confirm this reasoning.

In contrast to $KMnO_4$, $BaMnO_4$ operates at a cathode potential 0.9 v lower than the theoretical potential of the MnO_4^--MnO_2 couple and gives little capacity in the alkaline electrolyte.

$KReO_4$ also operates at a considerably lower cathode potential than $KMnO_4$ in alkaline electrolyte, as would be expected from the following standard potential data given by Latimer (3):

$$ReO_4^- + 2H_2O + 3e^- = ReO_2 + 4\ OH^-,\ E^\circ_R = -0.594\ v \quad [5]$$

$$ReO_4^- + 4H_2O + 7e^- = Re + 8\ OH^-,\ E^\circ_R = -0.584\ v \quad [6]$$

$KReO_4$ operates at a potential of from 0.15 to 0.20 v below its theoretical value, although it is uncertain whether the reduction of $KReO_4$ proceeds by Eq. [5] or [6]. On the basis of a 3 electron reduction step (Eq. [5]), it is calculated that this electrode would operate at an efficiency of 95%, if a −1.0 v end potential is assumed.

It is of interest to discuss the manganese dioxide electrode, which has long been used as a cathode material in primary cells because of its high theoretical electrode potential and coulombic capacity. Although the reduction of manganese dioxide is often represented by a simple equation such as the one calculated by Walkley (11) from thermal data,

$$MnO_2 + H_2O + e^- = MnOOH + OH^-,E^\circ_R = +0.17\ v \quad [7]$$

the half-cell potential discharge curve of this cathode exhibits a sloping characteristic as shown by the data in Fig 3. This suggests a complex reaction mechanism.

Recent studies of the alkaline reduction of manganese dioxide in dry cells by Cahoon and Korver (12) showed both divalent manganese, presumably formed as $Mn(OH)_2$ in the cathode, and an insoluble manganese oxide residue as the reduction products. That divalent manganese is an end product in the alkaline reduction of MnO_2 is evident from the half-cell potential discharge curves in Fig. 3 of electro-

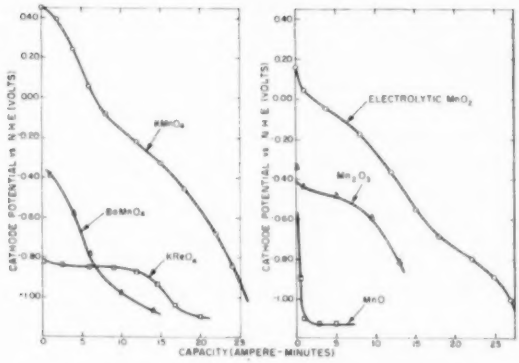

Fig. 3. Cathode potential of various group VIIb oxides discharged in 30% NaOH-70% H_2O, saturated with ZnO electrolyte at a rate of 0.005 amp/g.

lytic MnO_2 (85% MnO_2 content) and Mn_2O_3. For example, if end potentials of −0.40 v and −0.80 v are assumed for a one and two electron reduction, respectively, electrode efficiencies of 80 and 71% are obtained for MnO_2. For Mn_2O_3, an electrode efficiency of 62% is obtained if an 0.80 v end potential and a one electron change are assumed. However, the reduction of Mn_2O_3 may also take place according to the following idealized equations of Walkley (11):

$$3Mn_2O_3 + H_2O + 2e^- = 2Mn_3O_4 + 2\,OH^-, E^\circ_R = -0.18\text{ v} \quad [8]$$

$$2Mn_3O_4 + 2H_2O + 4e^- = 6MnO + 4\,OH^-, E^\circ_R = -0.39\text{ v} \quad [9]$$

Reduction ceases at the divalent manganese state, as evidenced by the discharge data for MnO. This effect is to be expected on the basis of the high negative potential of the $Mn(OH)_2$-Mn couple.

The slightly higher initial cathode potential of electrolytic manganese dioxide as compared to the potential given in Eq. [7] is thought to be due to the difference in the thermodynamic properties of the various oxides which differ chiefly in their E° values (11). These values for γ $-MnO_2$ are about 150 mv higher than those for pyrolusite.

Measurements conducted in acid solution (6) have shown that the E° values of the following reaction

$$MnO_2 + 4H^+ + 2e^- = Mn^{++} + 2H_2O, E^\circ_A = +1.23\text{ v} \quad [10]$$

depend on both the structural type of oxide and the value of n in the formula MnO_n. The variation in potential of various manganese dioxides in acid solution is illustrated by the half-cell potential discharge data in Fig. 4 for naturally occurring African MnO_2 and a synthetic electrolytic MnO_2. The discharge curves were obtained by discharging these compounds at a rate of 0.005 amp/g in 480 g/l $AlCl_3 \cdot 6H_2O$ electrolyte. A similar relationship between the two dioxides also exists in strongly alkaline solution (13).

The discharge curves for the two manganese dioxides in this acidic electrolyte are considerably flatter than those obtained for these compounds in solutions of higher pH. In addition, if an end potential of zero volt is assumed, both these compounds

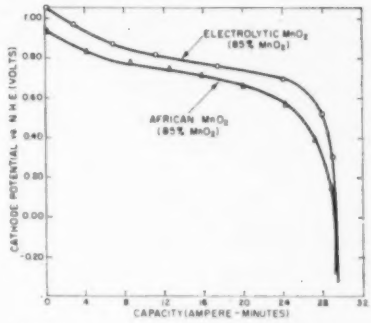

Fig. 4. Cathode potential of synthetic and naturally occurring manganese dioxide discharged in 480 g/l $AlCl_3 \cdot 6H_2O$ electrolyte at a rate of 0.005 amp/g.

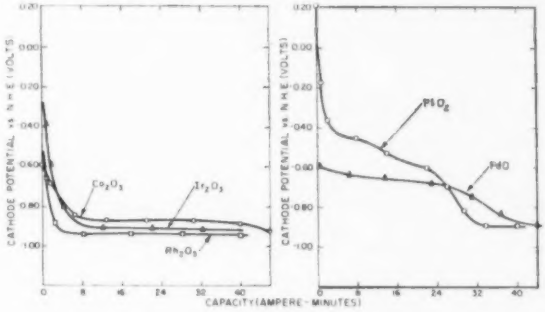

Fig. 5. Cathode potential of various group VIII oxides discharged in 30% NaOH-70% H_2O, saturated with ZnO electrolyte at a rate of 0.005 amp/g.

are reduced to the divalent manganese state with electrode efficiencies of 94%.

Group VIII oxides.—Figure 5 presents a comparison of the half-cell potential discharge curves of the oxides of the +3 valence state of cobalt, rhodium, and iridium, along with the discharge curves of PtO_2 and PdO_2 in alkaline electrolyte. Co_2O_3, Ir_2O_3, and Rh_2O_3 are reduced with difficulty in this electrolyte, and the flat potential-time discharge curve around −0.90 v probably represents the potential at which hydrogen ion is discharged. The discharge of hydrogen ion at the carbon electrode in this electrolyte occurs at a potential approximately 0.2 v less negative than usual (see Fig. 1), probably because of the presence of small amounts of these low hydrogen overpotential metals in the carbon mix. The low cathode potentials of these oxides would not be expected on the basis of Latimer's standard potential data.

Similarly, PtO_2 and PdO operate at potentials considerably below the theoretical values given by Latimer

$$Pt(OH)_n^{-} + 2e^- = Pt(OH)_2 + 4\,OH^-, E^\circ_R = +0.1 \text{ to } +0.4\text{ v} \quad [11]$$

$$Pt(OH)_2 + 2e^- = Pt + 2\,OH^-, E^\circ_R = +0.15\text{ v} \quad [12]$$

$$Pd(OH)_2 + 2e^- = Pd + 2\,OH^-, E^\circ_R = +0.07\text{ v} \quad [13]$$

Figure 5 indicates that the reduction of PtO_2 to Pt appears to take place in two steps, whereas PdO exhibits a flat potential-time discharge curve in the alkaline electrolyte. For these oxides, electrode effi-

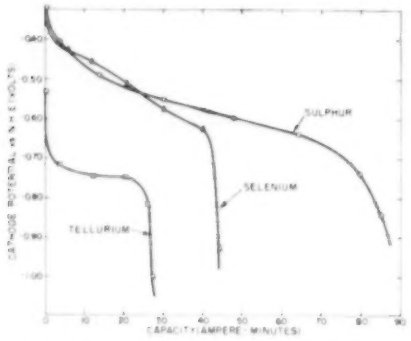

Fig. 6. Cathode potential of various group VIa elements discharged in 30% NaOH-70% H_2O, saturated with ZnO electrolyte at a rate of 0.005 amp/g.

ciencies of 100% are obtained to a −0.90 v end potential.

Group VIa oxides.—One of the most striking characteristics of the Group VIa potentials is the decrease in oxidizing power of the free elements with increasing atomic weight, as indicated by the following standard potential data (3)

$$S + 2e^- = S^=, E^\circ = -0.48 \text{ v} \quad [14]$$

$$Se + 2e^- = Se^=, E^\circ = -0.92 \text{ v} \quad [15]$$

$$Te + 2e^- = Te^=, E^\circ = -1.14 \text{ v} \quad [16]$$

The half-cell potential discharge data of Fig. 6 show that Se and Te in an alkaline electrolyte operate at cathode potentials considerably more positive than the values given by Latimer. The latter values are in doubt, however, because of the difficulty encountered in obtaining accurate thermodynamic data with which to calculate these potentials. S and Se, which have comparable sloping half-cell potential-time discharge curves, operate at approximately the same cathode potentials during the course of the discharge. This is in disagreement with the expected results based on the chemical reactivity of S and Se. If an −0.80 v end potential is assumed, electrode efficiencies of 82,100 and 100% are obtained from S, Se, and Te, respectively.

Figure 7 gives half-cell potential discharge data for various oxides of the +4 and +6 states of these elements. The oxides of Se and Te operate at cathode potentials of from −0.50 to −0.60 v in this alkaline electrolyte, although the corresponding sulfur compounds, Na_2SO_3 and Na_2SO_4, cannot be reduced under the present conditions of discharge.

It is apparent from the data that both the selenate and tellurate compounds are reduced with a corresponding eight electron change to the selenide and telluride ion, respectively. With an −0.80 v end-potential, electrode efficiencies of 93% and 80% are obtained for $NaTeO_4$ and $NaSeO_4 \cdot 10\,H_2O$. Recent work (14) on the controlled potential electrolysis of telluric acid at a mercury cathode further indicates that the reduction of +6 tellurium proceeds to −2 tellurium.

Similarly Lingane and Niedrach (15) showed by a coulometric technique that the reduction of +4 tellurium in alkaline medium proceeds to −2 tellurium according to the following equation:

$$TeO_3^= + 3H_2O + 6e^- = Te^= + 6\,OH^- \quad [17]$$

On the basis of a six electron change, electrode efficiencies of 57% and 65% have been calculated from the data in Fig. 7 for SeO_2 and TeO_2.

Group VIIa oxides.—The free halogens as well as the oxygen acids and their salts are powerful oxidizing agents with respect to their reduction to the halide. Oxides of the +5 and +7 oxidation states, because of their high theoretical capacity, are of principal interest for use as cathode materials in primary cells.

Figure 8 presents half-cell potential discharge curves of $KClO_3$, $KBrO_3$, and KIO_3 obtained when these compounds are discharged at a rate of 0.005 amp/g in strongly alkaline NaOH solution. In agreement with polarographic data (16), the reduction of bromate and iodate ions to the corresponding halide ions takes place in a single step. If an −0.80 v end potential and a 6 electron change are assumed for the reduction of $KBrO_3$ and KIO_3, these compounds operate at efficiencies of 92 and 91%, respectively.

The data in Fig. 8 and Latimer's standard potential data

$$IO_3^- + 3H_2O + 6e^- = I^- + 6\,OH^-, E^\circ_R = +0.274 \text{ v} \quad [18]$$

$$BrO_3^- + 3H_2O + 6e^- = Br^- + 6\,OH^-, E^\circ_R = +0.61 \text{ v} \quad [19]$$

show clearly that the reduction of both ions is irreversible. Despite the more positive standard potential of BrO_3^- as compared with IO_3^-, KIO_3, and $KBrO_3$

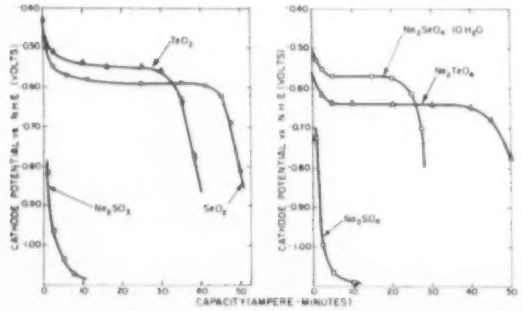

Fig. 7. Cathode potential of various group VIa oxides discharged in 30% NaOH-70% H_2O, saturated with ZnO electrolyte at a rate of 0.005 amp/g.

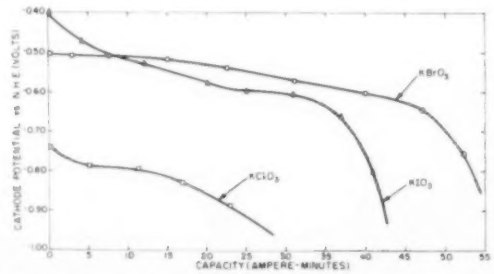

Fig. 8. Cathode potential of various halate salts discharged in 30% NaOH-70% H_2O, saturated with ZnO electrolyte at a rate of 0.005 amp/g.

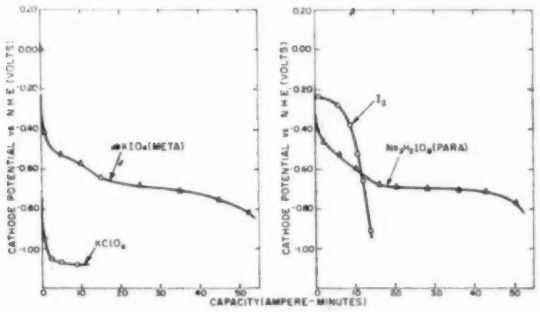

Fig. 9. Cathode potential of various perhalate compounds discharged in 30% NaOH-70% H_2O, saturated with ZnO electrolyte at a rate of 0.005 amp/g.

operate at comparable cathode potentials in the alkaline electrolyte. This is attributed to a higher overpotential for the reduction of BrO_3^- as compared with the reduction of IO_3^-. For example, at the dropping mercury electrode in acid medium, it has been found that the overpotential amounts to about 0.7 v for iodate and about 1.3 v for bromate (16).

The low cathode potential of $KClO_3$, as compared with $KBrO_3$ and KIO_3, is in agreement with observations that chlorate is not readily reduced at a cathode on electrolysis of a chlorate solution, nor is chlorate ion reduced at a dropping mercury electrode.

Figure 9 compares the half-cell potential discharge curves of sodium paraperiodate ($Na_3H_2IO_6$) and potassium metaperiodate (KIO_4) with that of potassium perchlorate. As expected from the highly negative cathode potential of $KClO_3$ given in Fig. 8 and from the fact that the oxidizing power of the oxy acids of chlorine (and their salts) decreases with increase in oxidation number of chlorine, $KClO_4$ cannot be reduced under the present conditions of discharge. The reduction of periodate, however, appears to take place with a two electron change to iodate, as follows:

$$H_3IO_6^{=} + 2e^- = IO_3^- + 3\,OH^-,\ E^\circ_R = \text{ca.} + 0.7\ \text{v} \quad [20]$$

The iodate ion subsequently is reduced to the iodide in accordance with Eq. [18]. If a −0.60 v end potential and a 2 electron change are assumed, both KIO_4 and $Na_3H_2IO_6$ are reduced to the iodate with electrode efficiencies of 86%. For reduction to the halides, KIO_4 and $Na_3H_2IO_6$ give electrode efficiencies of 90 and 100%, respectively, if an 8 electron change and an end potential of −0.80 v are assumed. Similarly, the electroreduction of periodate at the dropping mercury electrode in acid solution (17) shows two general waves corresponding to a reduction to the iodate and then to the iodide.

The high cathode potential of iodine shown in Fig. 9 further indicates that reduction of the iodate proceeds directly to the halide rather than through the halogen stage.

Manuscript received Oct. 8, 1959. This paper was prepared for delivery before the Ottawa Meeting, Sept. 28-Oct. 2, 1958.

Any discussion of this paper will appear in a Discussion Section to be published in the December 1960 JOURNAL.

REFERENCES

1. R. Glicksman and C. K. Morehouse, *This Journal*, **104**, 589 (1957).
2. C. K. Morehouse and R. Glicksman, *ibid.*, **103**, 94 (1956).
3. W. M. Latimer, "Oxidation Potentials," 2nd ed., Prentice-Hall, Inc., Englewood Cliffs, N. J. (1952).
4. M. von Stackelberg, P. Klinger, W. Koch, and E. Krath, *Tech. Mitt. Krupp Forschungsber*, **2**, 59 (1939).
5. J. J. Lingane and I. M. Kolthoff, *J. Am. Chem. Soc.*, **62**, 852 (1940).
6. A. D. Wadsley and A. Walkley, *J. (and Trans.) Electrochem. Soc.*, **95**, 11 (1949).
7. A. Walkley, *ibid.*, **93**, 316 (1948).
8. A. Walkley, *ibid*, **94**, 41 (1948).
9. L. V. Andrews and D. J. Brown, *J. Am. Chem. Soc.*, **57**, 254 (1935).
10. H. I. Schlesinger and H. B. Siems, *ibid.*, **46**, 1965 (1924).
11. A. Walkley, *This Journal*, **99**, 209C (1952).
12. N. C. Cahoon and M. P. Korver, *ibid.*, **106**, 745 (1959).
13. C. K. Morehouse and R. Glicksman, *ibid.*, **103**, 94 (1956).
14. E. Norton, R. W. Stoenner, and A. I. Medalia, *J. Am. Chem. Soc.*, **75**, 1827 (1953).
15. J. J. Lingane and L. W. Niedrach, *ibid.*, **71**, 196 (1949).
16. I. M. Kolthoff and J. J. Lingane, "Polarography," Vol. II, Chapt. XXXIV, Interscience Publishers, New York (1952).
17. R. H. Coe and L. B. Rogers, *J. Am. Chem. Soc.*, **70**, 3276 (1948).

Kinetics of the Dissolution of Copper in Aqueous Solutions of Aliphatic Diamines

S. C. Sircar[1] and D. R. Wiles[2]

Department of Mining and Metallurgy, University of British Columbia, Vancouver, Canada

ABSTRACT

The recent work on the mechanisms of the dissolution of copper in aqueous solutions of amines has been extended to the diamines. The chelating agents used were ethylenediamine, 1,3 propanediamine, and 1,4 butanediamine. The dissolution reaction is shown to involve two distinct steps. The first step is found to be an adsorption pre-equilibrium. In the second step, two types of reaction compete: chelation and attack by a second ligand. Desorption of the complex follows these steps. In 1,4 butanediamine, the chelation step is not observable, while in ethylenediamine the chelation appears to be so fast as to obscure the bimolecular reaction. In propanediamine, both are evident. The reactions of the singly protonated species have been found to be solely by bimolecular attack.

Recent studies (1-4) have done much to elucidate the mechanism of the dissolution of metallic copper in oxygen-containing solutions of various complexing agents. The work of Halpern (1) demonstrated that it is necessary to define two kinetic regions: the "low oxygen pressure" region, in which diffusion of reactants limits the rate, and the "high pressure region," in which the reaction rate is chemically controlled at the surface. Halpern also showed that the rates of dissolution by ammonia molecules and by ammonium ions were essentially independent, although some free ammonia must be present for any dissolution to occur.

Our recent study (4), involving dissolution of copper in solutions of ammonia, and methyl-, ethyl-, and n-butylamines, and their conjugate acids, led to a fairly clear picture of the reactions involved. It was concluded that the reactions take place in the following stages (where A represents the amine, and the subscript s designates species residing in the surface).

$$Cu + \tfrac{1}{2} O_2 \rightleftharpoons Cu_s\text{—}O \qquad \text{fast, } K \text{ large}$$

$$Cu_s\text{—}O + A \rightleftharpoons Cu_s\text{—}O(A) \qquad \text{fast, } K_1$$

$$Cu_s\text{—}O(A) + A \rightarrow Cu_s\text{—}O(A_2) \qquad \text{slow, } k_2$$

$$Cu_s\text{—}O(A_2) + H_2O \rightarrow Cu(A_2)^{++} + 2\,OH^- \qquad \text{fast}$$

Competitive with the attack by the second amine molecule is attack by a molecule of the conjugate acid, or "aminium" ion. Thus, the last two steps could occur in the following way:

$$Cu_s\text{—}O(A) + AH^+ \rightarrow Cu_s\text{—}O(A)(A\text{-}H^+) \qquad \text{slow, } k_3$$

$$Cu_s\text{—}O(A)(A\text{-}H^+) \rightarrow Cu(A)_2^{++} + OH^- \qquad \text{fast}$$

The pre-equilibrium appeared not to involve the aminium ion, a fact which accounts, at least in part, for the observed passivity of copper in ammonia-free solutions of ammonium salts (2, 4).

The rate of a reaction which proceeds according to the above mechanism can be expressed by the following equation:

$$\text{Rate} = \frac{d[Cu^{++}]}{dt} = \frac{K_1[A]S}{1 + K_1[A]} \cdot \{k_2[A] + k_3[AH^+]\} \qquad [1]$$

This equation was found to describe the observed rates very well for ammonia and the aliphatic amines studied. S represents the total surface area.

The observation of the bimolecular nature of the dissolution reaction led to the speculation that ethylenediamine may behave similarly. In this last case, however, the reaction would be monomolecular, because both attacking groups are attached to the same molecule. It seemed to be of interest, in view of this, to study the dissolution kinetics in solutions of longer chained diamines. In such case, one would expect the chelation step to become slower as the number of atoms in the chain increases.

It was with this in view that the present work was undertaken. The reagents used were ethylenediamine (en), 1,3 propanediamine (pn), and 1,4 butanediamine (bn), which form, on chelation, rings with five, six, and seven atoms, respectively. Data on the acid-base equilibria and the copper complexing equilibrium for these diamines are shown in Table I.

Experimental

The experimental methods used were the same as those of the previous work (3, 4). The experiments were performed in a 1-gal stainless steel autoclave fitted with a titanium liner. The oxygen pressure and stirring rate were maintained high enough to in-

[1] Present address: Bakhrabad, Cuttack 2, Orissa, India.
[2] Present address: Department of Chemistry, Carleton University, Ottawa, Ont., Canada.

Table I. Some equilibrium data for the diamines used in this work (5)

Equilibrium	Log K
Ethylenediamine (en)	
$Cu^{++} + en \rightleftharpoons Cuen^{++}$	10.73
$Cuen^{++} + en \rightleftharpoons Cuen_2^{++}$	9.30
1, 3 Propanediamine (pn)	
$Cu^{++} + pn \rightleftharpoons Cupn^{++}$	10.58
$Cupn^{++} + pn \rightleftharpoons Cupn_2^{++}$	9.08
1, 4 Butanediamine (bn)	
$Cu^{++} + bn$	No chelate*

* We have found only negative references to chelates involving 1, 4 butanediamine (6, 7). Pfeiffer (8) has made the $Cu(1, 4\ bn)_2^{++}$ chelate, but only in alcohol and ether solutions.

sure that the transport of reactants to the surface was not a factor in rate control. Samples withdrawn periodically from the autoclave were analyzed spectrophotometrically for copper by the carbamate method (9). As in our previous work, solutions were maintained at an ionic strength of 0.1 by adjustment with $NaClO_4$. All experiments were done at a temperature of 25.0° ± 0.1°C and at an oxygen pressure of 7.8 atm.

The 1,3 propanediamine and 1,4 butanediamine were obtained from K and K Chemicals Inc., and were used without further purification. On long standing the stock solutions of these reagents tended to become yellowish and were replaced. The ethylenediamine was obtained as 99% pure material from Carbide and Carbon Chemicals Corporation and was used without further purification. It had been found earlier (3) that fractional distillation of the ethylenediamine had no effect on the rate of dissolution.

Acid effects were studied after addition of measured amounts of reagent grade perchloric acid to the diamine solution.

Reproducibility of analyses and of rate measurements was very good, generally to within ±2%. At very high rates, there seemed to be greater scatter in the results. It is not understood why this is so, but it may be that transport control is becoming important.

Results

The experimental measurements made were on the systems under three different sets of conditions involving, respectively, the free diamines, the monoprotonated species (the first conjugate acids), and the free diamines with excess acid added.

Table II. Rates of dissolution of copper in diamine solutions

Ethylenediamine		1, 3 Propanediamine		1, 4 Butanediamine	
[en]	Rate (mg Cu cm^{-2} hr^{-1})	[pn]	Rate (mg Cu cm^{-2} hr^{-1})	[bn]	Rate (mg Cu cm^{-2} hr^{-1})
0.047	11.7*	0.0215	3.4	0.052	0.60
0.070	16.5	0.048	6.6	0.101	1.35
0.071	17.2*	0.091	10.8	0.229	4.05
0.095	22.8*	0.111	12.6	0.44	8.50
0.104	22.8	0.123	12.8	0.502	9.70
0.128	34.4	0.135	14.7		
0.143	31.3*	0.163	16.7		
		0.183	18.9		
		0.196	20.0		
		0.215	21.6		

* From Ref. 3.

Free diamines.—The results of rate measurements on the free diamines are summarized in Table II and shown graphically in Fig. 1, 2, and 3.

The forms of the curves for the three diamines are very different from each other, but can nevertheless be described quantitatively in terms of a single set of competing mechanisms, based on our earlier conclusion (4) that two amine groups coordinate with a copper atom before it enters the solution. If one suppose a surface, covered with adsorbed oxygen atoms, to engage in a fast equilibrium adsorption (K_1) of the diamine molecule, then the desorption of the complexed copper atom may follow after either chelation (k_1) by the diamine molecule al-

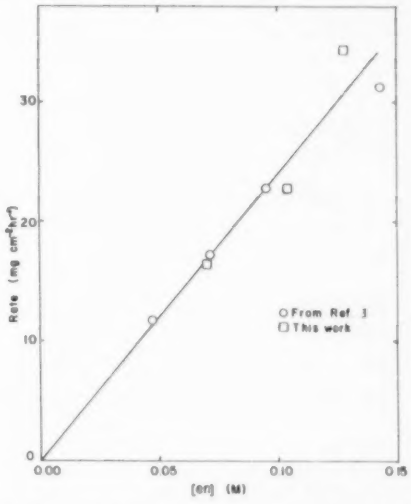

Fig. 1. Rate of dissolution of copper in free ethylenediamine (en) solution as a function of concentration.

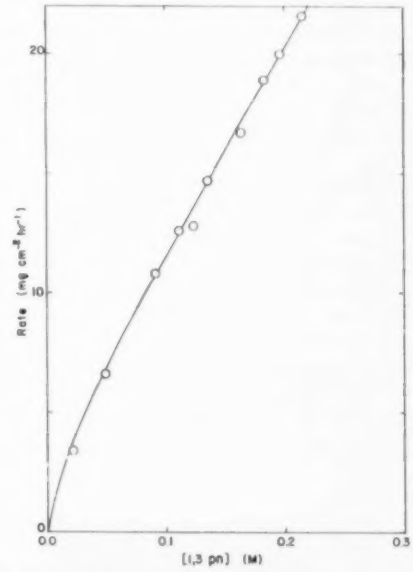

Fig. 2. Rate of dissolution of copper in 1,3 propanediamine (pn) solutions as a function of concentration. Solid line calculated using Eq. [2].

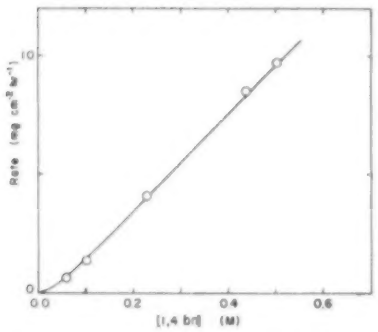

Fig. 3. Rate of dissolution of copper in 1,4 butanediamine (bn) solutions as a function of concentration. Solid line computed using Eq. [3].

ready attached, or attack (k_2) by a second molecule, such that each is coordinated at only one position. The over-all rate of dissolution is then given by Eq. [2]

$$\text{Rate} = \frac{d[Cu^{++}]}{dt} = \frac{K_1[X]S}{1 + K_1[X]}(k_1 + k_2[X]) \quad [2]$$

It is seen that where k_1 is very small, i.e., when chelation does not occur measurably, Eq. [2] reduces to:

$$\text{Rate} = \frac{K_1[X]S}{1 + K_1[X]} \cdot k_2[X] \quad [3]$$

Equation [3] is analogous to that used (4) to describe the bimolecular attack of the mono-amines on copper. It is found (Fig. 3) that this equation very well describes the observed effect of 1,4 butanediamine concentration on the dissolution rate.

If, on the other hand, k_1 is very large, (i.e., much larger than $k_2[X]$) for low values of $K_1[X]$, Eq. [2] reduces to

$$\text{Rate} = K_1k_1[X]S \quad [4]$$

This is equivalent to the expression used in earlier work (3) to describe the effect of ethylenediamine concentration on the rate of dissolution.

In the event that neither the chelation reaction nor the bimolecular attack can be ignored, then Eq. [2] must be used in full. This equation is seen in Fig. 2 to describe rather well the observed rates of dissolution of copper in 1,3 propanediamine.

The values found for the constants are given in Table III. The limits of error quoted are estimated by varying the constant enough to give a clearly bad fit of the data. It is these values for the constants which give the curves drawn in Fig. 1, 2, and 3.

Pure acid species.—Dissolution rates obtained in solutions of the mono-protonated species, ethylenediaminium and 1,3 propanediaminium, are given in Table IV.

The results can be interpreted satisfactorily by Eq. [5]

$$\text{Rate} = \frac{K_2[X]S}{1 + K_2[X]}(k_2 + k_3[X]) \quad [5]$$

where k_2 is found to be zero. It is evident from the form of Eq. [5] that dissolution in these solutions

Table III. Values found for the constants in Eq. [2] for the pure diamines

	en	1, 3 pn	1, 4 bn
K_1	$K_1k_1 = 240 \pm 10$	60 ± 5	22 ± 2
k_1	$K_1k_1 = 240 \pm 10$	5.0 ± 0.5	<0.1
k_2	$<<k_1$	85 ± 2	21 ± 0.5

Table IV. Rates of dissolution of copper in aqueous solutions of ethylenediaminium (enH^+) perchlorate and 1, 3 propanediaminium (pnH^+) perchlorate. These data are plotted in Fig. 4.

$[enH^+](M)$	Rate (mg cm^{-2} hr^{-1})	$[pnH^+](M)$	Rate (mg cm^{-2} hr^{-1})
0.022	4.8	0.17	2.40
0.039	8.6	0.040	6.40
0.061	16.2	0.060	9.8
0.071	19.6		
0.084	28.0		

occurs by bimolecular attack. The chelation step, corresponding to the constant k_2, evidently does not occur in the pure acid systems. The mechanism proposed for this dissolution is closely analogous to that described for the free amines.

The values for the constants for the above reactions are given in Table V. The curves shown in Fig. 4 were calculated using these values.

Mixed acid and basic species.—The "acid effect"–the change in rate on addition of acid to an excess of the free diamine–was studied only for 1,3 propanediamine. The results are given in Table VI.

It seems likely that the nature of the processes occurring in this mixed system are the same as those occurring in the pure systems, with two additional "cross-reactions" leading to the same reacting species

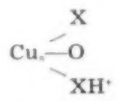

Since it is not possible kinetically to distinguish between the two paths by which this species can be formed, the observed cross-reaction rate will be best considered as the linear sum of the two independent

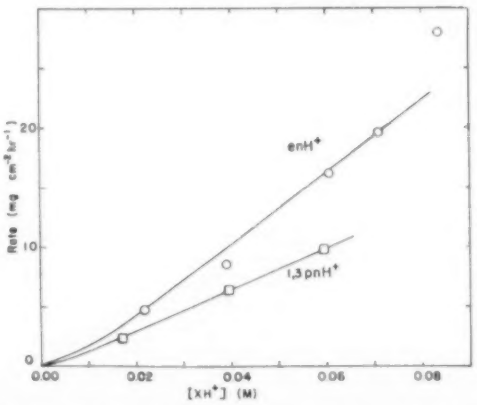

Fig. 4. Rate of dissolution of copper in solutions of ethylenediaminium (enH^+) and 1,3 propanediaminium (pnH^+) perchlorates. Solid lines calculated using Eq. [5].

Table V. Values for the constants in Eq. [5] for the pure mono-protonated diamines

	enH⁺	pnH⁺
K_2	120 ± 20	275 ± 25
k_2	0	0
k_4	310 ± 10	175 ± 10

Table VI. Rates of dissolution of copper in solutions containing both the acidic and basic forms of 1,3 propanediamine

[pn](M)	[pnH⁺](M)	Rate (mg cm⁻² hr⁻¹)
0.025	0.005	4.7
0.025	0.010	5.3
0.025	0.020	6.5
0.045	0.010	8.7
0.045	0.020	10.5
0.045	0.030	12.3
0.10	0.020	18.0
0.10	0.040	24.0
0.10	0.060	28.0

rates. Values were determined for the apparent rate constants by considering each reaction, in turn, to account for the whole of the cross reaction. Values are given in Table VII. This procedure necessarily will involve several sources of error. It is not surprising, then, that the values of the constants computed from the results of individual experiments showed a trend rather than a random scatter. The total range of the trend was only 40%, for reaction rates varying by as much as a factor of six, so it seems justifiable to give a 20% "confidence limit" on the mean values. The total experimental rates and computed rates are compared in Fig. 5.

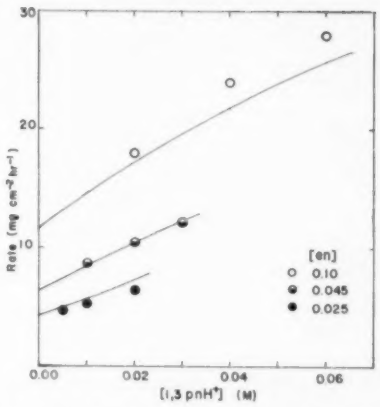

Fig. 5. Rate of dissolution of copper in mixed solutions of ethylenediamine (en) and ethylenediaminium (enH⁺) perchlorate: Comparison of experimental and calculated values.

Summary and Discussion

The dissolution of metallic copper in aqueous solutions of aliphatic diamines has been found to occur as the sum of a complex array of competing processes. These processes all give the same final product, that is, dissolved cupric ion, appropriately complexed, and the competing steps can be isolated only by studying extremes of pH, such that a small number of reactions are overwhelmingly predominant.

The reaction involves an oxygen-adsorption pre-equilibrium step

$$Cu_s + \tfrac{1}{2}\,O_2 \overset{fast}{\rightleftharpoons} Cu_s{-}O$$

followed by one of two competing pre-equilibria:

$$Cu_s{-}O + X \overset{fast}{\rightleftharpoons} Cu_s{-}O{-}X \qquad K_1$$

$$Cu_s{-}O + XH^+ \overset{fast}{\rightleftharpoons} Cu_s{-}O{-}XH^+ \qquad K_2$$

The first of these two adsorbed species can form a chelate complex and desorb:

$$Cu_s{-}O{-}X \overset{slow}{\rightarrow} Cu_s{=}O \rightarrow \qquad k_1$$

$$Cu_s{=}O + H_2O \overset{fast}{\rightarrow} CuX^{++} + 2\,OH^-$$

The competing step involving the acid species:

$$Cu_s{-}O{-}XH^+ \rightarrow Cu_s{=}O \qquad k_2$$

$$Cu_s{=}O \rightarrow CuX^{++} + OH^-$$

appears not to occur to a detectable extent. There is also a bimolecular attack, very much the same as that occurring with the mono-amines **(4)**:

$$Cu_s{-}O{-}X + X \overset{slow}{\rightarrow} Cu_s{-}O{-}X \qquad k_3$$

$$Cu_s{-}O{-}XH^+ + XH^+ \overset{slow}{\rightarrow} Cu_s{-}O{-}XH^+ \qquad k_4$$

and the corresponding cross reactions:

$$Cu_s{-}O{-}X + XH^+ \overset{slow}{\rightarrow} Cu_s{-}O{-}XH^+ \qquad k_5$$

$$Cu_s{-}O^+ + X \overset{slow}{\rightarrow} Cu_s{-}O{-}XH^+ \qquad k_6$$

Table VII. Summary of the equilibrium and rate constants

	K_1	K_2	k_1	k_2	k_3	k_4	k_5	k_6
en (K_1k_1 = 240 ± 10)	120 ± 20	—	0	$<<k_1$	310 ± 10	—	—
pn	60 ± 5	275 ± 25	5.0 ± 0.5	0	85 ± 2	175 ± 10	975 ± 200	210 ± 40
bn	22 ± 2	—	<0.1	—	21 ± 0.5	—	—	—

Each of these last steps is, of course, followed by hydration and desorption. The general equation to describe the rate gives the sum of all the six competing reactions.

$$\text{Rate} = \frac{d[Cu^{++}]}{dt} = \frac{S}{1 + K_1[X] + K_2[XH^+]}$$

$$\{K_1[X](k_1 + k_3[X] + ck_5[XH^+])$$

$$+ K_2[XH^+](k_2 + k_4[XH^+] + (1-c)k_6[X])\} \quad [6]$$

where c and $(1 - c)$ are normalizing constants. The values of the constants in Eq. [6] are summarized in Table VII.

A comparison of constants is very instructive in some respects, although it must be emphasized that because of the complex nature of the system, quantitative comparison of the constants may not be justified.

Of foremost importance is the relation between the competitive reactions of chelation and bimolecular attack, as shown by the constants k_1 and k_2 for the free diamines and by k_2 and k_4 for the first conjugate acids. It is found that ethylenediamine dissolves copper almost wholly by chelation, 1,4 butanediamine almost wholly by means of bimolecular attack, and 1,3 propanediamine by a combination of both. This trend is in agreement with what one would expect from a consideration of the length of the carbon chains involved.

The value 240 obtained for the product K_1k_1 for ethylenediamine is much smaller than one would expect from an extrapolation of the values of K_1 and k_1 obtained for 1,3 propanediamine and 1,4 butanediamine. It seems possible that the chelation may occur so rapidly that the preliminary adsorption cannot attain equilibrium, that is, the term $K_1[X]/(1 + K_1[X])$ of Eq. [2] and [6] does not give the true concentration of the species $Cu_{en}^{}$—O. If this is so, then this system should properly be studied by use of a steady-state treatment. Unfortunately not sufficient data are available to make this distinction meaningful.

In the acid system, it is found that neither ethylenediamine nor 1,3 propanediamine dissolves by the chelation mechanism. This is perhaps surprising in view of the effect of acid on promoting the bimolecular dissolution of copper in the aliphatic monoamines.

It seems significant that in all cases the attack of the surface by a protonated species is more rapid than by the free amine. This is true in the pre-equilibria, in the bimolecular attack and in the cross reactions. This generalization does not, however, hold for the chelation reaction, which does not occur in the acid system.

Keelen and Anderson (10), studying the dissolution of nickel in diamines, suggested that there is competitive adsorption involving the diamine and the solvent where both are necessary in the dissolving species. Thus, they concluded, the chelation can have an interfering effect. This situation is clearly different from the present one, in which contact at two points seems to be required for dissolution.

Acknowledgment

The financial support of the National Research Council (Canada) is gratefully acknowledged.

Manuscript received Aug. 10, 1959.

Any discussion of this paper will appear in a Discussion Section to be published in the December 1960 JOURNAL.

REFERENCES

1. J. Halpern, *This Journal*, **100**, 421 (1953).
2. J. I. Fisher and J. Halpern, *ibid.*, **103**, 282 (1956).
3. J. Halpern, H. Milants, and D. R. Wiles, *ibid.*, **106**, 647 (1959).
4. S. C. Sircar and D. R. Wiles, *ibid.*, **107**, 164 (1960).
5. H. Irving, R. J. P. Williams, D. J. Ferrett, and A. E. Williams, *J. Chem. Soc.*, **1954**, 3494.
6. A. E. Martell and M. Calvin, "Chemistry of the Metal Chelate Compounds," p. 138f, Prentice-Hall, New York (1952).
7. F. Basolo and R. G. Pearson, "Mechanisms of Inorganic Reactions," p. 20f, John Wiley & Sons, Inc., New York (1958).
8. P. Pfeiffer, *Naturwiss.*, **35**, 190 (1948).
9. E. B. Sandell, "Colorimetric Determination of Traces of Metals," p. 204, Interscience Publishers, New York (1950).
10. T. L. Keelen and R. C. Anderson, *J. Phys. Chem.*, **59**, 881 (1955).

Brief Communications

The JOURNAL accepts short technical reports having unusual importance or timely interest, where speed of publication is a consideration. The communication may summarize results of important research justifying announcement before such time as a more detailed manuscript can be published. Consideration also will be given to reports of significant unfinished research which the author cannot pursue further, but the results of which are of potential use to others. Comments on papers already published in the JOURNAL should be reserved for the Discussion Section published biannually.

Submit communications in triplicate, typewritten double-spaced, to the Editor, Journal of The Electrochemical Society, 1860 Broadway, New York 23, N. Y.

Dissolution of Single Crystals of Copper in Aqueous Ethylenediamine

Leslie H. Jenkins

Solid State Division, Oak Ridge National Laboratory,[1] Oak Ridge, Tennessee

ABSTRACT

The kinetics of the dissolution of preferentially oriented single crystal plates of 99.999% copper in stirred aqueous solutions of 10^{-2}M ethylenediamine containing oxygen have been studied. The dissolution rates, which were controlled by a transport process in solution, were a function of the temperature and stirring rate of the solution, but were independent of the crystallographic orientation of the exposed metal surface. From the examination of the facets developed during the course of the reaction on crystals with low index faces, it was concluded that the order of stability of the crystal faces was (100) > (110) > (111) in this particular system. Other than anomalous faceting observed in regions thought to correspond to grain boundaries, no correlation between chemical reactivity and crystal imperfections was observed.

The kinetics of the dissolution of polycrystalline copper in aqueous solutions which contain oxygen and a reagent capable of dissolving copper oxides have been studied extensively (1-3). These and other data show that by suitably varying the conditions under which the reaction is carried out, the type of kinetic control operative in any given system may be altered.

Halpern (1) rigorously defined such conditions for the oxidation of copper in aqueous ammonia solutions containing oxygen. More recently data have been obtained on the dissolution of copper in oxygen-containing solutions by several complexing agents, including ethylenediamine (3); however, the kinetic data reported is restricted to regions of high oxygen pressures where the rate is zero-order in oxygen and first-order in the complexing agent.

If single crystals of copper are exposed to environments such as these, facets and/or pits are developed on the surface of the metal. The geometrical symmetry of these facets or pits is a function of, among other things, the crystallographic orientation of the exposed face of the metal crystals. Also, it is generally believed that some of the pits and facets on the surface should bear a relationship to points where dislocations in the single crystals intersect the surface, since these are points at which the chemical potential is greater than that of an idealized atomically smooth surface. Kinks, steps, and other points of departure from the theoretically ideal surface should also be more favorable energetically as sites where reactions are initiated (4). Therefore, it appeared worthwhile to observe the changes in surfaces of single crystals of copper of various crystallographic orientations undergoing dissolution while gathering kinetic data on the system. The reaction of copper with oxygen in dilute aqueous ethylenediamine which is described by the following equation, was chosen for investigation:

$$Cu + 1/2\,O_2 + H_2O + 2\,en \rightarrow Cu(en)_2^{++} + 2\,OH^- \quad [1]$$

Conditions were such that a transport process in solution was rate-controlling. Future work will include observations on this and other aqueous systems under various types of kinetic control.

Experimental

Material.—American Smelting and Refining Company 99.999% material was used to grow copper single crystals of specific orientation by seeding from the melt in graphite crucibles. Specimens produced were parallelepipeds approximately 0.1 x 1 x 7 cm having the desired surface orientation on the 7 x 1 cm area. From these slugs three samples 0.1 x 1 x 2 cm were cut carefully with a jeweler's saw. Each crystal used was within three degrees of the desired surface orientation, and all data reported here were gathered on single crystalline material. A 1/16 in. diameter hole was drilled at one end of the crystal so that it could be suspended in the reaction vessel. The large sides of the crystal were lightly polished on a polishing wheel with 10μ Al_2O_3 to remove gross surface roughness. The sample was then cleaned by washing first in acetone, then in 2:1 HNO_3. A smooth, mirror-like surface was produced on the crystal by electropolishing, washing, and drying in the manner recommended by Young and Gwathmey (5). It was possible to use samples for more than one kinetic determination, if the surface was electropolished before each use; specimens whose surfaces were replicated for electron-micrograph studies were discarded after replication. It was felt that the process of stripping the replica film could introduce defects in the crystals by unknowingly bending or damaging in some other way.

Other than the exceptions noted below, all solutions were made from either CP or reagent grade chemicals and water which had been demineralized, distilled through a tin lined still, and stored in a seasoned polyethylene reservoir. Copper sulfate solutions were made by dissolving a weighed sample of AS&R 99.999% copper in excess, reagent grade

[1] Oak Ridge National Laboratory is operated by Union Carbide Corporation for the U. S. Atomic Energy Commission.

nitric acid. A 10% excess of standard sulfuric acid solution was added, and the mixture evaporated to dryness but not to SO_3 fumes. The residue was dissolved and diluted to volume in a volumetric flask. Portions of this solution were mixed with 10% excess ethylenediamine to prepare solutions of bisethylenediamine copper (II) sulfate. Hydrazine solutions were prepared from technical grade 85% hydrazine hydrate in water supplied by The Mathison Company. Since preliminary studies showed that identical results were obtained, both from the standpoint of kinetics and metal surface changes, whether solutions were prepared from triply distilled ethylenediamine or the 95-100% material supplied by Eastman Kodak Company, the latter material was used.

Hydrogen was purified by passing commercial grade tank gas first over hot copper and then through drying towers packed with magnesium perchlorate.

Oxygen-free solutions were prepared by bubbling about 100 ft³ of purified hydrogen saturated with water vapor through a fine fritted disk in the solution reservoir shown in Fig. 1 at a rate of 10 ft³ per day.

Apparatus.—The glass reaction vessel shown in Fig. 1 was designed to be used with solutions either free of oxygen or saturated with air. After placing a magnetic stirring bar sealed in glass in the bottom of the chamber, the polished copper crystal was suspended from the glass hook in the barrel of the vessel. The standard taper joint with bright platinum electrodes was placed in position and the entire apparatus attached to the filling rack.

If solutions free of oxygen were to be used, the system, exclusive of the solution reservoir, was alternately evacuated and filled with hydrogen. Twenty cycles were sufficient to remove all detectable traces of oxygen from the system. The volumetric bulb was then filled with about 82 ml

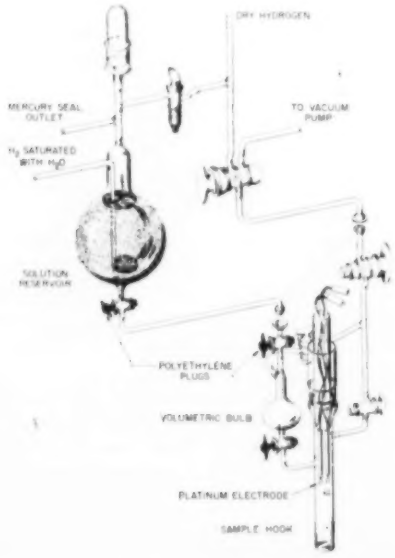

Fig. 1. Portion of filling rack with reaction chamber

of oxygen-free solution under its atmosphere of hydrogen from the storage reservoir, and the stopcocks sealing the bulb from the remainder of the system were closed. The system was again alternately evacuated and filled with hydrogen for a total of ten cycles. At the completion of these operations the solution and the sample were both at atmospheric pressure under hydrogen. A clamshell heater was placed about the reaction chamber, and the copper sample annealed at 450°C for 16 hr. The heater was then removed and the apparatus cooled to room temperature, removed from the rack, and placed in a water bath controlled to ± 0.02°C. After allowing 1 hr for temperature equilibrium to be established, the magnetic stirrer was engaged and all the solution allowed to flow from the volumetric bulb into the reaction chamber. The stopcocks isolating the reaction chamber were then closed.

When solutions saturated with air were desired the volumetric bulb was filled with 82 ml of solution and isolated from the rest of the system. The apparatus was attached to the rack and flushed with hydrogen for 20 cycles. The remainder of the procedure was repeated as on solutions containing no oxygen. By this method the copper sample did not have access to oxygen until contacted by the solution.

Progress of reactions was followed by observing conductivity changes in the solutions with time. Conductivity values were obtained with a Wheatstone bridge arrangement using an oscilloscope as a null detector. Maximum sensitivity of the system was such that the change in resistance produced by the dissolution of one atom layer of copper could be observed; however, in most cases the data were gathered under conditions in which the dissolution of 3-5 atom layers were required to produce an observable change in conductivity. Measurements were taken with the slide wire position held constant during the reaction. The null point was determined by adjusting a five decade standard resistance box.

Surface replicas.—Samples whose surfaces were to be replicated for observation with the electron microscope were removed from the reaction vessel after the desired amount of copper had been removed. They were washed quickly in a stream of distilled water for 1 min, then dried in a jet of oxygen. Surfaces were preshadowed with platinum at a 4:1 shadow angle and replicated with carbon.

Treatment of data.—At time t, the relative concentration of a component which determines the extent of a reaction may be expressed as a function of the observed conductivity values of the solution:

$$\% \text{ material unreacted} = \left(1 - \frac{\Delta\sigma_t}{\Delta\sigma_f}\right)100 \quad [2]$$

where $\Delta\sigma_t$ is conductivity change from time zero to time t and $\Delta\sigma_f$ is conductivity change from time zero to time reaction completed.

The first-order rate equation expressed in terms of conductivity is:

$$\log \frac{C_i}{C_i - C_i\left(\frac{\sigma_i - \sigma_t}{\sigma_i - \sigma_f}\right)} = kt/2.303 \qquad [3]$$

where C_i is initial concentration of reactant which controls extent of reaction, σ is the conductivity of the solution. The subscripts i, t, and f refer to the initial value before reaction has commenced, the value at time t, and the final value at completion of the reaction, respectively. If resistance values are substituted for conductivity terms, the equation becomes

$$\log \frac{R_f - R_i}{R_i} + \log \frac{R_t}{R_f - R_t} = kt/2.303 \qquad [4]$$

where R is the resistance of the solutions. Subscripts indicate values at times as above.

A plot of log $R_t/R_f - R_t$ vs. time should give a straight line, the slope of which is equal to $k/2.303$, if first-order kinetics are obeyed by the reactant controlling the extent of the reaction. It must be emphasized that Eq. [3] and [4] apply only to the component which governs the extent of the reaction. The denominator of the logarithmic term in Eq. [3] expresses the concentration of such a component at time t. Obviously, the expression is incorrect for a reactant present in excess of that demanded by the stoichiometry of the chemical reaction involved.

Experimental Results

Analytical data.—It is not necessary that the concentrations of the components be known for a kinetic treatment based on conductivity data, but at the completion of the reactions the solutions were analyzed for copper with a Beckman Model DU spectrophotometer using both the ethylenediamine method of Jonassen and Dexter (6) and the neocuproine method of Smith and McCurdy (7). The latter method is two orders of magnitude more sensitive. Data on the solubility of air in water (8) agreed with the copper analysis and showed that the extent of the reaction was limited by the amount of oxygen dissolved in the solutions when an excess of reagent capable of dissolving copper oxide was present.

These two methods of analysis offer sensitive means for determining the concentration of mono- and divalent copper in solutions of ethylenediamine. Tests proved that the cuprous complex of ethylenediamine does not adsorb light of 540 mμ, the wave length for maximum adsorption by the cupric complex (6). Any significant difference in copper concentration detected by the two methods can be attributed to the presence of monovalent copper in the ethylenediamine solution. No such differences were found.

Oxygen-Free Solutions

At 25°C the following solutions, each 10^{-2}M in the reagent listed, which had been deaerated in the manner described, were exposed to copper single crystals which had been annealed and maintained in an atmosphere of hydrogen: ethylenediamine; hydrazine sulfate; hydroxylamine sulfate; hydroxylamine; potassium cyanide (adjusted to pH 9 with KOH); HCl; H_2SO_4. Although it has been reported that in concentrated solutions KCN (9) will react with copper and water to liberate hydrogen, no copper was found in any of the solutions (limit of detection was 0.2 μg total Cu), and examination of the metal surface also showed no detectable changes.

The chemical reaction of major interest in this study was that shown in Eq. [1]. However, when all dissolved oxygen in the system had reacted, the solution contained copper ions in contact with copper metal. Since it represented a potential source of further reaction, the following equilibrium was investigated

$$2Cu^{+} \rightleftharpoons Cu^{++} + Cu^{0} \qquad [5]$$

To study this reaction, two solutions which had been freed of dissolved O_2 in the manner previously described were prepared; one 10^{-4}M $CuSO_4$ in 10^{-2}M H_2SO_4, the other 10^{-4}M $CuCl_2$ in 10^{-2}M HCl. Each solution, under a H_2 atmosphere in the solution reservoir, was introduced into the reaction vessel shown in Fig. 1 and exposed to a copper single crystal which had been annealed and maintained in a H_2 atmosphere. The apparatus was placed in a constant temperature bath at 25.00° ± 0.02°C. While in the bath the solutions were stirred continuously at a stirring speed of 500 rpm. After four days the solutions were analyzed for total copper by the method of Smith and McCurdy (7), and no change in copper concentration could be detected. In order to observe effects of complex species, an oxygen-free 10^{-4}M solution of a $Cu(en)_2SO_4$ in 10^{-2}M ethylenediamine was also exposed to a copper crystal under the conditions described above. Again, after four days no change in copper concentration could be detected. If the value of 10^{6} (see below) for the equilibrium constant of reaction [5] is correct, a change ~ 5 x 10^{-6}M in copper would be expected in the sulfate and chloride solutions. Such a concentration change would be detected easily by the analytical method used.

Bodlander and Storbeck (10) derived a value of 10^{4} for the equilibrium constant for reaction [5] from data on the solubility of copper (I) halides in solutions of alkali halides. Although they attempted to interpret the data to account for complex ion formation, it can be shown that in a 0.2M alkali halide solution containing 10^{-4}M copper (II) halide (these concentrations are typical of those studied by Bodlander and Storbeck), the equilibrium constant cannot be less than about 10^{6}, if no complex ions are formed and the solubility requirements of copper (I) halides are satisfied. Therefore, their interpretation of the data must not correct completely for copper (I) present as a complex ion.

Fenwick (11) avoided the problem of complex ions by determining the copper (I) present in solutions of $Cu(ClO_4)_2$ and $HClO_4$ exposed to metallic copper. The equilibrium constant was determined to be about 10^{6}. This value agreed, within the limits of experimental error, with that of Luther (12) which had been determined from solutions of $CuSO_4$ and H_2SO_4 exposed to metallic copper. It should be

pointed out, however, that sources of copper (I) other than that shown by Eq. [5] were available in these systems. Air-saturated solutions such as were used in both experiments contain dissolved oxygen capable of reacting with metallic copper to form Cu_2O which would dissolve in the concomitant acids. Also, a film of Cu_2O was surely present on the metallic samples before exposure to the solutions. And finally, the work of Kruger (13) and Miller and Lawless (14) on oxide films formed on copper in various solutions raises the question whether the solutions of Fenwick and Luther were at equilibrium with the metal or an oxide covered metal.

Although there is no proof that the results reported by the authors were obtained on systems at equilibrium, the four days allowed for equilibrium to be established was the same as that allowed by Fenwick. Also, it would appear that some doubt of the validity of previously reported equilibrium constants for the reaction in question is justifiable. It is clear that at the concentrations studied either equilibrium is established so slowly or the extent of reaction is so small that reaction [5] can be disregarded as a means of removing copper from the metal surface in a reasonable time.

Solution Saturated with Air

When saturated with air all the solutions previously mentioned did react with copper. Since it afforded an easy means of analysis for copper the ethylenediamine system was studied extensively. All data were gathered on solutions initially air-saturated which were 10^{-2}M in ethylenediamine. This concentration of complexing agent represents a tenfold excess over that necessary to react with all the copper oxide which could be formed by dissolved oxygen at 25°C.

Rate data were gathered at three different stirring speeds—200, 500, and 650 rpm, at temperatures of 7.50°, 25.00°, 34.47°, 47.04°, and 56.57° all ± 0.02°C. Since the sample was suspended about 2 in. above the impeller and due to the small cross section of the reaction chamber, the stirring efficiency was much less than that in the system described by Halpern (1). Dissolution rates were determined for crystals with surface orientations of (111), (100), (110), (611), and (210). The high index faces gave kinetic results identical to those obtained from the three close-packed faces; therefore, only results from the latter are reported here.

Figure 2 shows the percentage of the original oxygen remaining in solution as a function of time at a stirring speed of 500 rpm at various temperatures. It is obvious that the reaction rate was not affected by the different crystal faces exposed. This was true at all the temperatures which were investigated. Figure 3 demonstrates that an increased stirring rate increased the rate of dissolution but that the rate was not affected by crystal orientation. Again, this was true for the three stirring rates at all temperatures. Typical rate data from conductivity values are shown in Fig. 4. As previously stated, analysis for copper content at the completion of the reactions showed that the extent of the reaction was

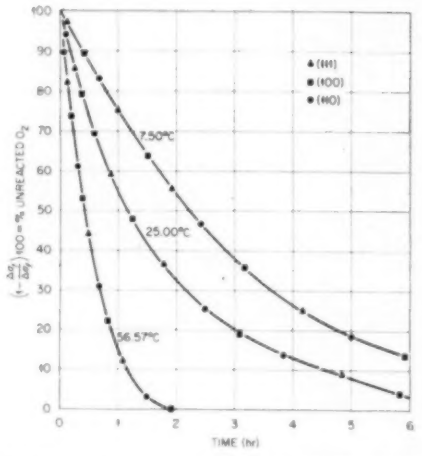

Fig. 2. Effect of temperature and crystallographic orientation on dissolution rate in 10^{-2} M ethylenediamine at a stirring velocity of 500 rpm.

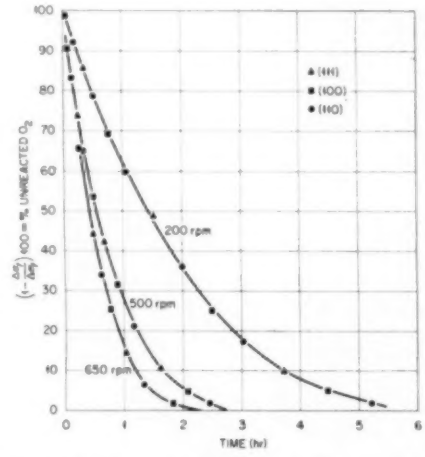

Fig. 3. Effect of crystallographic orientation and stirring velocity on dissolution rate in 10^{-2} M ethylenediamine at 47.04°C.

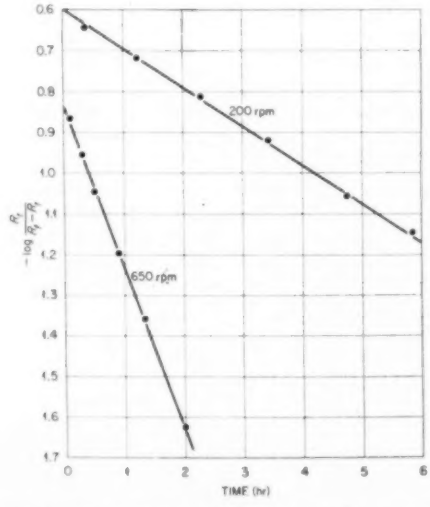

Fig. 4. Effect of stirring velocity on specific reaction rate at 25°C in 10^{-2} M ethylenediamine.

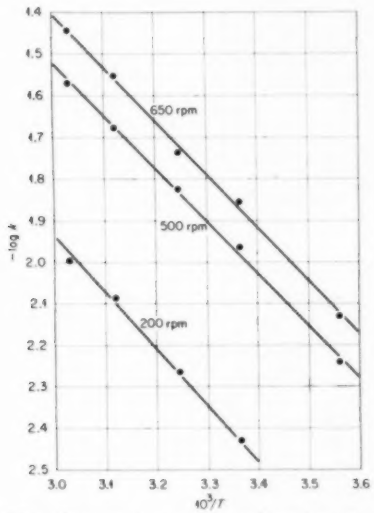

Fig. 5. Specific reaction rate as a function of stirring velocity and temperature in 10^{-2} M ethylenediamine.

determined by the amount of oxygen dissolved in the solutions. Therefore, the applicability of conductivity data to Eq. [2] and [4] demonstrates that the process was kinetically first-order with respect to oxygen and independent of the ethylenediamine concentration in these systems. A plot of log rate constants for the three stirring speeds is shown in Fig. 5 as a function of temperature. From the slopes of the lines, which are identical for the three stirring speeds, the apparent activation energy for the process was determined to be about 5800 cal mole^{-1}.

If air-saturated solutions were not stirred and thermal fluctuations in the temperature bath were very small, no reaction occurred at 25° and 35°C. Apparently a protective layer which prevents further reaction is formed over the reacting surface. Not only was no copper detected in the solution after 24 hr, but also there was no evidence of growth of a visible oxide film on the sample. The protective film is very unstable, for normal thermal agitation of unstirred solutions on the laboratory bench at room temperature is sufficient to cause reaction at a reasonable rate.

Experiments in which the stirred solutions were open to the atmosphere were also conducted. Under these conditions, conductivities of the solutions initially changed linearly with time. This is not unexpected if the rate of adsorption of oxygen from the air by the solution was at least as great as the rate at which oxygen reacted with copper. After a period of a few hours, depending on the temperature and the stirring rate, the reaction rate decreased, probably due to the decrease in concentration of free ethylenediamine. This point was not investigated further.

Oxide Film

In systems such as these the presence and possible role of oxide films is always open to question. In order to compare the behavior of these systems with one containing a film, a (110) crystal was oxidized in pure oxygen at 250°C until the sample was covered with a single-crystalline film of Cu_2O 700Å thick. The crystal was placed in the reaction chamber and the system flushed repeatedly with hydrogen. Obviously, it was impossible to anneal the specimen. The dissolution rate of the film in oxygen-free 10^{-2}M ethylenediamine, at a stirring speed of 500 rpm at 25°C, was determined from conductivity changes in the solution. Initially, there was an induction period of 30 min in which no conductivity change could be observed. (The reasons for the existence of an induction period in the dissolution of oxide films are not well understood, but such an observation is not unusual.) Dissolution then started and the conductivity changes were a linear function of time for a 2-hr period, at which time the rate decreased rapidly. About 80 min later the reaction was complete, and no further change with time was observed. The solution was analyzed for copper and the result was in excellent agreement with the amount of copper in an oxide film of this thickness. The decrease in rate at the end of the reaction could possibly be due to a slower dissolution rate of thinner oxide films which lie near the metal substrate; however, it seems more reasonable to assume that other factors, which are not understood at this time, caused the decreased rate.

Conductivity data indicated that at the completion of the 2-hr reaction period, the time at which the reaction rate started to decrease, about 630Å had been dissolved from the film. The copper required to form an oxide film of this thickness is equivalent to a dissolution of 375Å of metal. Air-saturated solutions of ethylenediamine under identical stirring and temperature conditions remove a corresponding amount of copper in about 15 min. While it is certain that the final reaction product in the air-saturated solutions studied is divalent copper, it is problematical whether the reaction proceeds through a Cu_2O or CuO mechanism. Although it is perhaps not permissible to compare the dissolution of Cu_2O films in oxygen-free solutions with other dissolution rates, it would appear that, if an oxide film is present on the crystals studied in air-saturated solutions, it must be an extremely thin one lacking the characteristics usually associated with a thick film.

Surface Effects

The (110) surface showed no substructural effects. At the very earliest point observed in the reaction no etch pits or subgrain boundaries could be seen; only faceting was observed. Figure 6 demonstrates the orderly progression of facet development on this surface. After an amount of copper corresponding to an average of 3000 atomic layers had been removed, the surface was no longer (110) but rather a series of facets thought to be (100) composed of long sharp-topped ridges separated by relatively deep valleys. It is difficult to obtain precise data about the depth of the valleys or the angle at which their sides intersect the base (110) surface from electron micrograph studies; however, it is certain that the facets lie in the (110)-(100) zone, and it is highly probable that the surfaces of the facets are (100) since the "subfaceting" on the

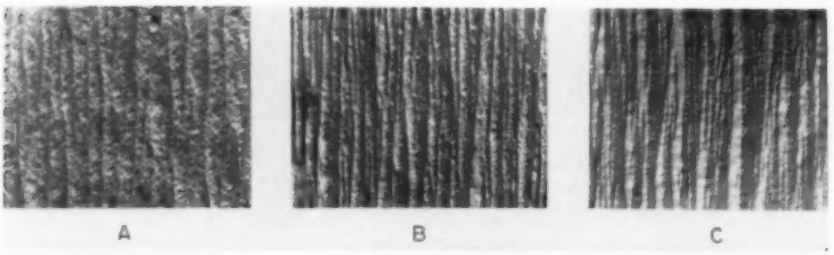

Fig. 6. Facet development on (110) surface. Average atomic layers of copper removed: A, 900; B, 1800; C, 3000. Magnification before reduction for publication: A, 50000X; B, 25000X; C, 8500X.

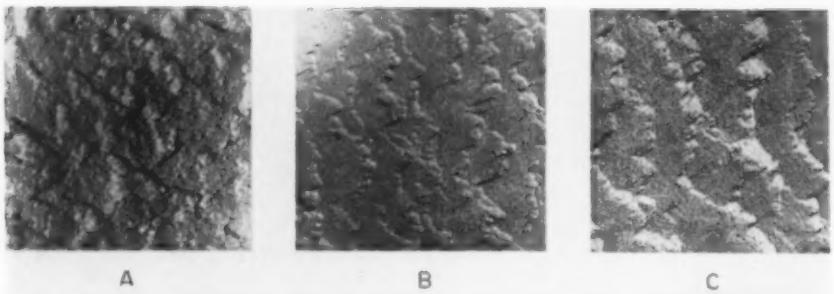

Fig. 7. Facet development on (111) surface. Average atomic layers of copper removed: A, 900; B, 1800; C, 3000. Magnification of A, B, C 17000X before reduction for publication.

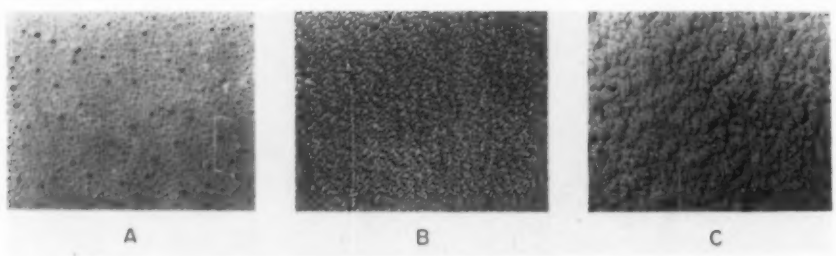

Fig. 8. Hillocks formed on (100) surface. Average atomic layers of copper removed: A, 900; B, 1800; C, 3000. Magnification before reduction for publication: A, 25000X; B, 12500X; C, 17000X.

sides of the valleys is identical with that of a (100) surface. If the fully developed facets are assumed to be (100), calculations of the amount of copper removed prove that the tops of the ridges certainly lie below the original (110) surface; however, the faceting process does start very early, and most of the material removed came from the valley areas.

Pitting is seen on the (111) surface at the earliest observable stages. Figure 7 illustrates how these pits grow and coalesce as the reaction proceeds to produce stepped facets which are oriented in two principal directions. From the orientation of the crystal and the shadows produced in the replication process, it is possible to prove that the facets are principally (110) faces. Furthermore, these facets start developing from pits very early in the dissolution process. Again, data on the total copper removed show that, at stages of the reaction where the facets are well developed, even the tops of the facets are well below the original surface. Also, at early stages of the reaction prior to extensive facet development it is possible to see pits which may have some relationship to the substructure of the crystal. A few of the pits are arranged in lines which apparently have some relationship to subgrain boundaries in the crystal.

Neither pitting nor oriented faceting is observed on the (100) surface even after the removal of copper corresponding to an average of 3000 atomic layers. From the beginning of the reaction rounded hillocks are seen on the surface. The development of these hillocks as the reaction proceeds is shown in Fig. 8. Arrangements of some of the hillocks in lines which may have some correspondence to subgrain boundaries are observed throughout the reaction.

Discussion

Kinetic Results

To prevent the formation of oxide films on a specimen before contact with the solutions it was desirable to anneal and maintain the copper crystal in an atmosphere of hydrogen. Therefore, it was not possible to mask the crystal edges of undesirable orientation from the solution. These edges of various orientations constituted 5-10% of the total exposed surface area. Also, electropolishing rounded off the edges of the crystal to produce other departures from the desired orientation. It seems clear then that if conditions had been such that the rate of oxidation at the crystal face was rate-controlling, no rate difference due to crystallographic orientation would have been observed since such differences would not be expected to be very large. However, the kinetic data at different stirring rates and temperatures demonstrate that conditions were such that a transport process in solution was rate-controlling. The activation energy determined for the reaction is of the magnitude anticipated for a process under transport control but certainly lower than expected for a system in which the rate-determining step is chemical in nature.

During the course of the reaction, the concentration of hydroxyl ion was constantly increasing in accordance with the requirements of Eq. [1]. This resulted in a corresponding decrease in the concen-

tration of the protonated form of ethylenediamine due to the equilibrium requirements of the reaction of ethylenediamine with water

$$en + H_2O \rightleftharpoons enH^+ + OH^- \quad [6]$$

Over-all, the concentration of hydroxyl ion increased about 10% while that of the ethylenediaminium ion decreased the same amount. No change in reaction rate due to these concentration changes was observed. Since initially both concentrations were only about 10% of that of the total ethylenediamine present, the changes in concentrations probably were not large enough to produce the effects observed in systems more concentrated in oxygen, ethylenediamine, and ethylenediaminium ion (3).

Experimental observation established that the reaction rate was directly proportional to the gross surface area of the sample, confirming the repeated observations of others; however, it is interesting that as the reaction proceeded there was no departure from first-order kinetics. Figure 6C shows the (110) surface at a time when the reaction was about 75% complete. At this time the surface area was approximately twice that of the original crystal before reaction started due to the troughs formed by removal of copper. As previously stated, the sides of the valleys show substructural developments like the (100) and certainly are not atomically smooth and, therefore, the roughness factors of this and the original surface can reasonably be assumed to be about the same. Since the average distance between crests of the troughs is about 7000Å these features cannot be considered negligible. Logically, it would be reasonable to expect deviations from first-order kinetics on all major faces of the crystals due to the increase in surface area, especially in the latter stages of the reaction when the change in surface area has reached a maximum. The observed structural effects would lead one to expect the greatest difference on the (110) and the least on the (111) in this particular system. These differences were, of course, not observed.

For such a system under kinetic control by a transport process, the critical area must be approximately that area of the solution which is circumscribed by the boundaries of the sample. Only macroscopic topographical deviations from a flat surface can alter this boundary area and, consequently, the reaction rates. Changes in surface area are effective only to the extent to which they contribute to such macroscopic fluctuations. Since the facets developed on the (110) were approximately 3500Å high, this suggests that the transport dependence observed is related to volume diffusion within the solution rather than diffusion across an interfacial barrier, for it seems clear that the area of such a barrier should be proportional to the microscopic surface area of the crystal.

Surface Orientations

In the system studied the (100) surface appears to be the stable orientation. At no time during the normal reaction is oriented faceting observed on surfaces of this type. However, if crystals of this orientation are reacted in systems with larger volumes so that more copper can be removed, faceting is observed as is demonstrated by the surface replica shown in Fig. 9. These facets consist of pits of various sizes, some of which have grown into each other to form large facets of random orientation. Over-all, there is clearly a tendency to maintain the (100) orientation. At higher magnifications the flat areas of this surface were seen to have a structure similar to that shown in Fig. 8A. It should be noted that casual observations would lead to the conclusion that the pits seen in Fig. 9 are associated with sites which are more reactive than the remainder of the surface. This cannot be the case, for Fig. 8 illustrates that the attack is a general one. The occurrence of pits under these conditions must be largely statistical and results from the propensity of the surface to maintain the more stable (100) orientation. The rapid development of (100) facets on the (110) surface supports the argument that the (100) is the stable orientation under these conditions. The development of facets, largely (110), on the (111) surfaces may represent a metastable condition. Since the (100) orientation is about 55° from the (111) and the (110) only 35°, the faceting observed may represent a progression to a surface state of lower energy as quickly as possible. These observations are complicated by the fact that the original surfaces of these specimens were about 2° removed from the (111). It is difficult to understand why original faceting of threefold symmetry illustrated in Fig. 7A should degenerate to twofold symmetry and why so much of the surface should maintain (111) orientation. It is reasonable to assume that if the surface were permitted to react to the point that it was covered with (110) facets, then the development of (100) facets on (110) facets would be observed; however, such arguments are questionable for the relationships between surface energies and surface area vs. total energy in systems of this type are not obvious. If no external forces are applied to the crystal, the relative stability of copper faces is (111)>(100)>(110). Since this relationship was not observed, it is possible that faceting is dependent on both the reagents in solution and their concentration.

Fig. 9. Facets on (100) surface after dissolution of an average of 30,000 atomic layers. Magnification 6500X before reduction for publication.

Fig. 10. Optical photograph of (100) surface shown in Fig. 8B. Magnification 200X before reduction for publication.

Only from replicas of the (111) surface in the early stages of reaction is it possible to obtain any information about the number of reaction sites. It is seen in Fig. 7A that the initial attack on the surface results in small triangular pits enclosed in larger ones. If each small pit is considered a nucleation point for reaction, then there are about 10^{11} such points per square centimeter of surface area. This number is much too large to be related solely to line defects in the crystal, and it is not certain that the number represents more than a limit to the means of observation.

On all (100) surfaces there are structural details like those shown in Fig. 10 which are thought to be related to subgrain boundaries within the crystal and which persist throughout the normal reaction. Similar patterns are observed on the (111) until faceting becomes so pronounced that they no longer are visible. No substructural effects of this type are observed on the (110). On the (100) these areas are hillocks raised above the rest of the surface indicating a decreased reactivity at these points, while on the (111) the lines are rows of pits which lie below the remainder of the surface, and the reactivity must be greater at such points. Whether or not such areas are representative of subgrain boundaries, their contradictory behavior is difficult to understand.

Conclusions

1. In the dilute, oxygen-free solutions studied, there is no measurable reaction between copper metal and divalent copper in solution. Either values quoted for the equilibrium constants are wrong or equilibrium is extremely slow in being established in these solutions.

2. The rate of dissolution of single crystalline copper in a closed system of air-saturated, 10^{-2}M solutions of ethylenediamine is controlled by a transport process in the solution. The rate is a function of the temperature and rate of stirring of the solution but is independent of the crystallographic orientation of the exposed metal surface. The activation energy determined is of the magnitude expected for a process under transport control.

3. While the dissolution rate appears to be directly proportional to the gross surface area of the sample, it seems likely that this is an oversimplification of a more complex relationship.

4. The dissolution rate of a Cu_2O film of predetermined thickness proved to be much slower than the removal of a corresponding amount of copper under similar conditions. If an oxide film was present on the crystals studied, it was an extremely thin one lacking the usual properties of a true film several angstroms thick.

5. The crystallographic orientation of facets developed on the metal surfaces during dissolution shows that the most stable face is not the close-packed (111). The relative stability of crystal faces in this particular system apparently is (100)>(110)>(111).

6. Nucleation of reaction sites appears to be a random process on all surfaces, and the number of such sites on the (111) face is much larger than would be permitted if reaction sites were limited to points where dislocations intersected the crystal surface.

7. The difference in reactivity of the areas thought to be subgrain boundaries on the (100) and (111) does not support the assumption generally made that these are regions of greater reactivity. At this time, no explanation of the lack of correlation between crystal imperfections and reactivity can be made.

Acknowledgment

J.O. Stiegler prepared all the surface replicas and electron micrographs, and R. M. Wallace is responsible for much of the supporting photographic work in this study. The oxide film on the (110) surface was prepared by the group headed by J. V. Cathcart in the Oak Ridge National Laboratory Metallurgy Division. The author is also indebted to F. W. Young, Jr., for many valuable discussions during the research and in the preparation of this paper. The contributions of all are gratefully acknowledged.

Manuscript received Nov. 4, 1959. This paper was prepared for delivery before the Columbus Meeting, Oct. 18-22, 1959.

Any discussion of this paper will appear in a Discussion Section to be published in the December 1960 JOURNAL.

REFERENCES

1. J. Halpern, *This Journal*, **100**, 421 (1953).
2. W. D. Robertson, V. F. Nole, W. H. Davenport, and F. P. Talboom, Jr., *ibid.*, **105**, 569 (1958).
3. J. Halpern, H. Milants, and D. R. Wiles, *ibid.*, **106**, 647 (1959).
4. N. Cabrera, "The Oxidation of Metals," "Semiconductor Surface Physics," R. H. Kingston, Editor, pp. 327-348, University of Pennsylvania Press (1956).
5. F. W. Young, Jr., and A. T. Gwathmey, *Acta Met.*, **4**, 145 (1956).
6. H. B. Jonassen and T. H. Dexter, *J. Am. Chem. Soc.*, **71**, 1553 (1949).
7. G. F. Smith and W. H. McCurdy, Jr., *Anal. Chem.*, **24**, 371 (1952).
8. N. A. Lange, Ed., "Handbook of Chemistry," 8th ed., p. 1082, Handbook Publishers, Inc., Sandusky, Ohio (1952).
9. N. V. Sidgwick, "The Chemical Elements and Their Compounds," Vol. I, p. 133, Oxford University Press, London (1950).
10. G. Bodlander and O. Storbeck, *Z. anorg. Chem.*, **31**, 458 (1902).
11. F. Fenwick, *J. Am. Chem. Soc.*, **48**, 860 (1926).
12. R. Luther, *Z. physik. Chem.*, **36**, 385 (1901).
13. J. Kruger, *This Journal*, **106**, 847 (1959).
14. G. T. Miller, Jr., and K. R. Lawless, *ibid.*, **106**, 854 (1959).

Studies on Cathodic Protection Using the Hull Cell

I. Action of Corrosion Inhibitors

K. S. Rajagopalan and Y. V. P. Ramachandra Row

Central Electrochemical Research Institute, Karaikudi, India

ABSTRACT

A new method of studying inhibitor action is proposed. It is shown that the action of acid inhibitors is changed profoundly under impressed current conditions. The study also reveals that the potential of the cathodically protected metal is not a fixed value as is usually believed but changes in the presence of inhibitor.

Cathodic protection is used in combination with another well-known method of corrosion prevention, viz., addition of corrosion inhibitor, in electrolytic derusting with acid solutions to prevent basis metal attack. It is, therefore, of considerable interest to know how the two methods function in conjunction with each other, in particular, how the current requirement for cathodic protection is influenced by inhibitor action. This aspect has apparently not received adequate attention so far. Preliminary experiments (1) carried out in this Institute have shown that the current requirement for cathodic protection can be conveniently studied by the Hull Cell technique (2, 3) which is so widely used in the study of electrodeposition and that precise information on inhibitor action under impressed current conditions can be obtained by this method. The application of this technique to the study of inhibitor action in sulfuric acid medium is considered here with reference to four commonly used acid inhibitors.

Experimental

Metal.—Mild steel having the following composition was used: C — 0.1 to 0.2%, Mn — 0.4 to 0.5%, P — 0.07 to 0.08%; S — 0.02 to 0.03%. Specimens of 18 gauge sheet steel cut to the size of Hull cathode and provided with a handle at the center were used in the Hull Cell experiments. Specimens of the same mild steel sheet 3 x 1 in. were used in independent experiments to determine weight loss at protection current. The specimens were initially freed of rust and scale, abraded with 120 emery, and degreased with methanol, hot benzene and hot acetone.

Set-up.—The Hull Cell used here (Fig. 1) is a small box of trapezoidal plan in which the cathode is placed at a fixed angle with respect to the anode (3). Both electrodes occupy the full cross section of the cell and the distribution of current density on the cathode for a 267 ml cell is given by the equation C. D. at any point. Amp/dm^2 = I (2.98-5.24 log L/2.54), where I is cell current in amperes and L is distance in centimeters of the point from the high current density end of the cell. The equation applies between the limits 1.3 and 6.4 cm. The dimensions of the Hull Cell are given in Fig. 1.

The cell was fabricated from ¼ in. thick perspex (trade product made from acrylic resin). To facilitate experimentation at elevated temperatures, the cell was placed inside a lead-lined brass bath of slightly greater height than the Hull Cell and both brass bath and the perspex Hull Cell filled with acid solution till acid level was nearly flush with the top of the cell. A lead anode was used.

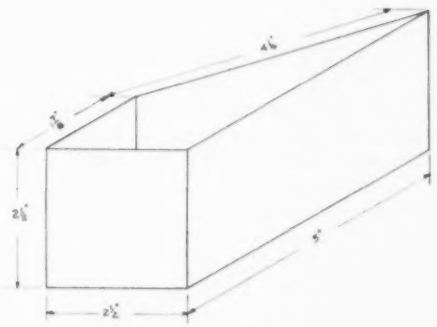

Fig. 1. Hull Cell

Procedure.—Experiments were made at various cell currents. The specimen was introduced into the cell after adjusting the current using a dummy specimen so that current started flowing to the specimen simultaneously with the immersion of the specimen. Immediately after test, the specimen was taken out and quickly reimmersed in a 0.5% NaOH solution followed by rinsing with cold water and drying to prevent attack by the acid after it was disconnected from the cell. The dried specimen was completely etched when the maximum current density obtained on the specimen was insufficient to give protection. An etched as well as a bright, unattacked region was observed when current densities required for complete cathodic protection were obtained in the Hull Cell. The line dividing these two regions were usually quite sharp and reproducible to the extent of less than 3 mm. All the results reported in the paper were obtained under conditions of uniform stirring with a mechanically driven glass stirrer rotating at an approximate speed of 750 rpm.

Results

Effects of temperature and acid concentration on the protection current.[1]—The effects of bath temper-

[1] The current density at which the dividing line is obtained.

Table I. Effects of some experimental variables on protection current.
Duration of test = 30 min

Protection line,** cm	Concentration of acid solution, moles/l	Temp, °C
—	0.5	60
—	0.5	60
6.1	0.5	60
6.1	0.5	60
6.1	0.5	60
5.8	0.5	60
5.8	0.5	60
NE	0.5	30
NE	0.5	40
NE	0.5	50
4.8	0.5	70
NE	0.05	60
E	21	60

** Distance of dividing line from high current density end. NE, no part of the surface got etched. E, completely etched.

ature and acid concentration on the current required for cathodic protection in 0.5 mole/l H_2SO_4 solution were studied in the first instance. The results obtained in replicate experiments for a cell current of 1.5 amp are given in Table I.

The metal remained practically unattacked at lower temperatures than 60°C as shown in Table I. As the temperature was increased beyond 50°C, etched and unattacked regions appeared. The dividing line shifted to higher current density values at 70°C as compared to 60°C. Apparently, at temperatures lower than 60°C the rate of corrosion is so low and the effect of even the lowest cathodic current obtainable on the plate are sufficiently marked to make the etching of the metal surface insignificant; while at 60°C and 70°C the corrosion rate is sufficiently high for etching to appear on unprotected regions within the duration of the test (30 min) for a cell current of 1.5 amp. At 2 M acid concentration the metal was practically completely etched and at 0.5 mole/liter the etched surface was not seen at all. The two regions became visible on the plate only at the intermediate concentrations of 0.5 mole/liter. The values obtained in 0.5 M acid solution at 60°C (see Table I) show that the position of the dividing line between the etched and the unattacked regions is quite reproducible. All the subsequent experiments were carried out at this temperature (60°±2°C).

Table II. Protection currents obtained for different cell currents.
Duration of test = 30 min

No.	Electrolyte	Cell current, amp	Protection line, cm	Current corresponding to protection line (calculated from Eq. [1]) ma/dm²
1	5% H_2SO_4	1.5	6.1	1500
		0.75	3.8	1400
2	5% H_2SO_4 + 0.01% Thiourea	0.75	NE	—
		0.5	6.4	450
		0.25	3.8	550
3	5% H_2SO_4 + 0.01% Gelatine	0.75	4.6	1300
		0.5	2.8	1400

Applicability of the Hull Cell equation.—The applicability of the equation given earlier, which gives the distribution of current density on the cathode, has been studied in several ways. First, the current densities for cathodic protection when different cell currents are employed have been compared. Results are given in Table II.

It is seen from Table II that a fairly good correspondence is observed between the protection currents obtained at different cell currents.

Losses in weight at the protection currents determined by means of independent experiments at similar current densities are given in Table III. It is seen that the corrosion rate is quite high in the absence of current and becomes negligible at the protection current. The protection currents themselves were calculated on the basis of the Hull Cell

Table III. Weight losses in the presence and absence of protection current, electrode potentials, and inhibitor efficiencies of four inhibitors
Duration of test = 30 min

			When protection current is not applied			When protection current is applied		
No.	Inhibitor	Concentration of inhibitor, %	Weight loss, g/dm²	Inhibition* efficiency, %	Electrode potential vs. SCE, v	Protection current, ma/dm²	Weight loss, g/dm²	Potential
1	Nil	—	2.8	—	—0.520	1500	0.017	—0.740
2	Quinoline	0.01	2.6	7	—0.500	800	0.011	—0.500
3	Quinoline	0.05	2.4	14	—0.490	700	—	—0.560
4	Quinoline	0.1	2.2	21	—0.480	500	—	—0.560
5	B-naphthol	0.01	2.6	7	—0.480	1100	0.014	—0.740
6	B-naphthol	0.025	2.3	18	—0.470	700	—	—0.740
7	B-naphthol	0.05	2.5	11	—0.460	500	—	—0.740
8	B-naphthol	0.1	2.3	18	—0.450	400	—	—0.740
9	Thiourea	0.01	0.15	95	—0.500	500	0.020	—0.720
10	Thiourea	0.025	0.07	98	—0.480	500	—	—0.720
11	Thiourea	0.05	0.05	98	—0.460	500	—	—0.720
12	Thiourea	0.1	0.05	98	—0.450	500	—	—0.720
13	Gelatine	0.01	1.2	57	—0.460	1400	0.007	—0.680
14	Gelatine	0.025	0.4	86	—0.440	1300	—	—0.680
15	Gelatine	0.05	0.3	89	—0.430	1000	—	—0.680
16	Gelatine	0.1	0.15	95	—0.430	800	—	—0.680

* Inhibition efficiency is calculated by the formula: $\left\{\frac{\text{Wt loss in the absence of inhibitor} - \text{Wt loss in the presence of inhibitor}}{\text{Wt loss in the absence of inhibitor}}\right\} \times 100$

equation. The results, therefore, suggest that the protection current can be predicted on the basis of the equation with a fair amount of accuracy. It may, however, be argued that a weight loss of 0.007 to 0.02 g/dm²/30 min cannot be strictly considered as representing complete cathodic protection. It is to be noted, however, that the present work relates to conditions which are connected with processes such as pickling operations which normally do not extend beyond 30 min. For this duration, the rate of loss as obtained should be considered very satisfactory. It may be pointed out in this connection that the maximum inhibition by the most efficient inhibitor used corresponds to a weight loss of 0.05 g/dm²/30 min with an inhibition efficiency of 95%. The combined effect of the two methods is appropriately studied keeping in view the highest order of protection obtainable with either method.

The Hull equation was derived from weight of metal deposited in different regions in various plating baths as well as by the direct determination of current distribution on the Hull plate. Measurement of current distribution on the cathode in Hull Cell under the conditions employed in the present study is of interest. This has been carried out using the strip method described by Hull (2). In this method a ¼ in. steel strip with a perspex back and edges painted with several coats of an acid resistant bituminous paint was used as the auxiliary electrode. It has been observed that current densities obtained by this method show fairly good correspondence with those calculated from the equation mentioned earlier in the region 1.3 to 6.4 cm from the high current density end of the cathode. At greater distances the measured values fall much more slowly than the equation would give. It may be noted in this connection that most of the measurements reported are confined to the region of 6.4 cm.

Protection current in relation to concentration of inhibitor.—The protection current at four concentrations of each of the four inhibitors considered, viz., B-napthol, quinoline, gelatine, and thiourea, are plotted against concentration in Fig. 2. It is seen from the figure that valuable information regarding the behavior of the inhibitors is given by this method. The effect of gelatine increases with concentration and does not reach a maximum value even at 0.1%. As compared to this, quinoline and thiourea make themselves more or less completely felt at the lowest concentration (0.01%), and further changes in concentration do not increase their effectiveness. These are also more effective than gelatine at all concentrations. In the case of B-naphthol, increase in concentration of inhibitor has a profound effect on the requirement of current and it reduces the current requirement more than quinoline and thiourea at 0.1%, although it is less effective than quinoline or thiourea at 0.01%.

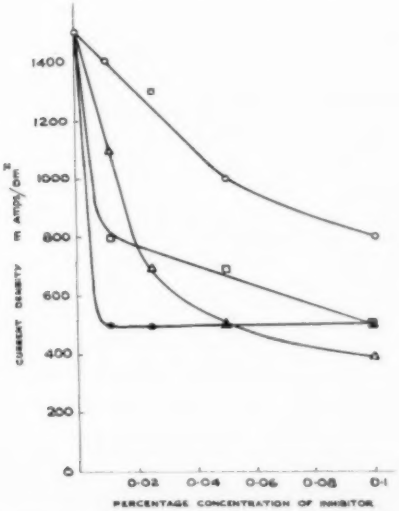

Fig. 2. Protection current vs. concentration of inhibitor. □ quinoline; △ B-napthol; ● thiourea; ○ gelatine.

Inhibition efficiences of the 4 inhibitors.—The inhibition efficiency of the four inhibitors are given in Table III in terms of weight loss data with and without inhibitor when no cathodic current is applied. It is seen from Table III that the efficiency of inhibition of the different inhibitors is in the order thiourea > gelatine > B-naphthol, quinoline. The inhibition efficiency of gelatine increases with concentration, and it becomes nearly as efficient as thiourea at 0.1%. Both B-naphthol and quinoline inhibit poorly at all concentrations. As compared to this, the effectiveness of the different inhibitors in reducing the current required for cathodic protection is in the order thiourea > quinoline > B-naphthol > gelatine at 0.01%. It may be mentioned in this connection that, although quinoline and B-naphthol inhibit poorly at 60°C (the temperature at which all the present experiments have been carried out), they inhibit to a greater extent of 25°C.[2] The loss in the inhibitive action of quinoline at elevated temperatures has been noticed by other workers also (4).

Electrode potentials at currents corresponding to protection currents.—The potentials were measured using an electronic millivoltmeter and saturated calomel electrode as the reference electrode. All the potential measurements were made in independent experiments at the protection current densities found by Hull Cell experiments. Potential data are given in Table III. It is seen that the potential corresponding to the protection current is not a constant value and varies with each system, but it remains the same for the same system at all concentrations though the protection current varies. The potentials before current is applied, however, vary with concentration of inhibitor.

The mechanism of cathodic protection as well as inhibitor action has been very satisfactorily interpreted in terms of the Evans diagram (5, 6). In the former case, cathodic protection is believed to have been attained when the metal is cathodically polarized to the open-circuit potential of the local anodes. In the latter case, the inhibitor increases either the anodic or cathodic polarization behavior

[2] It is necessary to draw the reader's attention here to the inhibition efficiency value given in ref. (1). This was obtained in experiment at room temperature as it was not expected that the extent of inhibition would change markedly with temperature. Our main interest at that stage was to bring out the reversal of the order under impressed current conditions.

of the local cells and brings about reduction in the corrosion rate. Both anodic and cathodic polarization behavior can also be influenced simultaneously. The direction in which the over-all potential will shift as a result of inhibitor action has been succinctly dealt with by Mears (7) as well as Hoar (8). In the present case, when no current is applied, the potential shift in all cases is in the nobler direction. Maximum shift is given by gelatine at 0.1% when the metal is 90 mv more positive than in uninhibited solution. This should indicate that all the inhibitors polarize the metal surface anodically and that this effect increases with concentration of inhibitor. On the other hand, the fact that all the inhibitors considered here reduce the current required for cathodic protection suggests that in the presence of inhibitor the metal is more cathodically polarized. It is further noticed that in the case of gelatine and quinoline the potential at which complete cathodic protection is obtained differs from that of uninhibited acid solution. It is reduced by 180 mv in the case of quinoline and 60 mv in the case of gelatine. Thus, it would appear that the action of corrosion inhibitors is a complex phenomenon in which not only increased anodic and cathodic polarization are involved but also a reduction in the potential requirement. Let us now consider the inhibition efficiencies of the different inhibitors given in Table III. Thiourea shows very high inhibition efficiency in the absence of current. This is observed even at the lowest concentration of the inhibitor employed.

The protection current is minimum in this case at 0.01% and there is no change of the protection current with concentration of inhibitor. The potential corresponding to satisfactory cathodic protection is the same as that of acid solution without inhibitor. It would, therefore, appear that thiourea increases the anodic and cathodic polarization characteristics of the metal surface considerably on addition and that this brings about the high inhibition efficiency in the absence of current as well as the lowering of the protection current in the experiments on cathodic protection. In the case of gelatine, the inhibition efficiency increases with concentration; so also the lowering of the protection current increases with concentration. The potential data indicate that the potential at which cathodic protection is obtained is lowered. So gelatine may be said to give cathodic protection and inhibition by lowering the potential requirement and by increasing the anodic and cathodic polarization characteristics of the metal surface and that these are a function of inhibitor concentration. B-naphthol and quinoline cause considerable lowering of the protection current at all concentrations although they give very poor inhibition in the absence of current. This suggests that these inhibitors become effective only in the presence of cathodic current. The conclusions drawn by Mann (9) and others (10) based on over voltage measurements and the theory put forward by Warner (11) that N-type inhibitors which can form quaternary ammonium ions can be adsorbed at cathodic areas when the metal is operating as cathode appears to have some validity in the light of the results obtained with quinoline and B-naphthol. The action of the inhibitors is seen only when cathodic current is applied. This should mean that these two inhibitors are adsorbed on the metal surface only at more negative potentials than the corrosion potential of steel in sulfuric acid [cf. (13)]. Quinoline apparently reduces the current requirement by lowering the potential requirement and B-naphthol by increasing cathodic polarization.

The factors determining the current required for complete cathodic protection have been the subject of a number of important studies. On the basis of practical experience it is believed that, if a steel structure is maintained at a potential of −0.77 v vs. saturated calomel electrode, it will be completely protected. This criterion has been widely used. Our study shows that even in the same electrolyte the presence of small quantities of inhibitors can bring about very substantial changes in the potential at which protection is obtained and that this change takes place to different extents in the case of the different inhibitors. It is, however, a constant value for each system. The theoretical studies of Wagner (12) appear to show that under certain conditions assumed by him the criterion for cathodic protection can be stated without recourse to Evans' diagram and that the current required for cathodic protection can be worked out on the basis of lowering the metal potential to a value 0.2 v more negative than the standard single electrode potential of the metal. The present work indicates that from a practical point of view much greater caution has to be exercised in using particular potential values as criteria for cathodic protection.

Acknowledgment

The authors gladly acknowledge the kind help and encouragement given by Professor K. S. G. Doss, Director, Central Electrochemical Research Institute.

Manuscript received Aug. 14, 1959.

Any discussion of this paper will appear in a Discussion Section to be published in the December 1960 JOURNAL.

REFERENCES

1. K. S. Rajagopalan and Y. V. P. Ramachandra Row, *Naturwissenschaften*, **46**, 319 (1959).
2. R. O. Hull, *Proc. Am. Electroplaters' Soc.*, **1939**, 52.
3. J. W. Cuthbertson, *Metal Ind.*, **79**, 87 (1951).
4. N. D. Rusyanova and N. V. Hoftmann, *J. Appl. Chem., USSR* (English Translation) **30**, 1630 (1957).
5. R. B. Mears and R. H. Brown, *Trans. Electrochem. Soc.*, **74**, 519 (1938).
6. T. P. Hoar, *J. Electrodepositor's Tech. Soc.*, **14**, 33 (1937).
7. R. B. Mears and R. H. Brown, *This Journal*, **97**, 75 (1950).
8. T. P. Hoar, Proc. International Cong. Surface Activity, Part III, Butterworths Scientific Publications, 81 (1957).
9. C. A. Mann, *Trans. Electrochem. Soc.*, **69**, 115 (1936).
10. J. O. M. Bockris and B. E. Conway, *J. Phys. Chem.*, **53**, 527 (1949).
11. J. C. Warner, *Trans. Electrochem. Soc.*, **55**, 287 (1929).
12. C. Wagner, *This Journal*, **99** (1952); **104**, 631 (1957).
13. L. I. Antropo, *J. Indian Chem. Soc.*, **35**, 309 (1958).

Particle Separations by Nonuniform Electric Fields in Liquid Dielectrics, Batch Methods

Herbert A. Pohl and James P. Schwar[1]

Plastics Laboratory, Princeton University, Princeton, New Jersey

ABSTRACT

The motion of suspended solids in nonuniform electric fields in liquid dielectrics is called dielectrophoresis. Some of the quantitative aspects of dielectrophoretic behavior of solids is reported herein. The yield of precipitated solids is seen to rise with applied voltage in cells of cylindrical geometry, until a critical or "sluff-off" voltage is reached. The yield is seen to decrease with increase of volume fraction of suspended solids in the range of 1 to 50% v/v. The yield depends on voltage gradient, applied potential, cell dimensions, and relative dielectric constants of solid and liquid. In particles of given size, yield is observed to be directly dependent on the dielectric constant. Moisture is shown to have a small but demonstrable effect. As expected, the amount and character of dielectrophoretic behavior is observed to be independent of the direction of the field applied.

Current flow during the process was observed to range up to about 20 $\mu\mu$a, and to indicate that a new method of conduction takes place with the particles present. It is suggested that this is due to ionic charging of the particles by usual current flow in the liquid dielectric, with the particles then aiding current flow and energy consumption (dielectric loss) by rotating.

The motion of suspended solids caused by nonuniform electric fields is called "dielectrophoresis" (1-3). The most polar material moves toward the place of greatest field intensity. Unlike electrophoresis, this does not require charged particles. Instead, it depends on the force felt by all polar material when in a nonuniform field. It may be described as arising from the unequal pulls exerted by the forward and backward direction of the electric field on the dipole produced in the particle by the field. Reversal of the field produces no change in the direction of the pull on isotropically polarizable particles.

Prior work on the more quantitative experimental aspects has shown that the field strength, electrode size, cell size, and particle size are important parameters affecting the yield of material held by the central electrode in a cell of cylindrical geometry. Field strength, electrode size, and particle size show criticality. At certain upper limiting voltages, small central electrode diameters, and small particle sizes, all precipitation appears to be prohibited. The work described here is a continued study of other such factors. The effects of varied dielectric constant of the powder, of the dryness of the system, of the polarity, and of the powder concentration are reported.

The apparatus and handling methods used in this study are essentially those as reported earlier.

Effect of Dielectric Constant of the Powder

As shown in the simplified theory (1, 2), the effect should be proportional to the difference in the dielectric constants of the liquid dielectric and the solid.

The following experiment was done in the apparatus previously described (3) with three powdered substances of differing polarizabilities. The dielectric constants of solid ammonium chloride, polyvinyl chloride (PVC), and sulfur are: 7.0, 4.6, and 3.67. The dielectric constant of the liquid dielectric, composed of carbon tetrachloride-benzene mixtures chosen to be equal in density to the solid in use, is approximately 2.26. In agreement with expectation, the amount of ammonium chloride precipitated in a given time at voltages below the critical voltage is found to well exceed that of the polyvinyl chloride or the sulfur. The amount of PVC pulled out in turn exceeds that of the sulfur. Data were obtained on particles of the same average particle size, namely, 163 μ (see Fig. 1 for details).

The critical voltage, i.e., the voltage at which the particles appeared to be no longer held by the central electrode, was observed to increase with increasing dielectric constant of the powder. That for NH_4Cl was 7.6 kv, that for PVC was 7.0 kv, that for sulfur was 5.2 kv under the following experi-

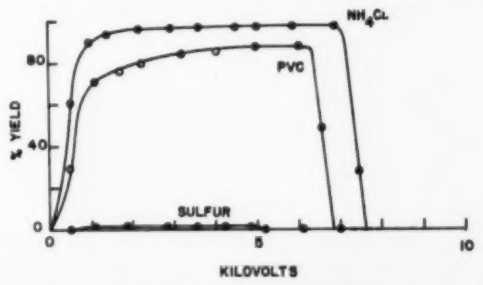

Fig. 1. Effect of varied dielectric constant of the solid powder on the precipitation yield during dielectrophoresis.

[1] Present address: Division of Engineering, Texas College of Arts and Industries, Kingsville, Texas.

mental conditions: powder suspended in CCl_4-benzene mixtures; alternating voltage used, reported as RMS: 60 cps; central wire diameter, 0.794 mm, Teflon coated to a thickness of 5 mils; test duration, 180 sec of flow at 12.5 ml/sec of feed liquid suspension: outer cell electrode diameter, 9.8 mm, ID.

Effect of Electrode Polarity

Data were obtained for the yield of PVC precipitated vs. the applied voltage in static fields, in which the polarity of the electrodes were reversed. The data of Table I show that while the central electrode is positive and the outer electrode negative the precipitation yield is identical to within experimental error with the condition of having the same but inverse voltage on the electrodes. This is in conformity with the view that the phenomenon is not electrophoresis, but is dielectrophoresis. Corona effects about the central electrode are thought to be present, especially at higher applied voltages, for when the field is suddenly reversed at very high voltages, the particles clinging to the central electrode suddenly are rapidly repelled to the cell wall. They will remain there for a time until the charge accumulated on the particles by their imbedment in the "corona region" about the central electrode leaks away. The particles then eventually migrate back toward the central electrode if the reverse voltage is maintained.

Effects of the Presence of Moisture

In an effort to find a factor effective in the behavior of the dielectrophoretic precipitations, the effect of careful drying was studied. The powdered material, in this case, polyvinyl chloride seived to pass 100 mesh, and stop on 140 U.S. mesh screen (nominal 127 μ average particle diameter), was used "as is" after long storage at room humidity, and after drying 24 hr at 105°C. The liquid dielectric, a mixture of CCl_4 and benzene, both of reagent grade, having the same density as the freshly wet powder, was used as received from the supplier, and also after drying over anhydrous $CaCl_2$ for one week. The precipitation yield was observed to be slightly higher (about 2% change in relative values) for the less dry materials. Perhaps this can be attributed to the slight changes in the dielectric constant of the liquid due to the water (see Fig. 2 for details). The critical cut-off voltage for the precipitation was rather higher in the case of the dry materials. This is probably due in part at least to the decreased conductivity of the liquid dielectric. Increased conductivity permits a higher rate of conductive counter-polarization of the particles, thus accelerating sluff-off. Numerically the critical voltages observed were: dry-8.6 kv; wet-7.9 kv.

Table I. Effect of field direction on the yield during dielectrophoresis

Data on particles of polyvinyl chloride of 126μ average particle diameter, suspended in CCl_4:C_6H_6 mixture of closely equivalent density between cylindrical electrodes, outer electrode, inner electrode, liquid velocity and test duration were as in the previous experiment.

Voltage	% Yield (central electrode positive)
500	20.4
1100	64.5
1900	70.1
2700	75.2
3400	78.6
3900	80.6
4600	82.6
5500	83.8
6400	83.8
6900	85.0
7800	24.7
Voltage	**% Yield (central electrode negative)**
500	19.6
1150	62.8
1900	69.4
2800	73.8
3600	77.2
4600	82.2
5500	83.5
6600	83.5
7800	23.9

Effects of Varied Particle Concentration

It is observed that, as the concentration of the solid suspended in the liquid dielectric increased, the yield of solid precipitated in a given time decreases. The experiments showing this were carried out in a cylindrical electrode cell of 9.8 mm ID, using a central wire electrode of 0.794 mm wire that was coated with 5 mil thick layer of Teflon. Polyvinyl chloride powder of spherical shapes, of nominal 127 μ average diameter, as in the above experiment, was used, at various concentrations in mixtures of CCl_4 and benzene adjusted to have similar density. The liquid velocity during the flow period of filling and draining was 12.5 ml/sec; the potential across the cell fixed at 2000 v. The test duration was 180 sec. The yield of powder collected at very low volume fraction (0.047) was 79% and fell smoothly with increase of volume fraction of powder to zero % yield at an extrapolated 51% volume fraction of powder, as the data in Fig. 3 show.

Current Flow during Dielectrophoresis

Preliminary measurements of the current flow taking place during the dielectrophoresis showed that breaks in the current vs. voltage curve occurred at points corresponding to obvious changes in the yield per cent vs. voltage curve. The current flow was observed to be greater with increased concentrations of powder, and to be greater with increase of particle size. Typical results obtained are shown in Table II and in Fig. 4. The data selected

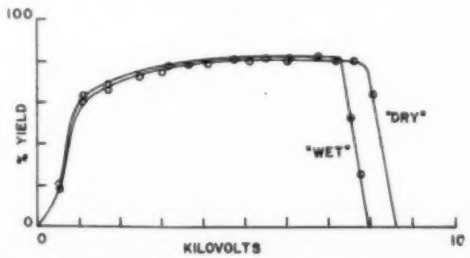

Fig. 2. Effects of moisture on the precipitation yield of polyvinyl chloride spheres during electrophoresis.

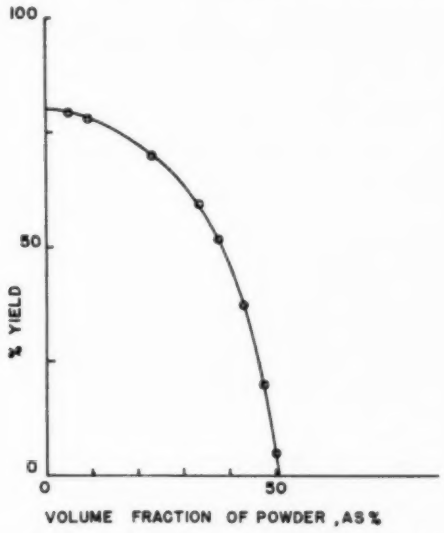

Fig. 3. Effects of powder concentrations on precipitation yield during dielectrophoresis.

Table II. Preliminary data on current flow as affected by concentration and particle size during dielectrophoresis

Particle size Mesh range	Nominal average particle diameter, μ	Current, $\mu\mu a$	Precipitate collected, as % of total	Volume fraction of powder in original suspension
−60, +80	213	2.0	60	0.091
−100, +140	127	1.06	81	0.091
−100, +140	127	2.7	68	0.250

for 2000-v potential across the cell in Table II do not show the break in the current-voltage curves observed but indicate the magnitudes of the currents and the relative changes observed on changing the particle size or concentration.

The data in Table II was obtained using a Kiethley electrometer across a high resistance in series with the cell and voltage supply circuit.

The greater conductivity of powder suspensions of larger particle size coincides with the observed lower critical voltage for sluff-off of the precipitated powder in those cases. The latter phenomenon is believed to be related to the current flow during dielectrophoresis, that current viewed as producing counter-polarization on the particles opposing the dielectrophoretic action. This effect—of current increasing with the particle size—and the observed direct dependence of the current on the

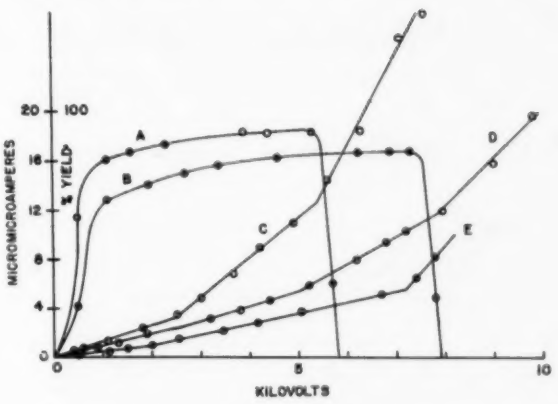

Fig. 4. Deposition and electric current characteristics during dielectrophoresis. Curve A: precipitation yield for PVC of 213 μ average particle diameter at 0.091 volume fraction in liquid dielectric. Curve B: precipitation yield for PVC of 127 μ average particle diameter at 0.091 volume fraction in liquid dielectric. Curve C: current flow during dielectrophoresis of 127 μ average particle diameter PVC at 0.25 volume fraction in liquid dielectric. Curve D: current flow during dielectrophoresis of 213 μ average particle diameter PVC at 0.091 volume fraction in liquid dielectric. Curve E: current flow during dielectrophoresis of 127 μ average particle diameter PVC at 0.091 volume fraction in liquid dielectric. Conditions: PVC powder suspended in CCl_4-benzene mixture of closely similar density; liquid velocity 12.5 ml/min; cell ID, 9.8 mm; wire electrode 0.794 mm and coated with 5 mils of Teflon; ***static field.***

particle concentration lend support to the view that a new method of current carrying is taking place. As suggested in an earlier paper (3), current flow through the liquid dielectric deposits ions on the suspended particles. A rotation of the particles, started, say, by Brownian motion, now acts to carry current across the volume occupied by the particles. This additional current carrying ability of the suspension is believed to be contributing here.

Manuscript received Sept. 23, 1959. This paper was prepared for delivery before the Philadelphia Meeting, May 3-7, 1959. A portion of the research reported in this paper was sponsored jointly by the Army Signal Corps and Office of Naval Research under Signal Corps Contract No. DA-039 sc-70154 and O.N.R. 356-375.

Any discussion of this paper will appear in a Discussion Section to be published in the December 1960 JOURNAL.

REFERENCES

1. H. A. Pohl, *J. Appl. Phys.*, **22**, 869 (1951).
2. H. A. Pohl, *ibid.*, **29**, 1182 (1958).
3. H. A. Pohl and J. P. Schwar, *ibid.*, **30**, 69 (1959).

Nonuniform Field Effects in Poorly Conducting Media

Herbert A. Pohl

Plastics Laboratory, School of Engineering, Princeton University, Princeton, New Jersey

ABSTRACT

A simplified theory of the behavior of suspended polymer particles in a real liquid dielectric is presented. It is becoming well known that nonuniform fields exert an attractive force of interesting magnitude on particles of high dielectric constant suspended in a liquid medium of lower dielectric constant. In a real dielectric there is an appreciable effect due to the very small currents (10^{-8} amp at kilovolts applied) which even good liquid insulators support.

It is shown that, in a real dielectric, the initial attraction to the central electrode felt by all particles due to the nonuniform field and its polarizing induction is gradually overcome by the repulsive effects of charge accumulated on the particles due to ionic conduction in the liquid. The "reversal time" for the particle motion is calculated and shown to be reasonable.

The ability of nonuniform electric fields to produce desirable separations of materials of differing dielectric constant is now well recognized. It is the purpose of this paper to help establish some of the more quantitative features of the phenomenon. Mueller (1), Pohl (2-4), and Loesche and Hultschig (5) independently examined the theory of the size and direction of the action of nonuniform fields on mixed dielectrics. Mueller concluded from his excellent analysis that the effects would not be appreciable for particles of molecular size. Loesche and Hultschig also concluded this from their theoretical and experimental study. However, it has been shown (2-4) that the action of nonuniform fields on macroscopic particles is indeed appreciable and can be used for certain separations. Debye (6-9) concluded from theoretical considerations that grading of macromolecules, such as high polymers, should be possible by this technique.

As defined earlier (2) "dielectrophoresis" is the motion of matter caused by polarization effects in a nonuniform electric field. Other effects interfere, such as conduction, thermal convection, diffusion, and the over-all effect of the sequence: charging (whether by electrode, particle, or ion contact) and followed by electrostatic repulsion. As expected, in dielectrophoresis the most polar material moves toward the region of greatest field intensity. However, all materials conduct. In this sense a theory developed on the assumption of no current flow in the electrical system, although helpful, is too simple. As a first step in considering the effects of conduction, the following rather elementary considerations are presented with no guarantee of having more than suggestive merit.

We may assume the particle to be in equilibrium with the various forces on it in a real dielectric

$$F_e + F_1 + F_d + F_v = 0$$

where F_e is the dielectrophoretic force, F_1 the force due to conduction-produced charge, F_d diffusional or osmotic force, and F_v = viscous drag force.

Dielectrophoretic force, F_e.—As shown in a prior paper (3), the dielectrophoretic force on a spherical particle in an electric field with uniform properties (i.e., "corona" effects absent) and cylindrical symmetry is

$$F_e = -4\pi a^3 \epsilon_0 K_1' \cdot \frac{(K_2'-K_1')\,V_1^2}{(K_2'+2K_1')\,r^3\left(\ln\frac{r_1}{r_2}\right)^2} \cdot r^0$$

$$= -4\pi \frac{a^3 \epsilon_0 K_1'(K_2'-K_1')}{r^3\ (K_2'+2K_1')} \cdot E_1^2 r_1^2 r^0$$

where ϵ_0 is permitivity of free space, r_2 the radius of outer, grounded cylinder, r_1 the radius of inner cylinder at potential V_1, r the distance of particle center from the axis, a the radius of particle, K_1' the relative dielectric constant of liquid medium, K_2' the relative dielectric constant of particles, r^0 the unit radius vector, V, V_1 the potential at r and r_1, respectively, and E, E_1 the field at r and r_1, respectively.

The negative sign indicates that the motion due to this force will be toward the axis. The motion will be strictly radial.

For present purposes we may gather all terms except those of immediate interest into a single constant, k_e,

$$F_e = \frac{-k_e a^3 V_1^2}{r^3\left(\ln\frac{r_1}{r_2}\right)^2} r^0$$

where

$$k_e = 4\pi\epsilon_0 K_1' \frac{(K_2'-K_1')}{K_2' + 2K_1'}$$

Electrostatic force, F_1, on current-induced dipoles.—The force on a particle carrying free electric charges in an electric field, E, is

$$F_1 = Q \cdot E$$

where Q is the free charge.

In a field of cylindrical symmetry it may be shown that

$$V = V_1 \ln\left(\frac{r}{r_2}\right) \Big/ \ln\left(\frac{r_1}{r_2}\right)$$

and

$$E = -\nabla V = -r^0 V_1 \Big/ \ln\left(\frac{r_1}{r_2}\right) \cdot \frac{1}{r} = E_1 \frac{r_1}{r}$$

The charge Q, accumulated by the particles during their life in the liquid and between discharging contacts with the outer electrode will be assumed to be proportional to their cross-sectional area and to the current density. The current in the real dielectric will be assumed due to ionic conduction in the liquid and to charge transfer between particles. It is assumed that voltage gradients sufficient to strip off electrons from the particles by field effects do not act here.

Consider the forces which arise on a particle sitting at rest in a field in which an ionic current flows. Let the particle be an insulator similar (but not necessarily identical) in dielectric constant and conductivity to the liquid medium. The motions of the ions in solution due to thermal motion and electrical forces cause them to diffuse through the liquid and, in particular, to collide with the particles of interest here. These ions generally adhere to the particles because of attractive electrical image forces. These forces arise as soon as the ion comes rather close to the particle. We may expect a high fraction of approaching ions to adhere until such time as the accumulated electric charge on the particle gives rise to a repelling field. The presence of the initial polarization on the particle gives rise to an initially attractive field for the approaching ions. This *induced* "surface" charge will make the surface field on the particle attractive to the ions until neutralized. Only then will the surface charge begin to be repellent to the oncoming ions. Our calculations from this point on largely concern themselves only with the period of ion-carried surface charging of the particle up to the point of neutralizing the induced surface charge, i.e., where no repulsion exists. Hence, we may assume for the present that all oncoming ions are picked up and held by the particle. Ionic current will then deposit equal numbers of positive and negative charge on opposite faces of the particle.

The charge density, q, will be proportional to the current density, j, to the time, t, of deposition; and to the projected area, $d\sigma$, of the area segment dA under consideration at P.

$$q = jt \frac{d\sigma}{dA}$$

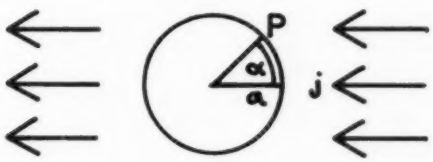

Now $\frac{d\sigma}{dA} = \cos\alpha$

therefore

$$q = j_1 t \cos\alpha - j_2 t \cos\alpha$$

where j_1 is the current in the liquid dielectric, j_2 is the current in the particle itself; therefore, $q_{net} = (j_1 - j_2)t \cos\alpha$.

the moment, $d\mu$, of that charge at P is

$$d\mu = 1 \cdot q \cdot dA$$

where $1 = a \cos\alpha$ = lever arm of moment. The total moment of the charged sphere is

$$\mu = \int_A lqdA$$

$$= \int_0^\pi (a\cos\alpha)(jt\cos\alpha)(2\pi a^2 \sin\alpha\, d\alpha)$$

$$= \frac{4\pi}{3} a^3 jt = jt \cdot (\text{volume})$$

Note that the moment turns out to be the volume of the particle times the total positive charge deposited.

This is also true for particles of other shapes. For example, consider a particle of nearly cubic shape, actually a particle of the shape of a sector of a cylindrical annulus sitting at an average distance, r, from the axis of the cylindrical electrode system. Let it have a length of side $2a$ in the radial direction, a length $2a$ in the cylindrical axis direction, and a median arc length also of $2a$ along the circumference of the imaginary cylinder axial to the electrode axis and passing through r. It may be shown that the moment is

$$\mu = 8a^3 jt = jt \cdot (\text{volume})$$

where $8a^3$ is the volume of the nearly cubical particle if $a << r$.

The translational force on a dipole in a nonuniform field is

$$F_j = \mu \cos\theta \cdot \nabla|E|$$

where θ is the angle the dipole makes with the impressed field. Here, $\theta = \pi$ $\cos\theta = -1$.

$$\nabla|E| = \nabla \left| \frac{E_1 r_1}{r} \right|$$

in a field of radial symmetry for

$$E = \frac{E_1 r_1}{r}$$

where E_1 is the field intensity at a distance r_1 hence

$$\nabla|E| = \frac{\partial}{\partial r} \frac{E_1 r_1}{r} = \frac{-E_1 r_1}{r^2}$$

and

$$F_j = \mu \frac{E_1 r_1}{r^2}$$

For a spherical particle laden with charge due to the current flow

$$F_j = \frac{4\pi}{3} a^3 jt \frac{E_1 r_1}{r^2}$$

As the current density, j_0, in an ohmic cylindrically symmetrical field is

$$(j_1 - j_2)_{r=r_0} = j_0 = \frac{E_0}{\rho_1} - \frac{E_0}{\rho_2} = \frac{E_1 r_1}{r_0} \cdot \frac{\rho_2 - \rho_1}{\rho_1 \cdot \rho_2}$$

where ρ_1 and ρ_2 are the specific resistivities of the liquid and the particle, respectively.

At the surface of a spherical particle of dielectric constant K_2' in a medium of dielectric constant K_1' the field E_{1s} is

$$E_{1s} = \frac{3K_1'}{K_2'+2K_1'} \cdot E_0$$

where E_0 is the field strength in the liquid, far from the particle.

The above relation, strictly speaking, applies only at the onset of current arrival. As the net polarization of the surface drops to zero (the conductance delivered charge equals the field induced polarization charge)

$$E_{1s} = E_0$$

However for $K_2' = 5$, $K_1' = 2$, as for representative pairs of materials,

$$\frac{3K_1'}{K_2'+2K_1'} = \frac{2}{3}$$

hence the variation of field at the surface during charging is not great in such cases. For later mathematical simplicity we choose to set

$$j = \frac{E_{1s}}{\rho} = \frac{3K_1'}{K_2'+2K_1'}\frac{E_0}{\rho}$$

where ρ is the specific resistivity. Hence

$$F_e = 4\pi a^2 t \cdot \frac{E_1^2 r_1^2}{r^2} \cdot \frac{K_1'}{K_2'+2K_1'} \cdot \left(\frac{\rho_2-\rho_1}{\rho_1\rho_2}\right)$$

Diffusional or osmotic force, F_d.—The osmotic pressure, Π, due to a set of suspended particles of concentration, n, per cc is

$\Pi = nkT$ [Van't Hoff equation (10)]

where k is Boltzmann constant and T is absolute temperature.

The pressure gradient along the r direction among the particles of varied concentration is

$$\frac{\partial \Pi}{\partial r} = kT\frac{\partial n}{\partial r} = \text{force per unit volume of particles.}$$

This pressure gradient or directed force per particle due to concentration gradient is then F_d, where

$$F_d = \frac{1}{n}\frac{\partial \Pi}{\partial r} = \frac{kT}{n} \cdot \frac{\partial n}{\partial r}$$

We may compare the magnitudes of the two forces as follows:

$$F_d = kT\,\Delta n/n \cdot 1/\Delta r$$

Now $\Delta n/n$ is the fractional change in concentration along r for any volume under consideration. The maximum relative change possible is unity (presence vs. absence of particles). The minimum change in radial distance having meaning can be considered to be equal to the diameter, $2a$, of the particle. Then

$$F_{d(max)} = \frac{kT}{2a}$$

For $a = 1\ \mu$, $T = 300°K$, $k = 1.38 \times 10^{-16}$ $\frac{\text{erg}}{(\text{deg.})(\text{molec.})}$

$F_{d(max)} = 2.07 \times 10^{-10}$ dynes per particle

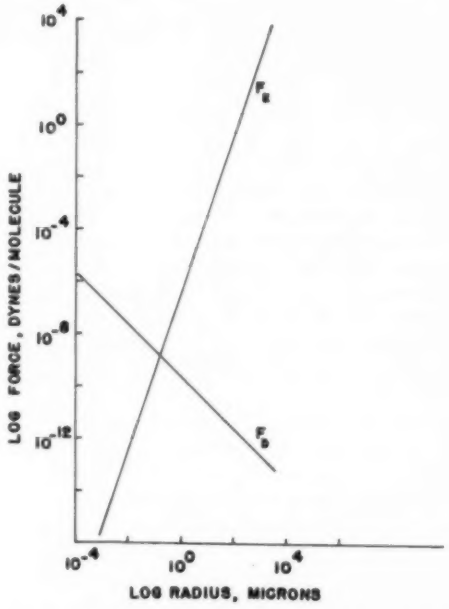

Fig. 1. Comparison of diffusional (osmotic) and dielectrophoretic forces for particles of various radii.

Values for other radii can be ascertained from Fig. 1.

An example of the magnitude of the force on a particle due to a cylindrically symmetrical electric field follows:

$$F_e = \frac{-4\pi a^3 \epsilon_0 K_1'(K_2'-K_1')E_1^2 r_1^2}{r^3(K_2'+2K_1')}$$

For

r = 1 mm = 10^{-3}m = distance from axis

r_1 = 0.5 mm = 5×10^{-4}m = radius of central electrode

r_2 = 5 mm = 5×10^{-3}m = radius of outer electrode

V_1 = 3000 v (outer electrode grounded)

$|E| = \frac{-V_1}{r \ln(r_1/r_2)} = 1.30 \times 10^6$ v/meter

ϵ_0 = 8.85×10^{-12} coul/(volt)(meter) = permittivity of space

a = $1\mu = 10^{-6}$m

K_2' = 5

K_1' = 2

$F_e = 3.15 \times 10^{-12}\left[\frac{\text{coulomb volts}}{\text{meter}} = \text{newtons}\right]$

$= 3.15 \times 10^{-7}$ dynes

which is much larger than the maximum osmotic force on this particle (2.07×10^{-10} dynes).

Values for other particle radii under these electrical conditions can be ascertained from Fig. 1.

For particles of over 1μ diameter this force may be shown to be negligible in comparison with the electrical ones.

Viscous drag.—For spherical particles one may use Stokes' law to find the force, F_η, required to keep spherical particles moving at a velocity, v, in a medium of viscosity, η.

$$F\eta = 6\pi a\eta v = 6\pi a\eta \, dr/dt$$

Particle path in nonuniform fields in real dielectrics.—It is reasonable, as said earlier, to assume that the particle is in effective equilibrium with the various forces on it, i.e.

$$F_e + F_j + F_d + F_\eta = 0$$

Combining equations for these values as given earlier, we find

$$\frac{-k_e a^2 V_1^2 r^6}{r^3\left(\ln\frac{r_1}{r_2}\right)^2}\,\frac{-V_1 r'' \dfrac{j_1 a^2 r_1}{r}\displaystyle\int_0^t \frac{dt}{r(t)}}{\ln\left(\frac{r_1}{r_2}\right)} + \frac{kT}{n}\cdot\frac{\partial n}{\partial r} + 6\pi a\eta\frac{dr}{dt} = 0$$

Deposition and dispersion of spherical particles in a cylindrical electrode cell in which ionic current flows.—For purpose of the present simplified calculations we neglect osmotic forces for particles over 1 μ size. We return then to our assumption of equilibrium among the dielectrophoretic, electrostatic, and viscous drag forces.

$$F_e + F_j = F_\eta = 6\pi a\eta v$$

or

$$6\pi a\eta v = -4\pi\epsilon_0 K_1'\frac{(K_2'-K_1')a^3}{(K_2'+2K_1')r^3}(E_1 r_1)^2 + \frac{4\pi a^3 t(E_1 r_1)^2(K_1')}{r^3(K_2'+2K_1')}\cdot\frac{\rho_2-\rho_1}{\rho_1\rho_2}$$

solving for $v = \dfrac{dr}{dt}$

$$\frac{dr}{dt} = v = \frac{(E_1 r_1)^2 a^2 K_1'\cdot 2}{3\eta(K_2'+2K_1')r^3}\left[-\epsilon_0(K_2'-K_1') + \frac{t\,(\rho_2-\rho_1)}{\rho_1\rho_2}\right]$$

collecting terms in r and t and integrating gives

$$v = \frac{-a^2 A}{r^3} + \frac{a^2 Bt}{r^3}\cdot\frac{\rho_2-\rho_1}{\rho_1\rho_2}$$

$$r^4 - r_0^4 = -4a^2 At + \frac{2a^2 Bt^2}{\rho_1\rho_2}(\rho_2-\rho_1)$$

where r_0 is initial radial distance of particle from axis of cylindrical electrodes, r the "final" radial distance after time, t,

$$A = \frac{2}{3}\frac{(E_1 r_1)^2 K_1'\epsilon_0(K_2'-K_1')}{\eta(K_2'+2K_1')}$$

$$B = \frac{2}{3}\frac{(E_1 r_1)^2 K_1'}{\eta(K_2'+2K_1')}$$

The variation of $r^4 - r_0^4$, a measure of the particle excursion, is seen to be parabolic with time. The furthest inward excursion for a particle is $r_0 - r_1$, which occurs, say, at $t = t_1$.

At $t = t_2 = 2t_1$, the particle originally at r_0 will have drifted out again to r_0. This is because of the eventual overcoming of the attractive dielectrophoretic force, F_e, by the growing repulsive force F_j due to ionic charging of the particle.

After $t = t_2$, the particles will be further out than at the start of the experiment.

At $t = t_1$, the velocity of the particles due to all forces is zero. We may term this "sluff-off time."

$$t_1 = \frac{A}{B}\frac{\rho_1\rho_2}{(\rho_2-\rho_1)} = \epsilon_0\frac{\rho_1\rho_2}{\rho_2-\rho_1}(K_2'-K_1')$$

(therefore the sluff-off time, t_1, is independent of voltage but is directly dependent on the resistance of solution)

$$t_2 = \frac{2A\rho\rho'}{B(\rho'-\rho)}$$

and

$$r_{0\max}^4 = r_1^4 + \frac{2a^2A^2}{B}\left(\frac{\rho_1\rho_2}{\rho_2-\rho_1}\right)$$

good up to $r_{0\max} = r_2$ for conducting particles

In the absence of corona-type effects, the sluff-off time, t_1 is of course expected to be independent of the applied voltage for the dielectrophoretic forces due to initial polarization and current-induced polarization depend in the same way on the voltage.

The maximum "yield" or fraction of the tube contents swept out is

$$y_{max} = \frac{\text{volume swept out}}{\text{total volume available}} = \frac{\text{amount of powder deposited}}{\text{total amount of powder available}} = \frac{\pi(r_{0\max}^2 - r_1^2)L}{\pi(r_2^2-r_1^2)L}$$

$$= \frac{\left(r_1^4 + \dfrac{2a^2A^2\rho_1\rho_2}{B(\rho_2-\rho_1)}\right)^{1/2} - r_1^2}{r_2^2-r_1^2} \quad \text{for } r_1 \leqq r_0 \leqq r_2$$

and if

$$r_1 << r_2$$

$$y_{max} \cong \left(\frac{2\rho_1\rho_2}{B(\rho_2-\rho_1)}\right)^{1/2}\frac{aA}{r_2^2}$$

At any time,

$$y = \frac{\left(r_1^4 + 4a^2At - 2a^2Bt^2\dfrac{\rho_2-\rho_1}{\rho_1\rho_2}\right)^{1/2} - r_1^2}{r_2^2-r_1^2}$$

and for

$$r_1 << r_2$$

$$y \cong \frac{a}{r_2^2}\left(4At - \frac{2Bt^2(\rho_2-\rho_1)}{\rho_2\rho_1}\right)^{1/2}$$

$$\cong \text{const.}\,\frac{V_1 a}{r_2^2}\left(\text{const.}\,xt - \text{const.}\,xt^2\frac{(\rho_2-\rho_1)}{\rho_2\rho_1}\right)^{1/2}$$

The above equations, then, suggest (*a*) that the sluff-off time, t_1, is relatively independent of voltage, (*b*) the sluff-off time, t_1, is directly proportional to the resistivity factor $(\rho_1\rho_2/\rho_1-\rho_2)$, (*c*) the deposit will first form, then suddenly unform, (*d*) the amount of deposition should be proportional to (i) particle size, (ii) voltage, (iii) inverse area of cell, (iv) time at short times, and (v) should be of

short life if the system resistivity is low and the resistivities are rather different; or long, if the conductivity of the particles matches or is greater than that of the liquid.

It need hardly be said that the simple theory mentioned can be expected to apply only roughly to systems in which there is superimposed annular fluid flow. Unfortunately, for experimental convenience, the experimental data available are on systems with appreciable annular flow. Only rough analogy may be made with the theory which is for a system with no liquid flow. Experiments designed to test the hypotheses above are under way.

As one check of the theory we can calculate a sluff-off time, t_1, using reasonable values for the indicated constants

$$t_1 = \frac{A}{B}\rho = \epsilon_0\rho\,(K_2' - K_1')$$

Let

$$\rho = 1.3 \times 10^{15} \text{ ohm meter}$$

$$\epsilon_0 = 8.85 \times 10^{-12} \text{ farad/meter}$$

$$K_2' - K_1' = 5 - 2 = 3$$

$$t_1 = 8.85 \times 10^{-12} \frac{\text{coul}}{(\text{volt})\,(\text{m})} \times 1.3 \times 10^{15} \frac{(\text{volt})\,(\text{sec})\,(\text{meter})}{\text{coul}} \times 3$$

$$= 1.15 \times 10^{4} \text{ sec, or about 3 hr.}$$

This value of 10^4 sec for an assumed specific resistance of 1.3×10^{15} ohm meters based on that measured for hexane in a similar system (11) turns out to be an entirely reasonable one and lends a measure of confidence to the theoretical results.

Manuscript received Sept. 23, 1959. This paper was prepared for delivery before the Philadelphia Meeting, May 3-7, 1960. A portion of the research reported in this paper was sponsored jointly by the Army Signal Corps and Office of Naval Research under Signal Corps Contract No. DA-36-039 sc-70154 and O.N.R. 356-375.

Any discussion of this paper will appear in a Discussion Section to be published in the December 1960 JOURNAL.

REFERENCES

1. F. H. Meuller, *Wiss. Veröffentl. Siemens-Werken*, **17**, 20 (1938).
2. H. A. Pohl, *J. Appl. Phys.*, **22**, 869 (1951).
3. H. A. Pohl, *ibid.*, **29**, 1182 (1958).
4. H. A. Pohl and J. P. Schwar, *ibid.*, **30**, 69 (1959).
5. A. Loesche and H. Hultschig, *Kolloid-Z.*, **141**, 177 (1955).
6. P. J. W. Debye, *Phys. Rev.*, **91**, 210 (1953).
7. P. Debye, P. P. Debye, B. H. Eckstein, W. A. Barber, and G. J. Arquette, *J. Chem. Phys.*, **22**, 152 (1954).
8. P. Debye, P. P. Debye, and B. H. Eckstein, *Phys. Rev.*, **94**, 1412 (1954).
9. W. A. Barber, P. Debye, and B. H. Eckstein, *ibid.*, **94**, 1412 (1954).
10. S. Glasstone, "Textbook of Physical Chemistry," p. 671, D. Van Nostrand, Inc., New York (1946).
11. Progress Report XXII, Laboratory for Insulation Research, M.I.T., December 1957.

Continuous Separations of Suspensions by Nonuniform Electric Fields in Liquid Dielectrics

Herbert A. Pohl and Charles E. Plymale

Plastics Laboratory, Princeton University, Princeton, New Jersey

ABSTRACT

Suspensions of various solids in organic dielectric liquids can be separated continuously into their components by pulsating direct or alternating current electric fields of modest strength. The method and its important variables are described, together with the results observed for several systems. It is found, for example, that there exists a critical lower voltage and a critical upper voltage between which the operation must take place if appreciable separation is to take place. Best results are obtained if the dielectric constant exceeds that of the liquid. Among other separations possible, it is shown that zircon-rutile particle mixtures readily separate under conditions of dielectrophoresis. These materials cannot be separated by density or magnetic methods. A simple theory for the forces exerted on the particles sitting in combined gravitational and nonuniform electric fields is given.

Suspensions of various solids in organic dielectric liquids can be treated continuously by pulsating direct or alternating current nonuniform electric fields of modest strength to clarify or enrich the suspensions. Materials of differing polarizability can be separated. The methods and some of the important variables are described in this paper. It is found, for example, that there exists a critical lower voltage and a critical upper voltage between which operations must take place if appreciable separation is to occur. Best results are obtained if the dielectric constant of the suspended solids exceeds that of the liquid dielectric. An increase in conductivity of both liquid dielectric and of suspension is observed to occur in the voltage range where dielectrophoresis changes. The results are analogous in many respects to those obtained in earlier batch studies (1-4).

Experiments were, speaking broadly, carried out under two types of conditions. In one set, cylindrically symmetrical electrodes were used while close match of densities of powder and liquid was main-

tained. In such an electrode system, the force exerted on the particles depends strongly ($1/r^3$) on the distance from the central electrode axis. In the other set of experiments, an attempt was made to operate between electrodes of such design that the force on the particles did not depend on geometrical position in the channel in which they moved ("isomotive" cell), while the particles fell freely through a liquid of rather lower density than themselves.

Experiments in the Cylindrical Electrode Geometry

As outlined above, particles of various materials were suspended in liquid dielectrics of closely matching density. These suspensions were then subjected to the action of the nonuniform field existing between cylindrically symmetrical electrodes. Flow was continuous and axial in the cell. The feed was at the top. The liquid was withdrawn simultaneously at the bottom from two outlets, one drawing material from the region close to the central electrode and the other drawing material from the periphery (see Fig. 1). The concentration of suspended solids in the two existing streams was compared optically using an electrophotometer. A plot of the observed concentration ratios showed that little effect was to be noted until at least a somewhat critical value of voltage was applied across the electrodes. Beyond this region, a sharp increase in pullout of material was noted at the axial region of the cell as the applied voltage was increased. This increase continued with increase of voltage until a rather sharp maximum was observed, following which a rapid decrease in pullout was displayed until, at a high and rather critical voltage, a return to equality of concentrations of the two exciting streams was observed.

The suspensions examined were (*a*) spherical particles of selected size ranges, e.g., 100-140 U.S. mesh, of polyvinyl chloride suspended in CCl_4-benzene mixture (see Fig. 2), and (*b*) powdered ammonium chloride particles of selected size range suspended in CCl_4-benzene mixture of similar density (see Fig. 3).

Current measurements made on the above systems showed the d-c current to be very small, about

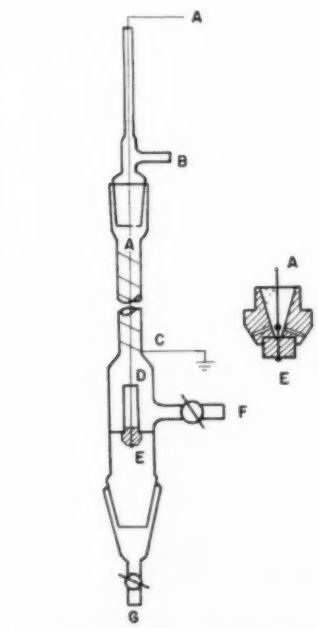

Fig. 1. Schematic diagram of cell used for continuous dielectrophoresis (cylindrical geometry). A, high potential (central) electrode; B, feed inlet; C, grounded outer electrode, consisting of bare wire wrapped onto glass tube; D, central takeoff tube; E, insulating (Teflon) central electrode support, perforated to pass suspension of particles; F, peripheral product vent; G, central product vent.

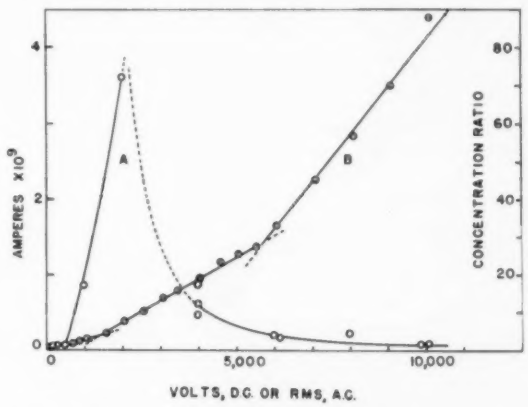

Fig. 2. Deposition and direct current flow during continuous dielectrophoresis of polyvinyl chloride. Curve A, Concentration ratio, central to peripheral, of exiting streams versus 60 cps, a-c rms voltage. Determined with swollen PVC; 90 μ average particle size; suspended in 1:1 v/v CCl_4-benzene mixture; space velocity of liquid, 10.5 cm/min: Teflon-coated central wire electrode, wire 0.74 mm diameter, 0.3 mm coating: Cell ID, 11 mm, powder concentration, 6% as volume fraction of suspension. Curve B, current vs. voltage for above system, but using static voltage.

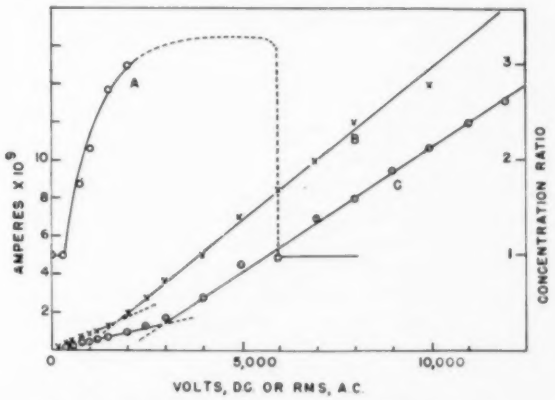

Fig. 3. Deposition and direct current flow during continuous dielectrophoresis of ammonium chloride. Curve A, concentration ratio, central to peripheral, of exiting streams vs. 60 cps, a-c rms voltage. Determined with NH_4Cl; 90 μ average particle size; suspended in 94:6 v/v CCl_4-benzene mixture; space velocity of liquid, 10.5 cm/min: Teflon coated central wire electrode, wire 0.74 mm diameter, 0.3 coating; cell ID, 11 mm; powder concentration, 2% as volume fraction of suspension. Curve B, current vs. voltage for above system, but using static voltage. Curve C, current vs. voltage in above geometry, using static voltage, and only flowing CCl_4 liquid in cell.

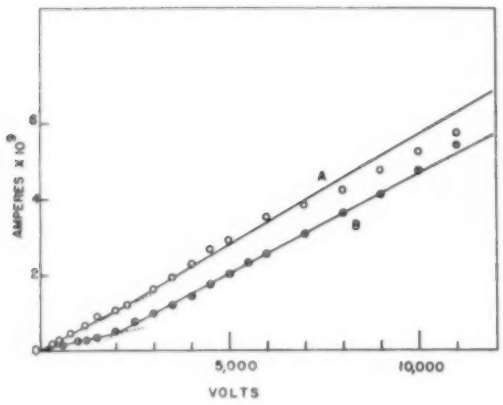

Fig. 4. Direct current flow in the liquid dielectric, 1:1 v/v CCl_4-benzene. Cylindrical cell geometry; liquid having space velocity of 10.5 cm/min, cell inside diameter, 11 mm. Curve A, data for bare 1.630 mm diameter wire. Curve B, data for bare 0.645 mm diameter wire.

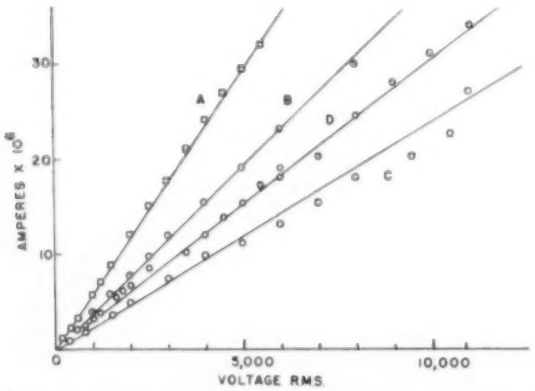

Fig. 5. Total current in electrode systems of cylindrical geometry containing a liquid dielectric. Alternating voltage applied; liquid having space velocity of 10.5 cm/mm, cell inside diameter, 11 mm, liquid dielectric, 1:1 v/v CCl_4-benzene; total current includes charging and loss currents. Curve A, data for bare 1.630 mm diameter wire. Curve B, data for bare 0.645 mm diameter wire, Curve C, data for bare 0.202 mm diameter wire. Curve D, data for Teflon covered wire; wire diameter, 0.74 mm, coating 0.3 mm thick.

1.0 to 100 $\mu\mu$a or slightly higher. The d-c current was measured using a Kiethley electrometer and appropriate shunts. The current was observed to be ohmic up to about the voltage at which the particles began to respond vigorously to the field. At this point a marked rise in current flow was observed, indicating a second mechanism of conduction had appeared (see Fig. 2-4). The data of Fig. 4 were made for comparison and were obtained on the pure liquid dielectric. The observed slight discontinuity in the current vs. voltage curves in the case of the pure liquid has not been elucidated. The discontinuities for the cases of solids present are rather larger. Alternating current measurements made on the above systems showed, as expected, that the dielectric loss current (10^{-8} amp) was too small to be detected easily in the presence of the relatively large charging current due to capacitance and stray inductances in the system (about 10^{-5}). Figure 5 shows this for 60 cps current vs. voltage for several inner electrode sizes.

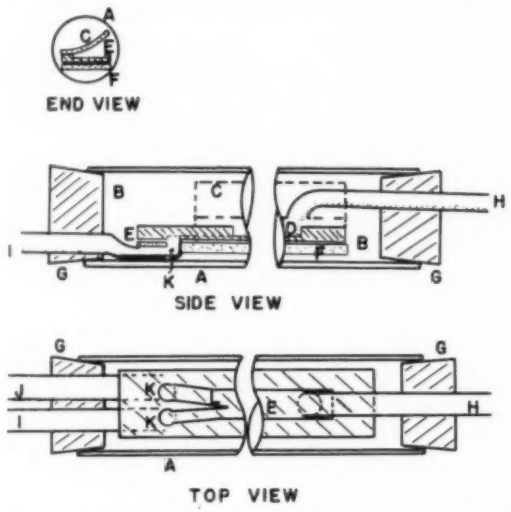

Fig. 6. Schematic diagram, isomotive cell for continuous dielectrophoretic separations. A, glass outer cell wall; B, dielectric liquid; C, curved upper brass electrode; D, solid particles lying in flat groove of Teflon insulator plate; E, Teflon plate, grooved; F, lower flat brass electrode; G, Neoprene stopper; H, Feed inlet, copper; I, lower exit tube, copper; J, upper exit tube, copper; K, exit holes; L, groove divider cut in Teflon.

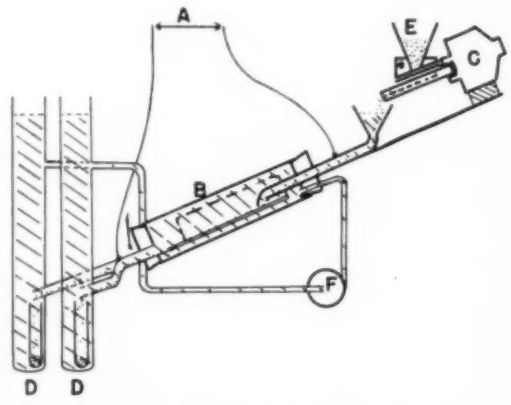

Fig. 7. Schematic diagram of isomotive cell operation. A, high voltage source; B, isomotive cell; C, vibrator; D, powder collectors; E, supply hopper for powder mixture; F, pump.

Experiments in "Isomotive" Cell Geometry

In these experiments, an attempt was made to have the solid particles pass through the nonuniform field cell in a long narrow tray in between electrodes of such a shape as to produce a force which was constant electrically and directed in opposition to that of gravity. Materials in powder form were then shaken down along this long narrow tray. The tray was given a slight tilt across its narrow dimension and a large inclination along its length (see Fig. 6 and 7). The dielectrophoretic force tended to hold particles up against the slight gravity pull exerted due to the tilt. Those particles most strongly pulled electrically would exit from

the lower end of the tray at one (uppermost) edge of the channel; those pulled least by the electrical force would tend to exit from the lower end of the tray at the other slightly lower edge of the channel. The angle of tilt was roughly estimated as 3° in experiments *A*, *B*, and *C* below. In experiments *D-H*, the tilt angle was more carefully measured by protracting.

The whole tray and electrode system was kept immersed in a low viscosity liquid dielectric (benzene or cyclohexane for experiments *A*, *B*, *C*; carbon tetrachloride for experiments *D-H*). Powders were fed in at the upper end and removed continually by sampling tubes at the lower end. After testing a number of cell designs to at least partially optimize performance, the following results on powders were obtained.

(*A*) Polyvinyl chloride powder was observed to be collectable at will in either of the exits from the cell, depending on the voltage applied. At very low or nil voltages, all of the powder collected in the lower exit. At medium voltages higher and higher fractions of the powder could be collected in the upper exit until, at about 1300 v, about 90% of the existing powder was observed to pass out the upper exit. As the voltage was increased beyond this range, the process was observed to become less selective, the powder behavior more erratic, and the proportion collected in the lower exit increased until the cell acted with very low selectivity (see Fig. 8).

(*B*) A powdered mixture of $Na_2Cr_2O_7 \cdot 2H2O$ and TiO_2, both of mesh size less than 80 was fed into the hopper and cell. At nil voltage very little of either kind of particle was observed to pass into the upper exit. As the voltage was increased a larger and larger fraction of TiO_2 was collected at the upper exit, until at about 300 v a maximum was observed. The proportion of the dichromate passing into the upper exit remained low until about 1000 v. At voltages higher than this (up to 2000 v a.c. rms) a lack of selectivity of the cell was observed, and a mixture of both solids was observed to go into the lower and upper exits (see Fig. 9).

(*C*) A mixture of 60-100 mesh rutile mineral (gray-black form of TiO_2) with 60-80 mesh polyvinyl chloride was passed through the cell. At nil voltage, neither type of particle passed out the upper exit. As the voltage was increased, a greater and greater fraction of the rutile passed into the upper exit, until at a voltage of about 750 v a.c., rms, slight quantities of PVC powder were observed to accompany it out the upper electrode. At higher voltage, as before, less selectivity in the separation was observed (see Fig. 10).

(*D*) The "operating curves" for the pure single components were determined by measuring the volume fraction of feed material which left by the high exit at various applied voltages. Samples of powders passing 100 U. S. mesh and resting on 140 U. S. mesh (nominal 127 μ average particle diameter) were used throughout the following experiments (see Fig. 11-14, e.g.). Following these determinations of the behaviors of the single components, the ability of the isomotive cell to separate 1:1 v/v mixtures of these powders was then determined. Compositions of the materials exiting from the low and high exits were determined by counting under a microscope. The following results (*E-H*) were obtained.

(*E*) *Silicon carbide-aluminum oxide*: Alumina and carborundum obtained from the Bay State Abrasives Company was screened and graded. Separation by dielectrophoresis of the carborundum from the alumina was found to be relatively easy. Figure 15 shows the percentage composition of the streams of powder coming from the high and low exits as a function of applied voltage. It may be seen that the carbide is readily pulled over to the high exit in preference to the alumina. At very

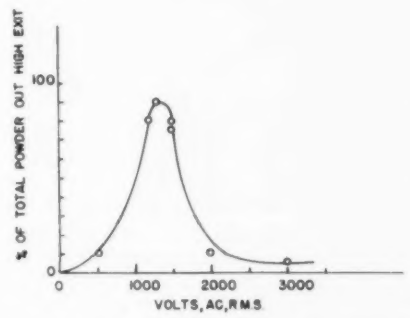

Fig. 8. Behavior of polyvinyl chloride spheres in isomotive cell.

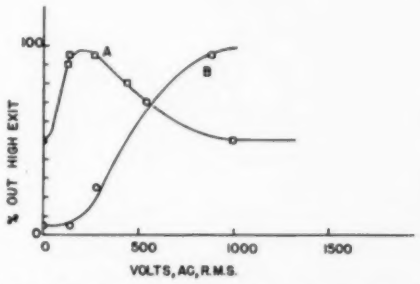

Fig. 9. Behavior of sodium dichromate-titanium dioxide particle mixtures in isomotive cell. Curve A, per cent of rutile in powder coming out high exit. Curve B, per cent of total powder coming out high exit.

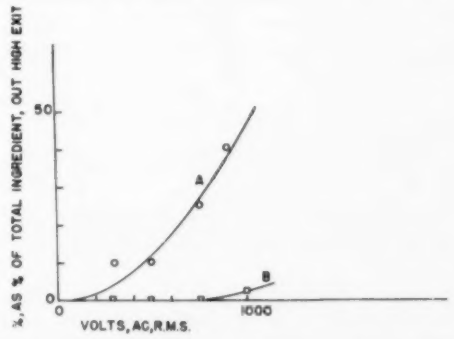

Fig. 10. Behavior of polyvinyl chloride-rutile mixtures in isomotive cell. Curve A, per cent of total rutile coming out high exit. Curve B, Per cent of total polyvinyl chloride coming out high exit.

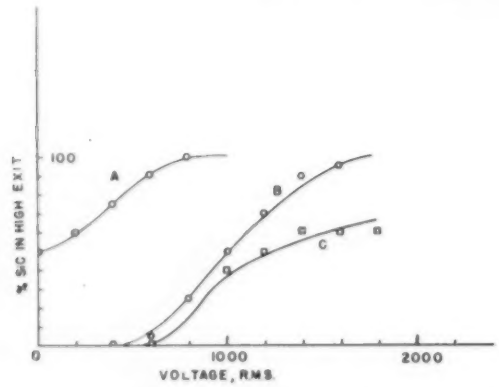

Fig. 11. Behavior of silicon carbide particles in isomotive cell. Curve A, 0° tilt. Curve B, 3° tilt. Curve C. 6° tilt.

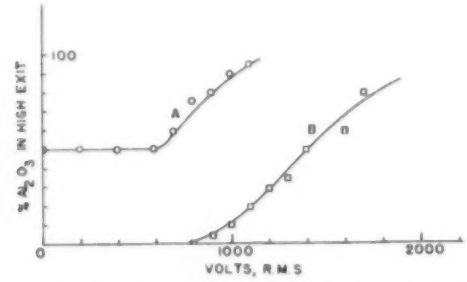

Fig. 12. Behavior of aluminum oxide particles in isomotive cell. Curve A, 0° tilt. Curve B, 3° tilt.

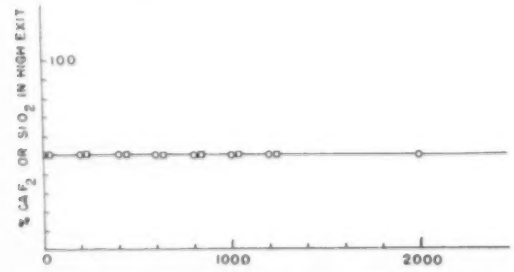

Fig. 13. Behavior of calcium fluoride (fluorite) and SiO_2 particles in isomotive cell. Circles, SiO_2; squares, CaF_2.

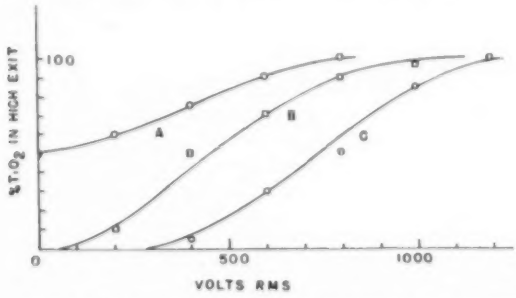

Fig. 14. Behavior of rutile (TiO_2) particles in isomotive cell. Curve A, 0° tilt. Curve B, 3° tilt. Curve C, 6° tilt.

low voltages, neither kind of particle succeeds in reaching the high exit. At low voltage the carbide in pure form succeeds in coming out the high exit. As the voltage increases beyond this point, a larger and larger fraction of it goes out the high exit, until as the lower critical voltage for the alumina is

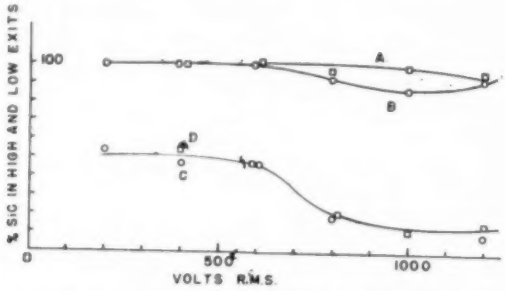

Fig. 15. Behavior of silicon carbide-aluminum oxide particle mixtures in isomotive cell. Composition at (A) high exit, 6° tilt; at (B) high exit, 3° tilt; at (C) low exit, 3° tilt; and at (D) low exit, 6° tilt.

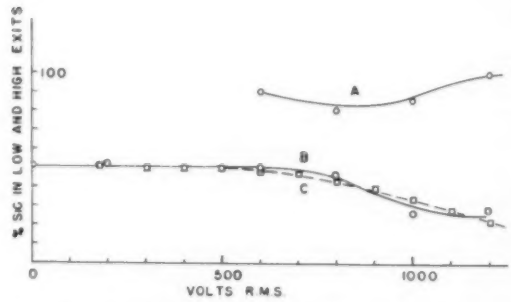

Fig. 16. Behavior of silicon carbide-silica mixtures is isomotive cell, cell at 3° tilt. Curve A, composition out high exit. Curve B, composition out low exit. Curve C, composition calculated from operating curves of pure components.

reached, a trace of alumina appears in it. As the voltage applied is increased still further almost all of the carbide and more and more of the alumina goes out the high exit, making the high exit stream steadily richer in alumina. The lower exit now delivers nearly pure alumina.

(*F*) *Silicon carbide-silicon dioxide*: Silicon carbide, as above, and purified "glass grade" sand, "Berkeley Fine Dry Special" from the Pennsylvania Glass Sand Corporation, seived and graded to pass 100 U. S. mesh and rest on 140 mesh (nominal 127 μ average particle diameter) were found to be easily separable by dielectrophoresis. Determination of the "operating curve" for the pure SiO_2 showed that in the present design of isomotive cell it would not come out of the high exit at any voltage applied if the tilt angle was as large as 3°. The curve for pure SiC is shown in Fig. 11. Separation curves are shown in Fig. 16. The behavior over-all resembled that for the Al_2O_3-SiC mixtures except for the nearly complete absence of SiO_2 in the upper exit. Some carry-over was experienced at the higher voltages, however. Experiments showed that SiO_2 particles alone did not move out the higher exit under any conditions of voltage applied at 3° tilt or greater.

(*G*) *Silicon carbide-calcium fluoride*: This mixture was studied because it formed an interesting example of an otherwise difficult separation. The closeness of the densities (SiC) $d_{25} = 3.17$; CaF_2, $d_{25} = 3.18$) and the absence of particularly outstanding magnetic properties precludes density or mag-

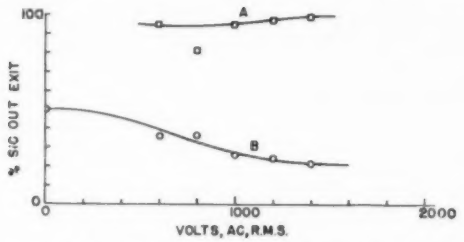

Fig. 17. Behavior of calcium fluoride (fluorite)-silicon carbide particle mixtures in isomotive cell. Curve A, high exit 3° tilt. Curve B, low exit 6° tilt.

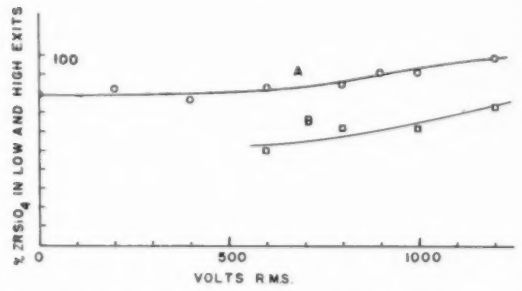

Fig. 18. Behavior of zircon-rutile particle mixtures in isomotive cell. Curve A, product in lower exit. Curve B, product in high exit, 3° tilt.

netic separations. As can be seen from Fig. 17, these two solids are readily separable by dielectrophoresis in the isomotive cell. CaF_2 like SiO_2 does not move out the high exit if alone at tilts of 3° or more.

(*H*) *Zircon-rutile*: This mixture of minerals which cannot be separated by density or magnetic methods proved readily separable by dielectrophoresis in the isomotive cell. Results are shown on Fig. 18. The separations were done on zircon sand from Yamba Beach, Australia. As received, it contained about 21% rutile from which it was readily separated by a preparatory cleanup run. Rutile, mineral, crushed and graded was used in making 1:1 v/v mixtures for this study. Zircon, like SiO_2, does not move out the high exit if alone in the cell at tilts of 3° or more.

Discussion of Results

It may be considered that forces on the particles in the tray come from at least five causes:

1. Osmotic.
2. Gravitational (corrected for bouyancy).
3. Dielectrophoretic, arising from the effect of the nonuniform electric field on the field polarized neutral particles.
4. Dielectrophoretic, arising from the effect of the nonuniform electric field on the current-induced (or produced) dipoles on the particle surface.
5. Electrophoretic, arising from the effect of the electric field on *excess* charges on the particles. Excess charges, may arise from several possible causes. A charge unbalance may arise from current-induced charging accumulating initially by image force adsorption in equal numbers, followed by local discharge due to "corona" effects at sharp edges on the particle. A charge unbalance may also arise from other causes such as contact or near contact with electrodes or other particles bearing an unbalance of charges. Still other mechanisms are possible. The nature of conduction in these organic liquid dielectrics is not completely clear, although ionic mechanisms appear to be prominent (6). The appearance of a break in the current-voltage curve of the liquid dielectric alone (Fig. 2-4) indicates that there may be some change in type of conduction even in the liquid without large amounts of suspended particles. This opens the question as to the cause of the several breaks observed in the curves for suspensions. It may be that in the present experiments that traces of powder impurity were present in the liquid dielectric studied. It may also be that the effect observed is due entirely to phenomena characteristic of particle-free liquid. Further studies of this intriguing problem are under way.

A simplified theory of the net force at any time after arrival in the field is given below for spherical particles, excluding the more difficult calculable electrophoretic forces arising from more or less random charging, and also excluding osmotic or concentration gradient forces which are generally negligible for particles above about 0.2 μ diameter.

The gravitational force, F_g, effective along the bottom of the tilted tray is

$$F_g = -\,i\,\frac{4}{3}\,(d_2-d_1)\,a^3 g \sin\alpha \qquad [1]$$

where a is the particle radius, d_2, d_1 the densities of particle and liquid dielectric, respectively, g the gravitational constant, and α the angle of tilt from horizontal.

As shown in earlier work (2) the dielectrophoretic force, F_e, arising from induction in a nonuniform field on neutral particles is

$$F_e = 2\,a^3 K_1' \epsilon_o \left(\frac{K_2'-K_1'}{K_2'+2K_1'}\right) \nabla |E|^2 \qquad [2]$$

where K_1', K_2' are the relative dielectric constants of the liquid and solid, ϵ_o is the permittivity of free space, and E the electric field at the particle.

In accord with results described elsewhere (5) it can be shown that the dielectrophoretic force, F_j, arising from the effect of a nonuniform field on current-induced dipoles on the surface of spherical particles is

$$F_j = i(\mu \cdot \nabla |E|) \qquad [3]$$

where

$$\mu = 4\pi/3\; a^3 j\, t \qquad [4]$$

μ is electric moment due to current-produced charge accumulation, and j is the net current arriving at surface of particle.

$$j = j_1 - j_2 \qquad [5]$$

j_1, j_2 is the current in medium and particle, respectively, i the unit vector in horizontal direction (unity if $\nabla |E|$ coincides with tray bottom direction), and t the time of flow of current.

By Ohm's law

$$j_1 = E_{1s}/\rho_1 \quad [6]$$

$$j_2 = E_{1s}/\rho_2 \quad [7]$$

where E_{1s} is the electric field at particle-liquid interface

$$E_{1s} = E\left(\frac{3K_1'}{K_2'+2K_1'}\right) \quad [8]$$

during most of the charging period and ρ_1, ρ_2 are the specific resistivities of the liquid and particles, respectively.

Combining equations

$$F_1 = 2\pi a^3 t\left(\frac{K_1'}{K_2'+2K_1'}\right)\left(\frac{\rho_2-\rho_1}{\rho_1\rho_2}\right)\nabla|E|^2 \quad [9]$$

The net force on the particle in the direction along the tray bottom is then, F_{net}

$$F_{net} = F_v + F_1 + F_g \quad [10]$$

$$F_{net} = 2\pi a^2\nabla|E|^2\left(\frac{K_1'}{K_2'+2K_1'}\right)\left[\epsilon_0(K_2'-K_1') + t\frac{(\rho_2-\rho_1)}{\rho_2\rho_1}\right] \quad [11]$$

$$-i\frac{4\pi}{3}a^3g(d_2-d_1)\sin\alpha$$

As a test of the above equations, we may examine a comparison of the calculated and observed forces. The electrical and gravitational forces are observed to be in balance, for example, when the voltage is just large enough to cause the particles to begin to go out the upper exit at a given tilt. Table I contains data relevant to this comparison. The voltage values, listed as "V critical" were found from use of data in Fig. 11, 12, 14, and 18, and were chosen at the point where the first particles could be detected in the higher exit during a 3° tilt. The value for the dielectric constant of silicon carbide is estimated from its behavior. The values of $\nabla|E|^2_{max}$ are those[1] calculated for a cylindrical electrode of radius 0.60 cm spaced 0.241 cm from a flat plate. The values of the calculated electrical and gravitational forces, F_e and F_g, were obtained using the given equations.

That the calculated values for the electrical force are less than those calculated for the gravitational at balance is believed to be due to what may be termed the "bunching effect." The electrical force is that calculated for lone spherical particles which are so small as to leave the acting electrical field unaffected. The experimental observations of the critical voltages were obtained instead using rather concentrated streams of particles. It is believed that considerable particle-particle and particle-field interactions exist in such circumstances which greatly accentuate the nonuniform field force on the aggregates. This is evidenced, for example, by the bridging effects already noted. This problem is under further study and it is hoped that further light can be shed on this phenomenon.

Table I. Comparison of the calculated electrical (dielectrophoretic) force and gravitional force on particles in a tilted tray (3° tilt) in a nonuniform electrical field due to combined flat and cylindrical plates

Substance	Density, g/cc	Dielectric constant	$V_{critical}$, v(rms)	$\nabla|E|^2_{max}$, $v^2/m^2 \times 10^{-12}$	F_e, newtons/m^3/unit vol.	F_g, newton/m^3/unit vol.
SiC	3.17	(10)	500	2.40	(38.2)	810
Al_2O_3	4.0	8.6	800	6.12	87.6	1230
TiO_2	4.26	70	150	0.216	5.8	1370
$ZrSiO_4$	4.7	12.5	600	3.44	61.8	1590

REFERENCES

1. H. A. Pohl, *J. Appl. Phys.*, **22**, 869 (1951).
2. H. A. Pohl, *ibid.*, **29**, 1182 (1958).
3. H. A. Pohl and J. P. Schwar, *ibid.*, **30**, 69 (1959).
4. H. A. Pohl and J. P. Schwar, "Particle Separations by Nonuniform Electric Fields in Liquid Dielectric, Batch Methods," Paper presented at The Electrochemical Society, May 6, 1959, Philadelphia, Pa.
5. H. A. Pohl, "Non-Uniform Field Effects in Poorly Conducting Media," *ibid.*
6. Progress Report XXII, Laboratory for Insulation Research, M.I.T., December 1957.

[1] For a cylindrical electrode above and parallel to a flat plate,

$$\nabla|E|^2_{max} = \frac{25}{54}\sqrt{5}\,\frac{V^2}{y_1^3\left[\ln\left|\frac{y_1-y_0}{y_1+y_0}\right|\right]^2}$$

where V is the voltage between electrodes, y_0 the least distance between cylinder and flat electrodes, $y_1 = \sqrt{(y_0+R)^2 - R^2}$, and R is the radius of curvature of the cylindrical electrode, and the field quantity is measured at the surface of the flat plate.

December 1960 Discussion Section

A Discussion Section, covering papers published in the January-June 1960 JOURNALS, is scheduled for publication in the December 1960 issue. Any discussion which did not reach the Editor in time for the June 1960 Discussion Section will be included in the December 1960 issue.

Those who plan to contribute remarks for this Discussion Section should submit their comments or questions in triplicate to the Managing Editor of the JOURNAL, 1860 Broadway, New York 23, N. Y., *not later than September 1, 1960*. All discussion will be forwarded to the author(s) for reply before being printed in the JOURNAL.

Electrodeposition of High-Purity Chromium from Electrolytes Containing Fluoride or Fluosilicate

N. Ryan

Aeronautical Research Laboratories, Australian Defence Scientific Service, Department of Supply, Melbourne, Australia

ABSTRACT

Investigation of the variables affecting the laboratory scale deposition of chromium from chromic acid electrolytes containing fluoride or fluosilicate has enabled the optimum conditions for the production of high-purity chromium (0.03-0.04 wt % oxygen, 0.0008-0.002 wt % nitrogen) at the highest current efficiency (38-45%) to be determined. This current efficiency is much higher than the 8-10% in the chromic acid-sulfate electrolyte in which chromium of a similar grade can be produced.

Continuous electrodeposition in a larger cell showed that the current efficiency in fluoride-containing electrolytes decreased progressively with time to a steady 25-30%. No explanation has been found for this decrease. After steady conditions have been achieved, the advantages in current efficiency of the fluoride over the sulfate bath remains substantial.

It has been known for several years that fluorides and fluosilicates are effective catalysts in chromium plating solutions. Electrolytes containing these anions have been used commercially, particularly in Germany, but they have not yet been used for the purpose of producing high-purity chromium.

In these laboratories the pure chromium (0.02 wt % O_2, 0.002 wt % N_2, 0.001 wt % max. metallic elements including C, S, Si) required for experimental work on the development of chromium-base alloys is produced from chromic acid electrolytes containing sulfate (1) at current efficiencies of 8-10%. It is known that improved current efficiencies are obtained when using electrolytes containing either fluoride or fluosilicate, and it was therefore decided to investigate solutions containing these anions to determine whether or not they could be used to produce a high-grade chromium deposit.

Work by Bilfinger (2) (reviewed by Hood) (3) on baths containing fluoride and fluosilicate resulted in a series of curves and tables which revealed the optimum deposition conditions necessary to maintain the highest current efficiencies at 55°C. In the present study, an electrolyte temperature of 100°C was chosen for the preliminary investigations, after a consideration of the results of work carried out by Brenner, *et al* (4). These workers showed that the relationship between electrolyte temperature and oxygen content of chromium deposited from chromic acid solutions containing fluoride was similar to that associated with the chromic acid-sulfate electrolytes, i.e., increasing electrolyte temperature resulted in a decrease in the oxygen content of the chromium deposit. The experimental program was therefore designed to yield, for a bath temperature of 100°C, information of a similar character to that previously obtained by Bilfinger at 55°C. This was done by studying independently each variable affecting the efficiency of deposition and purity of the product.

For ease of reading and brevity in this report the expressions "fluoride-containing electrolyte" and "chromium deposited from an electrolyte containing fluoride" will in general be replaced by the terms "fluoride electrolyte" and "fluoride chromium," respectively. The terms "fluosilicate electrolyte," "sulfate electrolyte," "fluosilicate chromium," and "sulfate chromium" have corresponding meanings.

Apparatus

The apparatus, holding 250-300 ml of solution, consisted of a glass vessel with inlet and outlet arms which were used for the electrode connections and for the introduction of the electrolyte. Gases evolved during electrolysis escaped via a reflux condenser, which assisted in maintaining a stable electrolyte concentration by eliminating fume and evaporation losses. Since fresh electrolyte was used for each experiment and deposition runs were limited to 1 hr, no precautions were necessary to counter fluosilicate contamination arising from the glass container. Chemical analysis of the deposited chromium confirmed the absence of silicon. The use of fresh electrolyte also helped to reduce the build-up of trivalent chromium, which would have introduced a further significant variable.

The electrolytes were prepared from high-grade chromic acid containing the following nominal impurities: 0.02% SO_4, 0.004% NO_3, 0.01% Fe, and 0.1% Na. Fluoride was added as hydrofluoric acid and fluosilicate as the potassium salt.

Chromium was deposited on ½ in. diameter copper tubes which were subsequently dissolved by digestion in nitric acid. High-purity lead was first used as the anode material, but this was found to become inactive within a very short period. It was therefore replaced by a 7% tin-lead anode, as used in some commercial fluoride baths. A heavy scale formed on this anode, and in the early test runs this was removed. However this practice was found to

Table I. Variables affecting the deposition of chromium in fluoride electrolytes

Run No.	Electrolyte composition		F/CrO_3, %	Temp, °C	Current density, amp/ft²	Current efficiency, %	Oxygen, wt %	Nitrogen, wt %
	CrO_3, g/l	F, g/l						
F1	315	3.0	0.96	101	1100	8	0.4	0.002
F2	310	10.0	3.20	102	1050	15	0.35	0.003
F3	300	5.65	1.81	102	1150	39	0.04	0.0012
F4	295	4.4	1.50	100	1150	40	0.04	0.003
F5	300	16.0	5.35	102	1100	No deposit	—	—
F6	200	2.5	1.25	102	1000	19.5	0.068	0.0016
F7	300	7.46	2.5	101	964	32.3	0.14	0.002
C1	100	1.75	1.75	101	950	33	0.037	0.005
C2	200	3.5	1.75	102	910	38.5	0.04	0.005
C3	300	5.25	1.75		910	45	0.04	0.005
C4	400	7.00	1.75		910	35	0.044	0.003
T1	300	5.14	1.71	55	1010	28.5	0.4	0.008
T2	300	5.14	1.71	70	1010	23.5	0.15	—
T3	300	5.14	1.71	82	1010	24	0.09	0.007
T4	300	5.14	1.71	92	1010	38	0.08	0.006
T5	300	5.14	1.71	30	1010	Black powdery deposit	—	—
CD1	300	5.25	1.75	101	1360	44	0.028	0.003
CD2	300	5.25	1.75	102	1125	48.5	0.035	0.003
CD3	300	5.25	1.75	102	670	39	0.035	0.003
CD4	300	5.25	1.75	102	1200	48	0.033	0.003

be unnecessary as the scale did not in any way affect the activity of the anode.

For a preliminary study of larger scale production, a plating cell consisting basically of an 8 in. diameter round bottomed "Hysil" glass vessel holding up to 10 l was constructed. A lid of laminated fiber board, coated with a heavy layer of polyvinyl chloride, served as a covering for the cell and held four 12 in. double-surface reflux condensers, the copper cathode (1 in. tube) and electrical connections to the annular anode made from a 7% tin-lead alloy (6 in. diameter, ⅜ in. thick). The volume of electrolyte normally used was 8 l, and as in the case of the small cell no precautions were taken to protect the glass from the action of the fluoride.

Power to this cell was supplied by a 250 amp capacity selenium rectifier. No heating of the electrolyte was necessary, other than bringing up to temperature prior to the commencement of a run, as the power input (200 amp at 5-6 v) was sufficient to maintain a boiling solution. Arrangements for continuous operation were not developed and plating times were limited to 6-7 hr runs.

Analysis

Oxygen analysis of the deposited chromium was carried out by the Adcock method and nitrogen was determined using the semi-micro Kjeldahl method. Fluoride and fluosilicate concentrations in the bath were determined by a modification of the steam distillation process used by Reynolds and Hill (5).

Conditions of Operation

The current efficiency-catalyst acid curves obtained by Bilfinger (2) at 55°C gave strong indications of the sensitivity of current efficiency to

Table II. Variables affecting the deposition of chromium in fluosilicate electrolytes

Run No.	Electrolyte composition		SiF_6/CrO_3, %	Temp, °C	Current density, amp/ft²	Current efficiency, %	Oxygen, wt %	Nitrogen, wt %
	CrO_3, g/l	SiF_6, g/l						
S1	300	3.4	1.14	101	900	26.5	0.12	0.0008
S2	300	6	2.00	101	900	39	0.04	0.0008
S3	300	4.50	1.50	101	870	35	0.06	0.0008
S4	300	7.50	2.50	101	730	22	0.12	0.0008
S5	300	5.25	1.75	101	915	36	0.054	0.0014
S6	300	6.75	2.25	101	900	33	0.10	0.0014
S7	300	5.62	1.87	101	880	38.5	0.04	0.0012
CS1	500	10	2	101	900	29.5	0.05	0.0008
CS2	400	8	2	101	875	35	0.06	0.0012
CS3	200	4	2	100	910	32	0.06	0.0016
CS4	100	2	2	100	906	19	0.04	0.0008
CS5	350	7	2	101	920	36.5	0.04	0.0008
TS1	300	6	2	70	900	26.5	0.2	0.004
TS2	300	6	2	85	940	37.0	0.08	0.0012
TS3	300	6	2	63	924	15*	0.25	—
TS4	300	6	2	92	885	38.5	0.06	0.001
DS1	300	6	2	102	1300	39.5	0.06	0.0008
DS2	300	6	2	101	610	28.4	0.084	0.001
DS3	300	6	2	101	1606	36.8	0.09	0.0012
DS4	300	6	2	101	1160	40.0	0.036	0.0008

* Powdery deposit, current efficiency value doubtful.

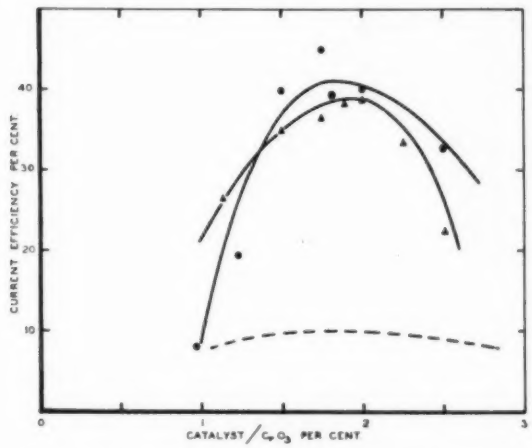

Fig. 1. Effect of catalyst-chromic acid ratio on current efficiency. •, Fluoride electrolyte; ▲, fluosilicate electrolyte; - - - -, sulfate electrolyte.

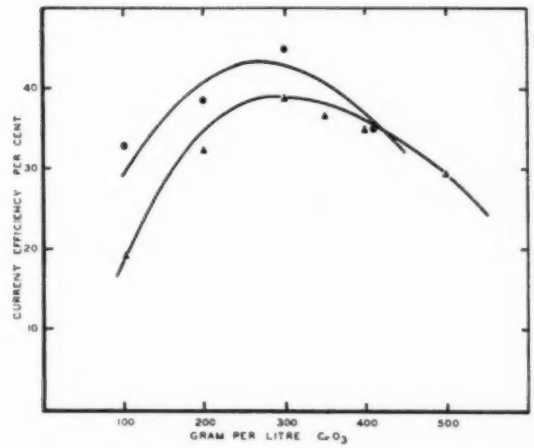

Fig. 2. Effect of chromic acid concentration on current efficiency. •, Fluoride electrolyte; ▲, fluosilicate electrolyte.

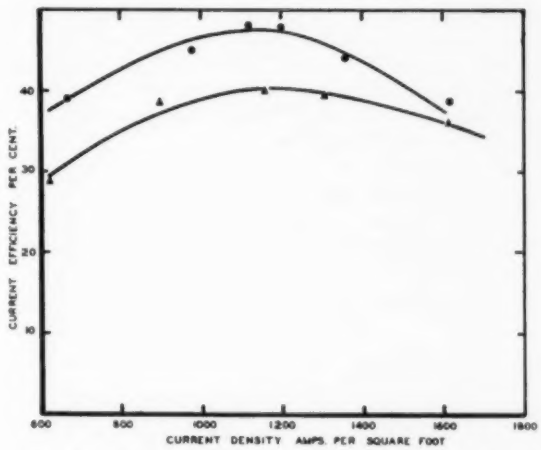

Fig. 3. Influence of current density on current efficiency. •, Fluoride electrolyte; ▲, fluosilicate electrolyte.

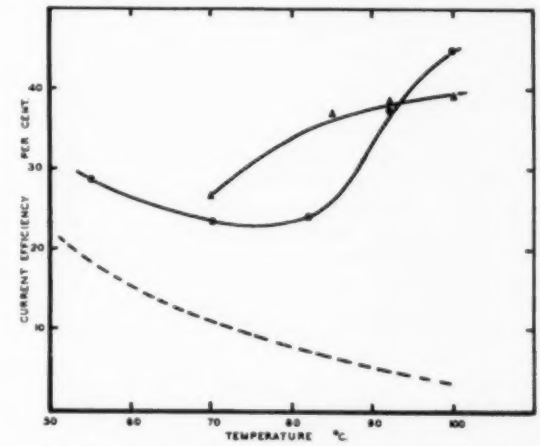

Fig. 4. Change in current efficiency with electrolyte temperature. •, Fluoride electrolyte; ▲, fluosilicate electrolyte; - - - -, sulfate electrolyte.

both fluoride and fluosilicate concentration in chromic acid electrolytes. For tests at 100°C, a chromic acid concentration of 300 g/l was selected, this being the standard concentration used in the production of sulfate chromium. Results are recorded in Tables I and II. The efficiency values are plotted against catalyst concentration in Fig. 1. The curve for sulfate electrolytes at 82°C is incorporated in Fig. 1 for comparison.

The results of the above test runs established the catalyst-chromic acid ratio at 1.75% for the fluoride electrolyte and 2% for the fluosilicate electrolyte. Several chromic acid solutions were prepared at concentrations ranging between 100 and 500 g/l CrO_3 each containing the required catalyst addition at the ratio cited above. These solutions were then electrolyzed at current densities of 880-950 amp/ft². The electrolyte temperature was maintained at 100°-102°C. The current efficiency data obtained are recorded in Tables I and II and illustrated graphically in Fig. 2.

From a study of the results obtained during this test series, chromic acid solutions of the following composition were prepared: (*a*) 300 g/l CrO_3, 5.25 g/l F; and (*b*) 300 g/l CrO_3, 6 g/l SiF_6. These solutions were electrolyzed at 100°-102°C using current densities ranging from 600 to 1600 amp/ft². Results are recorded in Tables I and II and shown in Fig. 3.

All of the above experiments were carried out in boiling electrolytes and the high current efficiencies obtained were particularly interesting. The association of high current efficiency with high temperature differed markedly from the behavior of sulfate electrolytes, i.e., decreasing efficiency with increasing temperature, and warranted further investigation. Hence electrolytes were prepared from 300 g/l solutions of chromic acid containing either 5 g/l fluoride or 6 g/l fluosilicate, and these were electrolyzed at various temperatures using current densities between 850 and 1010 amp/ft², as detailed in Tables I and II. The temperatures given in Tables I and II were measured by a thermometer attached to the cathode. It is possible however that the actual temperature at the cathode surface was slightly higher than those registered. The results of these experiments are given in Fig. 4, together with sul-

fate-electrolyte data (6). In the fluosilicate electrolyte, deposits at temperatures below 65°C were powdery, and the calculated current efficiency was thus doubtful. This may have been due to too high a current density which could result in some hydrolysis at the electrode surface.

The information obtained from these tests was both unexpected and interesting in that for both the fluoride and fluosilicate electrolytes current efficiency increased to a maximum value toward 100°C.

Gas Content of Electrodeposits (Oxygen and Nitrogen)

Oxygen.—Analysis of chromium deposited from the fluoride and fluosilicate baths at various temperatures showed that the oxygen content varied with temperature in much the same way as for sulfate chromium, i.e., as the electrolyte temperature was increased the oxygen content decreased rapidly between 50° and 80°C and then more gradually toward 100°C.

Results are recorded in Tables I and II and plotted in Fig. 5 together with the corresponding oxygen-temperature curve for a sulfate electrolyte. From these curves it is seen that while fluoride and fluosilicate chromium can be deposited with low oxygen content (0.03-0.05 wt %) they are unlikely to have as low an oxygen content as sulfate chromium produced under the optimum conditions. Against this, however, are the remarkably high current efficiencies of the fluoride and fluosilicate baths. At 100°C the efficiency of the sulfate electrolyte is 3% as compared with 40-45% for the fluoride and fluosilicate electrolytes.

Nitrogen.—The results suggest that the nitrogen content tends to decrease with increasing electrolyte temperature. However, this effect is doubtful, and other work (7) has shown that when higher nitrate impurity (0.1%) is present in the bath, the nitrogen content of the chromium is unaffected by electrolyte temperature.

Analysis of the chromium deposits from electrolytes of varying catalyst concentrations showed that the oxide impurity was particularly susceptible to changes in fluoride and fluosilicate concentrations. Low oxygen values occurred within the same catalyst concentration ranges which gave highest current efficiency. These values are recorded in Tables I and II and plotted against catalyst-chromic acid ratio in Fig. 6. Similar effects have been noted for the oxygen content of sulfate chromium, as is also indicated in Fig. 6. The nitrogen content was not affected.

Results recorded in Tables I and II show that variation in chromic acid concentration and current density have little or no influence on either the oxygen or nitrogen content in fluoride or fluosilicate chromium.

Electrodeposition from Fluoride Electrolytes in a 10-l Glass Cell

Using the information obtained from the preceding part of this investigation it was decided to carry out some preliminary tests in a larger scale apparatus as a step toward regular chromium production

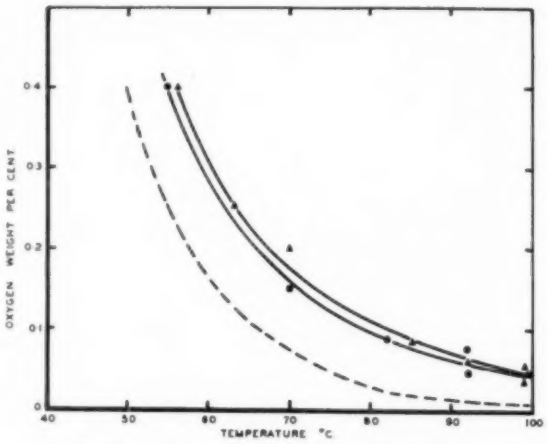

Fig. 5. Decrease in oxygen content with increasing electrolyte temperature. ●, Fluoride chromium; ▲, fluosilicate chromium; - - - - -, sulfate chromium.

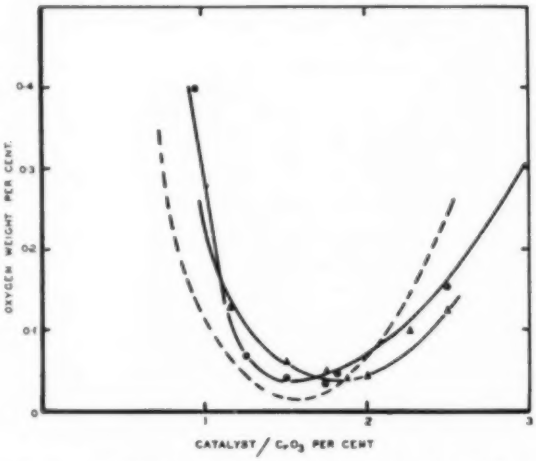

Fig. 6. Changes in oxygen content with various catalyst-chromic acid ratios. ●, Fluoride chromium; ▲, fluosilicate chromium; - - - - -, sulfate chromium.

from fluoride containing electrolytes. Table III which lists details of some of these preliminary runs shows that the current efficiency falls successively as the bath ages.

Factors which could have some influence on this current efficiency decrease are:

1. Trivalent chromium concentration which showed increasing values corresponding to the decreasing current efficiency results (see Table III).
2. The considerable build-up of nodules and the treeing of the deposits which upsets the effective current density by increasing the over-all cathode surface area and which produces a nonuniform distribution of current density over the cathode surface. In addition some loss of chromium results from the detachment of nodules from the cathode.
3. The possible formation of fluosilicate contamination by the chemical action of the fluoride electrolyte on the glass vessel.

Influence of trivalent chromium concentration.—In order to study the effect of this variable on the current efficiency a solution of known trivalent chro-

Table III. Electrodeposition in the 10-l glass cell

Run No.	L1	L2	L4	L6	L7
Electrolyte composition					
CrO_3 g/l	290	309	300	300	310
F g/l, start	4.5	5	5	5.6	5.4
F g/l, finish	4		5	5	5.25
Cr, g/l	1.2	1.32	2.32	5.14	5.2
Active age of bath, hr	7	11	25	40	47
Temperature, °C	102	102	102	102	102
Current density, amp/ft²	1150	1150	1150	1100	1150
Current efficiency, %	40	35	32	25	24
Oxygen, wt %	0.04	0.04	0.04	0.035	0.03
Nitrogen, wt %	0.0028	0.003	0.003	0.002	0.0012

mium concentration was prepared by adding a known amount of Cr_2O_3. This solution was electrolyzed in the small experimental cell. As indicated in Table IV, a current efficiency of 42% was recorded, which apparently indicated that the trivalent chromium concentration did not influence the current efficiency. However, reconsidering this factor it was thought possible that by introducing trivalent chromium into solution as Cr_2O_3, the trivalent chromium complex formed might not be the same as that which exists in the electrolyte as a result of natural aging. Hence a further solution was prepared in which the trivalent chromium was increased by artificially aging the electrolyte using a large cathode surface area separated from a small anode surface by means of a porous porcelain pot. In this way solutions containing 15 and 27 g/l trivalent Cr were prepared for electrolysis in the small cell. The results, recorded in Table IV again show that trivalent chromium added to the bath does not affect the current efficiency significantly.

Current density and nodule formation.—The above tests suggested the possibility that in the large cell much more chromium was being lost as nodules than had been expected. Work with sulfate electrolytes (1,6) has shown that nodule formation is influenced by current density, lower densities yielding smoother deposits. Tests were therefore carried out with the fluoride electrolyte at lower current densities in the large cell for 6- and 7-hr runs. It was noticed that treeing and nodule formation were reduced. In this way the effective current efficiency was increased to some extent as shown in Table V, but it did not return to the high values obtained (40-45%) in the survey investigation.

Table IV. Effect of trivalent chromium concentration

Electrolyte composition				Time of electrolysis, hr	Temp, °C	Current efficiency, %
CrO_3, g/l	F, g/l	Cr, g/l				
295	4.74	1.45 as Cr_2O_3		1	102	42
		Artificially aged				
		Start	Finish			
292	5.2	15	3	1	102	42
280	5.0	27	2.94	1	102	39.5

Table V. Effect of reduced current density on chromium recovery

Electrolyte composition		Current density, amp/ft²	Current efficiency, %
CrO_3, g/l	F, g/l		
300	5.24	1000	32
310	5.46	910	34.5
305	5.62	800	33.5
306	5.60	660	34.8

Fluosilicate contamination in fluoride electrolyte.—As stated previously no precautions were taken to protect the glassware from etching by the fluoride in the electrolytes used. In the 1-hr experimental runs this factor was considered negligible since the time was short and fresh electrolyte was used for each test. An analysis of the electrolyte which had been in the larger 10 l glass cell for a period of approximately 3 months showed a fluosilicate content of the order 0.6-0.7 g/l SiF_6. This represents a tie-up of 0.5 g/l fluoride which would upset the effective fluoride-chromic acid ratio. This fluosilicate contamination may have contributed to the continual decrease in current efficiency but only to a minor extent, by producing a slight variation in the chromic acid catalyst ratio which could be eliminated by using an inert cell lining.

Effects of Impurities in the Electrolyte

Sulfate.—Since high-purity chromic acid would be uneconomical for full-scale chromium production, some tests were carried out using a commercial grade of chromic acid having the following impurity levels: 0.5-0.8% SO_4, 0.003% NO_3, and less than 0.5% metallics. This was found to produce chromium at much lower current efficiencies than those obtained when pure chromic acid was used. It has been reported (2,8) that sulfate additions in fluoride and fluosilicate electrolytes are associated with a decrease in current efficiency. This led to a series of experiments in which sulfate was (*a*) purposely added to a pure chromic acid electrolyte and (*b*) completely removed from a commercial chromic acid electrolyte by precipitation with barium hydroxide, but without introducing excess barium as a further variable. Results are given in Table VI and show that the sulfate impurity in commercial chromic acid appreciably reduces the current efficiency of the fluoride electrolyte.

Tin.—The use of a 7% tin-lead alloy as an anode in the electrodeposition of fluoride chromium introduced the possibility of tin traces being entrapped in the chromium. Using spectrographic and polarographic analysis, 0.005 wt % tin was detected in the chromium. This was not considered of a sufficiently high value to influence the properties of the metal. Further tests were carried out using a pure tin

Table VI. Influence of electrolyte sulfate impurity

Electrolyte	Nominal composition CrO_3, g/l	F, g/l	SO_4, g/l	Current efficiency, %
Commercial CrO_3	300	5	0.65	26
	300	5	0.24	31
Commercial CrO_3 SO_4 pptd. with $Ba(OH)_2$	300	5	Trace	42
Pure CrO_3 with added SO_4	300	5	0.56	29

anode, but even in this extreme case the deposited chromium showed only 0.08% tin. These results are given in Table VII, which also shows that plating ceased during the run with the tin anode. This suggested that while tin might not cause serious contamination of the electrodeposit, it could have a deleterious effect on the performance of the electrolyte. This was confirmed by tests in electrolytes deliberately contaminated with tin, where the current efficiency decreased with increasing tin content, as indicated in Table VII. This factor is discussed further in the following section.

Alternative Anode Materials

As demonstrated above tin contamination of the electrolyte resulted in an efficiency decrease and may arise when using 7% tin-lead anodes continuously. Therefore several alternative anode materials were studied, the primary requirements being an alloy which would remain active and not contaminate either the electrolyte or the deposit. Alloys examined were Pb-7% Sn, -4% Sn, -1% Sn, and 0.5% Sn; Pb-2% Ag; Pb-2% Zn; Pb-2% Ag -2% Zn; Pb-1% Na, and Pb-0.5% Te. The alloys which proved to be most resistant to the fluoride solutions were the Pb-Sn alloys (0.5-4% Sn), Pb-Te, Pb-Ag, Pb-Na. The Pb-Na alloy was particularly brittle and for this reason was not selected. Using the Pb-2% Ag anode, silver was detected in the chromium. It was found that the concentration of tin in the lead anode could be reduced to 0.5% and still maintain an active anode. The probable level of contamination using this anode composition was considered negligible, and it was used in all further tests.

Chromium Deposition in a Polyethylene Lined Plating Cell

Because of the danger of fluosilicate contamination, inert lining materials were investigated. Polyethylene was found to be resistant to the highly active solution but it softened at the high temperatures. However, providing the lining was well supported this was not a major problem.

A polyethylene-lined vessel was designed which consisted essentially of a steel tank (10-12 l capacity) lined first with lead and then with polyethylene. To a lid, which was similarly lined, were attached the electrode inlets and the outlet for waste gases which included a polyethylene-tube spiral condenser. During electrolysis the lid was sealed to the cell with a polyethylene gasket.

The electrolyte, containing 300 g/l CrO_3-5.4 g/l F, was prepared from commercial grade chromic acid, the sulfate impurity being precipitated with barium hydroxide. The results of deposition in this bath are listed in Table VIII; all runs are of 6-7 hr duration. Simultaneous tests, using sample electrolytes from the large bath, were carried out in the small experimental cell and showed higher efficiency values (see Table VIII). These tend to show that the time for deposition or thickness of deposit is the main factor in the low efficiencies recorded in the larger scale cells. The chromium produced in the large cell was of a high order of purity and the current efficiency, although lower than anticipated, remained relatively constant during the tests.

Properties of "Fluoride" Chromium

Chromium deposited from the fluoride electrolyte has been arc-cast, extruded, swaged, and rolled using procedures similar to that already reported (9,10) for chromium deposited from the chromic acid-sulfate electrolyte. Thus it was possible to compare the properties of cold-worked and recrys-

Table VII. Effect of tin contamination in the electrolyte

Electrolyte composition CrO_3	F, g/l	Sn, g/l	Anode material	Tin in chromium, wt %	Current efficiency, %
300	5.4	—*	Pb — 7% Sn	0.005	42
300	5.4	—*	Pure Sn	0.08	Plating ceased during run
300	5.32	0.0	Pb — 0.5% Te	—*	38
300	5.32	4.6	Pb — 0.5% Te	Tin detected spectrographically	15.0
300	5.32	7.4	Pb — 0.5% Te		9.6

* Not determined.

Table VIII. Deposition of chromium in polyethylene-lined cell

Electrolyte composition CrO_3, g/l	F, g/l	Temp, °C	Current density, amp/ft²	Current efficiency, %	Current efficiency in test cell, %	Oxygen, wt %	Nitrogen, wt %
310	5.4	100-102	880	34	38	0.008	0.001
306	5.32	100-102	800	26	34	Not detected	Not detected
300	5.36	100-102	640	25	36	Not detected	Not detected
300	5.2	100-102	880	24.5	32	Not detected	Not detected
300	5.3	100-102	760	25	34	Not detected	0.0005

Table IX. Transition temperatures of rolled "sulfate" and "fluoride" chromium

Material	Composition, wt %		Ductile/brittle transition in bending °C		Hardness (V.P.N.)	
	O_2	N_2	As rolled	Recrystallized	As rolled	Recrystallized
Sulfate Chromium	—	0.002	—60	380	—	—
	0.012	0.001		195	185	130
Fluoride Chromium	0.025	0.002	—87	121	219	115

Table X. Room-temperature tensile properties of rolled "sulfate" and "fluoride" chromium

Material	Tensile strength, psi	Elongation on $4\sqrt{\text{area}}$, %	Reduction in area, %
Sulfate Chromium	100,000	40	50
Fluoride Chromium	88,000	57	55

tallized fluoride chromium with those of the sulfate material. The ductile-brittle transition temperatures and tensile properties of these materials in the form rolled strip are listed in Tables IX and X, and show that the fluoride chromium can be fabricated equally as well as chromium deposited from the chromic acid-sulfate electrolyte and has superior ductility values.

Discussion

The most puzzling feature of this investigation is the decrease in current efficiency on changing from the small test cell experiments to the pilot plant stage. At first sight it would appear that this current efficiency decrease was excessive and that some simple explanation might be found in that variables such as trivalent chromium concentration, fluosilicate contamination, or tin impurity could have a deleterious influence. However as has been shown above none of these factors had any appreciable influence on the current efficiency. It was demonstrated that the trivalent ion concentration did not have any influence. The source of the fluosilicate contamination was removed by using a polyethylene lined vessel, and tin contamination was greatly reduced by replacing the 7% tin-lead anode by one containing 0.5% tin.

In view of the above it was considered that the major effect might be due to the nodule growth, treeing, and the general roughness associated with the deposition of thicker coatings than those obtained in the small cell. By comparison with the sulfate bath (1, 6) where efficiencies of the order 14% are obtained for runs of 1 hr but drops to 6-7% for periods up to 72 hr, it may well be anticipated that a current efficiency of 42% in the small fluoride bath for hourly runs could drop to 20% for plating times of say 20 hr giving an equivalent thickness of chromium to that obtained in the sulfate bath. This current efficiency is in fact very close to the one obtained in this investigation which was 25% for 8-hr runs in the pilot plant equipment. By analogy with the operation of the sulfate bath where it is possible, by improved control of the operating variables (10) and also continual purification of the electrolyte by ion exchange, to obtain current efficiencies of 9-10% it should be possible to achieve current efficiencies of 27-30% in the fluoride bath.

It is true that this comparison does not in any way explain why treeing and general surface roughness occurs in aged baths, but it does help to put the drop in efficiency found in the fluoride bath in perspective. An explanation of the phenomenon must wait on a more fundamental attack on the more basic factors operating in the electrodeposition of chromium for considerable periods of time.

In the fluoride electrolyte a minimum current efficiency at electrolyte temperatures between 70° and 80°C was noted. The latter temperature is the maximum at which previous investigators had worked when examining plating conditions for fluoride electrolytes. Because up to this temperature the current efficiency in fluoride electrolytes shows the same downward trend as in sulfate electrolytes it has presumably been concluded that the current efficiency in the former would continue to decrease as the temperature is raised. No explanation for the minimum in the current efficiency-temperature curve can be given on the basis of the present results.

Conclusions

1. The optimum conditions for the deposition of high-purity chromium were (*a*) for the chromic acid-fluoride electrolyte: electrolyte composition, 300 g/l CrO_3, 5.25 g/l F; current density, 1150 amp/ft²; electrolyte temperature, 100°-102°C; giving a current efficiency of 40-45% in 1-hr runs. (*b*) for the chromic acid-fluosilicate electrolyte: electrolyte composition, 300 g/l CrO_3, 6 g/l SiF_6; current density, 1150 amp/ft²; electrolyte temperature, 100°-102°C; giving a current efficiency of 38-40% in 1-hr runs. These conditions yielded chromium containing 0.03-0.04 wt % oxygen and 0.0008-0.002 wt % nitrogen.

2. The oxygen content of the chromium was sensitive to changes in catalyst concentration. The catalyst concentration which gave the maximum current efficiency also gave the minimum oxygen concentration. This impurity concentration decreased with increasing electrolyte temperature in the same manner as found in the sulfate electrolytes, but the average minimum value was higher (0.03 wt %) than for the sulfate product (0.01 wt %). This minimum value was not influenced by changes in current density or chromic acid concentration.

3. The nitrogen impurity level was not changed in any consistent manner by any of the variables investigated.

4. Deposition of chromium from the chromic acid-fluoride electrolyte under semi-production conditions was accompanied by a progressive decrease in current efficiency with time to a steady value of 25-30%. The following are the conclusions from the investigation of some of the variables which could effect current efficiency: (*A*) The trivalent chromium concentration did not influence current efficiency. (*B*) A decrease in the current density for large-scale tests produced a slight increase in cur-

rent efficiency due apparently to a decrease in nodule formation (*C*) Tin was detected in both the chromium deposit and the electrolyte, and it was shown that tin contamination could reduce the current efficiency. (*D*) Any sulfate impurity in the chromic acid used must first be removed since sulfate contamination was shown to be associated with a reduction in current efficiency. However, the decrease in current efficiency with time was greater than could be explained by any combination of these factors.

5. "Fluoride" chromium fabricated by arc-casting, extrusion, swaging, and rolling at 700°C possessed mechanical properties which compared favorably with those of "sulfate" chromium prepared by similar means.

Acknowledgments

The author would like to thank Mr. E. J. Lumley for all nitrogen analysis and Messrs. J. B. Dance and A. R. Edwards for continued encouragement and helpful discussion in the preparation of this report. For permission to publish this paper acknowledgment is also made to the Chief Scientist, Australian Defence Scientific Service, Department of Supply, Melbourne, Australia.

Manuscript received Nov. 16, 1959.

Any discussion of this paper will appear in a Discussion Section to be published in the December 1960 JOURNAL.

REFERENCES

1. H. T. Greenaway, *J. Inst. Metals*, **83**, 121 (1954-1955).
2. R. Bilfinger, *Metallwirtschaft*, **22**, 466 (1943).
3. T. A. Hood, *Metal Finishing*, **50**, 103 (1952).
4. A. Brenner, Polly Burkhead, and C. Jennings, *J. Research, Nat. Bur. Standards*, **40**, 31 (1948).
5. D. S. Reynolds and W. L. Hills, "Applied Inorganic Analysis," Hillebrand, Lundel, Bright and Hoffman, John Wiley & Sons, New York.
6. H. T. Greenaway, Unpublished work.
7. N. Ryan and E. J. Lumley, *This Journal*, **106**, 388 (1959).
8. R. MacNair, *Metal Ind.*, **73**, 448 (1948).
9. H. L. Wain, S. T. M. Johnstone, F. Henderson, and N. Louat, *J. Inst. Metals*, **86**, 281 (1957-1958).
10. J. J. Dale, Private communication.

Polarization of Luminescence in ZnS and CdS Single Crystals

A. Lempicki

General Telephone and Electronics Laboratories Inc., Bayside, New York

ABSTRACT

The fluorescent emission from hexagonal ZnS and CdS single crystals is found to be polarized preferentially perpendicular to the c axis for both polarized and unpolarized excitation. Cubic ZnS crystals emit unpolarized radiation. The results are analyzed in terms of a simple dipole theory which is shown to be inadequate for the description of luminescent centers in these materials. Preliminary observations on the polarization of fluorescence of ZnO crystals are reported.

The so-called Weigert effect (1) or polarization of fluorescence has been known for many years. A large amount of work has been done on the properties of organic molecules in various media (1, 2). The method has not been applied extensively to the inorganic luminescent materials. A notable exception is found in the work of Lambe, Compton, West, and Klick (4-7) in this country and Feofilof (3) in Russia. The substances investigated by these authors were mostly halides.

Recent successes in the growth of single crystals of the sulfides (8, 9) made it possible to apply the polarization techniques to the study of the luminescent centers in these materials.

The simplest physical model of a luminescent center can be conceived as an atomic or molecular aggregate giving rise to a classical electric oscillator. If this is the case, the polarization studies should enable us to determine the components of the polarizability tensor and the orientation of the oscillator in the lattice.

Usually the measurement of polarization is made in the longitudinal direction as illustrated on Fig. 1. The fluorescent medium is at the origin of the coordinates O and is excited by an electromagnetic wave propagated along the $-x$ axis. The electric vector E is parallel to z. Observations are made through an analyzer A which can be rotated either parallel or perpendicular to E. One introduces a quantity p:

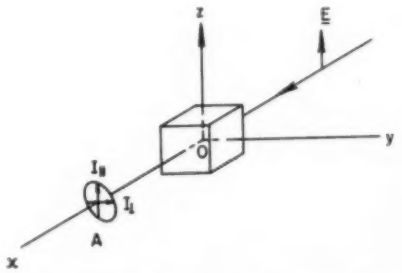

Fig. 1. Measurement of polarization-longitudinal experiments.

$$p = \frac{I_\parallel - I_\perp}{I_\parallel + I_\perp} \; ; \; -1 \leq p \leq 1 \qquad [1]$$

where $I_{\parallel}$ and $I_{\perp}$ are the observed intensities of fluorescence for the two directions. The theories of the effect aim at calculating p from a suitable model of the fluorescent center. There are various degrees of sophistication in these theories which are briefly described.

The Rayleigh-Tyndall model.—For monochromatic excitation one assumes that the fluorescence is essentially a scattering process without change of wave length. As in Rayleigh scattering the intensity in any given direction is proportional to the square of the dipole moment μ. This moment is determined by the polarizability tensor α through the equation

$$\mu = \alpha \underline{E}$$

In crystals it is assumed normally that the principal axes of this tensor are oriented along main crystallographic directions. In spite of the usually large Stokes shift ($\lambda_{absorption} < \lambda_{emission}$). This simple model has been used successfully in determining the symmetries of some luminescent centers in halides (4) and in diamond (10).

Separate absorption and emission oscillators.—It has been first pointed out by Perrin (11) in connection with work on fluorescent solutions that sometimes it may be necessary to postulate two different kinds of oscillators. The exciting energy is first absorbed by an absorption oscillator and then transferred to an emission oscillator. This formally allows for a shift in energy between absorption and emission and accounts for negative values of p sometimes observed in solutions. Feofilof has used essentially the same model in determining the symmetry of luminescent centers in CaF_2 and NaF (3). In this case the sign and magnitude of p change with the exciting wave length, and it is necessary to introduce two separate oscillators.

The models (a) and (b) are essentially classical although Jablonski (12) and Lafitte (13) have used quantum mechanical methods in describing the energy transfer between the two sets of oscillators.

Quantum mechanical treatment.—If the symmetry of the crystal and luminescent center are known, it is possible to write down selection rules for dipole transition (14). In a still more refined treatment the matrix elements could be computed, and from these one should be able to estimate p.

Experimental Methods

The experimental arrangement is represented schematically in Fig. 2. A mercury arc source is placed at S. The 3650Å radiation is isolated by means of filter 1 and passes through a Glen-Thompson polarizer which can be rotated about the x axis (θ). The fluorescence generated in specimen C passes through a polaroid analyzer and is detected by a photomultiplier Ph. Filter 2 has a sharp cut-off for the exciting radiation. The optical system of a Zeiss polarizing microscope was adapted for the measurements.

There are several important precautions which must be taken in order to obtain reliable results. Most important is that no polarized excitation reaches the detector. This is achieved by suitable

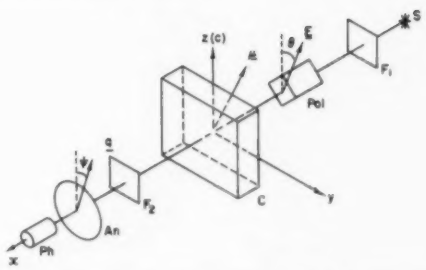

Fig. 2. Experimental arrangement for the measurement of polarization. S, radiation source; F_1, filter; Pol, polarizer; C, crystal; R_2, filter; An, analyzer; Ph, photomultiplier.

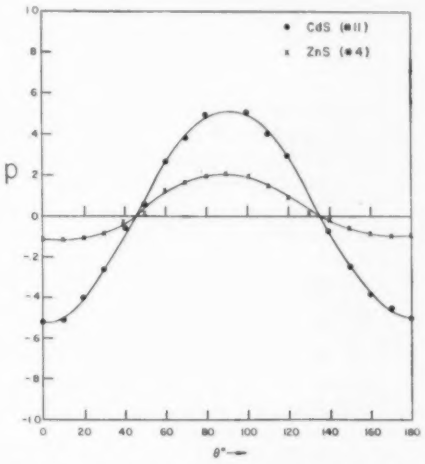

Fig. 3. Polarization factor p vs. the azymuth θ for a CdS and ZnS:Cu crystal. For θ = 0 the exciting electric vector is parallel to the c axis.

combinations of filters 1 and 2. The specimens in form of plates are mounted over a diaphragm. The exciting beam is made nearly parallel by removing the microscope condenser and using suitable stops. It is important that the numerical aperture of the objective gathering the fluorescence be as small as possible. The reason for this is given in the appendix.

Since the angles θ and Ψ can be set independently we can generalize Eq. [1] and define p as

$$p(\theta) = \frac{I(\Psi = \theta) - I\left(\Psi = \theta + \frac{\pi}{2}\right)}{I(\Psi = \theta) + I\left(\Psi = \theta + \frac{\pi}{2}\right)} \qquad [2]$$

In our measurements we have chosen the z axis to coincide with the c axis of the crystals. In case of excitation with natural (unpolarized) light the angle θ is, of course, not specified. We define then for this case

$$p_n = \frac{I(\Psi = 0) - I\left(\Psi = \frac{\pi}{2}\right)}{I(\Psi = 0) + I\left(\Psi = \frac{\pi}{2}\right)} \qquad [3]$$

It should be noted that measurements with natural light are much more sensitive than with polarized light. The reason for this is that, if the filter system

Table I. Polarization data

Type	Impurity, mole %	Fluorescence peak, Å	Structure	p(0°)	p(90°)	p_n
1. ZnS	Cu 2×10^{-4}		Hex.			−0.24
2. ZnS	Cu 2.10^{-4}		Hex.			−0.24
3. ZnS:Cu	0.02	4500	Hex.	−0.03	0.20	−0.12
4. ZnS:Cu	0.02	4500	Hex.	−0.11	0.20	−0.16
5. ZnS:Cu	0.02	4500	Hex. (cub)	−0.07	0.16	−0.09
6. ZnS	Cu 2×10^{-1}		Hex. (cub)	−0.08	0.12	−0.11
7. ZnS	Cu 0.01	4500	Cub.	0.00	0.00	0.00
8. ZnS:Mn	0.1	5750	Cub.	0.00	0.00	0.00
9. ZnS:Mn	1.0	5750	Cub. (hex)	−0.03	0.07	−0.05
10. ZnS:Mn	1.0	5750	Cub. (hex)	−0.06	0.02	−0.02
11. CdS		6800	Hex.	−0.52	0.51	−0.50
12. ZnO	Clear	5180	Hex.	0.00	0.00	0.00
13. ZnO	Clear	5180	Hex.	0.00	0.00	0.00
14. ZnO	Red	5130	Hex.	0.27	−0.25	0.28
15. ZnO	Red	5130	Hex.	0.48	−0.48	0.45

(1 and 2) is not ideal and the fluorescence weak, then an appreciable fraction of the excitation can reach the photomultipler. If it is polarized, it will affect the value of p. With natural light this leaking excitation can produce only a constant background independent of the setting of the analyzer.

Results

The ZnS crystals (Table I) used in this investigation were grown by a vapor phase method by Kremheller and Samelson of our Laboratories. Some of them were deliberately activated (by doping the starting powder) with Cu and Mn. Others were used as grown. The impurity concentration is given in the second column of Table I.

Specimens designated by ZnS:Cu and ZnS:Mn were doped intentionally during growth. Those designated by ZnS had only accidental impurities. The concentration of impurities was determined on a random selection of crystals from the same growth batch.

The requirements of bright fluorescence and plate-like geometry with the c axis in the plane of the plate seriously limit the number of suitable specimens. A fluorescent spectrum (under 3650Å excitation) was obtained on crystals which were sufficiently bright and the peak is given in the third column. X-ray analysis was obtained for all specimens. Crystals 1 and 2 are essentially free of stacking disorder and birefringence banding. All other ZnS specimens show varying amounts of both. Some, like 5, 6, 9 and 10, show, besides the main structure, diffraction spots due to the other phase. This is indicated in brackets. The remaining three columns of Table I give the values of p for excitation polarized parallel to c, perpendicular to c and natural light.

All the ZnS and CdS crystals, except 7 and 8, which are cubic, show a fluorescence preferentially polarized perpendicular to the c axis. The intensity was too weak for crystals 1 and 2 to measure p(0°) and p (90°), but these crystals have the highest values of p_n observed on any specimen of ZnS. The presence of disorder which is equivalent to the introduction of the cubic phase is seen to decrease the magnitude of p. Table I does not include numerous results obtained on cubic crystals many of which were electroluminescent. No polarization of fluorescence or electroluminescence was found in these. Unfortunately, no hexagonal ZnS:Mn crystals comparable in perfection with specimens 1 and 2 were available. This makes it difficult to distinguish between the property of the luminescent centers (Mn and Cu) and the lattice. It is impossible to compare ZnS:Cu an ZnS:Mn crystals which show different amounts of disorder.

Specimen 11 is a hexagonal CdS crystal with an emission peak near 6800Å.[1] Its fluorescence is also polarized perpendicular to c with a value of $|p| = 0.5$ considerably higher than in ZnS crystals.

Figure 2 gives the variation of p (θ) as a function of the azymuth θ for crystals 4 and 11. The CdS curve is symmetrical about the x axis and can be represented by an equation of the form $p(\theta) = -\frac{1}{2}\cos 2\theta$. If we make measurements with natural light excitation and plot p_n as a function of the angle Ψ we obtain a similar result $p_n = -\frac{1}{2}\cos 2\Psi$. This means that the polarization is quite independent of the mode of excitation. For ZnS the results are somewhat different. As seen from Table I and Fig. 2 we have in general

$$|p|\ (0°)\ | < |p_n| < |p\ (90°)$$

It should be stressed that quantitative measurements of polarization require a rather high degree of external crystal perfection. This is demonstrated by the following observations. One specimen of CdS consisted of a very clear plate joined to a thicker heavily striated part. Measurements of polarization were made in the two regions. In the clear portion p_n was about −0.3, whereas it decreased to almost zero in the less perfect part. To further check the effect of surface we have etched crystal 11 in HNO_3. The previously shiny surface turned rough and the polarization decreased from $p_n = 0.5$ to $p_n = -0.18$.[2] We believe that in specimens 1, 2, and 11 no surface depolarization effects were present.

Miscellaneous Observations

We have observed a polarization of the green electroluminescence in pure (nonphotoluminescent)

[1] The crystal was obtained from Dr. I. Broser of the Fritz Haber Institut der Max Planck Gesellschaft, Berlin. Beyond the presence of silver its exact impurity content is unknown.

[2] That a rough surface produces depolarization can be demonstrated by placing a ground glass plate between the crossed polarizers of a microscope. The field of view will not extinguish.

CdS. The crystals had Ga electrodes which had to be "formed" (15). These measurements were rather difficult because of the instability of emission. Values of p up to -0.3 were observed. The electroluminescence is thus also preferentially polarized perpendicular to c.

Some measurements were also made on ZnO crystals of two distinct types. Clear and transparent crystals (12, 13) obtained from vapor phase reaction show a weak *body* photoluminescence peaking at 5180Å. No polarization effects were observed on these. The second category (14, 15) obtained from zinc refineries have a deep red color and an intense fluorescence confined to a *surface* layer. The peak of the fluorescence confined to the surface layer is only slightly lower (5130Å) than that of the clear crystals. However, polarization is quite marked and in this case polarized preferentially parallel to c. A tentative explanation of this effect in terms of surface and volume properties has been proposed by Birman (16).

Discussion

One important question which must be settled before we draw conclusions from our results is the possible effect of dichroism. In ZnS, according to data of Piper, *et al.* (17) and Balkanski and Waldron (18), α ($\|$ c) $<$ α ($\perp$ c), where α ($\|$ c) and α ($\perp$ c) are the absorption constants for light polarized parallel and perpendicular to c. Hence, if fluorescence emission was initially unpolarized, it would become preferentially polarized parallel to c as it travels from the luminescent center to the surface of the crystal. This is contrary to our observations and thus dichroism cannot be responsible for the results. The situation is more complicated in the case of CdS for which α ($\|$ c) becomes larger than α ($\perp$ c) at wave lengths larger than 5350Å (12). Here dichroism could in principle produce the observed polarization at 6800Å. This point was checked directly by illuminating the crystal with unpolarized radiation approximating in wave length the fluorescent emission. The amount of polarization introduced by dichroism in both CdS and ZnS crystals was found to be below the experimental error and thus of no importance for our measurements.

In order to see whether the Rayleigh-Tyndall theory of scattering can account for the observed polarization we shall consider a very general model for the luminescent centers. Let us assume that there are n of them in the volume of the crystal under observation. Each center will be characterized by a certain polarizability tensor α^n_{ij}. The x, y, z coordinate system of Fig. 2 may or may not coincide with the principal axes system of some centers. The polarizability tensors of some centers may be identical.

The exciting radiation produces a dipole moment μ^n in each center. The direction of this moment is determined by the α^n_{ij} — s and the exciting electric field intensity E. Since observations are made along the x axis, only the components μ^n_y and μ^n_z will contribute to the observed intensity. These are given by

$$\mu^n_y = \alpha^n_{yy}\ \mathrm{E}\sin\theta + \alpha^n_{yz}\ \mathrm{E}\cos\theta$$
$$\mu^n_z = \alpha^n_{yz}\ \mathrm{E}\sin\theta + \alpha^n_{zz}\ \mathrm{E}\cos\theta \qquad [4]$$

Where θ is the angle between E and the z axis (Fig. 2). Since the polarizability tensor is symmetrical (19) only three components for each center (α^n_{yy}, α^n_{zz}, α^n_{yz}) determine the intensity.

The magnitude of the scattered (photoluminescent) intensity depends on the coherency of scattering from the various dipoles. In the absence of definite information about this we compute the intensity for both complete coherency (I_c) and complete incoherency (I_i). We have

$$I_c(\theta,\Psi) \sim \sum_n (\mu^n_y \sin\Psi + \mu^n_z \cos\Psi)^2$$
$$I_i(\theta,\Psi) \sim [(\sum_n \mu^n_y)\sin\Psi + (\sum_n \mu^n_z)\cos\Psi]^2 \qquad [5]$$

From Eqs. [5], [4], and [2] we can compute the polarization factors for both cases (Eq. [6] and [7]). The corresponding equations for natural light excitation are obtained by averaging Eq. [5] over θ and substituting in Eq. [3] (Eq. [8] and [9]).

$$p_c(\theta) = \frac{[2\mathrm{C}\,(\mathrm{B}^2\cos^2\theta + \mathrm{A}^2\sin^2\theta) + \mathrm{AB}\sin 2\theta]\sin 2\theta + [(\mathrm{B}^2\cos^2\theta - \mathrm{A}^2\sin^2\theta) - \cdots}{(\mathrm{B}^2\cos^2\theta + \mathrm{A}^2\sin^2\theta) + 2\mathrm{C}\,(\mathrm{B}\cos^2\theta + \mathrm{A}\sin^2\theta)\sin 2\theta + \cdots\cdots}$$
$$\cdots\cdots \frac{-(\mathrm{A}-\mathrm{B})\sin 2\theta - \mathrm{C}^2\cos 2\theta]\cos 2\theta}{+[(\mathrm{A}-\mathrm{B})\sin 2\theta + \mathrm{C}^2\cos 2\theta]} \qquad [6]$$

and

$$p_i(\theta) = \frac{(\mathrm{A}'\cos^2\theta - \mathrm{B}'\sin^2\theta)\cos 2\theta - \mathrm{C}' + (2\mathrm{C}' + \mathrm{F}')\sin^2 2\theta + 2(\mathrm{D}'\sin^2\theta + \cdots\cdots}{(\mathrm{A}'\cos^2\theta + \mathrm{B}'\sin^2\theta) + \mathrm{C}' + 2(\mathrm{D}'\sin^2\theta + \mathrm{E}'\cos^2\theta)\sin 2\theta + \cdots\cdots}$$
$$\cdots\cdots \frac{+\mathrm{E}'\cos^2\theta)\sin 2\theta + \frac{1}{2}(\mathrm{E}'-\mathrm{D}')\sin 4\theta}{+\frac{1}{2}(\mathrm{D}'-\mathrm{E}')\sin 4\theta} \qquad [7]$$

$$p_{rc}(\Psi) = \frac{\mathrm{B}^2-\mathrm{A}^2}{\mathrm{A}^2+\mathrm{B}^2+2\mathrm{C}^2}\cos 2\Psi + \frac{2(\mathrm{A}+\mathrm{B})\mathrm{C}}{\mathrm{A}^2+\mathrm{B}^2+2\mathrm{C}^2}\sin 2\Psi \qquad [8]$$

$$p_{ri}(\Psi) = \frac{\mathrm{B}'-\mathrm{A}'}{\mathrm{A}'+\mathrm{B}+2\mathrm{C}'}\cos 2\Psi + \frac{2(\mathrm{D}'+\mathrm{E}')}{\mathrm{A}'+\mathrm{B}'+2'\mathrm{C}}\sin 2\Psi \qquad [9]$$

The constants are

$$A = \sum_n \alpha^n_{yy} \qquad A' = \sum_n (\alpha^n_{yy})^2$$
$$B = \sum_n \alpha^n_{zz} \qquad B' = \sum_n (\alpha^n_{zz})^2$$
$$C = \sum_n \alpha^n_{yz} \qquad C' = \sum_n (\alpha^n_{yz})^2$$
$$D' = \sum_n \alpha^n_{yy}\alpha^n_{yz}$$
$$E' = \sum_n \alpha^n_{zz}\alpha^n_{yz}$$
$$F' = \sum_n \alpha^n_{yy}\alpha^n_{zz} \qquad [10]$$

Although the formulas are rather complicated, we can draw from them certain general conclusions, at least in the case of CdS. First, let us remark that for natural light excitation the polarization factors have the form $p_n \sim R \cos(2\theta + \phi)$, where R is an amplitude and ϕ a phase. Any partially polarized radiation must give rise to such a dependence. The important fact is that experimentally we find $R = -\frac{1}{2}$ and $\phi = 0$ (for CdS). This eliminates the sin 2Ψ term in Eq. [8] or [9]. Thus we must have $C = D' = E' = 0$. We now have to consider the coherent and incoherent case separately.

For the coherent case, the requirement $R = -\frac{1}{2}$ yields $A'^2 = 3B'^2$. If we substitute this into Eq. [6] we see that there is no way of reducing it to $-\frac{1}{2} \cos 2\theta$, which the experiment indicates.

For the incoherent case, we have from Eq. [9]:

$$\frac{B' - A'}{A' + B' + 2C'} = -\frac{1}{2}$$

Again, Eq. [7] cannot be reduced to the form $-\frac{1}{2} \cos 2\theta$ with the three arbitrary constants A', B', C' and the condition $A' \neq B'$.

Before we form our conclusions, let us dispose of a certain approximation which we have not mentioned explicitly. We have assumed that the exciting electric field components are $E \sin\theta$ and $E \cos\theta$ (see Eq. [4]). In fact, for ZnS at the excitation wave length of 3650Å the absorption constant α ($\perp$c) is larger than α ($\parallel$c). For CdS no measurements are available. If the same is true for CdS as for ZnS, we should use for the y component $E\,\sigma \sin\theta$ where σ represents an attenuation factor ($\sigma < 1$) as compared with the z component. If we recalculate the polarization factors Eqs. [6], [7], [8], and [9] in terms of σ we still cannot reduce simultaneously [6] and [8] or [7] and [9] to the experimentally observed form of $-\frac{1}{2} \cos 2$ (angle).

Thus, in the case of CdS, and in contrast to diamond and the halides, a model involving arbitrarily oriented anisotropic dipoles cannot account for the results.

The case of ZnS is more complicated because the $p(\theta)$ curves show an asymmetry (Fig. 2) and, therefore, a dependence of polarization of emission on the mode of excitation. It should be stressed that it is very important to obtain measurements of p as a function of θ over a whole period and not only at isolated points. Only then can one draw meaningful conclusions as to the adequacy of the dipole model of a luminescent center.

Finally, even in the case of CdS, it may be possible to construct a model involving two oscillators per center and account for the observations. In such a center an energy transfer would take place. This possibility has been discussed by Dexter (22) and lately by Malemed (23). On the other hand, it is possible to account for the polarization measurements qualitatively in terms of the symmetry of the valence bands in these materials rather than the center itself. A fuller discussion of the various possibilities is given in the accompanying paper by Birman (16).

Acknowledgments

The author is indebted to Drs. A. Kremheller and H. Samelson for the ZnS crystals, to I. Broser for the CdS crystal, to Dr. R. W. Smith, of RCA, for the electroluminescent CdS crystals and to Dr. A. R. Hutson, of B.T.L., for the ZnO crystals. Mr. V. A. Brophy and S. Kellner performed the x-ray analysis and Dr. J. L. Birman has contributed by his discussions and criticism.

Manuscript received Nov. 9, 1959. This paper was prepared for delivery before the Philadelphia Meeting, May 3-7, 1959.

Any discussion of this paper will appear in a Discussion Section to be published in the December 1960 JOURNAL.

REFERENCES

1. P. Pringshein, "Fluorescence and Phosphorescence," Interscience Publishers Inc., New York (1949).
2. T. Forster, "Fluorescenz Organischer Ferbindungen," Vandenloeck and Ruprecht, Gottingen (1951).
3. P. P. Feofilof, *J. Phys. Rad.*, **17**, 656 (1956).
4. J. Lambe and W. D. Compton, *Phys. Rev.*, **106**, 684 (1957).
5. W. D. Compton and C. C. Klick, *ibid.*, **110**, 349 (1958).
6. J. Lambe and E. J. West, *ibid.*, **108**, 634 (1957).
7. C. C. Klick and W. D. Compton, *J. Phys. Chem. Soc.*, **7**, 170 (1958).
8. A. Kremheller, *Sylvania Technologist*, **3**, 11 (1955).
9. L. C. Green, *et al.*, *J. Chem. Phys.*, **29**, 1375 (1958).
10. R. J. Eliott, I. G. Matthews, and E. W. J. Mitchell, *Phil. Mag.*, **3**, 360 (1958).
11. F. Perrin, *Ann Phys. Paris*, **12**, 169 (1929).
12. A. Jablonski, *Acta Phys. Pol.*, **10**, **33** (1950), **10**, 194 (1950).
13. E. Laffitte, *Ann. Phys. Paris*, **10**, 71 (1955).
14. J. L. Birman, *Phys. Rev. Let.*, **2**, 157 (1959).
15. R. W. Smith, *Phys. Rev.*, **105**, 900 (1957).
16. J. L. Birman, *This Journal*, **107**, 409 (1960).
17. W. W. Piper, *et al.*, *Phys. Rev.*, **110**, 323 (1958).
18. M. Balkanski and W. Waldron, *ibid.*, **112**, 123 (1958).
19. M. Born, "Optik," p. 308, Springer, Berlin (1933).
20. J. F. Nye, "Physical Properties of Crystals," p. 300, Clarendon Press, Oxford (1957).
21. C. W. Bunn, "Chemical Crystallography," Oxford (1946).
22. D. L. Dexter, *Phys. Rev.*, **108**, 630 (1957).
23. N. T. Malemed, *J. Phys. Chem. Soc.*, **7**, 146 (1958).

APPENDIX

Imagine the dipole moment μ (Fig. 2) of an oscillator to be decomposed into three components μ_x, μ_y, μ_z. By making $\psi = 0°$ or 90° we would like to obtain a signal due only to the components μ_z or μ_y, respectively. The intensity of radiation is zero along the axis of a dipole but increases as the square of the sine of the colatitude angle away from the axis. Thus, if the aperture is large, part of the radiation due to μ_z will also be intercepted by the objective. The ratio of the intensities due to the components μ_x, μ_y, μ_z is given by

$$\frac{I(\mu_x)}{I(\mu_z)} = f(\gamma)\frac{\mu_x^2}{\mu_z}; \quad \frac{I(\mu_y)}{I(\mu_z)} = f(\gamma)\frac{\mu_y^2}{\mu_z}$$

where sin γ is the numerical aperture of the objective. f (γ) can be obtained by computing the ratio of the fluxes through the objective from the dipole radiation intensity formula $I \sim \sin^2\theta\mu^2/r^2$. In Table II we give a few values of f (γ) for different objectives. If all the components of μ are equal the last column gives the percentage admixture of the unwanted $I(\mu_x)$ component. In most of our work we used the first objective.

Table II. Effect of numerical aperture

Sin γ	f(γ)	%I(μ_x)
0.08	332	0.30
0.22	48.4	2.06
0.45	11.2	8.92

Polarization of Fluorescence in CdS and ZnS Single Crystals

Joseph L. Birman

General Telephone and Electronics Research Laboratories Inc., Bayside, New York

ABSTRACT

The polarization of fluorescence in hexagonal (wurtzite) crystals of CdS and ZnS gives a clue to the symmetry of the states between which the luminescent transition occurred. Unfortunately this clue is at present equivocal; there are many models for the center which would be consistent with the observed polarization.

Various symmetry properties of the wurtzite structure are discussed; the band structure of CdS and ZnS at k = 000 is discussed. These symmetry and band structure considerations are used to set up and consider various models, Lambe-Klick, Schoen-Klasens, etc., which would be in accord with observation of polarization. It is concluded that the Lambe-Klick model is the simplest which is in accord with the presently available observations. Some experimental tests are proposed which should help the descision among the various models. In conjunction with other single crystal optical, electrical, and magnetic measurements, polarization studies may prove decisive in obtaining quantitative knowledge about the centers in sulfides.

Although the sulfide phosphors have been studied for many years and a great deal of progress has been made in rationalizing their luminescent, photoconductive, and electroluminescent properties by means of particular theoretical models, basic uncertainty remains concerning the chemical nature and energy level structure of the luminescent center in these materials. It was with the hope of contributing to the clarification of the energy level structure of certain important phosphors that the work reported by Lempicki (1) was undertaken. The problem of the chemical nature of the center (the local atomic constituents and configurations) is not discussed in this paper: rather we shall focus on the energy level structure of centers, in the simplest phosphors, which would be consistent with the polarization observations. Because of its simplicity we shall emphasize the Lambe-Klick model, without losing sight of the fact that at the present time no definitive choice of model can be made. Certain experiments will be suggested on the basis of which a decision may be made between the different models.

In Table I a summary is given of the major aspects of the experimental situation presented in Lempicki's paper. We note that the polarization of luminescence at room temperature (3650Å excited) in hexagonal CdS:Ag and ZnS:Cu is considerable but not complete. For CdS:Ag the degree of polarization of fluorescence is constant and independent of polarization of the exciting radiation. For ZnS:Cu we note structure sensitivity, as well as a slight dependence on the polarization of the exciting radiation (1). Some problems which the model should answer are: (*a*) origin of polarization; (*b*) the fact that polarization is not 100% at room temperature; (*c*) polarization of fluorescence is (in CdS:Ag) independent of polarization of exciting radiation; and (*d*) the sensitivity of the ZnS polarization results on the underlying crystal structure.

Table I. Summary of polarization experiments

Material	Radiation	Temp	$I_\perp/I_\parallel$
CdS:	EL	>300°C	1.5
	edge‡	liq N_2	6.3
CdS:Ag	6200	RT**	3
ZnS:Cu			
(hex)	4300	RT	~1.25
(cubic)	4500	RT	1*
ZnO			
(surface)	5130	RT	0.33†
(volume)	5180	RT	1*

* Unpolarized emission.
† Preferentially polarized || to crystal c axis.
‡ D. Dutton, *J. Phys. Chem. Solids*, 6, 101 (1958).
** RT signifies room temperature measurement.

No discussion of the ZnS:Mn results is given. Some possible models for the ZnO results are put forward in the Appendix.

Band Models for the Sulfide Centers

One common model which was introduced for the centers in the sulfides was the so-called Schoen-

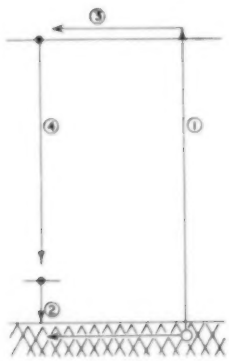

Fig. 1. Schoen-Klasens model for luminescent cycle in the sulfides.

Klasens band model (2). This model is illustrated in Fig. 1. According to the Schoen-Klasens model, the process of luminescence occurs as follows: If an incident photon is absorbed, with energy within the fundamental absorption edge, a free electron and a hole are created. The hole is captured by the center, which thus loses its electron. Since the energy level of the ground state of the center is assumed close to the valence band of the crystal, little energy is released when the hole is captured. (This energy is degraded in the form of infrared emission or thermal energy given up to the lattice.) The center, with a hole localized in it, at an energy level close to the valence band, is now in position to participate in the process of luminescence. Luminescence occurs when a free electron, which has been created by an incident photon, is captured by the hole localized at the center.

More recently, Lambe and Klick (3) have proposed an alternate model, which is shown in Fig. 2. In this model, the ground state of the center consists of an electron bound in an energy level close to the conduction band. As before, the process of luminescence may occur when an incident photon creates an electron and a hole in the crystal. However, if the center is filled initially, the first step, i.e., capture of a hole by the center, is the luminescent process. Subsequent capture of an electron by the empty center serves only to prepare the center again for later participation in further luminescent cycles. In this model, we see that in a certain sense

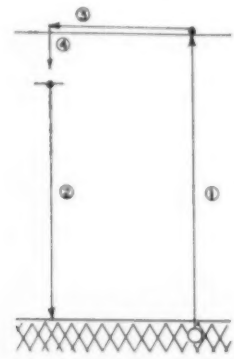

Fig. 2. Lambe-Klick model for luminescent cycle in the sulfides.

it is the free hole which dominates the process of luminescence.

In both the Schoen-Klasens and Lambe-Klick models, luminescence and photoconductivity are intimately connected by means of the energy bands in the phosphor—the luminescent process involving the transition of a "free" carrier in an energy band to a bound state (4). If this type of model is correct, it is understandable that the polarization results (1) could not fit into a simple classical oscillator picture: the band scheme is quantum mechanical, with no strict classical analogue. However, without further modification neither Schoen-Klasens nor Lambe-Klick models indicate how polarization may arise. While the weight of experimental evidence in the sulfides seems to favor either Schoen-Klasens or Lambe-Klick "band" models for the centers (5), other possible models cannot be ruled out. In particular, a "two oscillator" model—separate absorption and emission oscillators—may be at least mentioned. For example, in ZnS the absorbed 3650Å radiation may create excitons which then decompose at the center, emitting the characteristic fluorescence. (Even more general kinds of mechanisms might be envisioned for separate absorption and emission processes.) Such processes, within the two oscillator framework, would focus attention on the details of the recombination processes within a more or less isolated center, rather than upon band-center processes (within the context of such models the apparent connection between photoconductivity and luminescence would be more complex to explain than for the band models).

In any event to know how to get the necessary anisotropy to yield polarization requires study of the symmetry of the wurtzite lattice, both for examination of band-center processes and recombination processes within a center located at a particular site. In the next section, certain results pertaining to the effect of the symmetry of hexagonal (wurtzite) lattice on optical selection rules are summarized. An understanding of the effects associated with the symmetry of the hexagonal structure is necessary for us to proceed with further consideration of models.

Symmetry of Wurtzite and Zinc Blende Structures

All of the descriptive information about wurtzite or zinc blende structures is contained in their space group designations: C^4_{6v} for wurtzite, T^2_d for zinc blende (6). Actual experimental CdS crystals seem almost invariably to be of pure wurtzite structure; the ZnS crystals almost invariably are mixed structures, whether or not predominantly wurtzite or zinc blende. The symmetry groups of interest to us in each structure are: the point group of the space group, various site groups.

For zinc blende, the point group of the space group is T_d, for wurtzite it is C_{6v}. Now, in zinc blende there are sites with full symmetry T_d, while in wurtzite no site (occupied) has symmetry C_{6v}. Major interest in these particular symmetry groups arises from the energy band picture, since at k = 000 in the zone, the wave functions of the crystal must belong to

an irreducible representation of the point group of the space group (7). (If a function belongs to a particular irreducible representation of a group, its symmetry properties are specified when the operations [rotations, reflections, etc.] of the group are applied to it. Conversely, knowing the irreducible representations of a group it is possible to indicate the type of functions which may belong to it, that is 's', 'p_x', 'p_y', 'p_z', etc. In what follows we find both approaches helpful.) We also need to consider the spin orbit effect, particularly in sulfides, since this introduces certain effects of interest in the analysis. Formally, the procedure involved is a consideration of the irreducible representations of the "double group" of the particular group (7). The relationship between single and double group representations is easily obtained from the theory and physically corresponds to "turning on" (consideration of) the spin-orbit effect. After wave functions have been classified into symmetry types, the analysis may be carried one step further to a discussion of the allowed optical (electric dipole) selection rules. These rules tell us the states which may be connected by an allowed optical transition, and we shall indicate that a transition between states Γ_i and Γ_j is allowed optically by writing $\Gamma_i \leftrightarrow \Gamma_j$. If a limitation occurs, insofar as the optical transition is only allowed for particular polarization of the electric vector of the exciting radiation with respect to a crystal axis (e.g., the unique [c] or [00.1] of the wurtzite structure) it will be so indicated in the tables. If wave functions and selection rules were known, matrix elements and oscillator strengths of various optically allowed transitions could be computed. This degree of refinement does not seem warranted at the moment.

Since the cubic zinc blende does not possess a unique axis, no polarization effects arise; those states between which optical transitions can occur for point group T_d are so connected without any regard to polarization of excitation or emission. Results are given in Table II. For wurtzite, there exists a unique axis so that polarization effects may arise in addition to straightforward selection rules. Results are given in Table III for group C_{6v}. While at this time we present only the formal results of the group theory analysis, restricting ourselves to labeling the states by means of their symmetry designations, we shall later give a more physical picture of the states (in the band structure section). In any event, if we are given the information that radiation (absorbed or emitted) is, or is not, polarized, and that the "center" which (absorbs/emits) has effective net symmetry T_d, or C_{6v} in zinc blende or wurtzite, respectively, we may, by using Tables II and III, determine all the possible states for these symmetries between which optical transitions are allowed, and then further which states can give rise to polarization effects.

In Table IV similar information is given for the group C_{2v}, a subgroup of both T_d and C_{6v}. No point in crystal space in a wurtzite structure has this symmetry. In zinc blende, this group is a site group (see below).

The site symmetries (8) in zinc blende or wurtzite (that is, the point symmetry of the particular substitutional or interstitial site) are the following: in zinc blende, T_d, C_{3v}, C_{2v}, C_s; in wurtzite, C_{3v}, C_s. The main interest from the point of view of polarization effects would be in the site group C_{3v} in wurtzite structure, as this is the site for both substitutional and interstitial impurities. In addition, C_{2v} is the effective site symmetry in faulted zinc blende structures. In Table V selection rules are given.

Clearly, we are faced with formidable difficulties in attempting to interpret the observed polarization results in terms of the states between which optical transitions have occurred. There is a many-to-one correspondence between the observation of polarization and the pairs of states which might be involved, if these are the states of various "natural" groups in wurtzite. In zinc blende we expect no polarization, except perhaps in the case of faulted

Table II. Symmetry group Td*†

Single group representations: Γ_1, Γ_2, Γ_3, Γ_4, Γ_5
Double group representations: Γ_6, Γ_7, Γ_8
Optically allowed transitions:

$\Gamma_1 \leftrightarrow \Gamma_4$	$\Gamma_6 \leftrightarrow \Gamma_7$
$\Gamma_2 \leftrightarrow \Gamma_5$	$\Gamma_6 \leftrightarrow \Gamma_8$
$\Gamma_3 \leftrightarrow \Gamma_4$	$\Gamma_7 \leftrightarrow \Gamma_8$
$\Gamma_4 \leftrightarrow \Gamma_4$	$\Gamma_8 \leftrightarrow \Gamma_8$
$\Gamma_5 \leftrightarrow \Gamma_5$	
$\Gamma_5 \leftrightarrow \Gamma_5$	

* *See* G. Dresselhaus, *Phys. Rev.*, **100**, 581 (1955).
† In the text of the present paper, and in Fig. 4, Γ_4 is referred to as Γ_4'.

Table III Symmetry group C_{6v}*†

Single group representation: Γ_1, Γ_2, Γ_3, Γ_4, Γ_5, Γ_6
Double group representation: Γ_7, Γ_8, Γ_9
Optically allowed transitions:

$\Gamma_1 \leftrightarrow \Gamma_1$ ||c	$\Gamma_7 \leftrightarrow \Gamma_7$ $\perp$ and ||c
$\Gamma_1 \leftrightarrow \Gamma_5$ $\perp$c	$\Gamma_8 \leftrightarrow \Gamma_8$ $\perp$ and ||c
$\Gamma_2 \leftrightarrow \Gamma_2$ ||c	$\Gamma_7 \leftrightarrow \Gamma_9$ $\perp$c
$\Gamma_2 \leftrightarrow \Gamma_5$ $\perp$c	$\Gamma_8 \leftrightarrow \Gamma_9$ $\perp$c
$\Gamma_3 \leftrightarrow \Gamma_3$ ||c	$\Gamma_9 \leftrightarrow \Gamma_9$ ||c
$\Gamma_3 \leftrightarrow \Gamma_6$ $\perp$c	
$\Gamma_4 \leftrightarrow \Gamma_4$ ||c	
$\Gamma_4 \leftrightarrow \Gamma_6$ $\perp$c	
$\Gamma_5 \leftrightarrow \Gamma_5$ ||c	
$\Gamma_5 \leftrightarrow \Gamma_6$ $\perp$c	
$\Gamma_6 \leftrightarrow \Gamma_6$ ||c	

* The unique axis of this group is taken || to c.
† *See* J. Birman, *Phys. Rev.*, **114**, 1490 (1959).

Table IV. Symmetry group C_{2v}*

Single group representations: Γ_1, Γ_2, Γ_3, Γ_4
Double group representations: Γ_5
Optically allowed transitions:

$\Gamma_1 \leftrightarrow \Gamma_1$ ||x	$\Gamma_5 \leftrightarrow \Gamma_5$ $\perp$, and ||x
$\Gamma_1 \leftrightarrow \Gamma_3$ $\perp x$	
$\Gamma_2 \leftrightarrow \Gamma_4$ $\perp x$	
$\Gamma_2 \leftrightarrow \Gamma_2$ ||x	
$\Gamma_2 \leftrightarrow \Gamma_3$ $\perp x$	
$\Gamma_3 \leftrightarrow \Gamma_4$ $\perp x$	
$\Gamma_3 \leftrightarrow \Gamma_3$ ||x	
$\Gamma_4 \leftrightarrow \Gamma_4$ ||x	

* The unique axis of this group is taken || to x.
† G. Dresselhaus, *Phys. Rev.*, **100**, 581 (1955).

Table V. Symmetry group C_{3v}*

Single group representations: Γ_1, Γ_2, Γ_3

Double group representations: Γ_4, Γ_5, Γ_6

Optically allowed transitions:

$\Gamma_1 \leftrightarrow \Gamma_1$ || c	$\Gamma_4 \leftrightarrow \Gamma_4$ || c
$\Gamma_1 \leftrightarrow \Gamma_3$ $\perp$ c	$\Gamma_4 \leftrightarrow \Gamma_6$ $\perp$ c
$\Gamma_2 \leftrightarrow \Gamma_2$ || c	$\Gamma_5 \leftrightarrow \Gamma_5$ || c
$\Gamma_2 \leftrightarrow \Gamma_3$ $\perp$ c	$\Gamma_5 \leftrightarrow \Gamma_6$ $\perp$ c
$\Gamma_3 \leftrightarrow \Gamma_3$ || c, $\perp$ c	$\Gamma_6 \leftrightarrow \Gamma_6$ || c, $\perp$ c

* The unique axis of this group is taken || to c.

zinc blende crystal structure when the net site symmetry is reduced from T_d to effectively C_{3v}, and a unique axis has been introduced into the crystal structure. While polarization may arise in either wurtzite or faulted zinc blende structures, the values of the polarization must depend on the detailed energy level scheme. For example, it may be not observable if a cluster of closely lying states with different selection rules is optically accessible from a given initial state. In particular, while faulting formally reduces the site symmetry of a zinc blende structure to that of the wurtzite structure: e.g., from T_d to C_{3v}, the states split off by the lower symmetry may remain sufficiently close (if the perturbation is small) to be optically accessible, so that no observable polarization may result.

Conversely even though a particular optical transition may be allowed for both polarizations ($\perp$ and $\|$), the matrix elements whose values relate to the oscillator strength of the transitions for the two polarizations may be sufficiently different in magnitude so as to give an apparent polarization effect. These remarks are intended to emphasize the lack of uniqueness which obtains in assigning particular transitions as those involved in an observation of polarization.

We next discuss band structure of CdS and ZnS.

Energy Bands in the Sulfides

The complexity of the energy bands in some monatomic semiconductors (9) is indicative of what may be true also in the sulfides. On the other hand, we have not yet been driven by the weight of experimental evidence in the sulfides into the need for consideration of comparable complexity. In fact the simplest picture: tight binding (LCAO), extrema at k = 000, seems for the moment adequate, as well as simple, and we restrict our attention to this picture.

Since the outer valence electrons of both Zn (or Cd) and S are 's' and 'p' the states in the crystal are considered at k = 000 which can arise from these atomic orbitals. This means that we need to determine the crystal states (irreducible representations of T_d in zinc blende or C_{3v} in wurtzite) at k = 000 which can be obtained by combining 's' and 'p' orbitals. The states which are important from this point of view are illustrated in Fig. 3. The left side of the figure refers to zinc blende, the right to wurtzite. In Table VI the wave functions which are appropriate to the differently labeled states are indicated. From the figure we see a correlation between zinc blende states and the corresponding wurtzite states. In particular, we note the effect of the different wurtzite crystal symmetry, in causing a splitting of previously degenerate zinc blende states. The additional splitting due to spin orbit effect is also indicated for wurtzite.

Table VI. Wave function at a site

Basic set of s and p functions

$$\phi_{01} = s|\alpha\rangle \qquad \phi_{13} = y|\alpha\rangle$$
$$\phi_{02} = s|\beta\rangle \qquad \phi_{14} = y|\beta\rangle$$
$$\phi_{11} = x|\alpha\rangle \qquad \phi_{15} = z|\alpha\rangle$$
$$\phi_{12} = x|\beta\rangle \qquad \phi_{16} = z|\beta\rangle$$

Group T_d*:

Γ_1: ϕ_{01}; ϕ_{02}.

Γ'_5: ϕ_{11}; ϕ_{12}; ϕ_{13}; ϕ_{14}; ϕ_{15}; ϕ_{16}.

Γ_2: ϕ_{01}; ϕ_{02}.

Γ_7: $\{(1/\sqrt{3})[-i\phi_{11} - \phi_{13} + \phi_{16}]:\ (1/\sqrt{3})[i\phi_{12} - \phi_{14} - \phi_{15}].\}$

Γ_8: $\{(i/\sqrt{2})[\phi_{12} - i\phi_{14}];\ (i/\sqrt{6})[i(\phi_{11} - i\phi_{13}) + 2\phi_{16}];\ (i/\sqrt{6})[i(\phi_{12} + i\phi_{14}) + 2\phi_{15}];\ (i/\sqrt{2})[\phi_{11} + i\phi_{13}].\}$

Group C_{3v}†:

Γ_1: $\{a\phi_{01} + b\phi_{15};\ a\phi_{02} + b\phi_{16}.\}$

Γ_3: ϕ_{11}; ϕ_{12}; ϕ_{13}; ϕ_{14}.

Γ_7: $\{a\phi_{01} + b\phi_{13} + c/2(\phi_{11} + i\phi_{12});\ a\phi_{02} + b\phi_{16} + c/2(-\phi_{12} + i\phi_{11}).\}$

Γ_8: $\{(1/\sqrt{2})(\phi_{11}' - i\phi_{13});\ (-1/\sqrt{2})(\phi_{12} + i\phi_{14}).\}$

* For T_d, x, y, z are along the usual cartesian coordinate axes.

† For C_{3v}, x, y are perpendicular to z, and z is taken parallel to "C", the unique axis.

Table VII. Crystal wave functions

Zinc blende states at $\Gamma(k = 000)$; group T_d:

States with symmetry properties $\Gamma_1 - \Gamma_8$ may be formed (see Tables II and VI) by adding a function centered on one base site to that centered on the other, for example, for Γ_1 crystal function:

$$\Gamma_1: \{a\phi_{01}(Zn) + b\phi_{01}(S);\ a\phi_{02}(Zn) + b\phi_{02}(S)\}$$

see Table VI for definition of ϕ.

Wurtzite states at $\Gamma(k = 000)$ — group C_{3v}:

States with symmetry Γ_1, Γ_3, Γ_2, Γ_3 may be simply formed by adding functions centered at the site: Zn1, Zn2, S1, S2, where Zn1, etc., indicates the type of, and number of, the particular site. For a Γ_1 function

$$\Gamma_1: [a\phi_{01}(Zn1) + b\phi_{15}(Zn1)] + [a\phi_{01}(Zn2) + b\phi_{15}(Zn2)] + [a'\phi_{01}(S1) + b'\phi_{15}(S1)] + [a'\phi_{01}(S2) + b'\phi_{15}(S2)]$$

Wurtzite states at $\Gamma''(k = 0, 0, (2\pi)/c)$ — group C_{3v}:

Although $\Gamma'' = \Gamma$ in the reduced zone, it is helpful to consider it as distinct in the Jones or Energy zone. States Γ_2, Γ_3, Γ_3, at k = 0, $0(2\pi)/c$ are simply related to Γ_1, Γ_3, Γ_7, at k = 0, 0, 0 respectively. For example:

$$\Gamma_2: [a\phi_{01}(Zn1) + b\phi_{15}(Zn1)] - [a\phi_{01}(Zn2) + b\phi_{15}(Zn2)] + [a'\phi_{01}(S1) + b'\phi_{15}(S1)] - [a'\phi_{01}(S2) + b'\phi_{15}(S2)]$$

(cf. Γ_1 preceding.)

a, b, c, d are constants.

Physically, as earlier writers have indicated, the valence band consists mainly of electronic states localized about S while the conduction band has the states about Zn; this is, of course, an oversimplified picture. Table VI may be helpful in obtaining a physical picture of different wave functions associated with various states. In particular, we note that the zinc blende p-like (x, y, z) valence state Γ'_4 is split by the lower wurtzite potential into $\Gamma_5 + \Gamma_1$ which are, respectively, (x,y) and (s + z) orbital types. The spin-orbit effect in wurtzite causes $\Gamma_5 \rightarrow \Gamma_9 + \Gamma_7$ and it can be seen that Γ_9 remains (x,y) in orbital character, while Γ_7 contains a mixture of (x, y, s + z) states. Other changes caused by symmetry and spin-orbit effects can be easily obtained from Fig. 3 and Table VI.

The order of states, and separations, shown in Fig. 4 seem to be in accord with a variety of experiments in hexagonal CdS, including, absorption and reflection spectra, excitation spectrum of edge emission and of photoconductivity, and the exciton absorption spectrum (10). (On the other hand, preliminary cyclotron resonance results seems to indicate a more complex band structure for CdS, without agreeing or disagreeing with the separations shown in Fig. 4.) Again, the many-one correspondence between these experiments and band models needs emphasis, as some other band level schemes also consistent with the data could be proposed.

Figure 3 also reviews the polarization selection rules between certain states, which were already given in the various tables, and are now to be understood as restricting band-band optical transitions.

The band structure and order of states shown in Fig. 3 may be assumed also to apply to ZnS although there is at this time no comparably complete experimental evidence for ZnS. Numerical calculation, by the cellular method, of the band structure of ZnS in zinc blende and wurtzite structures (neglecting spin-orbit effect) gives an order of states in agreement with that illustrated in Fig. 3. In addition, the problem of crystal faulting is very significant in actual ZnS crystals, the faults causing barriers (11), changes in effective band gap (11) and, perhaps, changes in the order of states in the barrier (this seems unlikely although possible!). Hence, our major concern is with CdS center energy levels, even though actual major interest is in the ZnS luminescent systems.

It is now evident that the band models of Fig. 1 and Fig. 2 must be modified to take account of the actual band structures in the sulfides and that, in addition, if a symmetry designation is applied to the luminescent center state, polarization effects may be expected. While we work within the framework of the band scheme of Fig. 3 and 4 for the sulfides it is necessary to emphasize that the order of states and separations which have been assigned are provisional (although supported by the present weight of evidence).

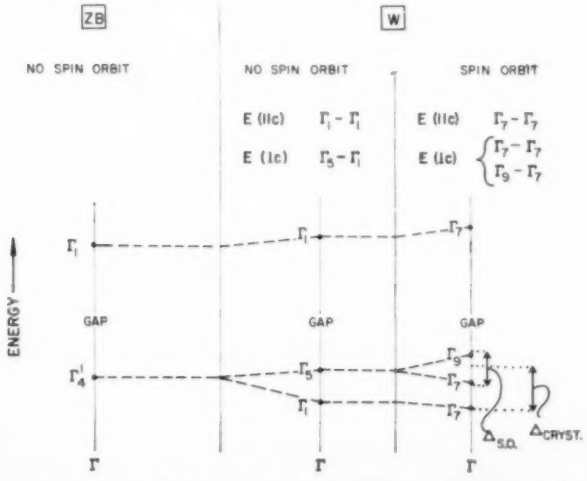

Fig. 3. Band structure, at k = 000 in zinc-blende and wurtzite structures showing the correlation between corresponding states. (This applies to the sulfides.)

Modified Band Models for Sulfide Centers

With the preceding development in mind, we are now in a position to formulate band models which, although still quasi-descriptive, are more refined than the simple S-K and L-K models. It will be possible then to evaluate alternate models and formulate (albeit tentatively) some opinion as to which model more simply accounts for polarization data.

It is evident from Fig. 4 that the valence and conduction band energy levels for a sulfide (particularly CdS) in hexagonal crystal structure, have particular symmetry properties (belong to particular irreducible representations). Similarly, the "center" state wave function must belong to some symmetry type. The simplest assumption one may make would seem to be: *the center has the maximum symmetry allowed for the crystal.* This would call for a center with Γ_7 symmetry, if we include the spin-orbit effect. Since the symmetry of the bands has been fixed (tentatively) by previous arguments we may rule out an S-K model for the moment, as the $\Gamma_7 - \Gamma_7$ transition is allowed for both $\perp$ and $\parallel$ polarizations. (S-K models are discussed below.) We are thus led to the L-K model modified for complex band structure: Fig. 5 in which a center with Γ_7 symmetry is placed near the conduction band. The process of luminescence then involves: (*a*) creation of free electrons and holes, by absorption of radiation whose energy is within the fundamental absorption edge, (b) attainment of thermal equilibrium by the holes, which populate the several

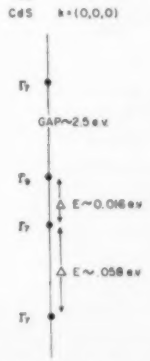

Fig. 4. Separations, in CdS, between states at k = 000. (Not to scale.)

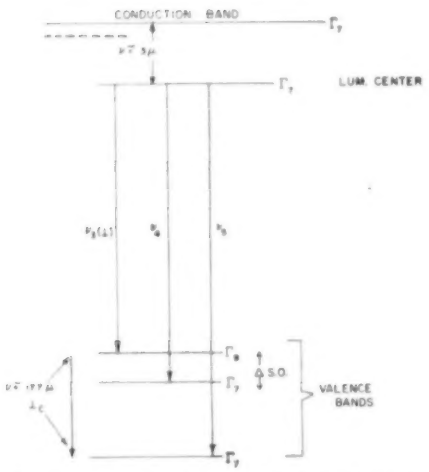

Fig. 5. Modified Lambe-Klick model for luminescent center and cycle. The 3 μ infrared luminescence quench, as well as the 17.7 μ absorption which should quench polarization are shown. Polarization of transitions can be obtained from Table III. The dotted line near the conduction band indicates the level from which edge emission is believed to occur.

valence bands as given by a Boltzmann factor, (c) recombination of the electron in Γ_7 center with a hole, and emission of characteristic radiation (ν_2 + ν_4 + ν_5) depending on the state of the hole at the moment of recombination, and finally, (*d*) capture of another electron by the center which is then returned to its initial state. If these are the steps involved in the production of preferentially polarized luminescence, then the L-K model leads to the following predictions for the luminescence (neglecting the lowest Γ_7 valence band):

(I) Both CdS edge emission (from a state closer to the band) and the 6200A (CdS) emission should be polarized, and both should obey the law for the temperature dependence of polarization

$$I_{\perp}/I_{\parallel} = a \exp(\Delta_{v_2}/kT) + b \qquad [1]$$

where $\Delta_{v_2} = 0.016$ ev for CdS if the previous assignments are correct. Note that the significant feature is not that a and b (or $I_{\perp}/I_{\parallel}$) be identical for the edge and 6200A emission, but that Δ_{v_2} be the same. Constants a and b depend on details of edge-center (trap) and luminescent center wave functions and would be only accidentally the same for the different emissions, as would the actual numerical values of polarization at any temperature. However, Δ which arises from the hole distribution between valence bands, must be the same if the L-K model of luminescence as we have presented it, and the accepted model of edge emission (12) are both correct in the approximation used.

(II) The excitation spectrum of luminescence and edge emission should be identical, since all that is involved in excitation is the creation of free electrons and holes (the latter being thermally distributed among the valence bands) and this is an intrinsic (host) property.

(III) The luminescence should be resolvable into several bands (centered on ν_2, ν_4, ν_5) of which ν_2 would be totally polarized $\perp$ to c, as given by selection rules.

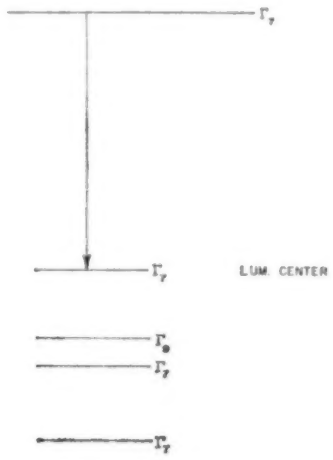

Fig. 6. Schoen-Klasens model with Γ_7 symmetry luminescent center.

(IV) The 6200A emission should be polarized independently of the polarization of exciting radiation since excitation only creates free carriers.

(V) Polarized infrared radiation (17.7μ) should quench the polarization of fluorescence by promoting the holes in the Γ_8 valence state to the lowest Γ_7 valence band: a hole in the latter does not give rise to polarized radiation.

(VI) The 3μ *IR* quench band, which promotes electrons from the "center" level to the conduction band should be operative for both polarizations.

As will be seen, these predictions should be helpful indeed to the decision among competing models.

While the polarization of the 4500A ZnS emission would be generally understandable in the identical type of L-K framework, the entire ZnS problem is complicated by the structure faulting which exists, and which contributes considerable complexity to the "band" structure of an actual specimen (11). A true test of (I)-(VI) above for ZnS should be made

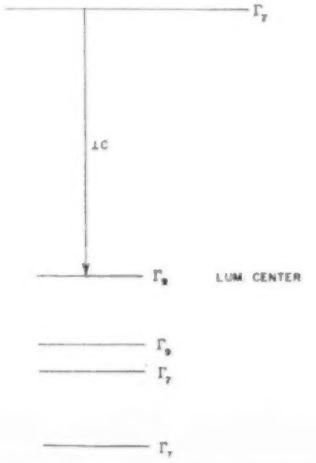

Fig. 7. Schoen-Klasens model with Γ_8 symmetry luminescent center.

on perfect hexagonal crystals, [cubic ZnS (zinc blende) shows no polarization (Table I)]. The structure sensitivity of the ZnS results, then, resides in the lack of polarization of emission in the "cubic" regions of a mixed crystal, as well as in the unknown effect which occurs for an activator within a fault plane region.

We now turn to some alternate models which would be consistent with polarization findings. The first class of alternate models we consider are S-K "band" models. Immediately we are led to several S-K models: one with ground state Γ_7, Fig. 6, one with ground state Γ_9, Fig. 7, and finally types whose ground "state" is actually a complex of several states, Fig. 8a, b. We shall, in the interest of brevity, only focus on salient features of each of these models, in particular emphasizing important differences which may be observed between each of these models and the L-K model which was discussed in some detail.

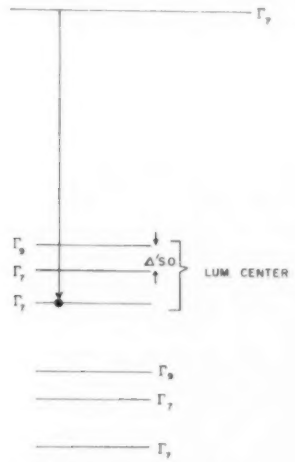

Fig. 8a. Schoen-Klasens model with three ground states. One electron is assumed in the center, normally, and the polarization should not be temperature dependent.

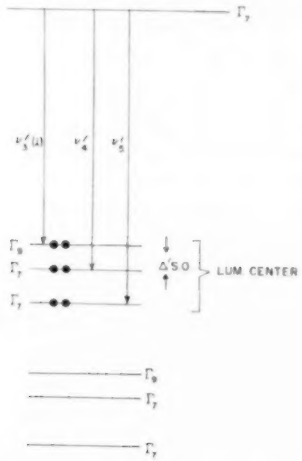

Fig. 8b. Schoen-Klasens model with three ground states. Six electrons are assumed in the "unexcited" ground state. Polarization may then be temperature dependent, if a single hole is captured by the center and reaches equilibrium among the three states.

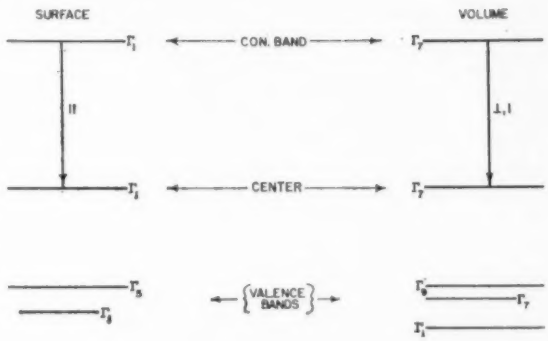

Fig. 9. Possible model for the ZnO polarization results. Assuming greater ionicity on the surface, we may classify states neglecting spin-orbit effect, while in volume the spin-orbit splitting is assumed necessary. This yields different selection rules on surface and volume.

The model in Fig. 6 requires that the transition $\Gamma_7 - \Gamma_7$, allowed for both polarizations by selection rules, shall have different strength for $\perp$ than for $\parallel$. (In particular $I_{\perp} > I_{\parallel}$). This model would predict a temperature independent polarization of luminescence.

The model of Fig. 7 would produce polarization ($\Gamma_7 - \Gamma_9$ transition) perpendicular to c, but to explain the lack of complete polarization some alternate mode of recombination with the center must be provided. As in the previous case, the polarization should be temperature independent.

A model more in the actual S-K spirit is that of Fig. 8a, b in which the ground "state" of the center consists of several levels, duplicating the valence band structure at k = 000, so a ground state trio of states is shown for the center. Now we may assume either that one, or six, electrons normally populate the ground states of the center. In the one electron in center case, Fig. 8a, according to the sequence which is assumed to apply for a S-K type model, at the instant of recombination, the free electron which will recombine to yield light sees the empty trio and recombines with any of the three available levels with some probability which is *a priori* fixed. If the center has only one electron in its normal ground state, it is clear that there will not be a temperature dependence for the polarization, since at the instant of recombination the entire ground state trio is empty. Temperature can only affect the state which the electron occupies after recombination, or before the valence band hole captures this electron to prepare the center for recombination. Neither of these will affect the polarization of emitted fluorescence. If in the unexcited state, the center is filled (13), i.e., consists of six electrons, Fig. 8b, (two in each doubly degenerate state of the trio) we have the possibility of temperature dependence of the polarization. This follows from the fact that the center will capture one hole, if the irradiation produces free holes and electrons, and this hole will reach thermal equilibrium between the various ground levels of the center. The particular state with the hole in it is the only state available for recombination; hence, the possibility of a tem-

perature dependence. If there is a temperature dependence, it should follow an equation formally identical to Eq. [1] as would the L-K model since the controlling factor is the Boltzmann distribution of hole occupancy of the center ground states. In fact, if the ground states of the center are replicas of the valence band k = 000 states, the only possibility for distinguishing this Schoen-Klasens model and the Lambe-Klick model would be in the *numerical values* of the constant Δ' arising in Eq. [1] for edge and 6200A emission, and in the IR quench frequency. It is unlikely that the center states' spacings and that of the valence bands at k = 000 should be identical, even though the various splittings arise, in the center as in the bands, from crystal symmetry and spin-orbit effects. Consequently, the decisive factors here will be the numerical values obtained if the fluorescence should prove temperature dependent. Note that the last three "S-K" models dispense with the assumption of a highly symmetric Γ_1 state for the "ground" state of the center, and may therefore be considered more "complicated" than the L-K model.

This concludes our consideration of simple "band" models which are in the spirit of L-K and S-K models and which would account for polarization. These band models are based on the k = 000 band order of states of Fig. 4, and would perhaps require revision if the band edges in particular sulfides were not at k = 000; certainly revision would be required if the order of band states were determined to be different from that we have taken. Rather than pretend to completeness by considering models based on these contingencies, we feel it preferable to consider the various possibilities already discussed (particularly, the simple L-K model) as working hypotheses and await the results of experiments—among them those proposed in (I-VI) above to help with the decision.

Two-Oscillator Models

As indicated in Lempicki's paper, models which involve separate absorption and emission oscillators have been successfully employed in accounting for fairly complicated data on polarization of fluorescence in solutions, and in certain ionic phosphors. In a certain (non-classical) sense the band models discussed above are two-oscillator models, since absorption in the lattice and emission at the center are distinct processes. However, more usual models of this class would be of a type where one "atom-like" center (polarizable dipole) absorbs the radiation and then either suffers some internal rearrangement (radiationless transition to another excited electronic state) and then emits, or actually transfers the excitation energy to another center where it is degraded by photon emission (14). A more recent variant of two-oscillator models would involve exciton creation (absorption step), migration, and then decomposition at the center (emission step) (15). Perhaps, even a single-triplet exciton conversion step may account for the needed stability of an exciton which would undertake such a process.

Assuming an absorption (excitation) process which would (for 3650Å irradiation) not leave a memory (i.e., polarization of fluorescence is seen to be independent of the polarization of the exciting radiation) the polarization of fluorescence then gives us information about the states involved in the emission. For processes of this kind, it is natural to assume that the emitting center will be located at a site and, therefore, possesses the site symmetry which, in wurtzite crystals, is C_{3v}. The wave functions of the emission center would then belong to irreducible representations of this site group (see Table V) and the optical selection rules would also then be appropriate. It would be then natural to construct as a model of the electronic states of the emitting center one derived from "s" and "p" type wave functions split in the appropriate manner in the existing crystal field. Such a model can easily be constructed from the information in Table V: depending on whether spin-orbit effect should be included will depend on the particular symmetry assignments of center states. Again, with respect to the L-K model more fully discussed above, it is evident that temperature and IR quench effects on the polarization, if they exist, should be quite different for the emission center-site model than for the L-K band model.

Discussion

It should be clear that the presently available polarization data alone are insufficient for the purpose of coming to an unequivocal conclusion about the nature of the centers, and in particular, even for deciding among the various band models or even between band models and "two-oscillator" models. We are led by a chain of plausibility arguments involving all the known properties of centers in the sulfides, to prefer band models, and within the class of band models to prefer the L-K model because of its relative simplicity. Many assumptions have been made in the process of formulating this chain including assumptions about the band structure (which seems supported by the evidence now available) and the symmetry of the center. Detailed theoretical analysis of the validity of the L-K model would be most fruitful if the model had been better established by virtue of additional experimental results.

In this context, then, we anticipate that the polarization studies can be most helpful in delineating properties of the various models which could be used to differentiate them, for example, by means of symmetry designations of the states of the center. In addition, one may make use of correlations by studying a simple sulfide system and then correlating the results and model obtained on such a system with that which would be appropriate for a more difficult system. For example, one may study polarization in hexagonal crystals and extrapolate the results to cubic systems since it is likely that a continuous correlation between hexagonal and cubic systems exists. In addition, the knowledge obtained for the 6200Å CdS emission by studying polarization may be carried over to the corresponding ZnS emission band (17): the former system being a "cleaner" one structurally and, hence, less ambiguous to interpret.

Acknowledgments

It is a pleasure to thank A. Lempicki for much discussion of his work. Dr. G. Neumark has also participated actively in discussions of the various models and her comments have been helpful, particularly in regard to S-K models. The author also wishes to thank Mrs. A. White for carefully typing the entire manuscript.

Manuscript received Nov. 9, 1959. This paper was prepared for delivery before the Philadelphia Meeting, May 3-7, 1959.

Any discussion of this paper will appear in a Discussion Section to be published in the December 1960 JOURNAL.

REFERENCES

1. A. Lempicki, *This Journal*, **107**, 404 (1960).
2. H. A. Klasens, *ibid.*, **100**, 72 (1953).
3. J. Lambe and C. C. Klick, *Phys. Rev.*, **100**, 573 (1955).
4. M. Schoen, *Physica*, **20**, 930 (1954).
5. C. C. Klick and J. H. Schulman, "Luminescence in Solids," in "Solid State Physics," Editors F. Seitz and D. Turnball, **5** (1957).
6. R. W. G. Wyckoff, "Crystal Structures," **I**, Interscience Publishers, New York.
7. G. F. Koster, "Space Groups and their Representations," in "Solid State Physics," edited by F. Seitz and D. Turnball, **5** (1957).
8. R. S. Halford, *J. Chem. Phys.*, **14**, 8 (1946).
9. F. Herman, *Rev. Mod. Physics*, **30**, 102 (1958); B. Lax, *ibid.*, **30**, 122 (1958).
10. D. Dutton, *Phys. Rev.*, **112**, 785 (1958); D. Dutton, *J. Phys. Chem. Solids*, **6**, 101 (1958); A. Lempicki, *Proc. Phys. Soc.* (in press); R. L. Kelly and W. J. Fredericks, *Phys. Rev. Ltrs.*, **2**, 389 (1959); R. G. Wheeler, *ibid.*, **2**, 463 (1959); also D. Thomas and J. Hopfield, *Phys. Rev.*, **116**, 573 (1959) and other references cited therein.
11. J. L. Birman, *Phys. Rev.*, **115**, 1492 (1959).
12. J. Lambe, C. C. Klick, and D. L. Dexter, *ibid.*, **103**, 1715 (1956).
13. Suggested by G. Neumark, and independently by W. Hoogenstraten, Private communication.
14. N. T. Melamed, *J. Phys. Chem. Solids*, **7**, 146 (1958).
15. S. Keller and G. Pettit, *Phys. Rev.*, **115**, 526 (1959).
16. W. Choyke, D. Hamilton, and L. Patrick, "Polarized Edge Emission of SiC," Scientific Paper #6-41003-1-P1, Westinghouse Research Labs., Pittsburgh, Pa., July 27, 1959; L. Patrick, "Polarization of Luminescence of Donor-Acceptor Pairs," Scientific Paper #6-40603-1-P1, Westinghouse Res. Labs., Pittsburgh, Pa., July 28, 1959. The author is indebted to Dr. Choyke for his kindness in providing him with preprints of these papers.
17. W. Van Gool, *Philips Research Repts.*, **13**, 157 (1958).

APPENDIX I

Temperature dependence of polarization.—Consider the conduction state Γ_{7c} and only the two uppermost valence states Γ_5 and Γ_{7v} (see Fig. 5). Let the number density of holes in either valence state be given by p_5 and p_7 and neglect the lowest Γ_7 valence band. Then the intensity of emission polarized perpendicular to c is given by

$$I_{\perp} \cong p_5[M(v_5)]^2 + p_7[M^{\perp}(v_7)]^2$$

where $M(v_5)^2$ involves some constants (effective mass, etc.) and the square of the matrix element for the optical transition Γ_7-Γ_5 from the center state to the valence band, and $(M^{\perp}(v_7)^2$ involves the square of the matrix element for the Γ_7-Γ_7 transition for light polarized to c. For the intensity emitted $\parallel$ c we obtain

$$I_{\parallel} \sim p_7[M^{\parallel}(v_7)]^2$$

where $M^{\parallel}(v_7)$ is similarly defined. Hence

$$I_{\perp}/I_{\parallel} = \frac{p_5}{p_7}a + b$$

where a and b are ratios of constants. Assuming a Boltzmann distribution of holes between the upper two valence states, which are separated by the spin-orbit splitting energy $\Delta_{s.o.}$, we obtain

$$I_{\perp}/I_{\parallel} = ae^{\Delta_{s.o.}/kT} + b$$

for the temperature dependence of fluorescence polarization.

APPENDIX II

Polarization in ZnO.—The zinc oxide results (Table I) are, of course, even more fragmentary and less capable of unique explanation than the corresponding results for the sulfides. However, some intriguing possibilities suggest themselves if we examine the selection rules for group C_{6v} (Table III). Again, we note that the measured polarization of room temperature surface luminescence (mainly *parallel* to c) is only partial, which suggests either a cluster of final (or initial) states or a transition between only two discrete states, allowed for *both* polarizations with different strengths depending on polarization.

It is possible to argue that the ZnO surface and volume luminescence are connected in the sense that they originate from the same center (atomic surroundings) but perturbed, with a wave function changed due to location on the surface or in the volume. Thus, we may imagine that

$$\Psi \text{ surface} = \Psi \text{ volume} + \lambda\Psi^{(1)}$$

for the center wave function depending on its location. Since a change in wave function in the first order (of a perturbation) will produce a second order change in energy, the luminescence may have approximately the same wave length, but considerably changed polarization properties, since polarization will involve the perturbation of the wave functions, through their optical matrix element, in the first order.

Suppose the surface of the crystal, due to distortions, is more ionic than the volume so that at the surface the net oxygen charge is nearly -2 while in the volume it is $-2 + \delta$ due to an overlap of charge density on the zinc ion, the latter having charge $(+2 - \delta)$. Since the net spin-orbit splittings will be a resultant of splittings on both Zn and O, with the latter's contribution small, we might expect to consider states on the surface nearly neglecting the spin-orbit effect while those in the volume include this. We are led to a model shown in Fig. 9 Physically, we are arguing that the surface Γ_7 state is more nearly Γ_1-like than the volume state and, hence, that $I_{\parallel}/I_{\perp} > 1$ at the surface.

Other speculations involving L-K models and the same argument about wave function distortion would make use of the Γ_5-Γ_5 selection rule (surface) and the change of $\Gamma_5 \rightarrow \Gamma_5 + \Gamma_7$ in volume, with a corresponding change of selection rules to allow both polarizations in emitted light.

Evidently, for ZnO, as well as for the sulfides, studies of the temperature and IR effects on the polarization are required.

Effect of CdS Addition in ZnS:Cu, In and ZnS:Ag, In Phosphors

Eugene F. Apple

Research Laboratory, General Electric Company, Schenectady, New York

ABSTRACT

ZnS:Cu,In and ZnS:Ag,In phosphors each can show two emission bands under 3650A excitation, namely, in the green (short) and orange (long) with Cu and in the blue and yellow with Ag activator. Addition of CdS causes the ratio of intensities of the short to long wave-length emission to increase. This observation is interpreted using the donor-acceptor associated pair model proposed recently for the long wave-length emission process.

ZnS phosphors coactivated with Ga or In and activated with Cu or Ag exhibit long wave-length emission bands (under u.v. excitation) in addition to the short wave-length emissions which peak at 5200A with Cu and 4450Å with Ag. Kroger and Dikhoff first reported the former emissions with peaks at 5700A and 6800Å in samples containing Ga and In coactivators, respectively. According to these authors (1) the spectral distributions of the bands were relatively independent of the particular activators involved.

More recently, Apple and Williams again studied the ZnS: (Cu or Ag), (Ga or In) phosphors and found that the spectral distribution of the long wave-length emission depends on the identity of the activator, as shown in Fig. 1, and the coactivator, as shown in Fig. 2. In most phosphors studied, both the long and short wave-length emission bands were observed. However, by changing the concentration of activator and coactivator, or the identity of the coactivator, or the temperature at which the phosphor was excited, the ratio of intensities of the short to long wave-length emissions, I_s/I_l, could be varied over a wide range (2).

The study reported in this paper concerns the effect of CdS addition on the ratio of emission intensities, I_s/I_l, in ZnS:Cu, In and ZnS:Ag, In phosphors. In ZnS phosphors exhibiting both the short and long wave-length emissions or the long wave-length emission only, addition of CdS causes an increase in I_s/I_l. Above 25-30 mole % CdS the long wave-length emission band is not observed at temperatures as low as −195°C. Effects of activator-coactivator concentration and temperature on the ratio I_s/I_l are included as well as typical glow curve measurements. These effects are interpreted using the model for the long wave-length emission proposed by Apple and Williams.

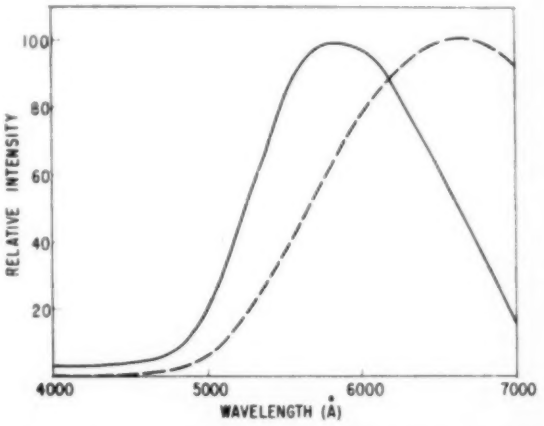

Fig. 1. Long wave-length emission spectra of hex. ZnS:10^{-4} Cu, Ga and hex. ZnS:10^{-4} Ag, Ga under 3650Å excitation at −196°C. Phosphors were fired in H_2S at 1150°C. ——— ZnS:10^{-4} Ag, Ga; - - - - - ZnS:10^{-4} Cu, Ga.

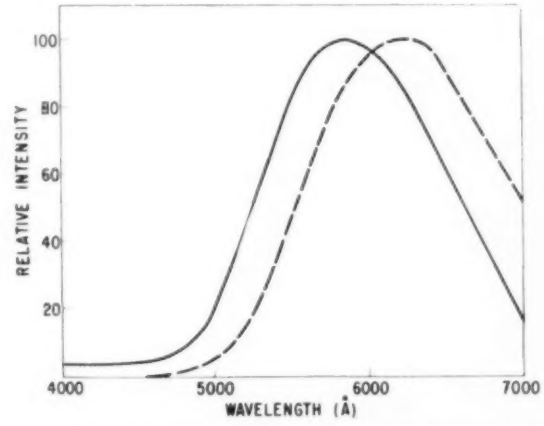

Fig. 2. Long wave-length emission spectra of hex. ZnS:10^{-4} Ag, Ga and hex. ZnS:10^{-4} Ag, In under 3650Å excitation at −196°C. Phosphors were fired in H_2S at 1150°C. ——— ZnS:10^{-4} Ag, Ga; - - - - - ZnS:10^{-4} Ag, In.

Experimental Results

Preparation of phosphors.—Mixtures of prefired ZnS and CdS (both from General Electric Company, luminescent grade) containing from 0 to 50 mole % CdS were ground and ballmilled until uniform. These mixtures were used in preparation of all the phosphors. The impurities, Cu, Ag, and In, were added to the mixtures as aqueous solutions. After slurrying with water the phosphor preparations were dried at 100°C, ground in a mortar, and fired at 1100°C in a stream of H_2S[1] for 2 hr. The phosphors were air-cooled to room temperature in the

[1] The H_2S (Matheson Co.) was bubbled through $Ba(OH)_2$ solution, then passed through columns containing silica gel and P_2O_5, and finally passed through a −50°C trap before coming in contact with the sample.

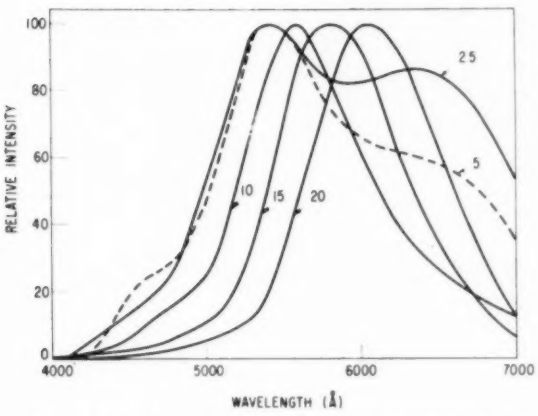

Fig. 3. Emission spectra for hex. (Zn,Cd)S:10^{-5} Cu, In under 3650Å excitation at room temperature. Mole per cent CdS is indicated. Phosphors were fired in H_2S at 1100°C.

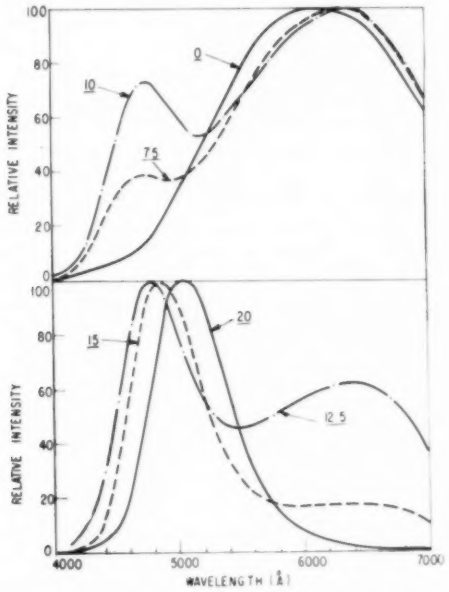

Fig. 4. Emission spectra of hex. (Zn,Cd)S:10^{-4} Ag, In under 3650Å excitation at room temperature. Mole per cent CdS is indicated. Phosphors were fired in H_2S at 1100°C.

H_2S stream. The mole % CdS and the gram-atom fraction of impurities identified with the samples throughout this paper correspond to the amounts present before firing.

Emission spectra at room temperature.—Emission spectra, under 3650Å excitation obtained from a G. E. mercury lamp, #H100-FL4, with Corning No. 5860 and Kopp No. 41 filters, were recorded on an automatic spectroradiometer which plots radiant energy flux vs. wave-length. Room temperature spectra of a typical series, hex. (Zn, Cd)S: 10^{-5} Cu, In are shown in Fig. 3. The spectra have been normalized so that the intensity of the predominant peak is 100. The ratio of relative intensities, I_s/I_l, which is about 1.16 in the 2.5% CdS sample, goes up with increasing CdS content until, with 20% CdS and above, the emission is entirely in the short wave-length band.

The emission spectra for hex. (Zn, Cd)S: 10^{-4} Ag, In at room temperature are shown in Fig. 4. In this series the phosphor with no CdS shows predominantly the long wave-length emission. As the CdS content is increased the relative intensity ratio, I_s/I_l, increases until at 20% virtually all the emission occurs in the short wave-length band. Hexagonal (Zn, Cd)S: 10^{-4} Cu, In gives similar results.

In both groups of phosphors the spectral distribution of the short wave-length emission as measured at the peak intensity moves to longer wave-lengths, i.e., lower energy, at the rate of about 0.017 ev/mole % CdS whereas the rate with the long wave-length emission is only about 0.003 ev/mole % CdS. The long wave-length spectra were measured at −195°C where the other emission does not interfere as much, as will be shown in the next section. However, because of the broadness of the spectra at the emission peak, the latter rate is only very approximate. Above 25% CdS, no long wave-length emission is observed even at −195°C in any of the samples measured. All the emission spectra were very reproducible on repeat samples prepared under the same conditions.

T dependence of emission.—The *T* dependence of emission was measured by recording spectra as the sample contained on a large Cu block was cooled slowly from about 250° to −195°C. Spectra for hex. (0.95 Zn 0.05 Cd)S: 10^{-5} Cu, In at temperatures from 245° to −80°C are shown in Fig. 5. This phosphor achieves its maximum brightness at about 210°C. The ratio of I_s/I_l increases with increasing temperature. Above about 0°C, a plot of log I_l/I_s vs. $1/T°K$ on any (Zn,Cd)S:Cu, In phosphor gives a linear relationship as is shown in Fig. 6. From the slope of this line, the difference in energies of the two types of centers is obtained (2). This energy decreases with increasing CdS content; for example, in (Zn, Cd)S: 10^{-5} Cu, In, it decreases from 0.34 ev to 0.24 ev in the range 0 − 10% CdS. Measurements were limited to samples containing 10% or less CdS because of the increased overlap of the short and long wave-length bands at higher CdS concentrations. In addition, the measurements were limited to Cu-activated phosphors because of the marked temperature quenching above 80°C observed in Ag-activated samples.

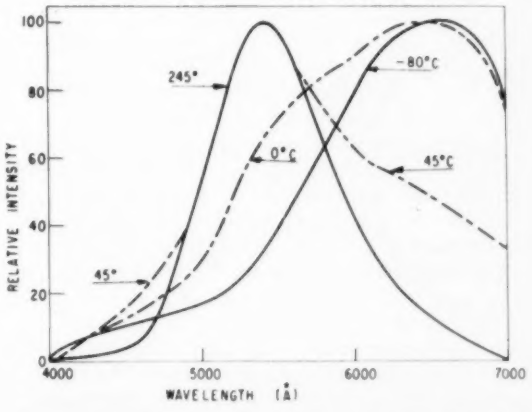

Fig. 5. Emission spectra of hex. (0.95 Zn, 0.05 Cd) S:10^{-5} Cu, In measured at the indicated temperatures.

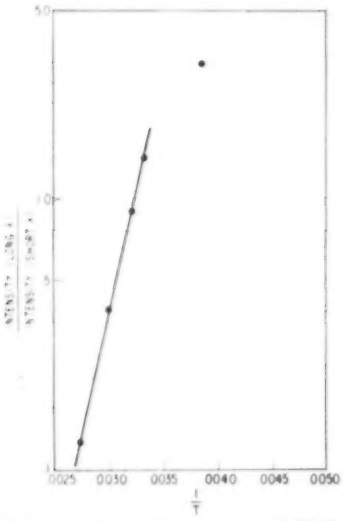

Fig. 6. T(°K) dependence of emission in (0.97 Zn, 0.03 Cd) $5{:}10^{-5}$ Cu, In under u.v. excitation.

Effect of activator-coactivator concentration.—In a particular series with constant Cd content, increase in the concentration of activator (and coactivator) over the range 10^{-5} to 5×10^{-4} g-atoms/mole (Zn, Cd)S results in a decrease in the ratio of relative intensities, I_r/I_t, when excited at a given temperature. This data on the effect of concentrations is consistent with that already reported for ZnS:Cu,In or ZnS:Ag, In phosphors (2).

Glow curve measurements.—Glow curve measurements were made on the hex. (Zn, Cd)S: 10^{-4} Cu, In series. The phosphors were excited for 5 min with a BH-4 lamp at −195°C after which they were warmed in the dark at a rate of 10°/min. An RCA 5819 PM tube was used as detector. The glow peaks shown in Fig. 7 move to lower temperatures with increasing CdS content. This effect of CdS is consistent with the results obtained by Hoogenstraaten with Al, Ga, and Cl donors (3).

Discussion

(Zn, Cd)S phosphors showing only what in this paper is called the short wave-length emission band have been studied extensively by many people. It has been shown that ZnS and CdS form solid solutions over the entire range and that in the 0-30 mole % CdS range, the absorption edge, as deduced from reflectance spectra, moves at the rate of about 0.020 ev/mole % CdS to lower energies (4). In turn, in (Zn, Cd)S:(Cu or Ag), (Al or Cl) phosphors the spectral distribution of the short wave-length emission moves to longer wave lengths, i.e., lower energies, at the rate of about 0.018 ev/mole % CdS (5). The donor levels assumed to be introduced by the coactivator become shallower with increase in CdS concentration as indicated by the thermal glow measurements. The rate in this case in the 0-30% region is about 0.012 ev/mole % CdS (3).

In the present study both the shift in the short wave-length emission to longer wave lengths and the shift in glow curve maxima to lower temperatures with increase in CdS content are qualitatively consistent with the data already reported by other

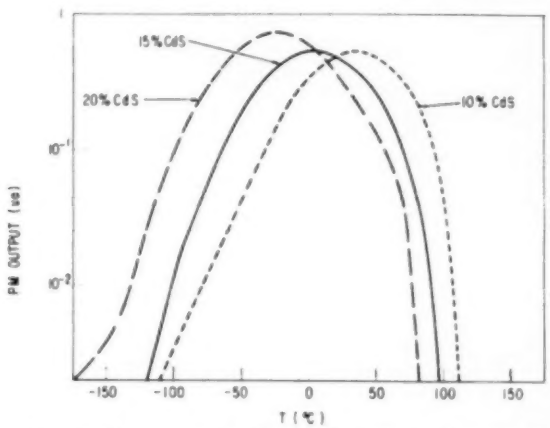

Fig. 7. Glow curves for (Zn,Cd)S:10^{-4} Cu, In. Numbers indicate mole per cent CdS. Excitation: BH-4 lamp at −195°C; heating rate 10°/min.

authors. Because of the very broad glow curves in evidence in (Zn, Cd)S:Cu, In phosphors it is probable that the ground states of the donor levels are distributed over a range of energies so that a unique value for a trap depth is not too meaningful. (In this paper, trap depth and ground state of the donor level are synonymous.) Johnson has obtained evidence that such a distribution exists in the several ZnS:Cu,Al and ZnS:Cu,In phosphors he has analyzed (6). The glow curves indicate, however, that the distribution of traps becomes shallower (with respect to the conduction band) with increasing CdS content. The temperature dependence of emission data for (Zn,Cd)S: 10^{-5} Cu,In also shows that the ground state of the donor level becomes shallower with CdS addition. The spectral distribution of the long wave-length emission in ZnS:Cu,In or ZnS:Ag,In changes at the rate of about 0.003 ev/mole % CdS in the 0-25% range.

In a phosphor showing both the long and short wave-length emission bands it would be expected that the bands should gradually merge with increasing CdS content because of their different rates of displacement. Beyond the point of mergence only one emission band should be observed since the donor levels are then shallow. As a result, transitions involving the ground state of the donor (between highly associated pairs) or an excited state of the donor (between loosely associated pairs) or the conduction band (between unassociated pairs) to the ground state of the activator would be virtually indistinguishable. In the (Zn,Cd)S:Cu,In or (Zn,Cd)S:Ag,In phosphors studied the bands are not observed to merge completely because the CdS, in addition to causing the bands to move as stated, also effects a change in their relative intensities. Increase in CdS content causes an increase in the ratio I_r/I_t so that (Zn,Cd)S phosphors showing both the short and long wave-length emissions or the long wave-length emission only, will, with substitution of 25-30% CdS for ZnS, show only the short wave-length emission even at −195°C. Perhaps the long wave-length emission could be observed at still lower temperatures. This newly observed effect of CdS on I_r/I_t is thought to be directly connected with the

decrease in donor (coactivator) depth attending the increase in CdS content.

Two models have been proposed for the long wave-length emission process in ZnS. Using the data of Kroger and Dikhoff, Klasens proposed that the long wave-length emission was due to the radiative recombination of a free hole with an electron trapped at a coactivator. As an alternative he suggested (7) that the radiative transition may involve recombination of a hole in a "waiting state" located above the filled band with an electron trapped at a coactivator. The nature of the waiting state was not clearly defined, but the idea was probably invoked to minimize the large difference in energies between the observed thermal and optical trap depths. The optical depth on the Klasens model, which would be approximately the difference between the band gap energy and the energy at the peak of the long wave-length emission, is about 1.3 ev greater than the thermal trap depth reported by Hoogenstraaten (3). Klasens also reported that the addition of 20% CdS in ZnS:Ag,In caused the peak of the long wave-length emission measured at −183°C to shift from 6100 to 6200Å or only 0.03 ev. This shift is considerably less energywise than the corresponding shift with CdS addition in the short wave-length emission.

More recently, Apple and Williams suggested another model for the long wave-length emission process which is based on the fact that the spectral distribution of this emission depends on the identity of both activator (Cu or Ag) and coactivator (Ga or In). They suggested that both species are involved in the luminescent center and concluded that the radiative transition giving rise to the long wave-length emission is between a coactivator-activator pair sufficiently close to each other in the lattice so that the ground state wave functions of the two overlap. This luminescent transition is shown on the band model in Figure 8a. In most of the phosphors they prepared, both the long and short wave-length emission bands were observed. By changing the concentration of activator and coactivator, or the coactivator identity, or the temperature at which the phosphor was excited, the ratio of intensities of the short to long wave-length emissions, I_s/I_l, could be varied over a wide range. Using an analysis based on the new model for the long wave-length center and on the Prener-Williams model for the short wave-length center (8) (shown in Fig. 8b) the authors were able to account qualitatively for the effects of the foregoing parameters on the ratio of intensities of the two emission bands. In the latter model, luminescence is attributed to transitions between coactivator-activator pairs which are not so highly associated as those giving the long wave-length emission.

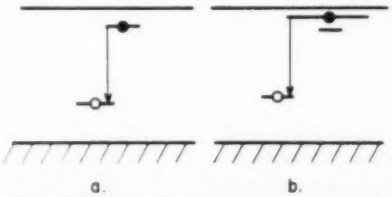

Fig. 8. Band theory models for the (a) long and (b) short wave-length (8) luminescent centers.

Apple and Williams suggested that the ratio of intensities of the short to long wave-length emission in ZnS: (Cu or Ag), (Ga or In) was dependent on at least two factors, the ratio of occupational probabilities of the emitting states of the short and long wave-length centers and the ratio of fractions of coactivator-activator (or donor-acceptor) pairs involved in each of the two types of centers. They said that the difference in the peaks of the emission spectra of the two bands is a measure of the difference in energies of the emitting states of the two types of centers and that the ratio of occupational probabilities, $P_{(e_s)}/P_{(e_l)}$, of the emitting states is given approximately by:

$$P_{(e_s)}/P_{(e_l)} \simeq e^{\frac{-he}{kT}\left(\frac{1}{\lambda_s}-\frac{1}{\lambda_l}\right)} \qquad [1]$$

where λ_s and λ_l are the wave lengths at the emission peaks of the respective bands. In ZnS phosphors this factor greatly favors the long wave-length emission; it is dependent on the depth of the ground state of the donor (which is the emitting state of the long wave-length emission). For example, at temperatures where thermal equilibrium applies, the ratio of intensities of the short to long wave-length emission is greater in ZnS:Ag,Ga than in ZnS:Ag,In because the ground state of Ga is 0.08 ev shallower than that of In (according to thermal glow measurements) (3). The value for $(1/\lambda_s - 1/\lambda_l)$ is smaller in the former case which leads to a more positive value of $P_{(e_s)}/P_{(e_l)}$. Also, at room temperature I_s/I_l is much larger in cubic than in hexagonal ZnS:Cu,In, due presumably to the fact that the donor ground state due to In is shallower in cubic than in the hexagonal phase (9).

The model suggested by Apple and Williams will be used to interpret the results of the effect of CdS addition on the emission in ZnS:Cu or Ag, In phosphor since this model is most consistent with the experimental results thus far obtained.

The increase in the ratio of intensities of the short to long wave-length emissions with increase in CdS content may be due to the change in the ratio of occupational probabilities of the emitting states, which change is a direct consequence of the gradual decrease in the depth of the ground state of the In level with CdS increase. From Eq. [1], I_s/I_l would increase with increasing CdS because the term $(1/\lambda_s - 1/\lambda_l)$ becomes smaller. As the short wave length approaches the long wave-length emission peak, $(1/\lambda_s - 1/\lambda_l)$ becomes so small that the actual mergence of the two peaks is not observed since before this point, the ratio of occupational probabilities has increased to such an extent that the short wave-length emission is overwhelmingly favored.

As was pointed out by Apple and Williams, the ratio of fractions of pairs contributing to the two emissions greatly favors the short wave-length emission and tends to balance out the occupational probability effect except where this ratio becomes large as with increasing CdS. In a series containing

a constant amount of Cd, the decrease in the ratio of intensities, I_s/I_l, with increasing concentration of activator and coactivator is due to the increase in the fraction of pairs contributing to the long wave-length emission. These results are consistent with those found previously for ZnS:(Cu or Ag), (Ga or In) phosphors.

In summary, CdS addition in ZnS:Cu,In or ZnS:Ag,In causes an increase in the ratio of short to long wave-length emission intensities. This increase is due to the increase in the ratio of the occupational probabilities of the emitting states of the two centers. Although other models could possibly be used to interpret these results, the fact that the spectral distribution of emission of the long wave-length center is dependent on the identity of both donor and acceptor is taken as evidence that the long wave-length luminescent transition is between associated donor-acceptor pairs as already pointed out (2).

Preliminary measurements show that CdS has the same general effect in ZnS:Cu,Ga or ZnS:Ag,Ga as in ZnS:Cu,In or ZnS:Ag,In.

Acknowledgments

The author wishes to thank the following people: Mrs. D. J. Weil for preparation of samples; Dr. F. J. Studer and Miss G. Lloyd for measurement of spectra; Dr. P. D. Johnson and Mr. F. C. Mostek for measurement of thermal glow curves; and Dr. J. S. Prener and Dr. F. E. Williams for review.

Manuscript received Nov. 16, 1959. This paper was prepared for delivery before the Philadelphia Meeting, May 1-5, 1959.

Any discussion of this paper will appear in a Discussion Section to be published in the December 1960 JOURNAL.

REFERENCES

1. F. A. Kroger and J. Dikhoff, *Physica*, **16**, 297 (1950).
2. E. F. Apple and F. E. Williams, *This Journal*, **106**, 224 (1959).
3. W. Hoogenstraaten, *ibid.*, **100**, 356 (1953); Thesis, University of Amsterdam, February 1958.
4. F. A. Kroger, *Physica*, **7**, 1 (1940).
5. S. Lasof, R. Shrader, and H. Leverenz, "Preparation and Characteristics of Solid Luminescent Materials," p. 224, John Wiley & Sons, Inc., New York (1946).
6. P. D. Johnson, Private communication.
7. H. A. Klasens, *This Journal*, **100**, 72 (1953).
8. J. S. Prener and F. E. Williams, *Phys. Rev.*, **101**, 1427 (1956); F. E. Williams, *J. Opt. Soc. Amer.*, **47**, 869 (1957).
9. E. F. Apple and D. J. Weil, Electrochem. Soc. Enlarged Abstracts, Electronics Div., Spring Meeting, Philadelphia, May 1959, p. 52.

Growth and Heat Treatment of Zinc Sulfide Single Crystals

A. Kremheller

General Telephone and Electronics Laboratories Inc., Bayside, New York

ABSTRACT

Zinc sulfide crystals grow readily from the vapor phase if small traces of certain impurities, such as zinc oxide and copper, are present. The decrease of ambient impurity concentration leads first to very thin, flexible, ribbon-like crystals which are hexagonal, and finally to nucleation with little growth. The purity of crystals depends not only on the composition of the starting material but also on the purity of the combustion tube employed; contamination during growth leads to an impurity gradient in crystals and to impurity variations among crystals. Crystals usually exhibit disorder of the crystal structure, although pure cubic or hexagonal structure can be achieved by annealing or quenching. Heat treatment also changes the impurity content and attendant properties, such as physical color, luminescence behavior, electrical properties, and disorder of the crystal structure.

There has been considerable interest in the growth of zinc sulfide single crystals during the past decade (1-3) because it is expected that the mechanisms of photoluminescence, photoconductivity, and electroluminescence will be better understood by studying single crystals. Natural zinc sulfide crystals are available in large size; however, they contain comparatively high impurity concentrations, usually of the order of 1% by weight. Since commercial applications of zinc sulfide phosphors require small quantities of additives, such as a few parts per million of activator and coactivator, natural crystals have been of but little importance in such researches.

Another requirement in preparing crystals for research purposes appears to be the proper control of the crystal structure (4). Synthetic crystals grown by the conventional vapor phase methods (3) exhibit one-dimensional disorder (3, 5-7, 8) consisting of randomness, mixed hexagonal-cubic structure in the same crystal, and the presence of polytypes which are intermediate between the hexagonal and cubic crystal systems.

Alfrey and Taylor (9) came to the conclusion that "unfortunately, single crystals (of zinc sulfide—the author) are difficult to grow and the amount and nature of the activators cannot be controlled, so that crystals grown by different experimenters will differ in constitution." The present paper shows how some of these difficulties have been overcome. It describes some experiments dealing with the preparation of zinc sulfide single crystals of controlled chemical composition and crystal structure. Previously reported observations (3, 8) are extended and, in many cases quantitatively corroborated;

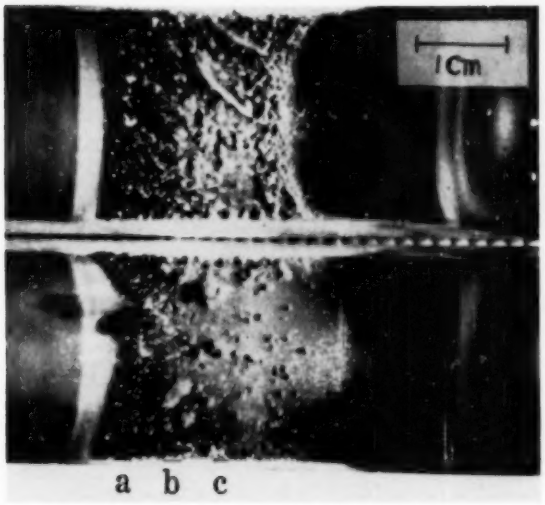

Fig. 1. Longitudinally split tube with crystals; regions a, b, c, as indicated in Table VII.

some new results are presented which appear to have experimental and theoretical implications as to the preparation of single crystals.

Experimental

The single crystals of zinc sulfide which have been investigated in the course of these studies were prepared from the vapor phase by sublimation. The growth method employing a U-shaped transparent quartz cooling finger which permits the control of nucleation, crystal structure, and morphology of crystals has been described previously (3). This technique is not described in any detail because the main experimental results are generally available (10). Recently Matsumura, *et al.* (11) have confirmed our observations (3, 8) in the course of investigating very thoroughly the growth and morphology of zinc sulfide single crystals obtained by the cooling-finger technique. Their observations are in essential agreement with many of our unpublished results; however, we were led by experimental circumstances to some additional investigations which are discussed here.

In another variation of vapor phase sublimation, a longitudinally split mullite tube is placed inside the mullite combustion tube (Fig. 1). This method leads to the growth of large voluminous crystals, which can be sampled readily and accurately from the various growth regions in the split tube. These large, oblong crystals were used mostly in the diffusion experiments described below.

Growth of pure single crystals.—The crystal growth on a cooling finger has been conducted as part of an attempt to prepare large crystals of high purity. Since the quartz combustion tube tends to break when cooled to room temperature after every experiment,[1] it was decided to keep the quartz tube continuously above 1000°C. In this way it was possible to conduct up to 30 growth experiments without loss of the quartz combustion tube. Consequently the cooling finger arrangement became a necessity for removing the crystals after growth was completed. In addition, since the cooling device can be removed rapidly from the hot zone, completely hexagonal crystals are obtained readily by temperature quenching.

[1] Quartz crystallizes in the tridymite form with an attendant volume increase of 15% when cooled to 900°C.

Table I. Decrease in impurity content,* in per cent by weight, of crystals grown on the cooling finger during consecutive growth experiments. (— not detected.)

Experiment No.	1	2	4	8
Cu	0.0005	0.0003	0.0002	<0.00001
Fe	0.0004	0.0002	0.0001	—
Pb	0.0003	0.00006	0.00002	<0.00001

* Quantitative spectrographic analysis by T. Veleker, Sylvania Electric Products Inc., Towanda, Pennsylvania.

Activated crystals are grown readily by this technique, with the desired level of activation depending on the additives physically admixed to the zinc sulfide powder or kept in a separate quartz boat; however, difficulties were met in preparing very pure crystals by the cooling-finger technique.

It was observed that the yield of crystals decreased with successive growth experiments. There was a trend to very thin, plate-like crystals with consecutive experiments. These thin tissue-like crystals were very flexible and exhibited interference colors in reflected light. After several experiments, nucleation still took place on the cooling finger, but the nuclei no longer grew into visible crystallites.

A correlation between the decrease in the rate of crystal growth and the increase in the purity of the crystals has been observed. Table I indicates that a gradual decrease of contamination occurs with successive growth experiments. It appears that the quartz tubes and boat are gradually cleaned, and the incorporation of impurities through the vapor phase and from the quartz substrate decreases accordingly.

There is additional proof that impurities are instrumental in the growth of zinc sulfide single crystals. The growth of crystals could again be brought about by using a quartz cooling finger which had not been used previously. The introduction of copper metal or zinc oxide powder into the boat was similarly effective in stimulating crystal growth.

Influence of tubing material.—The physical appearance, growth habit, and impurity content of crystals depend markedly on the tube material employed for crystal growth. As indicated above, there is a decrease in impurity levels with the successive use of a given transparent quartz tube. This purification effect occurs also with opaque quartz, while the increase in purity of crystals grown in consecutive experiments in mullite tubing has not been studied; however, crystals of successive batches became gradually light-yellowish to colorless in color and greenish-blue photoluminescent, while the first batch was dark-brown and nonphotoluminescent. Table II indicates average values of the tube composition and starting zinc sulfide powder which are based on several quantitative spectrographic analyses. The zinc sulfide powder is essentially spectrographically pure, while the tube ma-

Table II. Chemical composition of tube materials and original zinc sulfide powder, in per cent by weight

Element	Mullite	Opaque quartz	Transparent quartz	Zinc sulfide
Al	10-100	0.01-0.1	0.01-0.1	—
Ca	0.001	0.001	0.001	—
Cu	0.001-0.01	0.0001-0.001	0.0001	<0.00001
Fe	0.01-0.1	0.0001-0.001	<0.0001	<0.0001
Mg	0.01-0.1	0.0001-0.001	0.0001-0.001	0.0001
Mn	0.0001	0.0001	0.0001	0.00001
Ni	0.0001-0.001	—	—	<0.0001
Pb	0.0001	0.0001	<0.0001	<0.00005
Si	10-100	10-100	10-100	0.0001

Table III. Impurities in crystals grown in different tubes, in per cent by weight

Element	Mullite	Crystals grown in tubes of Opaque quartz	Transparent quartz
Al	0.0012	0.00025	0.00012
Ca	0.0004	0.0002	—
Cu	0.01	0.0013	0.0003
Fe	0.0007	0.0002	0.00015
Mg	0.0005	0.0002	0.0002
Mn	0.0001	0.00002	0.00002
Ni	0.00035	0.0001	<0.0001
Pb	—	—	—
Si	0.001-0.01	0.001-0.01	<0.001

terial is obviously the main source of contamination during growth.

The impurities are given as an average from several spectrographic determinations on randomly sampled crystals, Table III. One finds, as expected, that crystals grown in combustion tubes containing many impurities are contaminated accordingly. However, even the appearance and physical properties of the crystals depend on the kind of tubing material employed (Table IV).

One finds many crystals grown on the cooling finger that are not photoluminescent because they are very pure, while some crystals grown on the wall of the mullite tube are not photoluminescent because they contain too many impurities.

In general one observes also that the volume-to-surface ratio of crystals increases markedly with the impurity content. Some indication was found that traces of Ni, Co, and Fe in conjunction with Cu are very instrumental in introducing a brown to dark-brown physical color.

Nonuniformity in impurity content.—There has been considerable mention of the fact that the crystals of a specific batch differ widely with respect to purity and perfection of the crystal structure (9, 12, 13). While a partial analysis of these problems has already been presented (3, 8) in previous communications, additional evidence on the origin and elimination of these difficulties is given in the present paper. In this section three problems will be dealt with: (*a*) a comparison between the impurity level of the crystals and the material remaining in the boat, (*b*) spectrographic determination of impurities in the crystals grown in contact with the combustion tube wall and of the crystal fraction not in contact with the wall, and (*c*) the change of impurity level with location in longitudinally split tubes. The data are again averages of several experiments and show the typical features that cause the nonuniformity in purity from crystal-to-crystal and within single crystals grown by vapor phase methods.

Table V. Impurities, in per cent by weight, in single crystals and starting material after growth is completed

Element	Crystals on cooling finger	Powder in quartz boat
Al	0.001	0.0005
Ca	0.0002	0.0001
Cu	0.005	0.002
Fe	0.0007	0.0003
Ni	0.0005	0.0002

Table VI. Impurities, in per cent by weight, incorporated from the vapor phase and by solid-state diffusion

Element	Crystal fraction from wall	Crystal fraction not in contact with wall
Al	0.005	0.0005
Cu	0.015	0.003
Fe	0.001	0.0005

Table V shows that some impurities are incorporated preferentially in the single crystals on the quartz cooling finger in a mullite combustion tube. This becomes apparent when one compares the analyses of crystals with those of the contaminated residual starting material which was kept in a transparent quartz boat.

The powder in the boat also increased in particle size, but since the single crystals are much larger, one may assume that the impurities that are preferentially accumulated may cause the rapid growth, i.e., they may act as mineralizers.

In the second investigation, about half of every single crystal grown on the wall of the longitudinally split tube was broken off, and spectrographic analyses were run on both these and on the parts remaining in contact with the tube wall.

It was found, as indicated in Table VI, that the crystal fraction in contact with the wall contains a higher impurity level than crystals into which impurities were preferentially incorporated by vapor phase diffusion. This result confirms previous observations (14) which indicated an impurity gra-

Table IV. Properties of crystals grown in different combustion tubes

	Mullite	Opaque quartz	Transparent quartz
Physical color	Brown to dark brown	Yellow to whitish	Colorless
Transparency	Opaque or transparent	Some transparent	Most transparent
Electrical resistivity	Near 10^5 ohm-cm	10^9-10^{11} ohm-cm	$>10^{11}$ ohm-cm
Luminescence color	Green, orange, or none	Light green to blue	None or bluish

Table VII. Dependence of impurity content, in per cent by weight, of crystals on growth location in longitudinally split combustion tube, (regions a, b, and c of Fig. 1)

Element	Region a	Region b	Region c
Al	0.01	0.005	0.0005
Cu	0.012	0.006	0.002
Fe	0.002	0.001	0.0002
Ni	0.001	0.0006	0.0001

Table VIII. Purification of zinc sulfide single crystals by diffusion

Temperature, °C	before	800	1000	1100	1100
Time of annealing, hr	anneal	7	7	2	16
Per cent by weight of copper found	0.008	0.005	0.003	0.0025	0.00092

dient in cadmium sulfide crystals grown by a similar method.

The local impurity distribution from crystal-to-crystal can be studied when a longitudinally split tube is used, which also facilitates the sampling of crystals. Crystal growth starts at a sharp boundary which is near 1080°C (region a in Table VII and Fig. 1); the largest crystals grow in this region; they are brown to dark-brown in physical color. As the color lightens with the location farther from this dark region, the crystals become gradually smaller, the particle size following about an exponential dependence with the distance. Table VII shows the impurities found, and the photograph (Fig. 1) shows the split tube with crystals.

Control of impurity content and crystal structure by heat treatment.—It has been indicated above that the growth of very pure and large crystals in a reasonable reaction time leads to intrinsic difficulties. Therefore, it did not appear desirable to grow crystals of high purity, but instead an attempt was made to achieve this objective (i.e., the preparation of single crystals of controlled crystal structure and chemical composition) by heat treatment after crystal growth was completed.

Copper is considered to be the most important impurity because of its role as an activator and its relatively high concentration (Table III) in the large crystals which were grown in mullite tubing. The observation of Riehl and Ortmann (15) that copper diffuses readily into the zinc sulfide lattice suggested a method for purification. The purification method depends on impurity diffusion from the crystal into pure zinc sulfide powder in which the crystal is embedded. A variation of this method may also be used to activate crystals by diffusion in the opposite direction. The times and temperatures involved in purification by this process are indicated in Table VIII; some additional results are given in Fig. 2.

A large number of crystals have been heat treated in this way, and one observes that the purification process leads to various attendant changes. The brown physical color diminishes and the transparency increases; the electrical resistivity increases by

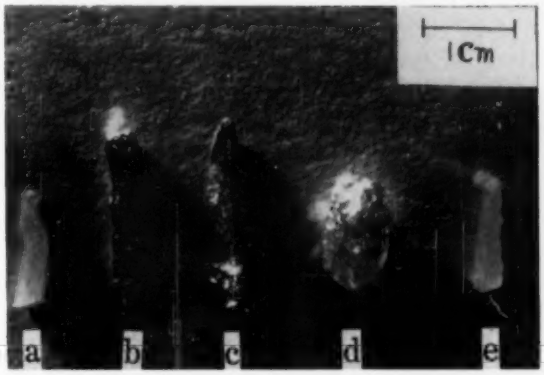

Fig. 2. Zinc sulfide crystals before and after annealing at 1000°C: (a) Piece of crystal b, annealed for 100 hr, pure embedding powder changed 3 times, (b) original, not annealed crystal, (c) crystal annealed for 32 hr in pure powder, (d) crystal annealed for 50 hr, and (e) crystal annealed for 200 hr, embedding powder changed 5 times. Crystals a-e were made cubic by a second annealing of 5 hours at 900°C in pure zinc sulfide powder.

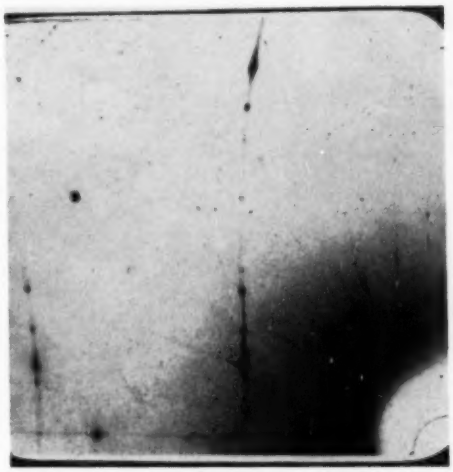

Fig. 3. X-ray diagram of a mixed hexagonal-cubic zinc sulfide crystal rotated about the c-axis; randomness, and 4- and 6-layer polytypes are observed.

several orders of magnitude; crystals turn photo- and electroluminescent or frequently change their emission color; changes in crystal structure also take place in many cases.

The crystal structure is usually quite disordered if zinc sulfide single crystals are grown on the wall of the combustion tube. The disorder consists of randomness, mixed hexagonal-cubic structure in the same crystal, and the presence of polytypes. An x-ray diffraction pattern of such a disordered crystal is shown in Fig. 3; the crystal has been rotated about the c-axis. The photograph shows the presence of mixed hexagonal-cubic structure, randomness as indicated by the blackening between the distinct spots, and the presence of 4- and 6-layer polytypes.

These disordered crystals are usually observed if one permits the furnace to cool at the rate governed by its heat capacity. If completely cubic crystals (Fig. 4) are desired, it is usually sufficient to keep

Fig. 4. X-ray diagram of cubic zinc sulfide single crystal rotated about the 111-direction.

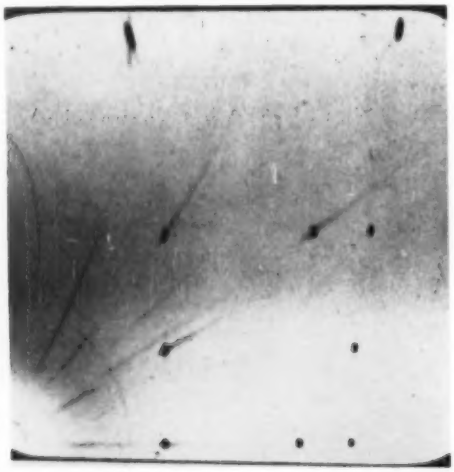

Fig. 5. X-ray diagram of hexagonal zinc sulfide single crystal rotated about the c-axis.

the crystals for 5 to 10 hr near 900°C. In this way one can combine the purification or activation of the crystal with the alteration of the crystal structure, so that a cubic crystal of controlled activator content is obtained.

The method employing the cooling finger also permits the preparation of completely hexagonal crystals (Fig. 5). The U-shaped cooling finger with crystals on the tip can be removed easily and rapidly from the hot condensation zone, so that the crystals are quenched after growth is completed (Fig. 6). It has been observed in all these cases that hexagonal crystals are formed, and therefore one may assume that crystals grew in this form under the growth conditions employed. This result is readily obtained when the cooling finger is used, while growth on the wall of the combustion tube does not permit rapid temperature quenching.

Hexagonal crystals can also be activated or purified by heat treatment after growth, although it is necessary to keep the annealing temperature below 800°C so that no transformation of the crystal structure (3) occurs while diffusion of foreign atoms

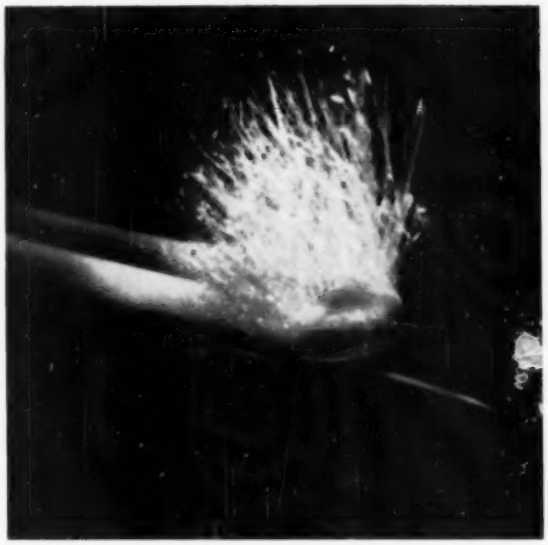

Fig. 6. Hexagonal crystals grown on the tip of the U-shaped quartz cooling finger.

(15) is taking place. In this way it has been possible to obtain pure or activated crystals belonging to the hexagonal system.

Conclusion

Certain impurities appear to be necessary when zinc sulfide single crystal growth is to proceed from nuclei. One may speculate that such mineralizers may facilitate the formation of screw dislocations, so that no need for the formation of a "two-dimensional nucleus" exists.

This behavior leads to inherent difficulties when an attempt is made to grow large pure crystals. Therefore, heat treatment with attendant diffusion has been employed in preparing large single crystals of controlled chemical composition. This annealing technique also eliminates the impurity gradient within a given crystal and impurity variations among crystals that depend on the growth site within the combustion tube.

Heat treatment also permits the deliberate control of the crystal structure, so that pure cubic or hexagonal crystals with or without a desired degree of randomness can be obtained, although the latter and the occurrence of polytypes appear to be markedly dependent on the presence of small amounts of foreign elements (3).

As a next step in investigating some pertinent problems, a detailed study of the impurity dependence of the crystal structure and disorder and their correlation with the appropriate free energy changes appears to be indicated. Such investigations should finally permit one to overcome the difficulties still remaining to be solved in the preparation of zinc sulfide single crystals of controlled chemical composition and crystal structure.

Acknowledgment

The author is greatly indebted for valuable contributions of D. J. Bracco, T. Veleker, R. Bastian, D. T. Palumbo, L. W. Strock, and V. A. Brophy. The

assistance of J. T. Ragusin and S. Faria with the experimental work is gratefully appreciated.

Manuscript received Dec. 16, 1959. This paper was prepared in part for presentation before the Chicago Meeting, May 2-6, 1954.

Any discussion of this paper will appear in a Discussion Section to be published in the December 1960 JOURNAL.

REFERENCES

1. D. C. Reynolds and S. J. Czyzak, *Phys. Rev.*, **79**, 543 (1950); S. J. Czyzak, D. C. Reynolds, R. C. Allen, and C. C. Reynolds, *J. Opt. Soc. Amer.*, **44**, 864 (1954); L. C. Greene, D. C. Reynolds, S. J. Czyzak, and W. M. Baker, *J. Chem. Phys.*, **29**, 1375 (1958).
2. Wm. W. Piper, *J. Chem. Phys.*, **20**, 1343 (1952).
3. A. Kremheller, *Sylvania Technologist*, **8**, 11 (1955).
4. A. H. McKeag and E. G. Steward, *This Journal*, **104**, 41 (1957).
5. C. Frondel and C. Palache, *Amer. Min.*, **35**, 29 (1950).
6. M. A. Short and E. G. Steward, *Acta Cryst.*, **8**, 733 (1955).
7. H. Mueller, *Neues Jb. Mineral. Abh.*, **84**, 43 (1952).
8. A. Kremheller, Heat Treatment of Zinc Sulfide Single Crystals, paper presented at the Spring Meeting of The Electrochemical Society at Chicago, May 1954.
9. G. F. Alfrey and J. B. Taylor, *Proc. Phys. Soc. (London)*, **68B**, 775 (1955).
10. "Methods of Experimental Physics," Vol. 6, Solid State Physics, edited by K. Lark-Horovitz and Vivian A. Johnson, Academic Press, New York, 1959, part B, p. 297.
11. T. Matsumura, H. Fujisaki, and Y. Tanabe, *Sci. Rep. Ritu*, **A10**, No. 6, 459 (1958).
12. D. R. Frankl, *Phys. Rev.*, **100**, 1105 (1955).
13. T. B. Tomlinson, J. Electronics, **2**, 293 (1956).
14. A. Kremheller, Ph.D. Thesis, Munich University, Munich, January 1952.
15. N. Riehl and H. Ortmann, *Z. Physik. Chem.*, **A188**, 109 (1941).

Characteristics of the {111} Surfaces of the III-V Intermetallic Compounds

Harry C. Gatos and Mary C. Lavine

Lincoln Laboratory, Massachusetts Institute of Technology, Lexington, Massachusetts

ABSTRACT

Surface characteristics of the {111} crystallographic planes of the III-V intermetallic compounds (zinc-blende structure), and in particular those of InSb, are discussed. The polarity of these compounds along the <111> directions leads to pronounced physical chemical differences between the {111} surfaces terminating with group III atoms and those terminating with group V atoms. Differences in etching, dislocation etch pit formation, and electrode potential are presented. Dislocation etch pits form on the group III surfaces and not on the group V surfaces of the six compounds investigated (InSb, GaSb, AlSb, InAs, GaAs, and InP). A proposed interpretation is based on the relative reactivity of the group III and group V atoms as affected by their bond configuration and the polarity of the zinc-blende structure.

A number of investigators have reported on the etching characteristics (1-5) and other surface properties of the III-V compounds (4, 6). InSb has been principally employed because of its availability.

Among the various crystallographic planes, the {111} are of special interest because the III-V compounds (zinc-blende structure) exhibit polarity along the <111>directions. Thus, there is significant difference between parallel {111} surfaces, arbitrarily designated as {111} and $\{\bar{1}\bar{1}\bar{1}\}$ as shown in Fig. 1. The outermost atom layer in each surface consists of either group III or group V atoms which are triply bonded to the lattice. This results from the fact that the {111} surfaces can be created only by cuts between planes such as AA and BB (Fig. 1) where atoms are singly bonded to one another. A surface configuration containing atoms singly bonded to the lattice, resulting, for instance, from a cut AA-B'B' is not stable (4, 5, 8). Furthermore, slip on the {111} planes occurs between AA and BB rather than AA and B'B'.

Dislocation etch pits are found only on the {111} and not on the $\{\bar{1}\bar{1}\bar{1}\}$ surface (1, 2, 5, 6). The identification of the two types of surfaces in InAs and GaSb was achieved recently by Warekois and Metz-

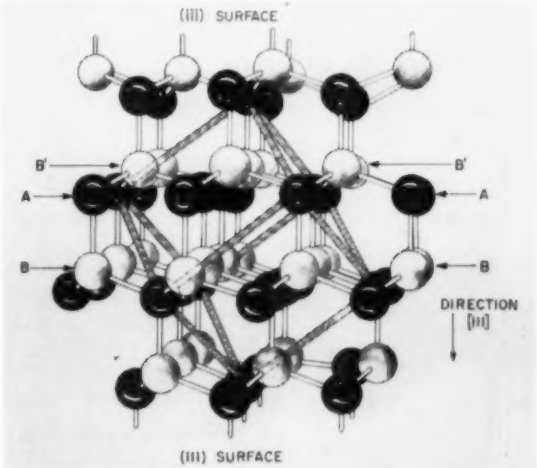

Fig. 1. Crystal structure (zinc-blende) of the III-V intermetallic compounds; the unit cell is indicated. •, group III atoms; ○, group V atoms.

ger (9). They showed by x-ray techniques that in InAs and GaSb the {111} planes developing dislocation etch pits terminate with the group III atoms. This has been also shown for GaAs (10), and for InSb and other III-V compounds (11).

In the present paper, the etching characteristics and the formation of dislocation etch pits in III-V compounds are discussed, and an interpretation is advanced for the observed differences between the two types of {111} planes and the formation of dislocation etch pits on the {111}and not on the $\{1\bar{1}\bar{1}\}$ surfaces.

Experimental

Reactivity of the {111} Surfaces

Quantitative differences in reactivity between the A[1] and B surfaces were determined by measuring their etching rates. For this purpose, high-purity InSb samples were employed having exclusively A or exclusively B surfaces. They were actually tetrahedrons having as all four sides either only A or only B surfaces. Each set of A and B tetrahedrons was prepared from the same single crystal of InSb by grinding the surfaces to the proper orientation as determined by x-ray diffraction. The geometric relationship between an A and a B tetrahedron is shown in Fig. 2 and can be conveniently related to the diagram of Fig. 1.

At room temperature and above, the etching rates of both types of surfaces in a number of oxidizing media are controlled by the diffusion of the oxidizing species in solution to the surface of the sample as has been shown for InSb and for other III-V compounds (12). Consequently, no difference in rates is observed at these temperatures. However, the etch patterns of the two types of tetrahedrons are different since the nature of the attack is not necessarily a function of the dissolution rate. On the A tetrahedron dislocation etch pits appeared on all four sides whereas no dislocation etch pits appeared on the B tetrahedron. This experiment certainly eliminates the possibility that the etching behavior of the crystallographic surface under study is affected by adjacent surfaces of different orientation and chemical reactivity.

The etching of both tetrahedrons proceeds at the same rate at 25°C with an activation energy of approximately 5 kcal, which is characteristic of diffusion-controlled dissolution processes (13, 14). At lower temperatures, however, the rates diverge, that of the A surfaces falling to one-tenth the rate of the B surfaces at 4°C. The activation energy associated with the etching of the A surfaces rises to approximately 25 kcal, which is characteristic of chemical activation-controlled processes, whereas the etching of the B surfaces remains diffusion-controlled. Clearly then, in the case of InSb, surfaces terminating with Sb atoms have a far greater tendency to react than those terminating with In atoms. This undoubtedly prevails at room temperature but cannot be detected by etching rate measurements since diffusion of the oxidizing species to the surface is the rate-determining step.

The above difference in reactivity was also confirmed by electrode potential measurements. InSb electrodes, one exposing an A surface and one exposing a B surface, were prepared from one single InSb crystal. In various etching media in the vicinity of 0°C, they exhibited significant differences in electrode potential (75 mv or greater). The electrode with the In surface was always more noble than that with the Sb surface, consistent with the rate measurements.[2] Electrodes prepared from different InSb ingots also showed the same potential difference as those prepared from the same ingot. On the other hand, electrodes with the same type of surface (either In or Sb) exhibited no potential difference within experimental error (5-10 mv).

[1] For convenience, group III atoms will be designated as A atoms and group V atoms as B atoms; {111} surfaces terminating with A or B atoms will be designated as A or B surfaces, respectively.

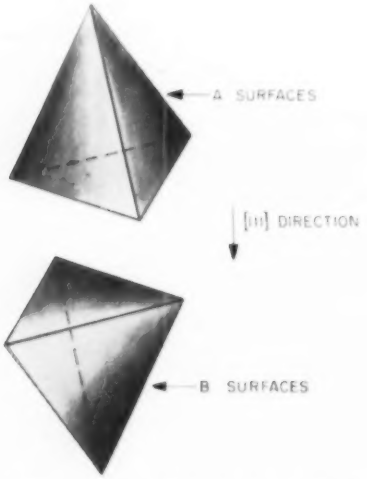

Fig. 2. Geometric relationship between tetrahedron A having exclusively group III atom surfaces, i.e., (111), $(\bar{1}\bar{1}1)$, $(\bar{1}1\bar{1})$, $(1\bar{1}\bar{1})$ and tetrahedron B having exclusively group V atom surfaces, i.e., $(\bar{1}\bar{1}\bar{1})$, $(\bar{1}11)$, $(1\bar{1}1)$, $(11\bar{1})$. Compare with Fig. 1.

Etching Characteristics

General Remarks.—Surface heterogeneities usually serve as centers for the initiation of preferential etching and etch pits. Such heterogeneities can result from cold work and from dislocations intersecting the surface. The morphological growth of etch pits or etch patterns, however, depends strongly on the nature of the chemical etchant. More often than not, slow acting etchants reveal surface heterogeneities (16). Fast etchants tend to dwarf local differences in surface reactivity and lead to chemical polishing.

In some instances virtually all of the dislocations can be revealed individually by employing slow etchants. The etch pit count can then serve for dislocation density determinations (17). In general, however, an etching agent which develops dislocation etch pits does not necessarily reveal all of the

[2] The dissolution rate of a metal in acid oxidizing media is usually determined by the reduction rate of the oxidizing agent (15), and the dissolution potential of the metal approaches its reversible value. This also applies to the present case, regardless of temperature. Thus, the more noble dissolution potential of the A surfaces clearly indicates that they have a lesser tendency to react than the B surfaces.

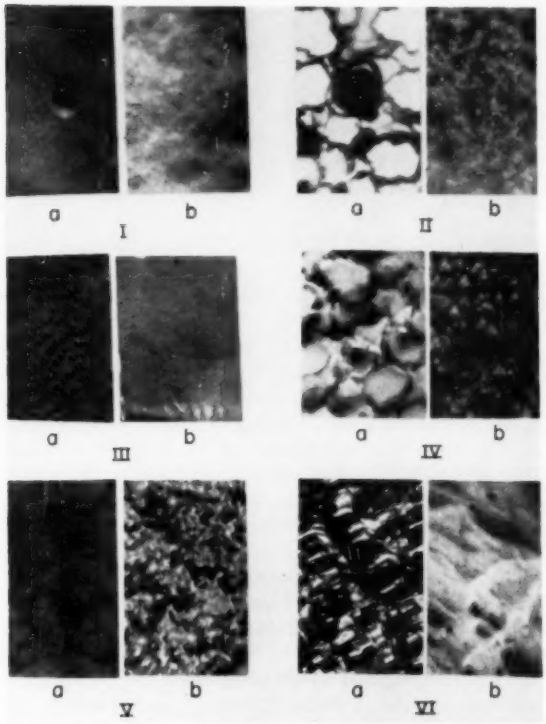

Fig. 3. {111} surfaces (a) terminating with group III atoms and $\{\bar{1}\bar{1}\bar{1}\}$ surfaces (b) terminating with group V atoms of III-V compounds. The compounds, the composition of the etchants in parts by volume, the etching time and temperature are: I, InSb; 2 conc. HNO_3:1 conc. HF:1 glacial CH_3COOH; 4 sec; 25°C.(315X). II, InAs; 0.4N Fe^{+++} in conc. HCl; 30 min; 25°C (525X). III, GaSb; 2 conc. HNO_3:1 conc. HF:1 glacial CH_3COOH; 15 sec; 25°C (315X). IV, GaAs; 0.2N Fe^{+++} in 6N HCl; 10 min; 82°C (1500X). V, AlSb; 1 30% H_2O_2:1 conc. HF:1 H_2O; 1 min; 25°C, followed by 1 conc. HCl:1 conc. HNO_3; 2 sec; 25°C (525X). VI, InP; 0.4N Fe^{+++} in conc. HCl; 1.5 min; 25°C (525X). (All magnifications are before reduction for publication.)

dislocations terminating at a given surface. The fact that distinct dislocation etch pits have not been observed on the $\{\bar{1}\bar{1}\bar{1}\}$ planes certainly does not imply that these surfaces are not intersected by dislocations.

Dislocation etch pits.—In order to establish whether or not the appearance of dislocation etch pits on the A surfaces alone is a general phenomenon, several III-V compounds were studied under varied experimental conditions. InSb, GaSb, AlSb, InAs, GaAs, and InP in single crystal form and of relatively high purity were employed. The surfaces were ground to within 1 degree of the desired orientation as determined by x-ray diffraction. A variety of etching media (inorganic and organic acids) were employed, containing different oxidizing agents such as HNO_3, H_2O_2, Fe^{+++}, MnO_4^-, $Cr_2O_7^=$, Ce^{++++}, and $V(OH)_4^+$ at various concentrations. Etching experiments were performed for periods ranging from a few seconds to 2 hr and at temperatures up to 82°C. Under such varying conditions, a multitude of etch figures were obtained. In no instance, however, were dislocation etch pits observed on the B surfaces of any of the compounds. Dislocation etch pits were developed on the A surfaces of all six compounds. This occurred in many preferential etchants (leading to etch figures) as well as in nonpreferential etchants (leading primarily to chemical polishing). Representative examples for the compounds employed are shown in Fig. 3. It should be noted that etchants acting preferentially on the A surfaces showed preferential action on the B surfaces also, but did not reveal dislocation etch pits on the latter.

Etch figures on the {111} surfaces of InSb.—In some instances, the same etchant can act both preferentially and nonpreferentially depending on the reaction time and surface pretreatment. Figure 4 shows A surfaces of InSb etched in Fe^{+++} etchant for various times. It is noted that the dislocation etch pits grow with time. Although not shown, the dislocation etch pits for the cases corresponding to Fig. 4-VI and 4-VII were larger than those in Fig. 4-V. Simultaneously the etch figures grow in size and merge into each other. They are shallow at all times with relatively flat {111} bottoms and grow sidewise. It is believed that in this case, heterogeneities originally present in the abraded surface contribute greatly to the initiation of the patterns shown in Fig. 4-I. As the cold worked layer is removed, etching proceeds rather uniformly and eventually leads to a chemical polish except for the areas immediately adjacent to the dislocations. For the same etchant, the cold-worked layer is removed in shorter times by increasing the temperature and therefore the etching rate. Figure 5-I shows that a

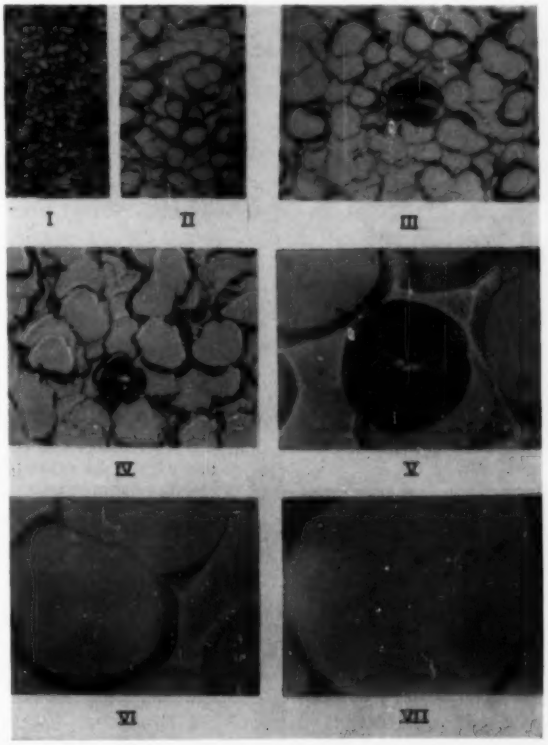

Fig. 4. {111} A surfaces of InSb etched in 0.4N Fe^{+++}—conc. HCl (515X) for various times. I, 5 min; II, 10 min; III, 15 min; IV, 20 min; V, 30 min; VI, 60 min; VII, 90 min.

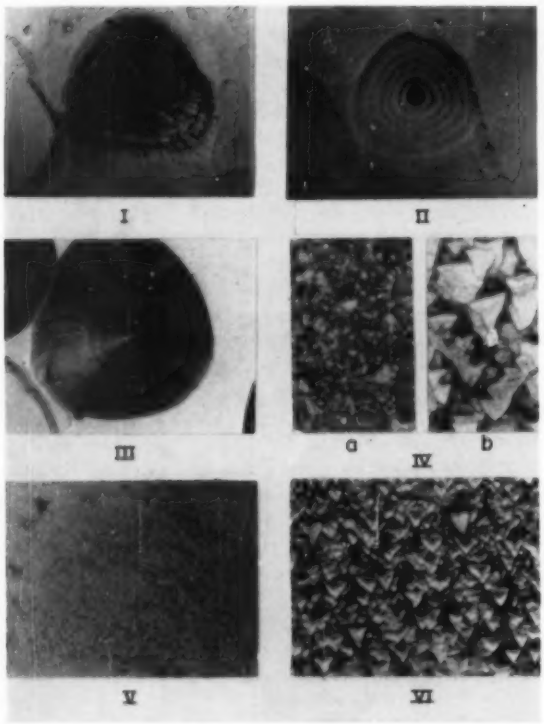

Fig. 5. {111} surfaces of InSb. I, Surface A etched for 5 min at 82°C in 0.4N Fe^{+++}— conc. HCl (515X). II and III, surface A etched for 4 sec in 2 conc. HNO_3:1 conc. HF:1 glacial CH_3COOH at 25°C, subsequently etched for 30 min in 0.4N Fe^{+++}—conc. HCl at 25°C (515X). IV, Surface B, etched for 5 min (a) and 90 min (b) at 25°C in 0.4N Fe^{+++}— conc. HCl (515X). V, Surface B of cases II and III (515X). VI, Surface B of case I (515X).

surface etched at 82°C for 5 min resembles that obtained at room temperature in 30 min. Consistent with this, essentially no preferential etch patterns appear if the surface is pretreated in a fast non-preferential etchant and subsequently etched by Fe^{+++}. Some dislocation etch pits, as the one shown in Fig. 4-II, did not form during the pretreatment with the fast etchant. Those developed during pretreatment (Fig. 5-II) grew further in the Fe^{+++} etchant (Fig. 5-III).

The etch patterns of the B surfaces persist longer than those of the A surfaces. It can be seen in Fig. 5-IV that in 90 min (Fig. 5-IVb) the growth of the etch figures on the B surface is appreciably less than the corresponding etch figures on the A surface of Fig. 4-VII. Figures 4-I and 5-IVa represent opposite sides of an {111} wafer; the same is true for Fig. 4-VII and 5-IVb for 5-II and 5-V, and finally for 5-I and 5-VI. Actually, in many cases, etch figures are revealed on the B surfaces while the A surfaces appear chemically polished.

Each side of the triangular patterns on the {111} surfaces is parallel to an <110> and perpendicular to a <211> direction. It is not uncommon for the A surfaces to develop hexagonal-type patterns with each of their sides again parallel to an <110> direction (Fig. 6-I). On occasion, the {110} planes develop intersecting the surface at an angle of 60°

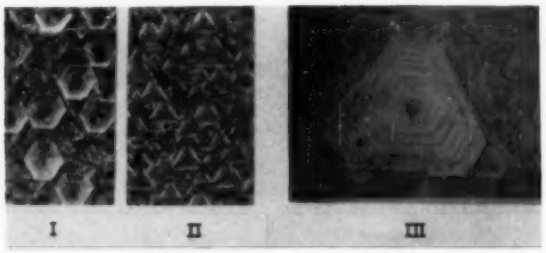

Fig. 6. {111} InSb surfaces etched for 30 min at 82°C in 0.2N Fe^{+++}—6N HCl. I, surface A (145X), II, surface B (145X), III, surface A (315X).

along the sides of the triangular or hexagonal patterns and lead to inverted pyramid-like etch patterns as can be seen in Fig. 6-I and to some extent in Fig. 6-II. An etch figure with a distinct terrace-like structure surrounding a dislocation etch pit is shown in Fig. 6-III.

Apparently, it is through the advancement of their sides that etch patterns grow. It will be recalled that at the temperature under consideration the over-all dissolution rate is the same for both A and B surfaces. The flat {111} bottoms of the etch figures on the A surfaces are not attacked as fast as the {110} planes mentioned above or any planes intersecting the surface at a steep angle along the sides of the etch figures. The chemical reactivity of the B surfaces on the other hand is much greater than that of the A surfaces. Consequently, the bottoms of the etch figures on the B surfaces are attacked appreciably, and their growth sidewise does not proceed as fast as on the A surfaces. This accounts for the fact that the etch figures of the A surfaces become rounded and grow faster than those of the B surfaces under the same experimental conditions. It is for the same reason that the etch figures of the B surfaces persist even under conditions under which the A surfaces appear chemically polished.

Discussion

Atomic Model for the A and B {111} Surfaces

Regarding the differences in behavior between A and B surfaces, it is proposed that the B surface atoms are very reactive chemically, since they are only triply bonded to the lattice, whereas their normal valence is five. Surface A atoms, also triply bonded to the lattice, must be appreciably less reactive since they are normally trivalent. The bond configuration of the zinc-blende structure (sp^3 tetrahedral hybrid orbitals) is illustrated schematically for the {111} direction (I). The formation of an A and a B surface (by a cut between planes AA

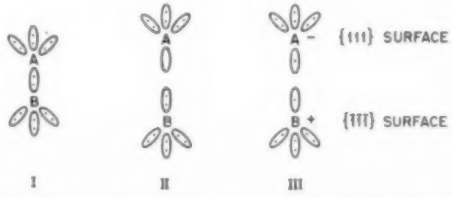

and BB of Fig. 1) can be represented as in II or III where both A and B atoms retain their tetrahedral

bond configuration. In II, atom B acquires both electrons; in III, atoms A and B acquire one electron each from the pair of electrons corresponding to the bond being broken. Case III is thermodynamically improbable since the ionization potential associated with the formation of B^+ is much greater than the electron affinity associated with the formation of A^-. Case II is considered as the most likely to occur as it leads to electrically neutral surfaces. In considering case II it is not possible to decide unambiguously whether or not A or B atoms are more reactive on the basis of the hybrid orbitals involved. However, it is reasonable to state that in etching processes where oxidizing (electrophilic) agents are involved, B atoms are more reactive than A because they have an unshared pair of electrons available for oxidation. Similarly, A atoms could possibly have a greater tendency to react with nucleophilic agents (unshared pair of electrons), but this case does not concern us at present.

The above valency or hybrid orbital model shows that B surface atoms should be more reactive than A in electrophilic ambients. Thus the model accounts for the observed differences between the A and B surfaces. It also accounts for the formation of dislocation etch pits on the A surfaces as shown below. The presence of the filled unshared electron orbitals on the B surfaces and the unfilled orbitals on the A surfaces points to pronounced differences in electronic phenomena between the two surfaces. These phenomena include surface conductivity, photoconductivity, surface recombination velocity, and others.

Obviously the model does not take into consideration possible surface states nor does it involve quantum mechanical aspects. However, it does account for the experimental results. A quantum mechanical verification should prove of considerable interest.

Edge dislocations in the zinc-blende structure.—It has been shown that in the zinc-blende structure, slip occurs on the {111} planes and along the <110> directions (5). The dislocation axis in this structure is parallel to the <110> direction and forms a 60° angle with the Burgers' vector (18). Considering the polarity of the zinc-blende structure it is apparent that $\alpha^{[3]}$ and β dislocations can intersect both the A and the B surfaces. Venables and Broudy (5) showed that for InSb, only one type of dislocations leads to the formation of dislocation etch pits on the {110} and probably on the {111} surfaces. If their work is viewed in the light of Warekois' (11) identification of the crystallographic polarity of InSb the observed dislocations are α (In) dislocations. Atom models of 60° edge dislocations intersecting an {111} surface are shown in Fig. 7 and 8.

Since dislocation etch pits result from only one type of dislocations and since these pits do not develop on both the A and the B surfaces, it appears that elastic strains associated with edge dislocations in the III-V compounds do not play a significant role in etch pit formation. Rather, the formation of dislocation etch pits is controlled primarily by the specific chemical differences between the A and the B atoms on the {111} surfaces and at the dislocations as affected by their bonding characteristics along the polar <111> direction and the dislocation axis.

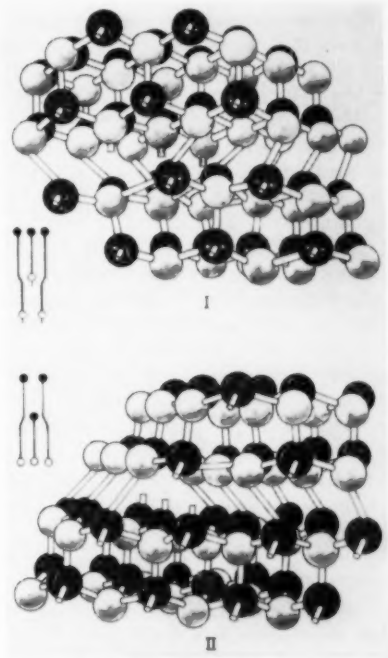

Fig. 7. Atom models showing a 60° edge dislocation intersecting the A surface. Surface of interest is defined by the atoms with protruding bonds. I, Dislocation terminating in a row of B atoms; II, dislocation terminating in a row of A atoms.

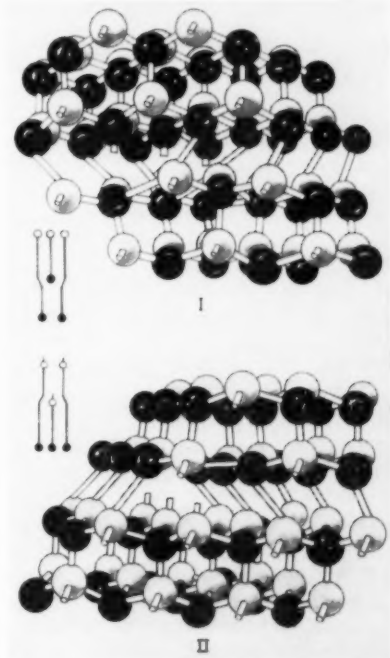

Fig. 8. Atom models of a 60° edge dislocation intersecting the B surface. Surface of interest is defined by the protruding bonds. I, Dislocation terminating in a row of A atoms; II, dislocation terminating in a row of B atoms.

[3] Dislocations with a row of triply bonded A atoms will be designated as α dislocations, and those with B atoms will be designated as β.

Etching and dislocation etch pit formation on the {111} surfaces.—Since both α and β dislocations intersect the A and the B surfaces, there are four possibilities: Aα, Aβ, Bα, and Bβ. As shown in Fig. 7 and 8 the α dislocations terminate with a divalent A atom (A_2) on the A surfaces and the β dislocations terminate with a divalent B atom (B_2) on the B surfaces. In the cases Aβ and Bα the terminal dislocation atom is trivalent (B_3 and A_3, respectively) and actually it does not lie in the outermost surface layer. Regarding the relative reactivities of the triply and doubly bonded surface atoms it is reasonable to state that $B_2 > B_3$ and $A_2 > A_3$ (it will be recalled that $B_3 > A_3$). Singly bonded A or B surface atoms are not being considered since such a surface configuration is unstable, as pointed out above. If it were stable, no difference in behavior would be expected between the A and the B surfaces. Finally, the quadruply bonded atoms immediately below the outermost surface layer are considered stable when compared with the triply bonded surface atoms.[4]

Etching and etch pit formation will be considered from an atomistic point of view. Although simplified, such an approach seems desirable at this time, particularly in dealing with covalent crystals.

Considering first {111} surfaces not intersected by edge dislocations (Fig. 1), it appears that the removal of triply bonded surface atoms (A atoms in the case of A surfaces and B atoms in the case of B surfaces) must be associated with the rate-determining step of the etching process. The atoms immediately below the outer surface atoms become singly bonded and, therefore, extremely unstable, as the outer surface atoms to which they are bonded are removed. It is because the outer surface atoms play such a significant role in the behavior of the {111} surfaces that major differences are observed between the A and the B surfaces.

The A and B surfaces intersected by edge dislocations are now considered:

Case Aα (Fig. 7-II).—The terminal A_2 atom of the dislocation is the first one to react. Then two B_3 adjacent atoms, which will react faster than any A_3 surface atoms, are exposed. As these B_3 atoms react, four A_2 surface atoms are exposed as well as an A_2 atom of the dislocation. Thus, it is apparent that the attack proceeds faster along the dislocation than over the rest of the surface leading to the formation of a dislocation etch pit.

Case Aβ (Fig. 7-I).—Strictly speaking the terminal B_3 atom of the dislocation does not belong to the outermost surface atom layer, and its role in the etching process is not expected to be of primary importance. Even if this B_3 atom is attacked before the A_3 surface atoms, then two A_2 surface atoms are exposed but the next atom of the dislocation remains bonded to three A_3 atoms. It is apparent from the diagram that in such a case the attack does not necessarily proceed preferentially along the dislocation, but rather in a layer-like fashion over the surface.

Case Bα (Fig. 8-I).—This case is in many respects similar to the Aβ case. Actually, the formation of dislocation etch pits is even less favorable here. The terminal atom of the dislocation is A_3 which is less reactive than the surface B_3 atoms.

Case Bβ (Fig. 8-II).—Although this case is analogous to Aα, it does not lead to the formation of dislocation etch pits. As the terminal dislocation atom B_2 is attacked, two A_3 atoms are exposed which will not react as fast as the B_3 surface atoms. These A_3 atoms delay the exposure of the next B_2 dislocation atom until the surrounding B_3 surface atoms are attacked. Hence, no preferential attack along the dislocation axis takes place.

[4] Surface configurations with "steps" and "kinks" will not be considered at this time. They will be treated in a future communication.

Summary

Dislocation etch pits were observed on the {111} surfaces terminating with group III atoms in six III-V intermetallic compounds (InSb, GaSb, AlSb, InAs, GaAs, and InP) in a number of etching solutions. In all six compounds no dislocation etch pits were observed on the {111} surfaces terminating with group V atoms. In addition to this difference, at low temperature the group III {111} surfaces exhibit appreciably smaller etching rates and more noble electrode potentials than the group V surfaces. Furthermore, etch figures develop on the group V surfaces in etchants which chemically polish the group III surfaces. This applies even under conditions in which both types of {111} surfaces exhibit the same etching rates.

An atomic model is proposed with unshared filled tetrahedral orbitals in the case of B surfaces and unfilled orbitals in the case of A surfaces. The model accounts for the observed differences between the two types of surfaces and points to further differences in electronic properties.

Acknowledgment

The authors are indebted to Mrs. M. J. Button for assisting with the experiments, to E. P. Warekois for identifying the surfaces by x-ray diffraction, and to Dr. A. J. Rosenberg for suggesting the use of tetrahedrons in determining the etching rates of the A and B surfaces.

Manuscript received Oct. 8, 1959. This paper was prepared for delivery before the Columbus Meeting, Oct. 18-22, 1959. The work reported in this paper was performed by Lincoln Laboratory, a center for research operated by Massachusetts Institute of Technology with the joint support of the U. S. Army, Navy, and Air Force.

Any discussion of this paper will appear in a Discussion Section to be published in the December 1960 JOURNAL.

REFERENCES

1. H. A. Schell, *Z. Metallkunde*, **48**, 158 (1957).
2. J. W. Allen, *Phil. Mag.*, **2**, 1475 (1957).
3. W. Bardsley and R. L. Bell, *J. Electron*, **3**, 103 (1957).
4. M. C. Lavine, A. J. Rosenberg, and H. C. Gatos, *J. Appl. Phys.*, **29**, 1131 (1958).
5. J. D. Venables and R. M. Broudy, *ibid.*, **29**, 1025 (1958).
6. R. E. Maringer, *ibid.*, **29**, 1261 (1958).
7. J. F. Dewald, *This Journal*, **104**, 244 (1957).
8. P. Haasen, *Acta Met.*, **5**, 598 (1957).
9. E. P. Warekois and P. H. Metzger, Pittsburgh Diffraction Conference Abstracts, p. 48, November 1958; *J. Appl. Phys.*, **30**, 960 (1959).
10. J. G. White and W. C. Roth, *J. Appl. Phys.*, **30**, 946 (1959).
11. E. P. Warekois, Unpublished results.

12. M. C. Lavine, A. J. Rosenberg, and H. C. Gatos, To be published.
13. M. B. Abramson and C. V. King, *J. Am. Chem. Soc.*, **61**, 2290 (1939).
14. W. W. Harvey and H. C. Gatos, *This Journal*, **105**, 654 (1958).
15. H. C. Gatos, *Corrosion*, **12**, 322 (1956).
16. H. C. Gatos, W. W. Harvey, and M. C. Lavine, *Rev. Met.*, **55**, 1149 (1958).
17. S. A. Kulin and A. D. Kurtz, *Acta Met.*, **2**, 354 (1954).
18. W. T. Read, Jr., *Phil Mag.*, **45**, 775 (1954).

Etching Behavior of the {110} and {100} Surfaces of InSb

Harry C. Gatos and Mary C. Lavine

Lincoln Laboratory, Massachusetts Institute of Technology, Lexington, Massachusetts

ABSTRACT

Preferential and nonpreferential etching characteristics of the {110} and {100} surfaces of InSb were investigated. Since {111} facets develop in the etch figures of these surfaces, the morphology of the etch figures reflects the crystallographic polarity of InSb along the <111> directions. Dislocation etch pits were found both on the {110} and on the {100} surfaces. The role of the relative reactivities of the various crystallographic planes in the over-all etching behavior of InSb and the effect of cold work are discussed.

InSb and other III-V intermetallic compounds with the zinc-blende structure have two types of {111} surfaces, i.e., one type terminating with group III atoms (A surfaces) and one terminating with group V atoms (B surfaces). The two types of surfaces, resulting from the crystallographic polarity of the <111> directions, exhibit markedly different physical chemical properties (1). Thus, it was found that the B surfaces of InSb are far more reactive than the A surfaces in oxidizing (electrophilic) agents. It is expected that the same applies to the {111} surfaces of the other III-V intermetallic compounds. This difference in reactivity was shown responsible for the fact that dislocation etch pits appear on the A surfaces and not on B surfaces of six III-V compounds investigated (InSb, GaSb, AlSb, GaAs, InAs, InP).

Since the zinc-blende structure exhibits no polarity in the <110> and <100> directions, no differences in behavior are expected among the various {110} surfaces or the various {100} surfaces. It will be shown, however, that in certain etchants {111} facets develop on the {110} and {100} surfaces, and consequently the <111> polarity of zinc-blende structure is reflected in the etching behavior of these surfaces.

It is the purpose of the present paper to demonstrate the role of the <111> crystallographic polarity on the etching behavior of the {110} and {100} surfaces of InSb and show that this behavior is consistent with the atomic model proposed to explain the relative reactivities of the A and B surfaces of the III-V intermetallic compounds (1). The effects of surface heterogeneities introduced by cold work are also discussed.

{110} Surfaces

In the present study wafers used were cut from high-purity InSb single crystals. The parallel sides of the wafers were ground to within 1° from the {110} orientation as determined by x-ray diffraction. Before etching they were ground with 1600 mesh garnet powder.

Two types of etchants were employed: (*a*) preferential etchants leading to the formation of etch figures, and (b) fast nonpreferential etchants resulting in the formation of dislocation etch pits on an otherwise chemically polished surface. A number of nonpreferential etchants can be employed successfully; among various preferential etchants studied the one consisting of 0.2*N* Fe^{+++} ions in 6*N* HCl was found the most suitable.

Typical results obtained with the preferential etchant are shown in Fig. 1-I. Upon cursory exami-

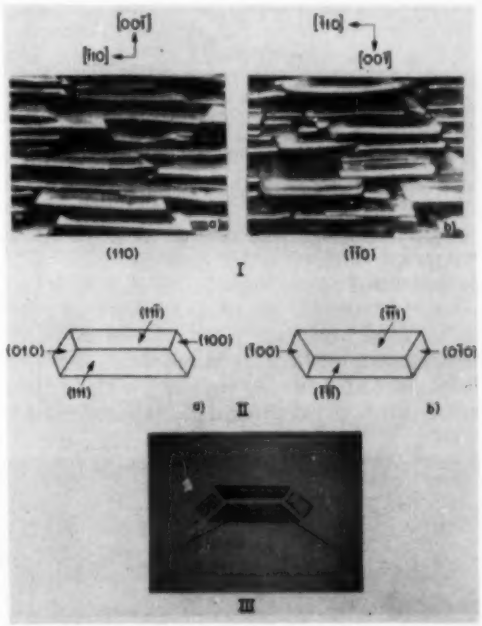

Fig. 1. Etch figures on {110} surfaces of InSb developed with 0.2N Fe^{+++} in 6N HCl at 82°C. I, opposite faces of an {110} wafer, 1500 X. II, schematic diagram of individual etch figures. III, exploded view of an etch figure; each facet was photographed individually while positioned parallel to the field of observation; arrows point to dislocation etch pits (approx. 800 X). (All magnifications are before reduction for publication.)

nation no difference is apparent between the two etched sides (Ia and Ib) of these wafers. Goniometric analysis of the etch figures shows that their elongated facets are {111} planes bounded by {100} planes as illustrated schematically in Fig. 1-II. The planes designated as (111) and $(\bar{1}\bar{1}1)$ are A planes whereas those designated as $(11\bar{1})$ and $(\bar{1}\bar{1}\bar{1})$ are B planes. It can be seen that in an etch figure the A planes develop to a greater extent being less reactive than the B planes. As a result of this, and by considering the geometry of the zinc-blende structure and the relative position of the A and B planes (1), the trapezoid-like figures on the opposite {110} faces should appear inverted when the wafer is rotated about the $[\bar{1}10]$ direction as it can be seen clearly in Fig. 1-II.

The difference in size between the A and B facets of the etch figures varies according to the etching conditions. If the {110} surfaces are exposed to the preferential Fe^{+++} etchant without first removing the cold worked layer introduced by abrasion, the difference in over-all size between the A and B planes is not very pronounced. However, if the cold worked layer is removed by a fast nonpreferential etchant and then the surface is etched with the Fe^{+++} etchant, the A planes essentially predominate over the B planes and the {110} surfaces acquire a scale-like (shingle-like) appearance.

It was considered of interest to find out whether or not the etching behavior of the microscopic A and B facets of the etch figures resembles that of the A and B surfaces of InSb. It was possible to develop dislocation etch pits on the A facets of the etch figures but not on B facets, in accord with the behavior of ordinary A and B surfaces. Furthermore, the A and B facets of the etch figures were unambiguously distinguishable by their over-all appearance which was typical of the A and B surfaces, respectively, etched in the Fe^{+++} etchant. It should be pointed out that the A and B facets are best examined microscopically when positioned parallel to the field of observation. They form a 35° angle with the {110} surface. In the present case an ordinary metallograph was employed and the {110} wafers were positioned at the appropriate angles by means of suitable platforms. An exploded view of an etch figure is shown in Fig. 1-III. The arrows in the A facet point to dislocation etch pits.

Nonpreferential etching revealed distinct dislocation etch pits in a background of chemically polished {110} surface as shown in Fig. 2-I. The over-all etching rate of the {110} surfaces was determined by employing samples bounded entirely by {110} surfaces. Results are shown in Table I together with rates of the A, B, and {100} surfaces. It is seen that in the Fe^{+++} etchant the various surfaces exhibit essentially the same etching rate since, in this case, the over-all etching process is controlled by the transport of oxidizing species of the etchant to the InSb surface. Consequently, no conclusions can be drawn about the relative reactivity of the various surfaces. In the nonpreferential etchant, at 4°C, the A surfaces exhibit the lowest rate. Under these conditions etching of the A and the {110} surfaces is under chemical activation control (activation energy approximately 25 kcal/mole) whereas etching of the B and the {100} surfaces is under diffusion control (activation energy approximately 5 kcal/mole). These results are discussed further below.

Table I. Etching rates of various crystallographic planes of InSb

Plane	Etching rate: Etchant 1, mg/cm²/min	Etching rate: Etchant 2, mg/cm²/sec
{111}—B	0.2$_5$	7.8
{100}	0.2$_5$	7.8
{110}	0.2$_5$	2.5
{111}—A	0.2$_5$	0.5

Etchant 1: 0.2*N* Fe^{+++} in 6*N* HCl; 10°C; Etchant 2: in parts by volume, 2 conc. HNO_3; 1 conc. HF; 1 glacial CH_3COOH; 4°C.

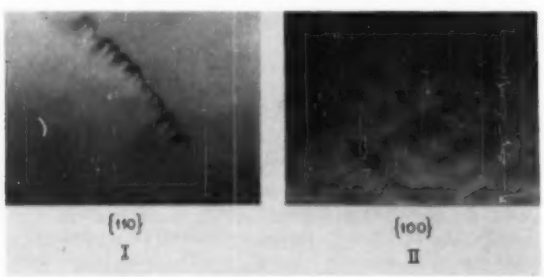

Fig. 2. Dislocation etch pits on the {110} and {100} surfaces (540 X). Etchant (in parts by volume): 5 conc. HNO_3; 5 conc HF; $2H_2O$.

{100} Surfaces

The {100} wafers employed in these experiments were prepared as the {110} wafers. As shown in Fig. 2-II, dislocation etch pits are revealed by nonpreferential etching, but they are appreciably smaller than the etch pits developing on the A or even the {110} surfaces under similar experimental conditions. Dislocation etch pits on the {100} surfaces of InSb or other III-V intermetallic compounds have not been reported in the literature. Yet, {100} surfaces like the {111} and {110} surfaces are intersected by the 60° edge dislocations of the zinc-blende structure.

On the {100} surfaces of InSb preferential etchants develop etch figures which are similar to those reported for GaAs (2). Figures 3-Ia and 3-Ib show the preferentially etched parallel surfaces of an {100} wafer. It is seen that the longer dimension of the rectangular etch figures on the one side of the {100} wafer is at a right angle to the longer dimension of the etch figures on the opposite side of the wafer. The etch figures are bounded by <110> directions.

Goniometric examination revealed that the etch figures are truncated tetragonal pyramid structures, the four sides being {111} planes. The top plane of the truncated pyramid is either flat {100} or has higher order planes (usually {411}) forming a shallow angle (approximately 19°) with the <100> direction. Between individual truncated pyramids occasionally pits are observed which are inverted pyramid-like depressions with flat {100} bottoms. The geometry of the etch figures is shown in Fig.

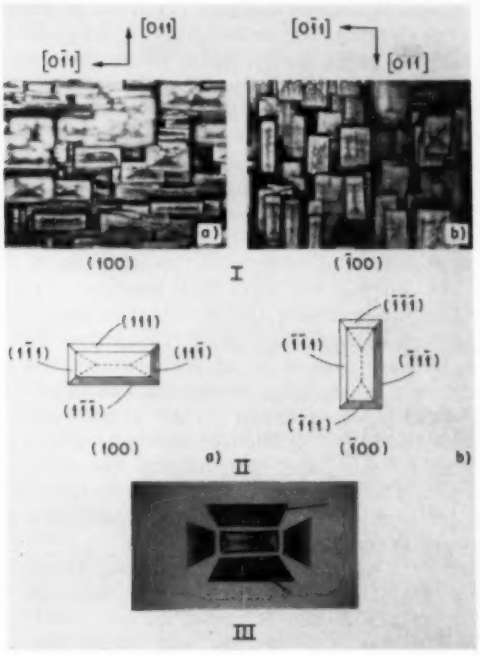

Fig. 3. Etch figures on {100} surfaces of InSb developed in 0.2N Fe^{+++} 6N HCl at 82°C. I, opposite faces of an {100} wafer, 1500 X. II, schematic diagram of individual etch figures; higher order planes occasionally present are indicated with dotted lines. III, exploded view of an etch figure; each facet was photographed individually while positioned parallel to the field of observation; arrows point to dislocation etch pits (approx. 800 X).

3-II. Here also the A facets [(111), (1$\bar{1}$1), (11$\bar{1}$), and ($\bar{1}\bar{1}\bar{1}$)] of the etch figures develop to a greater extent than the B facets [($\bar{1}$11), ($\bar{1}\bar{1}$1), (1$\bar{1}\bar{1}$), and (11$\bar{1}$)] and the etch figures appear as rectangular parallelograms rather than squares when viewed parallel to the <100> direction.

With techniques similar to those employed in the case of the {110} surfaces it was possible to develop and record conical dislocation etch pits on the A facets of the etch figures and to reveal on the individual facets the typical appearance of preferentially etched A and B surfaces. An exploded view of an etch figure is shown in Fig. 3-III. The arrows in the A facets point to dislocation etch pits.

If the cold-worked layer of the {100} surfaces is removed by chemical polishing prior to preferential etching the A facets develop to a much greater extent than the B facets. In addition the flat {100} facets are not developed and the etch figures become elongated structures as shown in Fig. 4.

The over-all etching rates of the {100} surfaces shown in Table I were obtained with samples bounded entirely by {100} surfaces.

Discussion

The development of certain crystallographic planes during crystal growth, as well as the distribution and morphology of etch figures, is associated with mechanisms which constitute a complex and controversial problem. The present results contribute to the elucidation of one of the aspects of this problem, i.e., the role of relative reactivity of the various crystallographic planes in the formation of dislocation etch pits and the morphology of etch figures. Of particular interest in the present case is the fact that two types of crystallographically equivalent {111} planes are involved.

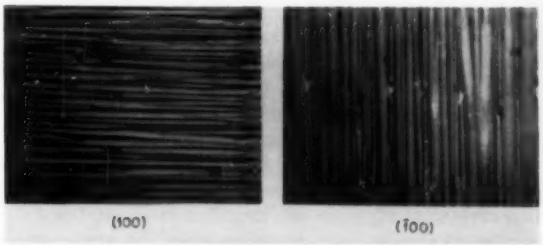

Fig. 4. Opposite faces of an {100} wafer of InSb etched with 0.2N Fe^{+++} in 6N HCl at 82°C following removal of the abraded surface in a nonpreferential etchant (1500 X).

In the case of InSb it was shown conclusively that in oxidizing etchants the A surfaces are far less reactive than the B surfaces [see Table I and also ref. (1)]. This difference in reactivity was considered the controlling factor for the observed differences in etching behavior between these two types of surfaces and in particular for the formation of dislocation etch pits on the A surfaces and not on the B surfaces. In the present study it was possible to confirm these differences in behavior on microscopic A and B facets of individual etch figures.

Differences in etching rates among the various surfaces of InSb are masked in many oxidizing media, as in the case of the Fe^{+++} etchant (Table I), since the etching rates are controlled primarily by transport processes in the etchant, even at low temperatures. However, as evidenced by the results of Table I for the nonpreferential etchant, it is believed that the reactivity of the principal crystallographic planes of InSb decreases in the following order (3)

$$B\ \{111\} \gtrsim \{100\} > \{110\} > A\ \{111\}$$

The {110} surfaces have both A and B atoms triply bonded to the lattice and, therefore, are more reactive than the A surfaces but less reactive than the B surfaces. Ideally {100} surfaces can consist of either A or B atoms; however, real {100} surfaces consist of both A and B atoms which are only doubly bonded to the lattice. Consequently the {100} surfaces are more reactive than the {110} surfaces. This reasoning does not show clearly whether or not the {100} surfaces are less reactive than the B surfaces. Doubly bonded B atoms are more reactive than triply bonded B atoms but doubly bonded A atoms are most likely less reactive than triply bonded B atoms (1). As will be pointed out below, however, the reactivity of the {100} surfaces is probably somewhat smaller than that of B surfaces.

For a dislocation etch pit to develop (or an etch pit in general) it is necessary that etching proceeds faster in the direction of the pit than on the surface surrounding it. It was shown (1) that this condition is met in oxidizing media only when dislocations consisting of a row of triply bonded A

atoms (α dislocations) intersect the A surfaces of III-V compounds. Apparently, in the zinc-blende structure, the elastic strains present in the direction of the dislocations do not enhance the reactivity to an appreciable extent under the present etching conditions. The conical etch pits presently observed on the {100} surfaces are attributed to dislocations on the basis of their morphology, which is typical of dislocation etch pits in the diamond and zinc-blende structure, and because rows of such etch pits were observed along low angle boundaries on the {100} surfaces. Like the etch pits of the A and {110} surfaces, the etch pits of the {100} surfaces are also believed to be due to α and not due to β dislocations [cf. ref. (4)].

By employing suitable InSb cylinders Venables and Broudy (4) found that dislocation etch pits become smaller in going from the {111} to the {110} surfaces. They reported no dislocation etch pits on the {100} surfaces. The conditions for dislocation etch pit formation on the {110} surfaces are not as favorable as on the A surfaces where the relatively low reactivity of the A surface atoms is essentially responsible for the formation of pits. The high reactivity of the atoms of the {110} surfaces and especially of the {100} surfaces prevents pronounced preferential attack along the dislocation axis.

The etch figures appearing during preferential etching of InSb surfaces consist of low indexed crystallographic facets and represent limiting etch forms. The elongated shape of the etch figures of the {100} surfaces (Fig. 4) is the result of the very high reactivity of the B planes. On both the {110} and {100} surfaces the more reactive B {111} facets develop to a lesser extent than the A facets. Since slow reacting planes predominate during etching of concave surfaces, the development of the etch figures is probably preceded by the formation of concave etch pits. No effort was made to follow the growth steps of the etch figures under the present, very rapid etching rates.

As in the case of {111} surfaces of InSb (1) here also cold work modified the preferential etching behavior. Cold-worked surfaces develop better defined etch figures than the surfaces from which the cold work has been removed (compare for example Fig. 3-I and 4). Actually in the case of {111} surfaces it was found that certain etchants act preferentially when cold work is present and lead to chemical polishing in the absence of cold work. Cold-worked surfaces are heavily populated with imperfections such as complex networks of dislocations, presenting numerous high energy centers which react appreciably faster than the rest of the surface and lead to the formation of etch pits.

Since the thickness of the cold-worked surface layer is estimated to be of the order of a few microns, these pits do not propagate to any great extent but rather develop into the steady-state shape of the etch figures. The observed excessive overlapping of the etch figures (Fig. 1 and 2) is suggestive of the multitude of centers for the initiation of etch pits. The varying size of these primary etch pits is very likely responsible for the varying dimensions of the etch figures. High reactivity centers for pit nucleation are present in all real surfaces but obviously to a much lesser extent than in those with a damaged layer. If active centers are assumed as necessary for the initiation of etch pits which develop into etch figures, then no etch figures should be expected to form on a flat, imperfection-free surface [cf. ref. (5)]. Such surfaces are not encountered in reality.

Cold work usually results in enhanced reactivity. In the case of the {100} surfaces the enhanced reactivity of the A and B planes decreases the difference in their reactivities and, thus, the etch figures of the {100} surfaces become rectangular as shown in Fig. 3 rather than elongated shapes as shown in Fig. 4.

From the experimental results and the preceding discussion it is apparent that the formation of dislocation etch pits and the over-all morphology of the etch figures is strongly affected by the relative reactivity of the principal crystallographic planes.

Manuscript received Oct. 8, 1959. This paper was prepared for delivery before the Columbus Meeting, Oct. 18-22, 1959. The work reported in this paper was performed by Lincoln Laboratory, a center for research operated by Massachusetts Institute of Technology with the joint support of the U. S. Army, Navy, and Air Force.

Any discussion of this paper will appear in a Discussion Section to be published in the December 1960 JOURNAL.

REFERENCES

1. H. C. Gatos and M. C. Lavine, *This Journal*, **107**, 427 (1960).
2. H. A. Schell, Z. *Metallkunde*, **48**, 158 (1957).
3. See also M. C. Lavine, A. J. Rosenberg, and H. C. Gatos, *J. Appl. Phys.*, **29**, 1131 (1958).
4. J. D. Venables and R. M. Broudy, *ibid.*, **29**, 1025 (1958).
5. A. P. Honess, "The Nature, Origin and Interpretation of the Etch Figures on Crystals," pp. 33-37, John Wiley & Sons, Inc., New York (1927).

Polarographic Reductions of Benzyl Halides

Leland W. Marple, Leif E. I. Hummelstedt,[1] and L. B. Rogers

Department of Chemistry and Laboratory for Nuclear Science, Massachusetts Institute of Technology, Cambridge, Massachusetts

ABSTRACT

A polarogram for benzyl chloride in a supporting electrolyte of lithium chloride has a dip in the limiting current due to electrostatic repulsion from the interface of the monovalent anion produced by transfer of the first electron. The dip is decreased by the presence of electronegative substituents on the ring and is eliminated by a moderate concentration of surface-active tetramethylammonium ions in the solution.

Benzyl bromide and iodide each undergo two widely separated one-electron reduction steps at concentrations less than 10^{-4} *M*. At higher concentrations, adsorption phenomena are encountered in the region of potential between the two waves due to the presence of bibenzyl, a by-product of the first reduction step.

The exploratory work of von Stackelberg and Stracke (1) showed that reductions of organic halogen compounds became easier on going from chloride to bromide to iodide. The over-all reaction usually involved replacement of the halogen atom with a hydrogen atom. The half-wave potentials were independent of pH, showing that addition of hydrogen did not occur in the rate-determining step, but after the transfer of electrons.

The steps in the polarographic reduction of an organic halogen compound, RX, can be represented by the following reactions (1, 2):

$$RX + e^- \rightarrow RX^- \quad [1]$$

$$RX^- \rightarrow R\cdot + X^- \quad [2]$$

$$R\cdot + e^- \rightarrow R^- \quad [3]$$

$$R^- + H_2O \rightarrow RH + OH^- \quad [4]$$

In some cases, side reactions (1),

$$2\,R\cdot \rightarrow R:R \quad [5]$$

or (3)

$$RX + Hg \rightarrow RHgX \quad [6]$$

are known to occur. It is generally assumed that addition of the first electron is the slow step and that reactions [2], [3], and [4] are relatively rapid because only one wave is usually observed for each halogen atom replaced.

Most aliphatic halogen compounds appear to reduce like carbon tetrachloride, for which no stable intermediates (ions or radicals) are believed to exist. Although the over-all reaction usually involves replacement of the halogen with a hydrogen atom, in the reduction of 1,2-dibromoethane, the principal product is reported to be ethylene (1). This reduction must involve virtually simultaneous transfer of two electrons, followed by elimination of two bromide ions and formation of a double bond. Normally, formation of a divalent negative intermediate must be considered improbable.

We felt that the addition of an aromatic ring to the carbon having the halogen atom, or the presence of a double bond in the 2-position should tend to increase the stability of intermediates in the reduction process. This was indeed found to be so. The first intermediate formed by benzyl chloride, the monovalent negative ion, $[C_6H_5CH_2Cl]^-$, appears to have a relatively long life-time. The chief evidence for the existence of such a long-lived intermediate is the appearance of a dip in the limiting current plateau. (Ring-substituted derivatives of benzyl chloride also have dips in their polarograms.) Similar dips in the polarograms for inorganic anions have been studied extensively by Frumkin and his coworkers (3, 5). It is generally agreed that the phenomenon is the result of electrostatic repulsion of a reducible anion from the negative electrode surface.

Current dips were not observed for either benzyl bromide or iodide. Instead, the present study indicates that a long-lived neutral species, either a stable free-radical or a dimer is formed. Mass-spectrometric evidence has confirmed the latter. The only other case where a stable product of a one-electron transfer has been reported is that for reductions of allyl mercury halides (3).

Results

Benzyl Chloride

The polarogram for this compound conformed to the general description of the process for the removal of a halide insofar as a single wave was obtained and its position was relatively independent of pH (see Fig. 1). Unlike most organic halides, its polarogram had a marked dip in the limiting-current plateau, a phenomenon that was observed under a variety of conditions. The dip was eliminated by the presence of 0.07*M* tetramethylammonium ion. Because dips in the limiting currents of anions are similarly affected, a negatively charged species of relatively long lifetime must be involved.

The polarograms can be explained by assuming that the limiting current prior to the onset of the

[1] Present address: Eastern Laboratory, E. I. du Pont de Nemours & Co., Inc., Gibbstown, N. J.

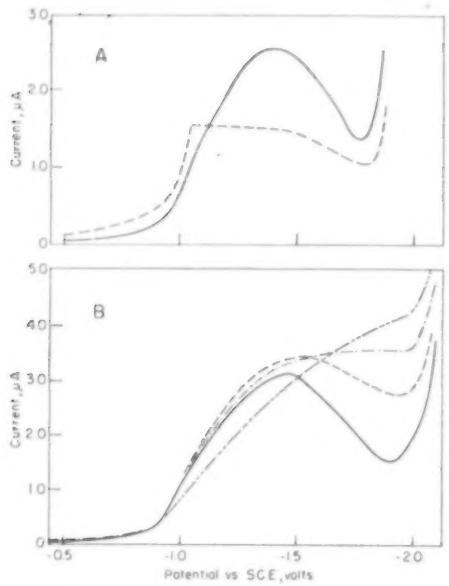

Fig. 1A. Polarograms of 1.17×10^{-3} M benzyl chloride in 0.092M NaOH. - - - - in 2.0% methanol; ——— in 51.0% methanol. Fig. 1B. Effect of $(CH_3)_4$ NCl on polarograms of 1.04×10^{-3} M benzyl chloride in 51.0% CH_3OH and 1.0M LiCl. ——— No $(CH_3)_4$ NCl added; - - - - - 0.030M $(CH_3)_4$ NCl; — · — · — · 0.070 M $(CH_3)_4$ NCl; — · · — · · — 0.47M $(CH_3)_4$ NCl.

dip corresponds to a two-electron transfer. As the potential of the electrode becomes more cathodic, progressively more of the product formed by reaction [1] is repelled from the surface of the electrode before reaction [2] (followed by [3] and [4]) can take place. In the presence of tetramethylammonium ion, however, repulsion of the ion is not as significant so that reaction [2], and those that follow, can proceed to completion. In that connection, it is interesting to note that the presence of calcium ion (0.49*M*) had no effect on the current dip. According to Reinmuth (6), this indicates that ion-pair formation is not the primary effect, but instead the structure of the double-layer. In addition, a temperature increase to 35°C, which would favor more rapid dissociation of the intermediate ion, did eliminate the dip.

There are two additional points of interest in connection with the effect of tetraalkylammonium salts. First, von Stackelberg and Stracke, in their broad survey of the polarography of organic halides, used 0.1*M* tetraethylammonium bromide as a background electrolyte. As a result, they observed no dips in their limiting currents. Second, in the present investigation it was found that large amounts of tetraalkylammonium salts produced a cathodic shift in the wave (Fig. 1) which was attributed to blocking of the electrode surface (7-9). Hence, the use of tetraalkylammonium salts to eliminate such current dips may result in shifts of the half-wave potential in either direction (2, 10).

In the case of benzyl chloride, the dip in the limiting current reached a value approximately one-half the maximum, indicating complete repulsion

Table I. Compounds exhibiting dips in the limiting current plateau in 1.0M LiCl and 51.0% CH_3OH

Compound	Conc, moles/liter	"$E_{1/2}$" v vs. S.C.E.	$\frac{i_{min}}{i_{max}}$
Benzyl chloride	1.04×10^{-3}	−1.066	0.45
α-Chloro-p-xylene	1.44×10^{-3}	−1.071	0.47
α, o-Dichlorotoluene	1.57×10^{-3}	−0.923	0.75
α, p-Dichlorotoluene	1.40×10^{-3}	−1.011	0.64
α, 2, 4-Trichlorotoluene	1.40×10^{-3}	−0.898	0.94
α, 3, 4-Trichlorotoluene	1.40×10^{-3}	−0.908	0.87
1-(Chloromethyl) naphthalene	8.3×10^{-4}	−0.953	0.85

of the organic ion. The fact that the value for limiting current was not corrected for a change in $m^{2/3}t^{1/6}$ with potential probably accounts for a ratio slightly smaller than 0.5. At potentials of −1.3, −1.5, and −1.7 v, the current proved to be diffusion controlled. Furthermore, the relative size of the dip appeared to be independent of concentration as low as $10^{-3}M$ where the correction for residual current was larger than the reduction current.

In Table I are listed the results on other related compounds which showed current dips. Note that the compound having two chlorine atoms in the ring gave the smallest dip, the compound with one chlorine in the ring, next. There may be many contributing factors but, in this case, the chief factor appears to be the greater distribution of charge which decreases the repulsion of the anion by the electrode. This hypothesis is supported by the smaller dip found on going from a benzene ring to a naphthalene ring. Furthermore, the presence of only 0.01*M* tetramethylammonium ion was sufficient to eliminate the small dip obtained with α-chloromethyl naphthalene.

Substitution in the ortho position appears particularly efficient in decreasing the dip. This suggests that there is a steric factor that aids the elimination of chloride ion.

Finally, Table I indicates that the presence of a larger number of chlorine atoms on the ring appears to produce a less cathodic half-wave potential. However, it should be pointed out that the locations of the waves are strongly influenced by adsorption.

The presence of adsorption effects is clearly evidenced in the original polarograms for benzyl chloride, particularly in low percentages of methanol. The dashed curve in Fig. 1A was obtained in 2% methanol. During the drawn-out initial portion of the wave, the individual drop shapes were quite characteristic of adsorption. Following the gradual rise at the beginning of the polarographicwave, the current increased rapidly to the limiting-current plateau. Much the same behavior was found in 20% methanol, but at 51% methanol adsorption behavior had almost disappeared. At 80% there was no evidence for adsorption either in the individual drop shapes or in the polarograms as a whole. All of the compounds in Table I showed similar adsorption behavior although most of them showed more evidence of it in 51% methanol than did benzyl chloride. Adsorption effects will be discussed later in more detail.

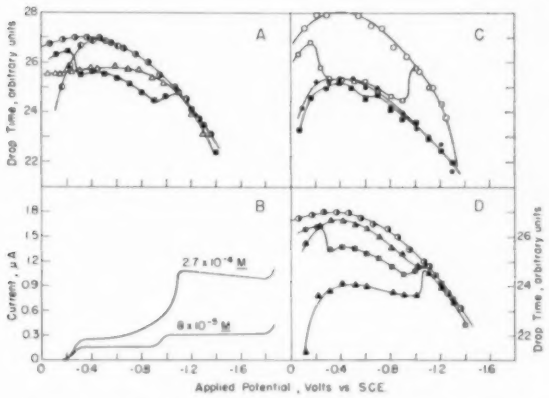

Fig. 2. Effects on electrocapillary curves of supporting electrolyte, solvent composition, and reducible species. Supporting electrolyte only.
Open circle, 2% MeOH-0.092 N NaOH; circle, solid right half, 51% MeOH-0.092 N NaOH; circle, solid left half, 51% MeOH-0.100 N KBr; solid circle, 80% MeOH-0.092 N NaOH.
Benzyl bromide, 1.13 x 10^{-3}M. open square, 2% MeOH-0.092 N NaOH; square, solid left half, 51% MeOH-0.092 N NaOH; solid square, 80% MeOH-0.092 N NaOH.
Open triangle, Bibenzyl, 2.83 x 10^{-4}M in 51% MeOH-0.092N NaOH; triangle, solid right half, benzyl chloride, 1.40 x 10^{-3}M in 51% MeOH-0.092N NaOH; solid triangle, benzyl iodide, 0.85 x 10^{-3}M in 51% MeOH-0.092N NaOH.

Benzyl Bromide and Benzyl Iodide

While polarograms for benzyl bromide had no current dips, they did show two distinct reduction steps at concentrations from 1 x 10^{-5} to about 1 x 10^{-4}*M*. Only below 1 x 10^{-4}*M* were two diffusion-controlled waves of equal height obtained. A typical polarogram is shown in Fig. 2B.

It is clear that each wave must correspond to a one-electron reduction. The first wave must be due to formation of the monovalent ion. The large separation of the first and second waves indicates that the radical produced by decomposition of the monovalent ion is not easily reduced further, probably because of a rapid conversion to bibenzyl according to Reaction 5. The absence of a current dip in the plateau of the second wave indicates that decomposition of the monovalent ion is, as expected, much faster in the case of the bromine compound than for chlorine.

The behavior of benzyl iodide, at concentrations between 1 x 10^{-5} and 2 x 10^{-4}*M*, was virtually identical with that of benzyl bromide. Not only were two diffusion-controlled waves of equal height obtained but, in addition, the half-wave potentials for the first and second waves agreed, within experimental error, with the values obtained for benzyl bromide. Again, no dip in the limiting current was observed.

At concentrations higher than about 10^{-4}*M*, the first waves of both benzyl bromide and benzyl iodide did not increase with concentration as fast as the second. Although the limiting current for the second wave had normal drop shapes and continued to be diffusion controlled, the shapes of the tracings for individual drops became increasingly characteristic of strong adsorption in the range of potential covered by the first wave. Changes in limiting current with mercury height gave plots falling between diffusion and adsorption control. The limiting current had a temperature coefficient of 2% per degree which did not differentiate between the two but did rule out kinetic control. Furthermore, the foot of the second wave acquired the desorption characteristics reported previously for the benzyl chloride wave (Fig. 2B). At concentrations greater than millimolar, behavior was quite erratic and two additional poorly shaped waves appeared between the usual first and second waves.

The electrocapillary curves shown in Fig. 2 not only confirm the presence of adsorption but give further insight with respect to the differences that were observed. A comparison of Fig. 2A and 2B shows that a marked decrease in drop time occurred in the region of the first wave and continued to the second wave. Upon passing through the second reduction the drop time returned to that of the background electrolyte. The decrease in the region of the plateau of the first wave is not attributable to bromide ion produced in the reduction or by the slow hydrolysis of benzyl bromide. (Note the negative slope of the limiting-current plateau in Fig. 2B. However, the presence of 0.1*M* bromide ion did affect the electrocapillary curve on the positive side of the maximum.) In the limiting-current region of the first wave, bibenzyl is strongly adsorbed whereas toluene, the final reduction product, and benzyl alcohol, the hydrolysis product, are not adsorbed at the millimolar level. This indicates that the product of Reaction 5, bibenzyl, was the main source of the adsorption effects.

Adsorption of the reduction product of the first wave is less pronounced at higher concentrations of alcohol. Figure 2C shows that there is little adsorption in 80% methanol probably due to greater competition for the surface from methanol as well as to greater solubility of the product. The somewhat greater adsorption found in the case of benzyl iodide in alkaline solutions of 51% methanol may reflect the faster decomposition in this medium of its monovalent ion compared to that formed by benzyl bromide (see Fig. 2D). As a result, a somewhat higher concentration of bibenzyl would be produced at the surface.

Other aspects of adsorption were examined briefly. First, it was possible to show that, at low concentrations of benzyl bromide, the half-wave potential for the first reduction was sensitive to the presence of surface-active anions and hydroxide; in the presence of 0.092*M* sodium hydroxide or 0.10*M* potassium bromide the wave appeared at more cathodic potentials than in the presence of chloride, in which the wave was, in turn, more cathodic than that in nitrate. There was also a corresponding shift in the electrocapillary curve.

The effect of the presence of bromide ion was studied originally because of its presence due to decomposition of benzyl bromide in alkaline solutions. Hydrolysis led to erratic results for half-wave potentials, particularly in the case of benzyl iodide, which decomposed even faster. Decomposition was slower in higher concentrations of methanol and at the same time, the half-wave potentials were shifted

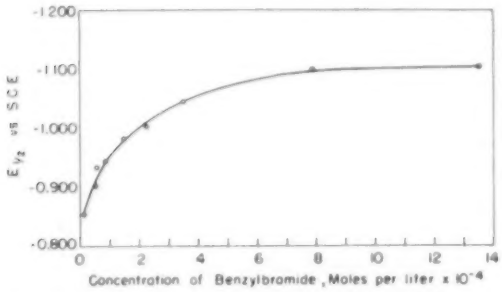

Fig. 3. Effect of concentration of benzyl bromide on its half-wave potential in 51% methanol that is 0.092M in sodium hydroxide.

to more cathodic values. These shifts indicated that a charged species was being produced by the reaction and ruled out the possibility that the neutral halide was undergoing ionization prior to reduction.

The position of the second wave for benzyl bromide was a function of concentration. Thus, there was approximately a 250 mv cathodic shift on going up from 1 x 10^{-5} to 1 x 10^{-3}*M*. At higher concentrations the wave remained constant, probably due to attainment of maximum sorption (see Fig. 3). Benzyl chloride showed a similar but much smaller dependence on concentration.

It is important to note that the half-wave potential for each wave of benzyl bromide agreed with the corresponding one for benzyl iodide within experimental error. Agreement of the first waves, which involve different reducible species, was surprising but can be rationalized in terms of virtually simultaneous electron transfer and halide elimination. On the other hand, agreement of the half-wave potentials for the second waves is to be expected because the same intermediate, the benzyl radical, is undergoing further reduction in each case. The resulting carbanion undoubtedly reacts with the solvent to form toluene.

From the electrocapillary curves in Fig. 2, it was quite clear that bibenzyl, or a closely related compound, must have been formed in the first reduction steps of the bromide and iodide derivatives. However, the presence of bibenzyl was later confirmed by making mass-spectrometric studies of products isolated from extracts of large-scale electrolyses. A 10^{-1}*M* solution of benzyl bromide in 50% methanol containing 0.1*M* potassium bromide was electrolyzed at −0.5 v vs. S.C.E. using a mercury-pool cathode until the current had decreased to a negligible value. The solution was again made 10^{-1}*M* in benzyl bromide and electrolysis continued. A white solid precipitated before the end of the electrolysis, and it gave the typical mass-spectrometric pattern of bibenzyl. Masses of 182 and 91 were particularly prominent. The original benzyl bromide showed no trace of mass 182.

Another electrolysis was carried out in which droplets of excess benzyl bromide were present at all times. A mass spectrogram of an ether extract, from which the more volatile materials had been pumped off, clearly indicated the presence of large amounts of $C_6H_5CH_2C_6H_4CH_2Br$ (masses 260 and 262), or one of its isomers, and $C_6H_5CH_2C_6H_4CH_2$ (mass 181) and the corresponding metastable peak at 126. The presence of relatively small amounts of bibenzyl was indicated by the small peak at mass 91 and the fact that mass 182 was somewhat higher than that expected from the isotopic ratio of carbon in a fourteen-carbon species. The formation of such a halide can be explained easily by the presence of the large excess of benzyl bromide in the solution. A reaction product of this type might well lead to the appearance of the additional polarographic waves which appeared in millimolar solutions of benzyl bromide (and iodide). Large peaks at masses 165 and 166 were also found in this extract but could not be explained satisfactorily.

Neither of the above electrolysis products gave any indication of masses for $C_6H_5CH_2HgBr$ or $C_6H_5CH_2Hg$. Generally, the peaks for HgBr and $HgBr_2$ were roughly equivalent and were found to the same extent in blank electrolyses. However, as one might expect small amounts of benzylmethyl ether (mass 122) formed by solvolysis were present but there was no benzyl alcohol (mass 108).

A similar experiment, in which an air-free suspension of benzyl bromide (in 50% methanol containing 0.1*M* potassium bromide) was shaken with mercury (no potential applied), showed no evidence of a spontaneous reaction leading to an organo-mercury compound. The small amounts of mercury present were also found in the blank. Therefore, there is no basis for suggesting that the electrochemical reduction of benzyl bromide (and probably the iodide) is preceded by a reaction with mercury or that the benzyl radical attacks mercury after being formed. In the case of the corresponding allyl halides, prior chemical reaction may indeed occur (3), but the proposed dissociation to form $RHg^{\cdot}$ prior to reduction seems unlikely, except for one of the compounds, because of the reported cathodic shift in reduction potential as the dielectric constant of the medium was lowered.

Experimental Details

Polarograms and electrocapillary curves were obtained as before (10). The organic halides were the purest obtainable from Eastman Kodak Company and were used as received. Stock solutions were prepared in pure methanol from which aliquots were taken to prepare polarographic solutions. Polarograms were run at 25°C and a line drawn through the maximum currents for use in the figures. Limiting currents were tested for diffusion control by plotting reduction current vs. square root of the mercury height; a straight line was interpreted as an indication of diffusion control. Temperature coefficients of the limiting currents were also studied between 2° and 35°C and, except for the dip of benzyl chloride, were found to be close to 2%/C°.

Mass spectrometric studies were made on a CEC Model 21-103C. In every case, masses were scanned to at least 400.

Acknowledgment

The authors are very much indebted to Professor Klaus Biemann and his associates for running the mass spectrometric analyses and providing vital de-

tails for interpretation of those results. This work was supported in part by the United States Atomic Energy Commission under Contract AT(30-1)905.

Manuscript received June 26, 1959. This paper was prepared for delivery before the Columbus Meeting, Oct. 18-22, 1959.

Any discussion of this paper will appear in a Discussion Section to be published in the December 1960 JOURNAL.

REFERENCES

1. M. von Stackelberg and W. Stracke, *Z. Elektrochem.*, **53**, 118 (1949).
2. J. L. Lothe and L. B. Rogers, *This Journal*, **101**, 258 (1954).
3. A. Kirrmann and M. Kleine-Peter, *Bull. Soc. Chim., France, 1957*, 894; see also, G. Costa, *Ricerca Sci.*, **22**, S133 (1952).
4. A. Frumkin, "Adsorption of Organic Substances at the Metal-Electrolyte Solution Interface and Its Influence on Electrochemical Processes" in "Electrical Phenomena and Solid-Liquid Interface," p. 58, Academic Press, New York (1957).
5. A. Frumkin, N. Nikolajeva-Fedorovich, and R. Ivanova, *Can. J. Chem.*, **37**, 253 (1959).
6. W. H. Reinmuth, Paper presented at the 134th Meeting of the American Chemical Society, Chicago, Illinois, September 1958.
7. A. A. Kryukova and M. A. Loshkarev, *Zhur. Fiz. Khim.*, **30**, 2236 (1956).
8. M. A. Loshkarev and M. G. Dikova, *Ukrain. Khim. Zhur.*, **22**, 457 (1956).
9. M. A. Loshkarev and A. A. Kryukova, *Zhur. Fiz. Khim.*, **31**, 452 (1957).
10. L. E. I. Hummelstedt and L. B. Rogers, *This Journal*, **106**, 248 (1959).

Preparation of Boron from Boron Carbide

David R. Stern

American Potash & Chemical Corporation, Whittier, California

ABSTRACT

A process to prepare elemental boron from boron carbide is presented. Included is evidence that the process is one of anodic transfer. Boron of at least 99.8% purity can be made directly from technical grade materials. Purity is a function of electrolysis voltages and boron carbide purity. Current efficiencies in excess of 95% are obtained and preferred electrolysis conditions are stated.

Preparation of elemental boron has been discussed by a large number of investigators (1-19). Not all processes give sufficient purity. Filament and arc discharge techniques have generally been regarded as the preferred methods of securing a high-purity crystalline boron (2, 3, 5-8, 11, 12, 17, 19). New interest in elemental boron as thermistors and possible semiconductor devices has reemphasized the problem of attaining higher purities. McCarty and coworkers (18) have discovered new low-temperature crystalline modifications of elemental boron.

Vapor phase deposition techniques are generally limited by metallic filament contamination. Impurities are generally tantalum, tungsten, molybdenum, carbon, and titanium (2, 3, 7, 11, 12, 17, 19). Another disadvantage with these contaminants is that they are not removed with secondary upgrading techniques. Deposition on a filament of elemental boron and lower decomposition temperatures are significant contributions (7, 19).

Desire for a potentially higher purity product without heavy metal contamination focused attention on an electrolytic approach. Andrieux, Cooper, and others have developed electrolytic reductions (4, 9, 10, 14-16).

This research effort has resulted in an electrolytic process for boron, which is an anode transfer technique (13). This transfer technique has been applied both to elemental boron and boron carbide. Feasibility studies were conducted on a laboratory exploratory basis in small cells. The scope of this paper is limited to the bench scale preparation of elemental boron from boron carbide.

Experimental Procedure

Cell.—A cross section of the cell used in this investigation is presented in Fig. 1 The unit consisted of a porous carbon basket with a porous carbon diaphragm. Carbide was packed between the diaphragm and porous basket. This cartridge unit was lowered into a dense graphite crucible by steel rods. Removal and recharging with boron carbide could be accomplished without a complete cell shutdown.

External heating was accomplished using graphite resistors. Cell temperatures were measured with Chromel-Alumel thermocouples inserted into the recesses in the centering post and the hollow cathode which was also a thermowell.

An argon blanket could be maintained over the entire cell.

Electrolyte.—The electrolyte consisted of sodium chloride, potassium chloride, and potassium fluoborate with an initial composition of 40-40-20 wt %, respectively. During the course of electrolysis, cathode deposits are withdrawn periodically. Occluded electrolyte is water leached and can be recovered and recycled.

Electrolysis.—After the anode compartment was packed with boron carbide, sufficient predried salt is added to cover the carbide. This cartridge charge was then placed in the heating furnace and melted under argon. Whenever fresh salts, a new diaphragm, or new crucible were used, pre-electrolysis was performed at 2.5 v from ½ to 1 hr before actual electrolysis. The pre-electrolysis deposit acted as a scavenger of impurities and was a direct means of purifying the electrolytic system. A cathode was

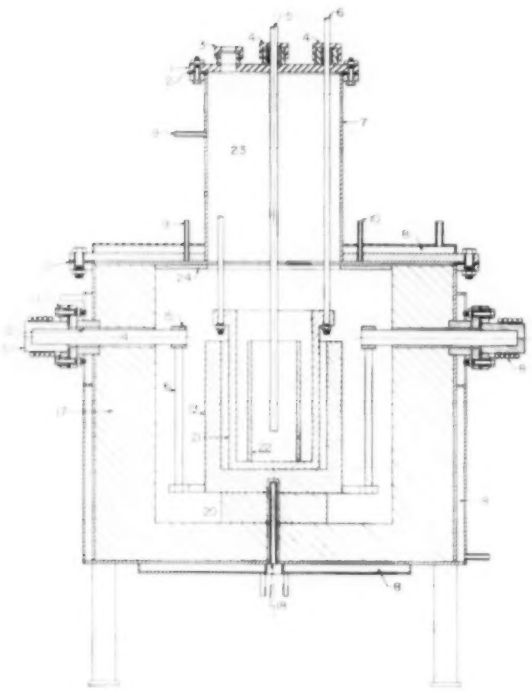

Fig. 1. Bench scale boron carbide cell: 1, stainless (316) lid; 2, Neoprene gasket; 3, sight glass; 4, packing glands; 5, cathode; 6, anode tie rods; 7, mild steel shell; 8, water jackets; 9, argon inlet; 10, argon outlet; 11, insulating bushing; 12, Vycor tube; 13, copper a-c electrode connector assembly; 14, main graphite electrode lead; 15, graphite a-c electrode connector; 16, a-c graphite resistor rod; 17, magnesia insulating bricks; 18, centering post; 19, dense carbon cup; 20, carbon pedestal; 21, porous carbon basket; 22, porous carbon diaphragm; 23, cooling chamber; 24, heat baffle.

then inserted to a known depth so that a given cathodic current density could be set initially.

At completion of electrolysis the cathode was raised and allowed to cool. To recharge the boron carbide, the cartridge unit was raised, salt allowed to drain, and a new unit inserted.

Processing.—Figure 2 is a photograph of a typical cathode deposit. This deposit was placed in a polyethylene beaker of distilled water on removal. Upon standing in the water the deposit would break off the rod and was wet ground in an iron mortar and leached twice with 10% hydrochloric acid. It was then washed free of acid, rinsed with acetone, and vacuum dried under argon.

The final sample was then weighed and analyzed. Most samples were analyzed for total boron content, sodium, iron potassium, silicon, nitric acid insolubles, and water soluble boron.

Fig. 2. Typical cathode deposit

Experimental Results

Product purity.—The purest elemental boron resulting from this investigation was 99.8%. This purity was obtained using commercial reagents without any prior purification or recrystallization. Control of the electrolysis and atmosphere were the only precautions taken. Major impurities were sodium, silicon, iron, and carbon. These generally could be limited to less than a total of 0.2%. Lower levels of impurities were sodium 0.05%, silicon 0.07%, iron 0.05%, and carbon (as B_4C) 0.06%. These lower levels, however, were not obtained simultaneously in one sample.

Effect of cell voltage.—An important factor contributing to product purity is cell voltage. A typical relationship between sodium impurity and cell voltage is presented in Figure 3. At voltages between 0.9–1.0 v sodium contents were as low as 0.05%, but no smooth correlation was obtained. It must be pointed out that anodic current density is not constant in this system.

A similar relationship can be shown for the silicon and iron impurities, but the final level of these impurities are also dependent on the processing technique.

These results indicate that the concentration of major impurities in the product is a direct function of cell voltage, the higher the cell voltages the higher the impurities.

Electrolytic decomposition of the fluoborate and alkali halides occur at higher voltages. These reactions are indicated by the liberation of chlorine and adversely affect the current efficiency of the process as well as product purity.

As long as sodium is a component of the electrolyte, there will be some sodium contamination, but by maintaining voltage below 1.2 v, sodium content may be kept below 0.2%.

Origin of other contaminants.—Table I lists the typical spectrographic analyses of the new raw materials entering the process and the materials of con-

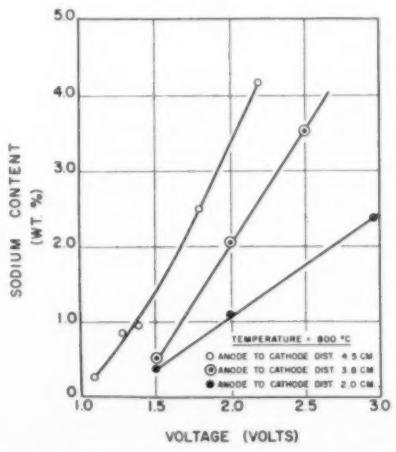

Fig. 3. Sodium content of boron product as a function of cell voltage.

Table I. Semi-Quantitative spectrographic analyses

Constituent	Weight per cent			
	B_4C*	KBF_4*	Carbon†	Graphite‡
Boron	Major	Major	—	0.0008
Silicon	0.17	0.02	0.017	0.012
Iron	1.2	0.015	0.045	0.032
Magnesium	0.26	0.00092	0.0068	0.0016
Titanium	0.10	nil	0.0018	0.0036
Copper	0.0072	0.0011	0.0013	0.00044
Manganese	0.16	nil	—	—
Calcium	0.026	0.26	0.038	0.018
Zirconium	0.20	nil	—	—
Aluminum	0.3	0.0034	0.012	0.030

* Technical grades.
† Grade 20 porous carbon.
‡ C. S. Graphite.

struction. Boron carbide contains the major contaminants except for the calcium in the fluoborate. Thus, purity of the elemental boron is closely allied to the purity of boron carbide. Silicon and iron are anodically transferred in this process.

Pre-electrolysis yields a deposit containing approximately 14% iron, 12% silicon, and only 16% boron.

Figure 4 presents product purity as a function of cumulative electrolysis. These results indicate that whenever a new charge is electrolyzed the purity is low probably due to moisture and the impurities in the boron carbide and the salts.

After an initial conditioning period the purity increases and remains high during most of the remaining electrolysis. Drop off in purity is attributed to higher transfer voltages resulting from the build-up of carbon in the anode compartment as boron is depleted. If the product covering 90% of the electrolysis time were combined into a single sample, an average product purity of 98% would result. The maximum purity attained was 99.8% boron.

Effect of temperature.—High-purity product is obtained at good current efficiencies within a temperature range of 700°-850°C. No definite relationship between temperature and product purity has been noticed within this range. Although a detailed study of the phase relationship of the KCl-NaCl-KBF_4 mixture has not been made, operation above the KCl-NaCl eutectic 660°C must be employed. Above 850°C loss of the fluoborate increases

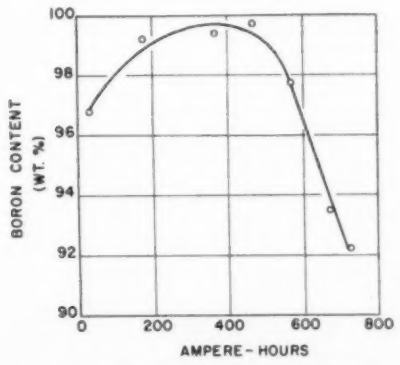

Fig. 4. Product purity as a function of cumulative ampere-hours.

and deposits tend to fall from the cathode. A compromise temperature of 800°C was adopted for the major part of this investigation.

Current density.—Cathodic current density has been varied between 12 to 75.0 amp/dm^2. High current efficiencies are obtained throughout this range. No significant correlation was found between initial current density and boron purity.

Boron material balance.—It has been stated that boron was derived from the carbide and that fluoborate was only a carrier salt. Previous electrolysis systems (4, 9, 10, 13-16) have operated at higher voltages and consequently have not been anodic transfer processes.

Table II lists some experiments, which offer some proof that in this system boron is derived from the anodic boron carbide.

The following points should be noticed: (*a*) experiments conducted without boron carbide (regardless of a carrier) gave no product below 1.3 v; (*b*) experiments conducted without fluoborate (with B_4C) also gave no product even up to 2.2 v; (*c*) the solvent for the carrier salt may be pure KCl, NaCl, or halide mixtures; (*d*) at voltages higher than 3 v boron trichloride is formed.

Analyses of the boron carbide also give evidence of the boron being extracted. These data are presented in Table III.

Final proof of boron transfer is presented in Table IV. Examination indicates that a total of 61 g of elemental boron was extracted on the cathode deposit during electrolysis, whereas only 12 g of boron was available initially in the fluoborate and 11 g of this were accounted for at the completion of electrolysis.

Cell electrolyte.—Cell electrolyte analyses have indicated that concentrations of sodium, potassium,

Table II. Electrolytic systems

Electrolyte	Anode	Voltage	Yield
KCl-KBF_4-NaCl	None	<1.0	None
KCl-KBF_4-NaCl	None	>1.3	Some
KCl-KBF_4	None	<1.0	None
KCl-NaCl	Boron carbide	2.2	None
KCl-NaCl	Boron carbide	3.2	None*
KCl-NaCl-NaF	Boron carbide	1.2	None
KCl-KBF_4	Boron carbide	<1.0	Yes
KCl-KBF_4-NaCl	Boron carbide	<1.0	Yes
LiCl-KF-KBF_4	Boron carbide	2.8	Some
KCl-KF-KBF_4	Boron carbide	<1.1	Yes

* BCl_3 fumes.

Table III. Anodic transfer of boron from boron carbide

	Weight per cent	
	Before electrolysis*	After electrolysis†
Total B	75.4	18.8
H_2O Sol. B	0.05	—
HNO_3 Ins.	98.2	83.58
Fe	0.11	0.04
Si	0.16	—
B in HNO_3 Ins.	76.58	19.61

* Technical grade powder B_4C.
† Analysis after 1063 amp-hr of electrolysis.

Table IV. Boron balance in boron carbide cell

	g	g
Total boron in cell initially:		
As B_4C	74	
As KBF, (electrolyte)	12	
		86
Total boron remaining in cell after electrolysis:		
In anode charge	13	
In electrolyte	8	
		21
Total boron removed from cell during electrolysis:		
By deposition	61	
By salt drag out and sampling	3	
		64
Total boron accounted for		85
Boron unaccounted for		1

and chloride ions do not change appreciably during electrolysis. Concentrations as a function of cumulative ampere-hours are presented in Fig. 5. All concentrations are relatively constant except that of the fluoride ion. This is contrary to what is expected in the electrolysis of a halide-fluoborate system where the potassium fluoride concentration increases as boron fluoride is reduced to boron. The boron concentration at the start increases for a short period of time. This probably represents the solution of boron from the carbide. This observation is illustrated vividly in Fig. 6 when the fluoride to boron mol ratios are plotted as a function of electrolysis time. The ratio in fluoborate is four, while an inspection of the curve shows a decrease to a ratio of two. Chemical analyses of the purge gas indicate that some fluoride is lost from the system as boron trifluoride, but the rate of solution of boron from the carbide more than compensates for that volatized from the system. Material balance data indicate that the physical quantity of fluoborate lost is relatively small and can be made up by fluoborate additions.

Electrolysis data.—Current efficiency for this system is based on the following electrode reaction:

$$B^{+3} + 3e \rightarrow B^{\circ} \qquad [1]$$

Some data on electrolysis are presented in Table V. High current efficiencies are obtained and energy consumption is low. A pound of 94-99% boron requires from 3-4 kwhr of electrical energy.

Summary and Conclusions

An electrolytic anode transfer process for the preparation of high-purity elemental boron from boron carbide has been presented. Evidence that the process is one of anodic transfer is included.

The following conclusions concerning this method of preparing elemental boron can be set forth:

1. Boron of at least 99.8% purity can be made directly from technical grade materials without prior purification treatment.
2. Elemental boron can be prepared in purities at least equal to that attained via vapor deposition processes without the corresponding heavy metal contamination.
3. Major impurities are sodium, silicon, iron, and carbon. The total of these impurities can be reduced to 0.2% or less.
4. Impurity levels in the boron are a function of the electrolysis voltage and purity of the boron carbide.

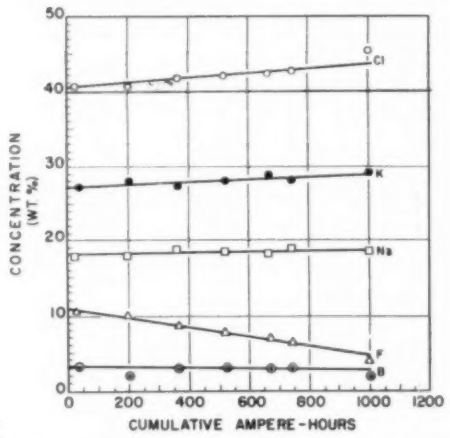

Fig. 5. Electrolyte composition as function of cumulative ampere-hours.

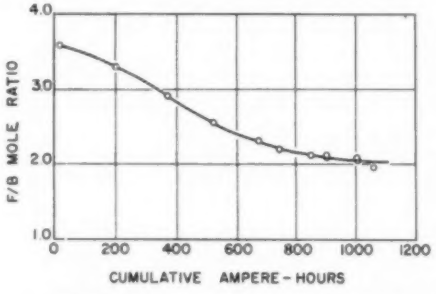

Fig. 6. Fluoride boron mole ratio as a function of cumulative ampere-hours.

Table V. Electrolysis data

Temp, °C	Voltage, v	Current, amp	Time, hr	Final deposit weight, g	Cathodic current density, amp/dm²	Current efficiency, %	kwhr/lb Boron
735	1.1	6.9	24	21	16.6	92.0	3.9
740	1.1	6.5	23	18.8	14.4	90	4.0
725	1.1	3.5	29.5	12.0	11.9	81	4.3
790	1.0	7.9	19.0	17.4	13.5	96	3.9
800	1.0	6.9	19.0	17.5	14.0	98	3.4
800	1.0	4.2	24.0	12.7	9.0	90	3.6
795	1.0	5.3	23	17.1	11.3	97	3.2
800	1.0	3.7	23	12.9	8.4	101	3.0
810	0.9	5.8	52.5	39.6	10.7	90	3.1
810	1.0	4.1	66	35.7	8.2	94	3.4
800	1.0	5.7	30	21.7	5.1	92	3.6

5. Voltages less than 1.2 v, cathodic current densities between 12.0 and 75.0 amp/dm², and 800°C are the preferred conditions of electrolysis.

6. Current efficiencies for this anodic transfer process are high. Efficiencies in excess of 95% are easily obtained. Energy consumption is 3-4 kwhr/lb boron.

7. The application of this technique as a secondary upgrading technique for higher purity borons has been postulated.

Acknowledgment

The author would like to express his appreciation to Mr. Aiji Uchiyama and Mr. Quentin H. McKenna who conducted both the laboratory and bench scale work on this project.

Manuscript received Oct. 12, 1959. This paper was prepared for delivery before the Chicago Meeting, May 1-5, 1960.

Any discussion of this paper will appear in a Discussion Section to be published in the December 1960 JOURNAL.

REFERENCES

1. H. Moissan, *Ann. chim. et. phys.*, **6**, 296 (1895).
2. E. Weintraub, *Trans. Am. Electrochem. Soc.*, **16**, 165 (1909).
3. A. E. Van Arkel, U.S. Pat. 1,774,410, Aug. 26, 1930.
4. J. L. Andrieux, *Ann. chim.*, **12**, 423 (1929).
5. L. Hackspill, A. Stieber, and R. Hocart, *Compt. rend.*, **193**, 776 (1931).
6. D. P. Mellor, S. B. Cohen, and E. B. Underwood, *Australian Chem. Inst. J. & Proc.*, **3**, 329 (1936).
7. A. J. Laubengayer, D. T. Hurd, A. E. Newkirk, and J. L. Hoard, *J. Am. Chem. Soc.*, **65**, 124 (1943).
8. M. Formstecher and E. Ryskevic, *Compt. rend.*, **221**, 747 (1945).
9. H. S. Cooper, U.S. Pat. 2,572,248, Oct. 23, 1951.
10. H. S. Cooper, U.S. Pat. 2,572,249, Oct. 23, 1951.
11. G. H. Fetterley, U.S. Pat. 2,542,916, Feb 20, 1951.
12. G. M. Murphy, "Separation of Boron Isotopes," National Nuclear Energy Series, Vol. 3, U.S. Atomic Energy Commission, Oak Ridge, Tennessee (1952).
13. Norton Co., Australian Pat. 164,170, July 18, 1955.
14. J. L. Andrieux and W. J. Deiss, *Bull. soc. chim., France*, 838 (1955).
15. N. P. Nies, E. W. Fajans, L. L. Thomas, L. E. Hiebert, and V. Morgan, U.S. Pat. 2,832,730, Apr. 29,1958.
16. N. F. Murphy and R. S. Tinsley, U. S. Pat. 2,848,396, Aug. 19, 1958.
17. D. R. Stern and L. Lynds, *This Journal*, **105**, (11) 676 (1958).
18. L. V. McCarty, J. S. Kasper, F. H. Horn, B. F. Decker, and A. E. Newkirk, *J. Am. Chem. Soc.*, **80**, 2592 (1958)
19. K. E. Bean and R. J. Sparks, "Research Investigation of Physical Chemistry and Metallurgy of Semiconductor Materials," 2nd Quarterly Report, Mar. 1, 1959-June 1, 1959, Signal Corp, Contract DA-36-039-SC-78246.

Contribution to the Theory of Current Distribution in Local Cells

Carl Wagner

Max-Planck-Institut für physikalische Chemie, Göttingen, Germany

ABSTRACT

The distribution of the anodic current density in local cells involving anodic dissolution of a metal and reduction of oxygen as the cathodic reaction is calculated for a diffusion controlled limiting cathodic current density.

Statement of the Problem

Corrosion of metals in aqueous solutions may in general be accounted for by the superposition of anodic and cathodic reactions. The anodic reaction which is the dissolution of a specified metal is inherently confined to the surface of that metal. Cathodic reactions involve reduction of oxidizers, e.g., reduction of elemental oxygen to water, or evolution of hydrogen from hydrogen ions. If only one metal without inhomogeneities is present, anodic and cathodic reactions occur randomly at its surface (1), and the net current density vanishes everywhere. In the presence of chemically inert inclusions, conducting oxide layers, or other electronic conductors which are in electrical contact with the metal, cathodic reactions may also occur at the surface of these materials. In the latter case referred to as local cell action, there is a net current flowing inside the electrolyte from the metal which is dissolved as anode to the other material as cathode. The occurrence of cathodic reactions at the other materials increases inherently the rate of dissolution of metal as the anodic reaction and thus aggravates corrosion. If the dissolving metal is directly adjacent to cathodic areas, the rate of attack is especially high at the boundary. Thus conditions favoring local cell action are to be avoided if possible in order to minimize corrosion. This, however, is not always easy to accomplish. Therefore, it is desirable to formulate rules of thumb in order to estimate the potential dangers resulting from local cell action.

Current distributions in local cells have been calculated by Waber and his associates (2-7). For coplanar adjacent cathodes and anodes shown in Fig. 1, the current density next to an anode-cathode boundary becomes infinite if polarization is disregarded (2). Thus for a realistic approach, polar-

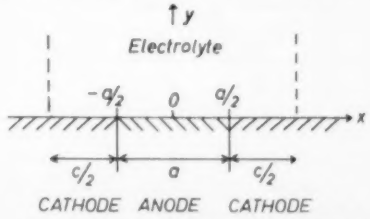

Fig. 1. Anode with adjacent cathodes

ization must be taken in account in estimating the maximum local corrosion rate at an anode-cathode boundary. If both the anodic and the cathodic polarization curve can be approximated by straight lines involving the same slope, the potential distribution in the electrolyte can be obtained in terms of a Fourier series or integral and therefrom the local current density can be calculated (3,4). Calculations for other conditions seem desirable. In what follows calculations are presented for a diffusion controlled limiting cathodic current density in solutions containing oxygen.

In accord with Waber it is assumed that there are no solid corrosion products which impede diffusion and conduction in the electrolyte.

General Presuppositions

The electrical potential ϕ in an electrolyte involving a constant electrical conductivity obeys the Laplace equation

$$\text{div grad } \phi = 0 \qquad [1]$$

For a single cathodic and a single anodic reaction and for a constant electrical potential in the metallic conductors, the boundary conditions can be formulated as (8)

$$\phi \text{ (anode)} + \eta_a(J_a) = \Phi_a \qquad [2]$$

$$\phi \text{ (cathode)} - \eta_c(J_c) = \Phi_c \qquad [3]$$

where ϕ (anode) and ϕ (cathode) are the electrical potentials in the electrolyte next to the anode and the cathode, respectively, Φ_a and Φ_c are constants, and η_a and η_c, respectively, are the absolute values of the overpotentials of the anodic and the cathodic reaction corresponding to the absolute local current densities J_a and J_c. Since cations are supposed to migrate from the anode toward the cathode, ϕ (anode) is more positive than ϕ (cathode).

At the anode, metal is dissolved and simultaneously the oxidizer, e.g., oxygen, is reduced cathodically. The net current density at the anode, $J_a - J_c$, is equal to the product of the specific conductivity σ of the electrolyte and the absolute value of the local potential gradient, $\partial\phi/\partial n$, normal to the surface of the electrode according to Ohm's law,

$$[J_a - J_c = \sigma\,|\partial\phi/\partial n\,|] \text{ anode} \qquad [4]$$

At the cathode, reduction of oxidizer, e.g., oxygen, is supposed to be the only electrode reaction. Thus

$$[J_c = \sigma\,|\partial\phi/\partial n\,|] \text{ cathode} \qquad [5]$$

To obtain solutions for the potential and the current distribution from Eq. [1] to [5], the polarization curves must be known for both the anodic and the cathodic reaction. In particular, it is possible to calculate the local current densities at both the cathode and the anode as the intensities of sources and sinks with the help of an integral equation (8). This method has been found to be profitable for calculating the current density distribution in cells used for the deposition of metals. So far, linear polarization curves have been assumed. It is possible, however, to formulate and to solve the integral equation also for other types of cathodic or anodic polarization curves with the help of numerical methods.

Under most practical conditions, the polarization curves are not known and not easy to determine. Consequently, for practical purposes one has to rely on direct observations of corrosion rates rather than on calculations based on polarization curves. Direct observations always refer to a special set of conditions. To predict corrosion rates under somewhat different conditions, it is, therefore, necessary to make conjectures and extrapolations. To this end, this paper presents calculations for conditions which are idealized yet characteristic of practical situations.

In most practical cases, corrosion involves reduction of oxygen as the cathodic reaction. The current density J_c at the cathode as a function of the negative value of the local single electrode potential rises first exponentially owing to activation control and finally tends to a limiting value $J_{c(\max)}$ corresponding to diffusion control. The value $J_{c(\max)}$ is proportional to the concentration of oxygen in the bulk electrolyte and moreover depends on the convection of the electrolyte. This type of polarization curve is well known from polarographic investigations. The behavior of the cathode may, therefore, be approximated by

$$J_c \cong 0 \text{ if } -E_c < -E_{c(1/2)} \qquad [6]$$

$$J_c \cong J_{c(\max)} \text{ if } -E_c > -E_{c(1/2)} \qquad [7]$$

where $E_{c(1/2)}$ denotes the half-wave potential at which $J_c = J_{c(\max)}/2$.

According to Delahay (9), the value of $J_{c(\max)}$ may not be single-valued because oxygen is reduced either to H_2O_2, or to H_2O especially at lower single electrode potentials. In the latter case the maximum current density is twice as much as for reduction to H_2O_2. This, however, is irrelevant for the calculation of the order of magnitude of local cell action.

The equilibrium single electrode potential $E_{a(eq)}$ of the dissolving metal is assumed to be more negative than the half-wave potential $E_{c(1/2)}$ of oxygen where signs of potentials are chosen in accord with the Stockholm convention. The difference

$$\Delta E = E_{c(1/2)} - E_{a(eq)} \qquad [8]$$

is, therefore, assumed to be positive.

In a solution containing oxygen and under conditions precluding local cell action, a metal exhibiting a high activation polarization on dissolving may assume essentially the half-wave potential of oxygen. Under these conditions ΔE is balanced mainly by the overpotential of the dissolving metal,

$$\Delta E \cong \eta_a(J_a = J_{c(\max)}) \qquad [9]$$

Thus neither increase of oxygen supply nor local cell action affects the rate of metal dissolution to a significant extent.

The following considerations refer, therefore, to more reactive metals such as zinc which exhibit a relatively low activation polarization on dissolution. It is assumed that without local cell action the corrosion rate is controlled by diffusion of oxygen, i.e.,

$$J_a \cong J_{c(max)} \quad [10]$$

Moreover it is assumed that the anodic polarization curve may be approximated by a straight line over a sufficiently wide range corresponding to the relation

$$E_a - E_{a(eq)} = \eta_a = J_a h_a \quad [11]$$

where E_a is the electrode potential of the anode with a current density J_a and $h_a = dE/dJ_a$ is a constant.

In the case of local cell action, the maximum corrosion rate is attained if the dissolving metal is polarized to the half-wave potential $E_{c(1/2)}$ of the cathodic reaction. The corresponding potential shift is $\eta_a = \Delta E$ and the current density J_a is equal to $\Delta E/h_a$ according to Eq. [11]. For a significant rise of the anodic dissolution rate of a metal due to local cell action it is, therefore, necessary that $\Delta E/h_a >> J_{c(max)}$, or

$$\Delta E/h_a J_{c(max)} >> 1 \quad [12]$$

Coplanar Cathodes and Anodes

Coplanar cathodes and anodes are considered as one of the most important practical cases involving local cell action. The two-dimensional geometry of the electrodes is shown in Fig. 1 and is identical with the geometry considered by Waber and Rosenbluth (3). The anode is supposed to have a finite width a. The cathodes at either side of the anode are supposed to consist of another chemically inert material involving a high electrical conductivity. The width of the cathodes and the depth of the electrolyte are assumed to be infinite.

According to previous calculations for similar situations (3, 4, 8), one may anticipate two different limiting cases determined by the magnitude of the dimensionless ratio a/k_a where a is the width of the anode and $k_a = \sigma h_a$ is the so-called polarization parameter.

I. If $a << \sigma h_a$, polarization enforces a nearly uniform anodic current density, the potential drop in the electrolyte becomes insignificant, and $E_a \cong E_{c(1/2)}$. Hence, in view of Eq. [8] and [11]

$$J_a = \Delta E/h_a \quad [13]$$

II. If $a >> \sigma h_a$, the potential in the electrolyte along the anode is nearly constant whereas the anodic current density varies greatly and is especially high at the anode-cathode boundary. Under these conditions, an approximate solution of the current distribution may be obtained by calculating first the potential and current distribution in the electrolyte for vanishing polarization of the anode and introducing subsequently the effect of anodic polarization as a perturbation.

In view of Eq. [6] and [7], the Laplace equation for the electrical potential ϕ in the electrolyte as a function of the coordinates x and y is to be solved for the boundary condition

$$\phi = 0 \text{ at } |x| \leq a/2,\ y = 0 \quad [14]$$

$$\partial\phi/\partial y = J_{c(max)}/\sigma \text{ at } a/2 \leq |x| \leq (a+c)/2,\ y = 0 \quad [15]$$

$$\partial\phi/\partial y = 0 \text{ at } |x| > (a+c)/2,\ y = 0 \quad [16]$$

Equation [14] refers to the anode of width a at which the potential ϕ is supposedly constant and equal to zero by definition. Equation [15] refers to those sections of the cathodes where the single electrode potential is more negative than the half-wave potential. Equation [16] refers to farther sections of the cathode.

The distance $(a+c)/2$ at which the local single electrode potential is equal to the half-wave potential $E_{c(1/2)}$ of the cathodic reaction is not explicitly given but implicitly by the condition that the electrical potential ϕ at $|x| = (a+c)/2$, $y = 0$ must be equal to the negative value of the difference ΔE between the half-wave potential $E_{c(1/2)}$ of the cathodic reaction and the equilibrium single electrode potential $E_{a(eq)}$ of the anode,

$$\phi[|x| = (a+c)/2,\ y = 0] = -[E_{a(eq)} - E_{c(1/2)}] = -\Delta E \quad [17]$$

An approximate solution may be obtained by disregarding the occurrence of current lines beyond the broken lines in Fig. 1 corresponding to the boundary condition

$$\partial\phi/\partial x = 0 \text{ at } |x| = (a+c)/2,\ y > 0 \quad [18]$$

An analogous problem has been considered in conjunction with cathodic protection (10). Using Eq. [36] of a previous paper (10) with the notation of the present paper, one has

$$\phi = \frac{J_{c(max)}}{\sigma}\left\{ y + \frac{a+c}{\pi}\,\mathrm{Re}\left[i \sin^{-1}\frac{\sin \pi z/(a+c)}{\sin \pi a/2(a+c)} \right] \right\} \quad [19]$$

where $z = x + i\,y$ is the complex variable used in conformal mapping. Equation [19] satisfies the Laplace equation and the boundary conditions stated in Eq. [14], [15], and [18].

Substitution of Eq. [19] in Eq. [17] yields

$$\frac{\sigma\,\Delta E}{J_{c(max)}} = c\left\{ \frac{1 + c/a}{\pi\, c/a} \cosh^{-1}\frac{1}{\sin[\pi/2(1+c/a)]} \right\} \quad [20]$$

The expression in braces is equal to ½ if $c/a << 1$, and equal to 2.28 if $c/a = 1000$. Thus, for most practical situations, the expression in braces may be assumed to be equal to unity in order to obtain the order of magnitude of c. Hence

$$c \sim \sigma\,\Delta E/J_{c(max)} \quad [21]$$

The value of c may be considered as the effective width of the cathodic areas which determines the magnitude of the amount of oxygen reacting at the cathode.

The potential at the anode is equal to zero by definition according to Eq. [14]. The potential at the cathode is given by Eq. [19],

$$\phi(|x| > a/2,\ y = 0) = -\frac{(a+c)\,J_{c(max)}}{\pi\,\sigma} \cosh^{-1}\frac{\sin[\pi x/(a+c)]}{\sin[\pi a/2(a+c)]} \quad [22]$$

From Eq. [19] and Ohm's law the net current density $J_a - J_{c(max)}$ at the anode is obtained as

$$J_z - J_{z\,max} = -\sigma \left(\frac{\partial \phi}{\partial y} \right)_{|x| < a/2,\, y = 0}$$

$$J_{z\,max} \left\{ \frac{\cos\left(\frac{\pi x}{a+c}\right)}{\left[\sin^2\left(\frac{\pi a/2}{a+c}\right) - \sin^2\left(\frac{\pi x}{a+c}\right) \right]^{1/2}} - 1 \right\} \quad [23]$$

The validity of Eq. [19] to [23] is restricted because of the underlying approximations. First, it must be recalled that the cathodic current density is a continuous function of the electrode potential in contrast to the step function suggested in Eq. [6] and [7] on which Eq. [15] and [16] are based. Second, current lines spread beyond $|x| = (a+c)/2$ in contradistinction to the boundary condition in Eq. [18] used instead of Eq. [16]. Third, anodic polarization has been ignored but must be considered.

If $c >> a$, i.e., according to Eq. [21], if

$$\sigma \, \Delta E / a J_{z\,max} >> 1 \quad [24]$$

most of the potential drop in the electrolyte occurs in front of the anode where current lines are crowded. Approximations used for the calculation of the potential ϕ far away from the anode, especially at $x \geq (a+c)/2$, are, therefore, virtually irrelevant for the validity of Eq. [23]. Deviations from Eq. [23] are mainly due to anodic polarization. Pertinent calculations are presented below.

If conversely $c << a$, i.e., if

$$\sigma \, \Delta E / a J_{z\,max} << 1 \quad [25]$$

most of the potential drop in the electrolyte occurs in front of the cathodes where current lines are crowded. Consequently, if $c << a$, use of approximations at the outer boundary of the cathodes, i.e., $|x| \geq (a+c)/2$ causes a much greater error than in the former case where $c >> a$. Even if $c << a$, however, Eq. [22] and [23] yield the correct order of magnitude of ϕ and J_z next to the anode-cathode boundary if anodic polarization is negligible.

Since current lines ending at the cathode at $|x| < (a+c)/2$ spread beyond $|x| = (a+c)/2$, the decrease of the potential along the cathode with increasing distance x is less steep than has been calculated from Eq. [19] based on Eq. [18] according to which current lines beyond $|x| = (a+c)/2$ are precluded. The magnitude of this error may be estimated by comparing the variation of the potential at the surface of a galvanic couple involving constant current densities J at the cathode and the anode of equal width b/2 for conditions indicated in Fig. 2a and 2b. The potential distribution in the electrolyte can be calculated readily by superimposing the potentials resulting from line sources and sinks (11). In this way the change in the potential along the cathode of Fig. 2a without current lines beyond the boundaries of the electrodes is found to be

$$\phi(x = b/2) - \phi(x = b) = \frac{bJ}{\pi^2 \sigma} \left[\int_{\pi/4}^{2\pi/4} \ln \sin \eta \, d\eta - \int_{0}^{\pi/2} \ln \sin \eta \, d\eta \right] \quad [26]$$

$$= 0.74 \; (bJ/\sigma)$$

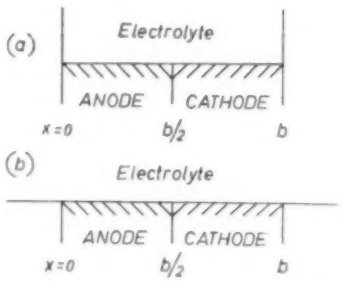

Fig. 2. Galvanic couples for estimating the effect of sidewise spreading of current lines on the potential drop along the cathode according to Eq. [26] and [27].

whereas for conditions shown in Fig. 2b with current lines expanding sidewise,

$$\phi(x = b/2) - \phi(x = b) = [(2 \ln 2)/\pi] \; (bJ/\sigma) = 0.44 (bJ/\sigma) \quad [27]$$

The ratio of the values calculated in Eq. [25] and [26] is 1.7. Thus cutting off the space for the spreading of current lines beyond $|x| = (a+c)/2$ in Fig. 1 by using Eq. [18] instead of Eq. [16] does not affect the order of magnitude of the above calculations even if $c << a$ as far as the vicinity of the anode-cathode boundary is concerned.

According to Eq. [23], the anodic current density at the anode-cathode boundary $x = a/2$ tends to infinity as in other problems where polarization at a boundary is disregarded (2, 3, 8). Thus polarization must be taken in account in order to obtain a realistic result. To this end, an approximate method indicated in Fig. 6 of a previous paper (8) may be employed as is shown in what follows.

Equations [22] and [23] have been derived for vanishing anodic polarization. If anodic polarization is considered to be a minor perturbation, Eq. [22] and [23] may still be used as first-order approximations except for the immediate vicinity of the anode-cathode boundary.

For each of the limiting cases $c >> a$ and $c << a$, one obtains from Eq. [22] and [23]

$$J_z(x \leq a/2) = A(a/2 - x)^{1/2} \quad [28]$$

$$\phi(x \geq a/2) = -B(x - a/2)^{1/2} \quad [29]$$

The symbols $\leq$ and $\geq$ mean "slightly smaller than" and "slightly greater than," respectively. The constants A and B are calculated below in Eq. [39] and [42] for $c >> a$ and in Eq. [48] and [52] for $c << a$.

Since anodic polarization does occur, the potential at the anode is lowered by $h_a J_z$. In view of Eq. [14]

$$\phi = -h_a J_z \text{ if } x < a/2 \quad [30]$$

Substitution of Eq. [28] in Eq. [30] yields

$$\phi(x \leq a/2) \cong -h_a A/(a/2 - x)^{1/2} \quad [31]$$

In Fig. 3 the potential in the vicinity of the anode-cathode boundary is shown as curve I and curve II calculated from Eq. [31] and [29], respectively. Two divergent branches are obtained. This divergence is due to the fact that the anodic current density tends

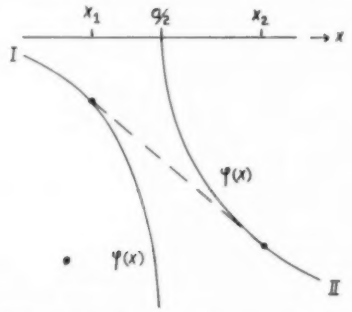

Fig. 3. Potential ϕ (x, y = 0) near the anode-cathode boundary at x = a/2.

to infinity at x = a/2, y = 0 if anodic polarization is disregarded. Actually, the potential must be represented by a smooth curve. To obtain an approximation, one may draw the common tangent line pertaining to curves I and II, which is indicated by the broken line between the coordinates x_1 and x_2 in Fig. 3.

Equating the slopes of the tangent lines at $x = x_1$ and $x = x_2$ and the slope of the broken line in Fig. 3, one obtains with the help of Eq. [29] and [31]

$$-\frac{h_a A}{2(a/2 - x_1)^{3/2}} = -\frac{B}{2(x_2 - a/2)^{1/2}} = \frac{-B(x_2 - a/2)^{1/2} + h_a A/(a/2 - x_1)^{1/2}}{x_2 - x_1} \quad [32]$$

Upon solving Eq. [32] for $(a/2 - x_1)$ and $(x_2 - a/2)$, it follows that

$$a/2 - x_1 = 3^{1/2} h_a A/B \quad [33]$$

$$x_2 - a/2 = 3^{1/2} h_a A/B \quad [34]$$

With the help of Eq. [31] and [33] the potential at the cathode boundary is obtained as

$$\phi(x = a/2, y = 0) = \phi(x = x_1, y = 0) + (a/2 - x_1)(\partial\phi/\partial x)_{x=x_1, y=0} \cong -(3^{3/4}/2)(h_a AB)^{1/2} \quad [35]$$

Hence the anodic current density at the anode-cathode boundary (x = a/2) is found to be

$$J_a = -\phi(x = a/2)/h_a \cong (3^{3/4}/2)(AB/h_a)^{1/2} \quad [36]$$

Next the values of A and B for the two limiting cases c >> a and c << a are calculated.

1. If c >> a, the cosine in Eq. [23] is nearly equal to unity and the sine functions may be approximated by their arguments. Hence Eq. [23] becomes

$$J_a \cong \frac{(a + c)}{\pi(a^2/4 - x^2)^{1/2}} J_{c(max)} \text{ if } c >> a \quad [37]$$

For the vicinity of the anode-cathode boundary at $x \gtrsim a/2$, it follows from Eq. [37] that

$$J_a \cong \frac{a + c}{\pi[a(a/2 - x)]^{1/2}} J_{c(max)} \cong \frac{c}{\pi[a(a/2 - x)]^{1/2}} J_{c(max)} \quad [38]$$

Upon comparing Eq. [28] and [38] it follows that

$$A \cong \frac{J_{c(max)}\, c}{\pi\, a^{1/2}} \text{ if } c >> a \quad [39]$$

If c >> a and $x \gtrsim a/2$, the sine functions in Eq. [22] may be approximated by their arguments. Thus

$$\phi(x \gtrsim a/2, y = 0) \cong -\frac{a+c}{\pi\sigma} J_{c(max)} \cosh^{-1}(2x/a) \quad [40]$$

For $x \cong a/2$, the inverse hyperbolic cosine function has an argument close to unity and therefore may be approximated by

$$\cosh^{-1}(2x/a) = \cosh^{-1}[1 + 2(x - a/2)/a] \cong 2[(x - a/2)/a]^{1/2} \quad [41]$$

Substitution of Eq. [41] in Eq. [40] yields Eq. [29] with

$$B \cong \frac{2}{\pi} \frac{(a + c)\, J_{c(max)}}{\sigma\, a^{1/2}} \cong \frac{2}{\pi} \frac{c\, J_{c(max)}}{\sigma\, a^{1/2}} \text{ if } c >> a \quad [42]$$

Upon substituting Eq. [39] and [42] in Eq. [36], using Eq. [21], and omitting numerical factors of the order of unity, the anodic current density at the anode-cathode boundary is found to be

$$J_a(x = a/2) \sim \left(\frac{\sigma}{a\, h_a}\right)^{1/2} \Delta E \text{ if } c >> a \quad [43]$$

2. If c << a and $x \sim a/2$, the trigonometric functions in Eq. [22] and [23] may be approximated by the following expressions

$$\sin\frac{\pi x}{a + c} = \cos\left[\frac{\pi}{2}\left(\frac{a + c - 2x}{a + c}\right)\right] \cong 1 - \frac{1}{2}\left(\frac{\pi}{2}\frac{a + c - 2x}{a + c}\right)^2 \quad [44]$$

$$\sin\frac{\pi a/2}{a + c} = \cos\left(\frac{\pi}{2}\frac{c}{a + c}\right) \cong 1 - \frac{1}{2}\left(\frac{\pi}{2}\frac{c}{a + c}\right)^2 \quad [45]$$

$$\cos\frac{\pi x}{a + c} \cong \cos\frac{\pi}{2}\frac{a}{a + c} = \sin\frac{\pi}{2}\frac{c}{a + c} \cong \frac{\pi}{2}\frac{c}{a + c} \quad [46]$$

Upon substituting Eq. [44] to [46] in Eq. [23] and omitting terms of higher order, it follows that the current density J_a next to the anode-cathode boundary $(a/2 - x << c)$ is

$$J_a \cong \frac{c}{2[c(a/2 - x)]^{1/2}} J_{c(max)} \quad [47]$$

Upon comparing Eq. [28] and [47], it follows that

$$A = (c^{1/2}/2)\, J_{c(max)} \text{ if } c << a \quad [48]$$

Substitution of Eq. [44] and [45] in Eq. [22] yields the potential at the cathode next to the cathode-anode boundary,

$$\phi(x \gtrsim a/2, y = 0) = \frac{(a + c)\, J_{c(max)}}{\pi\sigma} \cosh^{-1} f(x) \quad [49]$$

where

$$f(x) = \frac{1 - \frac{1}{2}\left[\frac{\pi}{2}\frac{a + c - 2x}{a + c}\right]^2}{1 - \frac{1}{2}\left[\frac{\pi}{2}\frac{c}{a + c}\right]^2} \quad [50]$$

If $c << a$ and $(x - a/2) << c$, $f(x)$ may be approximated by

$$f(x) \cong 1 - \frac{1}{2}\left[\frac{\pi}{2}\frac{a + c - 2x}{a + c}\right]^2 + \frac{1}{2}\left[\frac{\pi}{2}\frac{c}{a + c}\right]^2 \cong 1 - \frac{1}{2}\left[\frac{\pi^2 c(a/2 - x)}{(a + c)^2}\right] \quad [51]$$

Substituting Eq. [51] in Eq. [49] and using the first term of a series expansion for the inverse hyperbolic cosine function involving an argument close to unity, one obtains Eq. [29] with

$$B \cong \frac{c^{1/2} J_{c(max)}}{\sigma} \quad \text{if } c << a \quad [52]$$

Upon substituting Eq. [48] and [52] in Eq. [36], using Eq. [21], and omitting factors of the order of unity, the anodic current density at the anode-cathode boundary is found to be

$$J_a(x = a/2) \cong \left[\frac{\Delta E\, J_{c(max)}}{h_a}\right]^{1/2} \quad \text{if } c << a \quad [53]$$

For the current density J_a at the center of the anode the following relations are obtained.

1. If $c >> a$, it follows from Eq. [37] for $x = 0$ with the help of Eq. [21] and omission of factors of the order of unity that

$$J_a(x = 0) = \frac{2(a + c)}{\pi a} J_{c(max)} \cong \frac{\sigma \Delta E}{a} \quad [54]$$

2. If $c << a$, it follows from Eq. [23] and [46] that

$$J_a(x = 0) \cong J_{c(max)} \quad [55]$$

i.e., local cell action at the center of a sufficiently large anode is insignificant since J_a tends to the value determined by the local rate of oxygen supply.

Discussion and Conclusions

According to the foregoing considerations the local current density J_a for dissolution of a metal may be determined

1. by the rate of oxygen diffusion

$$J_a \cong J_{c(max)} \quad [56]$$

in accord with Eq. [10], or

2. by the potential drop in the electrolyte (resistance control) corresponding to the relation

$$J_a \sim \sigma \Delta E/a \quad [57]$$

which is deduced in Eq. [54] for the center of an anode of width a with adjacent cathodes if $c >> a$, or

3. by anodic polarization control corresponding to the relation

$$J_a = \Delta E/h_a \quad [58]$$

which has been obtained above as Eq. [13] for sufficiently narrow anodes ($a << \sigma h_a$).

The current density J_a at an anode-cathode boundary may be given by Eq. [43] if $c >> a$ and thus be equal to the geometrical mean of the right-hand members of Eq. [57] and [58] corresponding to a combination of resistance and anodic polarization control.

Alternatively, J_a at an anode-cathode boundary may be given by Eq. [53] if $c << a$ and thus be equal to the geometrical mean of the right-hand members of Eq. [56] and [58] corresponding to a combination of oxygen diffusion and anodic polarization control.

The validity range of the various approximations is determined mainly by the values of two dimensionless groups, N_1 and N_2,

$$N_1 = a/k_a = a/\sigma h_a \quad [59]$$

$$N_2 = \Delta E/h_a J_{c(max)} \quad [60]$$

The group N_1 is the ratio of the width a of the anode and the corrosion parameter k_a which in turn is defined as the product of the conductivity σ and the slope h_a of the potential-current density curve of the anodic reaction. The corrosion parameter $k_a = \sigma h_a$ is equal to the thickness of the electrolyte which yields a potential drop equal to the overpotential η_a of the anodic reaction at a given current density. The value of $N_1 = a/\sigma h_a$ is decisive for the uniformity of the current density at the anode. If $N_1 << 1$, the anodic current density is virtually uniform. Conversely, if $N_1 >> 1$, the anodic current density is much higher at the edges of the anode than at the center.

The group N_2 is the ratio of the potential difference ΔE defined in Eq. [8] to the overpotential $\eta_a = h_a J_{c(max)}$ pertaining to an anodic current density which is equal to the cathodic current density $J_{c(max)}$. The corrosion rate is significantly increased by local cell action only if $N_2 >> 1$,

The increase in corrosion rate due to local cell action may be represented by the ratio Q of the current density of metal dissolution with local cell action to that without local cell action. If the latter value is equal to the maximum current density of oxygen reduction in accord with Eq. [10], the value of Q becomes

$$Q = J_a/J_{c(max)} \quad [61]$$

So far, limiting cases have been considered, and it has been assumed that either $N_1 << 1$, or $N_1 >> 1$, etc. Since the approximate formulas for $N_1 << 1$ and $N_1 >> 1$ become identical if $N_1 = 1$, etc., it is not necessary to state $N_1 << 1$ or $N_1 >> 1$ but simply $N_1 < 1$ or $N_1 > 1$. Thus one has four principal cases listed in Table I whose occurrence is determined by the values of the dimensionless groups N_1 and N_2. Figure 4 shows the ranges of these cases graphically.

The summary presented in Table I involves considerable simplifications since factors of the order of unity have been omitted. Such a simplified rep-

Table I. Limiting cases of local cell action for conditions shown in Fig. 1

($N_1 = a/\sigma h_a$; $N_2 = \Delta E/h_a J_{c(max)}$; $Q = J_a/J_{c(max)}$)

Case	I	II	III	IV
Range	$N_2 < 1$	$N_1 < 1; N_2 > 1$	$N_1 > 1; N_2 > N_1$	$N_1 > 1; N_2 < N_1$
c/a	—	$c > a$	$c > a$	$c < a$
J_a (center)	$J_{c(max)}$	$\frac{\Delta E}{h_a}$	$\frac{\sigma \Delta E}{a}$	$J_{c(max)}$
J_a (edge)	$J_{c(max)}$	$\frac{\Delta E}{h_a}$	$\left(\frac{\sigma}{a h_a}\right)^{1/2} \Delta E$	$\left(\frac{J_{c(max)} \Delta E}{h_a}\right)^{1/2}$
Q (center)	1	N_2	N_2/N_1	1
Q (edge)	1	N_2	$N_2/N_1^{1/2}$	$N_2^{1/2}$

resentation seems to be adequate for most purposes because in practice the basic data for a rational analysis such as the rate of oxygen supply and the slope of the anodic polarization curve are, in general, estimated rather than precisely known.

To illustrate the significance of the various cases, representative values of N_1 and N_2 are calculated. The value of ΔE is of the order of 1 v. The value of $J_{c(max)}$ depending on convection of the electrolyte can be expected to lie between 10^{-5} and 10^{-3} amp/cm^2. The electrical conductivity σ ranges in most cases between 5×10^{-4} for fresh water and 5×10^{-2} ohm^{-1}cm^{-1} for sea water. The slope $h_a = dE/dJ_a$ of the anodic polarization curve of a fairly reactive metal such as zinc in a 10^{-4}M Zn^{2+} ion solution is estimated to be of the order of 10^2 v/amp cm^{-2} corresponding to an exchange current density of 10^{-4} amp/cm^2, whereas less reactive metals such as iron or nickel exhibit higher values depending on the value of J_a.

For reactive metals, $N_2 = \Delta E/h_a J_{c(max)}$ lies, therefore between 10 and 10^3, i.e., is greater than unity. Consequently, cases II, III, and IV are expected to occur. According to Table I, $Q(edge) = J_a(edge)/J_{c(max)}$ is equal to N_2, $N_2/N_1^{1/2}$ and $N_2^{1/2}$ for cases II, III, and IV, respectively. For $\Delta E = 1$ v, $h_a = 10^2$ v/amp cm^{-2}, and $J_{c(max)} \cong 10^{-4}$ amp/cm^2 one obtains, therefore, values of Q(edge) between 10 and 100.

To have a value of $N_1 = a/\sigma h_a < 1$ corresponding to case II with uniform corrosion, the width a of the anode must be less than 5×10^{-2} cm in fresh water and less than 5 cm in sea water. Otherwise, case III or IV involving a higher corrosion rate at the edge of the anode than at the center occurs. If $N_2/N_1 = \sigma \Delta E/aJ_{c(max)} > 1$, case III occurs. If conversely $N_2/N_1 < 1$, case IV occurs. For $\Delta E = 1$ v, and $J_{c(max)} = 10^{-4}$ amp/cm^2, the width of the anode for a transition from case III to case IV is $a \cong 5$ cm in fresh water and $a \cong 500$ cm in sea water. If the width of the anode is less, i.e., case III prevails, the current density J_a decreases with increasing width a of the anode at both the center and the edge. If conversely the width of the anode exceeds 5 cm in fresh water, or 500 cm in sea water, i.e., case IV prevails, J_a (center) tends to $J_{c(max)} = 10^{-4}$ amp cm^{-2} and J_a(edge) is found to be 10^{-3} amp cm^{-2} independent of the width of the anode and the conductivity of the electrolyte if $h_a = 10^2$ v/amp cm^{-2}.

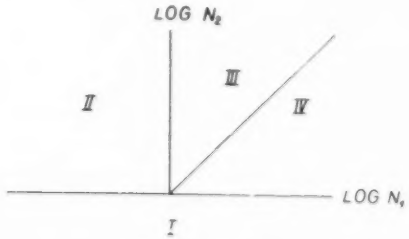

Fig. 4. Ranges of the dimensionless group $N_1 = a/\sigma h_a$ and $N_2 = \Delta E/h_a J_{c(max)}$ for the limiting cases I, II, III, and IV listed in Table I.

The foregoing calculations refer to a value of $J_{c(max)} = 10^{-4}$ amp/cm^2 as an average representative value. In view of a rather large variability of $J_{c(max)}$ with the oxygen concentration in the bulk electrolyte and the intensity of convection, the dependence of the various phenomena on the magnitude of $J_{c(max)}$ is of special interest. If $N_1 > 1$ and $N_2 > N_1$, i.e., $J_{c(max)} < \sigma \Delta E/a$, case III is realized. The values of J_a at both the center and the edge of the anode are independent of $J_{c(max)}$, i.e., the rate of oxygen supply. On increasing the oxygen supply, N_2 becomes less than N_1 and, accordingly, case IV is realized. Then J_a(edge) is proportional to the square root of $J_{c(max)}$ and J_a(center) $\cong J_{c(max)}$. It is noteworthy that J_a is found to be virtually independent of the rate of oxygen supply if the supply is low, in particular if the oxygen concentration in the electrolyte is low. This is an important characteristic of local cell action contrary to usual rules of kinetics. The lower the oxygen concentration in the electrolyte, the greater is the effective area of the cathodes to which oxygen diffuses. In view of this compensation the rate of corrosion for cases II and III is controlled not by oxygen diffusion but by the resistance of the electrolyte and by anodic polarization.

The scheme in Table I and Fig. 4 is not strictly applicable to less reactive metals such as iron or nickel involving higher values of $h_a = dE/dJ_a$ which are not constant but depend on J_a. Under these conditions, only certain trends can be stated. First, in the case of metals exhibiting a large activation overpotential on dissolving, case I corresponding to a value of $N_2 < 1$ is favored, i.e., local cell action is not likely to enhance corrosion of a metal such as nickel. Second, if $N_2 > 1$, case II involving uniform attack is expected to occur with anodes of greater width than has been calculated above for a more reactive metal such as zinc since $N_1 = a/\sigma h_a$ is inversely proportional to h_a. The lower the reactivity of a metal, the lower is the rate of attack since J_a for case II is inversely proportional to h_a. Third, the less reactive a metal, the lower is the effect of

local cell action at edges since J_a(edge) is inversely proportional to $h_a^{1/2}$ for cases III and IV according to Eq. [43] and [53], respectively, if $h_a = dE/dJ_a$ is constant.

Although local cell action aggravates corrosion, the potential danger is not unlimited as is shown by the foregoing discussion. In many practical cases, the effect of local cell action is even less severe, if in contradistinction to an important presupposition introduced above, solid corrosion products are formed and constitute some kind of protective layer especially at locations involving a high initial attack.

The foregoing considerations refer to reduction of oxygen as the cathodic reaction. It is important to recall that evolution of hydrogen is another cathodic reaction which does occur in parallel and may prevail under certain conditions. The characteristics of local cell action due to oxygen reduction and to hydrogen evolution differ in some respects. In particular, in the case of hydrogen evolution as the predominant cathodic reaction the corrosion rate is increased considerably by small areas of a material involving a low hydrogen overpotential in a matrix of a less noble metal such as zinc at which the hydrogen overpotential is high. In contrast, in most practical cases where corrosion is due to reduction of oxygen, the cathodic current density is independent of the nature of the solid conductor because J_c is close to the limiting value $J_{c(max)}$. Under these conditions, inclusions of foreign materials affect the corrosion rate only to a minor extent. For this reason, only large cathodic areas have been considered above.

The conclusions drawn in this paper differ in some respect from those drawn by Waber and his associates (2-7, 12) because the analysis in the present paper presupposes a limiting current density of the cathodic reaction, whereas Waber, *et al.* assume linear polarization curves for both the cathodic and the anodic reaction. Both approaches supplement each other. In particular, if hydrogen evolution rather than oxygen reduction takes place as the cathodic reaction, and local depletion of hydrogen ions is not a decisive factor, Waber's analysis may be considered to be more relevant.

Manuscript received Sept. 1, 1959.

Any discussion of this paper will appear in a Discussion Section to be published in the December 1960 JOURNAL.

REFERENCES

1. C. Wagner and W. Traud, *Z. Elektrochem.*, **44**, 391 (1938).
2. J. T. Waber, *This Journal*, **101**, 271 (1954).
3. J. T. Waber and M. Rosenbluth, *ibid.*, **102**, 344 (1955).
4. J. T. Waber, *ibid.*, **102**, 420 (1955).
5. J. T. Waber and B. Fagan, *ibid.*, **103**, 64 (1956).
6. J. T. Waber, J. Morrissey, and J. Ruth, *ibid.*, **103**, 138 (1956).
7. J. T. Waber, *ibid.*, **103**, 567 (1956).
8. C. Wagner, *ibid.*, **98**, 116 (1951).
9. P. Delahay, *ibid.*, **97**, 198, 205 (1950).
10. C. Wagner, *ibid.*, **99**, 1 (1952).
11. C. Wagner, *ibid.*, **104**, 631 (1957).
12. J. T. Waber, *Corrosion*, **13**, 95t (1957).

Effect of Hydrogen Pressure on the Hydrogen Overvoltage on Bright Rhodium

Sigmund Schuldiner

U. S. Naval Research Laboratory, Washington, D. C.

ABSTRACT

The effect of hydrogen pressure on the hydrogen overvoltage on bright, active rhodium was determined. The data indicated that the overvoltage mechanism was controlled by the $2H_{ads} = H_2$ step. Kinetic parameters for the mechanism were quantitatively determined including the surface coverage with adsorbed atomic hydrogen. A Langmuir adsorption isotherm resulted from the relationship between surface coverage with atomic hydrogen at equilibrium and the partial pressure of molecular hydrogen above the solution.

It has been shown in a previous study of the effect of hydrogen pressure on the overvoltage on bright platinum (1) that pressure effects can be used to determine kinetic parameters and to establish a reasonable reaction mechanism. In the investigation reported here pressure effects on hydrogen formation and ionization reactions on bright rhodium were studied. By using this metal in rapidly stirred, strong acid solution, diffusion effects were virtually eliminated, and it was possible to make a quantitative determination of the kinetic parameters.

Experimental

Breiter, Kammermaier, and Knorr (2) showed that the properties of an "aged" rhodium electrode are different from those of a "new" electrode. This was confirmed by this investigation. On a new rhodium electrode it was found that at first the overvoltage was relatively high, but that on repeated anodic and cathodic cycling to high polarization values (-0.4 v cathodic and > 1 v anodic) a reproducible electrode of high activity was obtained.

The general experimental techniques were the same as those previously used (3, 4). The cell was constructed of Teflon and is shown in Fig. 1. The rhodium (99.5 + %) cathode was prepared by melting the tip of a 0.025 in. thick rhodium wire with a hydrogen/oxygen flame and forming a small sphere. The wire was then inserted into the 0.02 in. hole

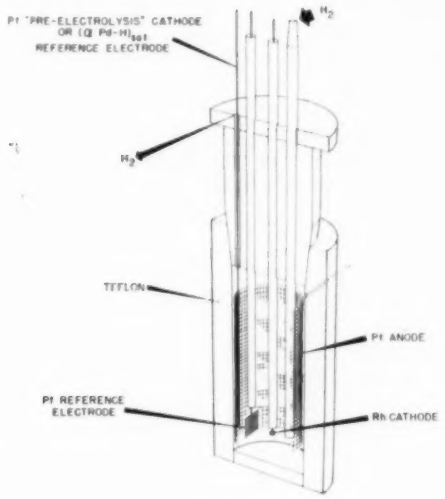

Fig. 1. Electrolytic cell

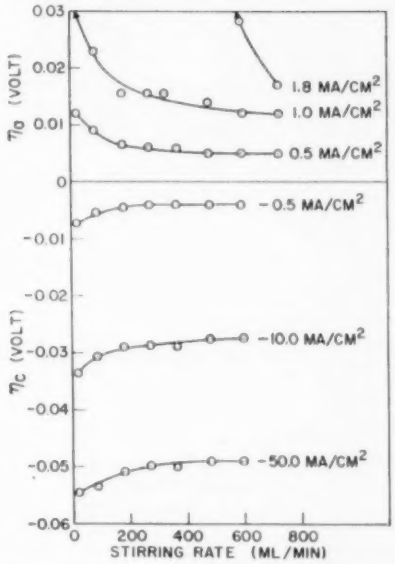

Fig. 2. Effect of stirring rate ($P_{H_2} = 1$ atm) on η_c and η_a

in the Teflon rod shown in Fig. 1. A molten polyethylene seal was made between the bottom of the Teflon rod and the rhodium wire. The resulting rhodium electrode then consisted of a bead at the end of a 2 mm exposed length of wire. The total apparent area of exposed rhodium was 0.10 cm². The solution was in all cases 1M H_2SO_4. Purified gases consisting of either pure hydrogen or mixtures of hydrogen and helium were bubbled through the acid solution in the cell. The method of preparation of the gas mixtures and the determination of the hydrogen partial pressure are described in a previous paper (1).

After the solution was pre-electrolyzed and the rhodium electrode was activated by repeated anodic and cathodic polarization, repeated measurements were taken at each partial pressure of hydrogen under both anodic and cathodic polarization. Overvoltages at each current density were time independent. The reference electrode to cathode interface *IR* drop was determined by interrupter measurements (3). The data given are average values of individual runs. The precision of an individual reading was better than 0.5 mv. The maximum deviation of the average values was ±0.5 mv at low overvoltages and ±2 mv at high overvoltages. The temperature was 27° ±1°C.

Experimental Results

Concentration polarization effects were minimized by rapid stirring with gas. Figure 2 shows the effect of stirring rate on overvoltage for pure hydrogen. The data show that a value is reached after which the overvoltage is independent of stirring rate. Stirring rates in excess of these values were used for all measurements.

Cathodic overvoltage, η_c, vs. log apparent current density curves at different hydrogen pressures are shown in Fig. 3. Figure 4 shows the anodic overvoltage, η_a, vs. log apparent current density curves. At low current densities a linear relationship between the anodic and cathodic overvoltages and apparent current density was found and these results are shown in Fig. 5.

From the experimental data shown in Fig. 3-5, kinetic parameters and a reaction mechanism can be determined.

Calculation of Kinetic Parameters

The Tafel slopes of ~0.0295 shown in Fig. 3 indicate that the reaction mechanism is a fast discharge of hydronium ions followed by a slow combination of hydrogen atoms, H_{ads}, to molecules;

$$H_3O^+ + e^- = H_{ads} + H_2O \qquad [1]$$

$$2H_{ads} \xrightarrow{\text{slow}} H_2 \qquad [2]$$

This mechanism is confirmed by the limiting anodic current densities found in Fig. 4. These limiting current densities would be caused by the coverage of adsorbed hydrogen atoms on the rhodium surface dropping to zero. It will be shown later that the limiting current densities shown in Fig. 4 are not due to a diffusion process.

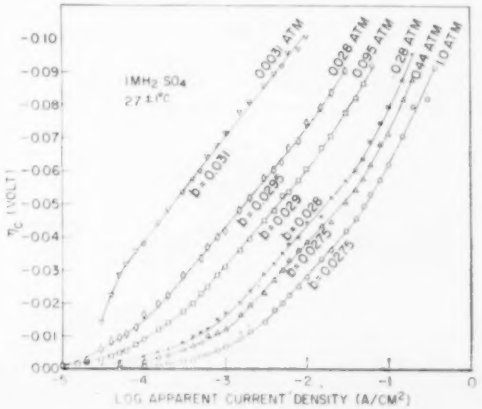

Fig. 3. Relations for η_c vs. log ($-i_c$)

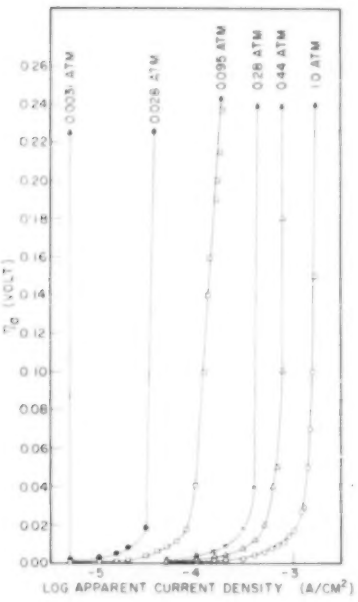

Fig. 4. Relations for η_a vs. log i_a

The equations (1) for this mechanism are:

$$i_c = i_{o,c}\frac{(1-\theta)^2}{(1-\theta_o)^2}[\exp(-2\eta_c\mathbf{F}/RT)-1] \qquad [3]$$

$$i_a = i_{o,a}\frac{(1-\theta)^2}{(1-\theta_o)^2}[1-\exp(-2\eta_a\mathbf{F}/RT)] \qquad [4]$$

where i_c, i_a are the applied cathodic and anodic current densities respectively; $i_{o,c}$, $i_{o,a}$ are the cathodic and anodic exchange current densities, respectively; η_c, η_a are the cathodic and anodic overvoltage, respectively; θ is the fraction of available surface covered with atomic hydrogen; θ_o is the fraction of available surface covered with atomic hydrogen at zero current density, (equilibrium); and R, T, and $\mathbf{F}$ are the gas constant, absolute temperature and the Faraday, respectively.

At overvoltages near equilibrium $\theta = \theta_o$ and Eq. [3] and [4] can be simplified to:

$$i_c = i_{o,c}[\exp(-2\eta_c\mathbf{F}/RT)-1] \qquad [3a]$$

$$i_a = i_{o,a}[1-\exp(-2\eta_a\mathbf{F}/RT)] \qquad [4a]$$

The values of $i_{o,c} = -i_{o,a}$ can therefore be determined for various values of hydrogen partial pressure, P_{H_2}, by plotting i_c vs. $[\exp(-2\eta_c\mathbf{F}/RT)-1]$ and i_a vs. $[1-\exp(-2\eta_a\mathbf{F}/RT)]$. These plots are shown in Fig. 6.

The values of θ_o and θ can be determined in the following way. If one plots i_c vs. $[\exp(-2\eta_c\mathbf{F}/RT)-1]$ throughout the entire range of values determined, the curves shown in Fig. 7 are obtained. The deviation at higher current densities, where θ is significantly greater than θ_o, from the straight line fit found

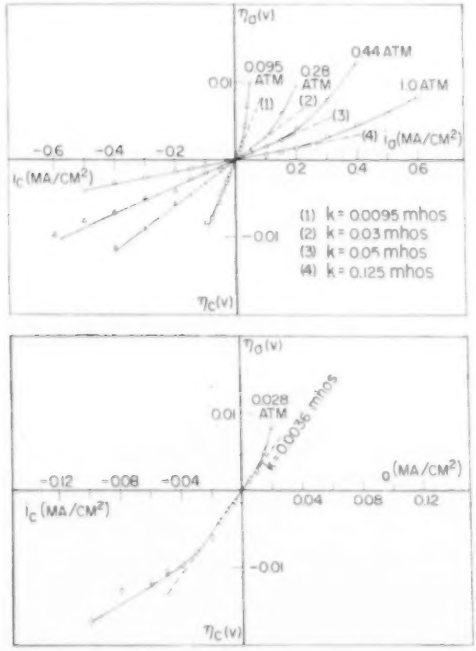

Fig. 5. Low current density relationships for η vs. i

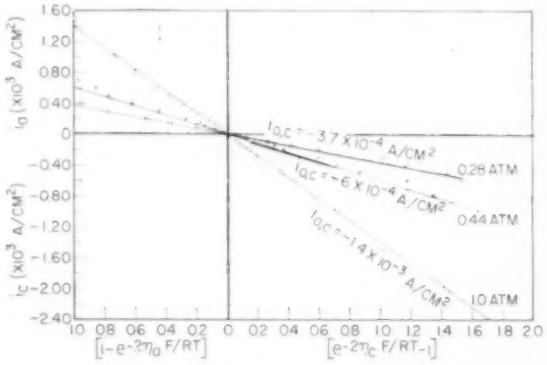

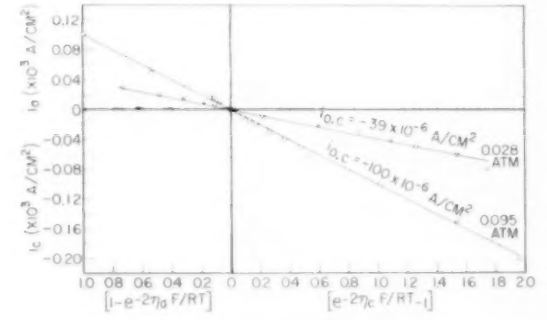

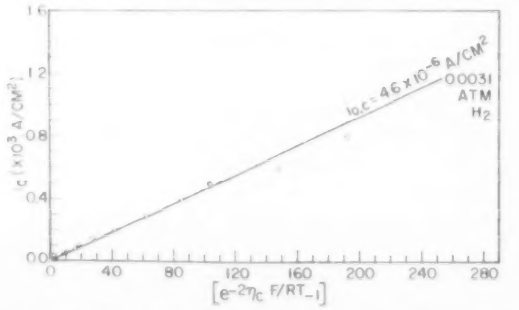

Fig. 6. Values of $i_{o,c}$ as determined by plotting i_a vs. $[1-\exp(-2\eta_a F/RT)]$ and i_c vs. $[\exp(-2\eta_c F/RT)-1]$.

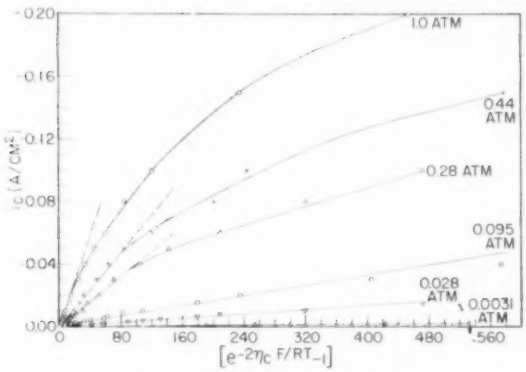

Fig. 7. i_c vs. $[\exp(-2\eta_c F/RT) - 1]$

at low current densities is a function of the ratio $(1-\theta)^2/(1-\theta_o)^2$. Hence in order to linearize these curves one would have to plot i_c vs. $(1-\theta)^2/(1-\theta_o)^2$ $[\exp(-2\eta_c \mathbf{F}/RT)-1]$. One can then solve for $(1-\theta)^2/(1-\theta_o)^2$ using Eq. [3]. Since the slow combination step, Eq. [2], of the reaction mechanism in the absence of a back reaction can be written as follows

$$i_c = \vec{k}_c \theta^2$$

and since

$$i_{o,c} = \vec{k}_c \theta_o^2$$
$$i_c/i_{o,c} = \theta^2/\theta_o^2 \qquad [5]$$

By simultaneous use of Eq. [3] and [5] one can solve for θ_o and θ when $\eta_c > 0.03$ v, then

$$\theta_o = \frac{[\exp(-2\eta_c \mathbf{F}/RT)-1]^{1/2} - (i_c/i_{o,c})^{1/2}}{(i_c/i_{o,c})^{1/2}\{[\exp(-2\eta_c \mathbf{F}/RT)-1]^{1/2}-1\}} \qquad [6]$$

and

$$\theta = (i_c/i_{o,c})^{1/2}\,\theta_o \qquad [7]$$

The limiting cathodic current densities, $i_{c,L}$, were determined from Eq. [5]. When $i_c = i_{c,L}$, $\theta = 1$, hence

$$i_{c,L} = i_{o,c}/\theta_o^2 \qquad [8]$$

The limiting anodic current densities, $i_{a,L}$, were determined from Eq. [4]. When $i_a = i_{a,L}$, $\theta = 0$ and since η_a is a large positive number, $\exp(-2\eta_a \mathbf{F}/RT) = 0$, hence

$$i_{a,L} = i_{o,a}/(1-\theta_o)^2 \qquad [9]$$

The rate constants for the over-all reaction, $k = \pm(di/d\eta)_{\eta\to 0}$ (the sign is negative for the cathodic and positive for the anodic directions) near equilibrium where there is a linear relation between η and i were determined from Fig. 5. The stoichiometric numbers, μ, were calculated from the Horiuti (5) relationship

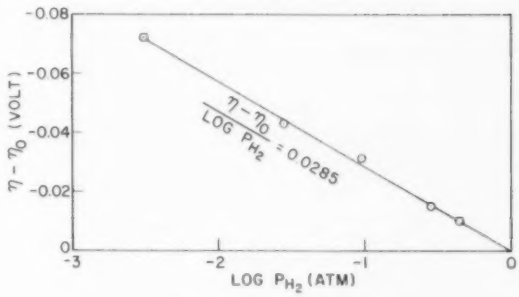

Fig. 8. η-η_o vs. log P_{H_2}

$$\mu = 2i_{o,c}\mathbf{F}/kRT \qquad [10]$$

Table I lists the kinetic parameters which were determined as indicated above. In addition the experimentally determined values of $i_{a,L}$ are shown for comparison with the calculated values.

Discussion

Several investigators have established (1, 6-11) that at a given current density in the linear Tafel region the hydrogen overvoltage on a cathode is related to the hydrogen pressure by the expression

$$\eta = \eta_o + (RT/2\mathbf{F}) \ln P_{H_2} \qquad [11]$$

where η, the overvoltage, is defined as the potential difference between the working electrode and a reversible hydrogen electrode in the same solution, η_o is the overvoltage at 1 atm of hydrogen and P_{H_2} is the partial pressure of hydrogen above the solution. A plot of $\eta - \eta_o$ vs. log P_{H_2} for the data which was taken at 27°C should therefore give a straight line with a slope of 0.0295 v. Figure 8 shows such an experimental plot with a slope of 0.0285 v. The agreement is very good which not only confirms Eq. [11] but also serves as a verification of the hydrogen partial pressure values.

The effects of current density on surface coverage with atomic hydrogen, θ, for various P_{H_2} values are shown in Fig. 9. Here i_c is plotted vs. θ^2. According to Eq. [5], when the back reaction is negligible there should be a linear relation between i_c and θ^2 with a slope of $i_{o,c}/\theta_o^2$. As shown by Eq. [8], when $i_c = i_{c,L}$ the slope is simply $i_{c,L}$. Since, when the back reaction is negligible, the surface coverage should be only a function of current density independent of P_{H_2}, a slope of $i_{c,L}$ should apply for all the data shown in Fig. 9. The average $i_{c,L}$ values of -1.49 amp/cm² given in Table I has been drawn through each set of points shown in Fig. 9. As can be seen the fit of this

Table I. Kinetic parameters

P_{H_2}, atm	$i_{o,a} = -i_{o,c}$, amp/cm²	θ_o, average values	Calc. $i_{a,L}$, amp/cm²	Expt. $i_{a,L}$, amp/cm²	$i_{c,L}$, amp/cm²	k, mhos/cm²	μ
1.0	1.4×10^{-3}	0.029	1.48×10^{-3}	1.87×10^{-3}	−1.66	0.125	0.87
0.44	6.0×10^{-4}	0.020	6.24×10^{-4}	8.5×10^{-4}	−1.50	0.050	0.93
0.28	3.7×10^{-4}	0.015	3.81×10^{-4}	4.5×10^{-4}	−1.64	0.030	0.96
0.095	1.0×10^{-4}	0.008	1.02×10^{-4}	1.9×10^{-4}	−1.56	0.0095	0.82
0.028	39×10^{-6}	0.0053	39.4×10^{-6}	35×10^{-6}	−1.40	0.0036	0.84
0.0031	4.6×10^{-6}	0.0020	4.62×10^{-6}	$\sim 5 \times 10^{-6}$	−1.15	—	—
				Avg	−1.49		0.88

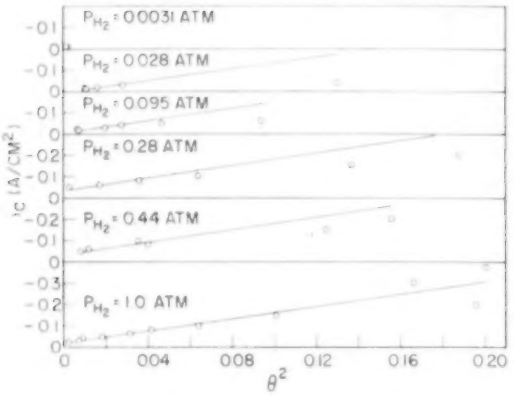

Fig. 9. Relations between i_c and θ^2

slope through the points at θ^2 values below 0.06, which corresponds to a θ value of 0.245, is good. The poorer fit at higher θ^2 values is undoubtedly due to the assumption of a Langmuir isotherm (12) in the derivation of Eq. [3] and [4]. A better fit would probably be obtained by use of a Temkin (13) isotherm at coverages above 0.2. However, the use of the Langmuir isotherm for the calculation of kinetic parameters in the present paper is valid since θ_o, and $i_{o,L}$ represent low and zero coverage, respectively, whereas $i_{c,L}$ represents full coverage. The Langmuir isotherm does apply to these conditions.

The Langmuir isotherm is

$$\theta_o^2/(1-\theta_o)^2 = KP_{H_2} \qquad [12]$$

The data for this isotherm is plotted in Fig. 10 and an excellent fit to a straight line intersecting the zero point is obtained. The calculated K value is 0.0009. The Langmuir isotherm shown in Fig. 10 confirms the fact that the atomic hydrogen coverage of the rhodium surface at equilibrium is low. It also confirms the electrode mechanism postulated and the method of calculating the kinetic parameters. In addition, since the anodic part of the curves shown in Fig. 6 show a good linear fit from zero overvoltage to about the point where the limiting anodic current density is reached, one can conclude that $\theta_o << 1$. This is because during anodic polarization the value of θ must range from θ_o at equilibrium to zero at the limiting current density. If this range of values was a significant fraction of unity then one could not obtain a linear fit using Eq. [4a].

A further confirmation of the applicability of the calculations used is the stoichiometric number, μ,

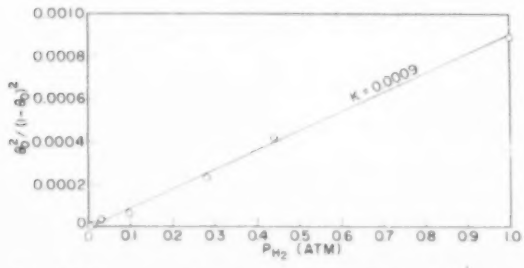

Fig. 10. Langmuir adsorption isotherm, $\theta_o^2/(1-\theta_o)^2$ vs. P_{H_2}

being close to unity and the agreement between the experimental and calculated anodic limiting current densities shown in Table I. There is always a possibility that some hydrogen is dissolved in the metal near the surface, and this would tend to result in making the experimental error in the direction of higher $i_{o,L}$ values. This is generally observed in Table I comparing the experimental $i_{o,L}$ values with the calculated values.

Ershler (14) by use of charging curves, Eucken and Weblus, and Breiter, Knorr, and Völkl (15) from a-c impedance measurements have concluded that the surface of a platinum metal is covered largely with atomic hydrogen at the hydrogen equilibrium potential. The results given here and in previous papers from this laboratory (1, 16) have shown that the surface of platinum metals is covered only sparsely with atomic hydrogen at equilibrium. It is conceivable that both results may be correct. For example, a layer of atomic hydrogen may exist just beneath the metal surface or is so incorporated in the metal surface that it is in effect a part of the metal. If this atomic hydrogen is not in equilibrium with the molecular hydrogen in solution, then it may be detected by charging curves, or by a-c methods but would not play a part, except possibly as a catalyst, in the hydrogen surface potential-determining reaction at equilibrium. It could be that such a layer is formed by the activation procedures used with platinum metals which generally consist of alternate anodic and cathodic treatment. Such a layer may also exist even at very low hydrogen partial pressures. It is noteworthy that the a-c impedance measurements of Breiter, Knorr, and Völkl (15) gave virtually the same high surface coverage for Pt metals in both hydrogen and nitrogen saturated solutions. The transitory nature of highly activated platinum (17-19) in highly purified solutions may be due to such a layer of atomic hydrogen being decreased in time rather than to the accumulation of impurities on the surface.

Diffusion effects in this investigation must be negligible under the experimental conditions used. The reason for this can be seen from the fact that $i_{o,L}$ values are always greater than $i_{o,a}$ values. If diffusion were important, when $\theta_o << 1$, $i_{o,L}$ values must always be smaller. This can be seen from the relation

$$1/i_{o,L} = (1-\theta_o)^2/i_{o,a} + 1/i_{o,d} \qquad [13]$$

where $i_{o,d}$ is the so-called diffusion exchange current density. This means that for the system reported here $i_{o,d}$ must be much larger than $i_{o,a}$.

Another verification of the kinetic analysis used in this paper would be an experimental determination of $i_{c,L}$. This was impossible to achieve with the technique used in this investigation. This is due primarily to the large coverage of the metal surface with hydrogen bubbles at current densities approaching 0.5 amp/cm^2. New techniques are being considered with which it is hoped that this difficulty may be overcome and a determination of $i_{c,L}$ may be possible.

Manuscript received Aug. 27, 1959.

Any discussion of this paper will appear in a Dis-

cussion Section to be published in the December 1960 JOURNAL.

REFERENCES

1. S. Schuldiner, *This Journal*, **106**, 891 (1959).
2. M. Breiter, H. Kammermaier, and C. A. Knorr, *Z. Elektrochem.*, **60**, 119 (1956).
3. S. Schuldiner, *This Journal*, **99**, 488 (1952).
4. S. Schuldiner, *ibid.*, **101**, 426 (1954).
5. J. Horiuti, *J. Research Inst. Catalysis, Hokkaido*, **1**, 8 (1948).
6. S. J. Bircher and W. D. Harkins, *J. Am. Chem. Soc.*, **45**, 2890 (1923).
7. M. Knoble, *ibid.*, **46**, 2751 (1924).
8. H. M. Cassel and E. Krumbein, *Z. physik. Chem.*, **A171**, 70 (1934).
9. G. Schmid and E. K. Stoll, *Z. Elektrochem.*, **47**, 360 (1941).
10. J. O'M. Bockris and R. Parsons, *Trans. Faraday Soc.*, **45**, 916 (1949).
11. K. J. Vetter and D. Otto, *Z. Elektrochem.*, **60**, 1072 (1956).
12. I. Langmuir, *J. Am. Chem. Soc.*, **54**, 2798 (1932).
13. M. I. Temkin, *Z. Fiz. Khim.*, **15**, 296 (1941).
14. B. Ershler, *Acta Physicochim.*, **7**, 327 (1937).
15. A. Eucken and B. Weblus, *Z. Elektrochem.*, **55**, 114 (1951); M. Breiter, C. A. Knorr, and W. Völkl, *ibid.*, **59**, 681 (1955).
16. S. Schuldiner, *This Journal*, **106**, 440 (1959).
17. A. N. Frumkin, *Z. Physik. Chem.*, **207**, 321 (1957).
18. A. N. Frumkin and E. Aikasjan, *Dokl. Akad. Nauk SSSR*, **100**, 315 (1955).
19. M. Breiter, H. Kammermaier, and C. A. Knorr, *Z. Elektrochem.*, **60**, 37 (1956).

Technical Notes

Effect of Oxygen on the Active-Passive Behavior of Stainless Steel

Norbert D. Greene[1]

Metals Research Laboratories, Union Carbide Metals Company, Division of Union Carbide Corporation, Niagara Falls, New York

The usefulness of potentiostatic polarization methods for studying passivity of metals has been demonstrated (1-7). These techniques are used here to determine whether dissolved oxygen has any effect on the active-passive behavior of stainless steel. The passivating inhibitor mechanism proposed by Stern (8) assumes that the presence of small quantities of oxidizing agents (or passivators) does not affect appreciably the anodic dissolution kinetics of a metal. This study is a direct test of this assumption. Further, it is also useful in testing the validity of theories which attribute passivity to the retardation of anodic dissolution by adsorbed oxygen from solution (9-11).

Type 430 stainless steel in sulfuric acid was chosen for this study because its active-passive transition is reproducible and does not vary with time, and the critical anodic current density is sufficiently high so that spontaneous passivation does not occur in oxygen-saturated solutions.

Experimental

Potentiostatic anodic polarization measurements were conducted with apparatus and techniques described in detail elsewhere (7, 12). Electrodes were machined from Type 430 stainless steel (15.90% chromium, 0.30% manganese, 0.054% carbon, 0.31% silicon, 0.005% phosphorus, and 0.011% sulfur) furnace-cooled after 1 hr at 780°C. Polarization measurements were conducted in hydrogen- and oxygen-saturated sulfuric acid solutions.

[1] Present address: Department of Metallurgical Engineering, Rennselaer Polytechnic Institute, Troy, New York.

Electrodes were pre-exposed to the test solutions for 15 to 20 hr prior to polarization measurements. All tests were performed at 24° to 26°C.

Results

Figure 1 shows anodic polarization data for Type 430 stainless steel in hydrogen-saturated normal sulfuric acid. The active corrosion potential is indicated on the ordinate. This curve is typical of most active-passive metals (1-7). As the potential is increased, current density increases to a maximum, here called critical anodic current density, I_c. The corresponding potential is called the primary passive potential, *Epp*. At potentials more noble than *Epp*, current decreases, eventually to very small values, and becomes time-dependent. Above approximately 0.900 v, current again increases with potential and oxygen evolution occurs. The current maximum at 0.050 v is not significant in the passivation process and is not considered further here.

Although Fig. 1 is an applied current polarization curve, other studies, to be reported later, demonstrate that it closely approximates actual anodic dissolution rate over a wide range of potentials. At potentials above reversible oxygen potential (0.900 v) and within approximately 50 mv of the active corrosion potential, significant distortion occurs because of contributions from oxygen and hydrogen evolution, respectively.

Figure 2 shows the polarization of Type 430 stainless steel in oxygen-saturated normal sulfuric acid. In contrast to the behavior in hydrogen-satu-

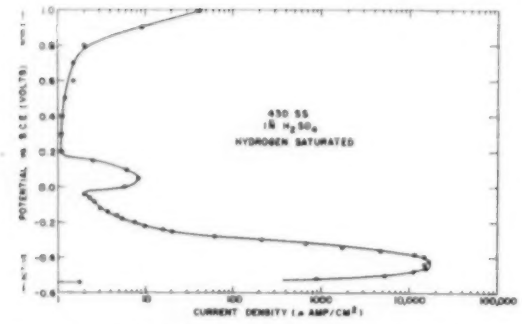

Fig. 1. Anodic polarization of Type 430 stainless steel in hydrogen-saturated 1N sulfuric acid.

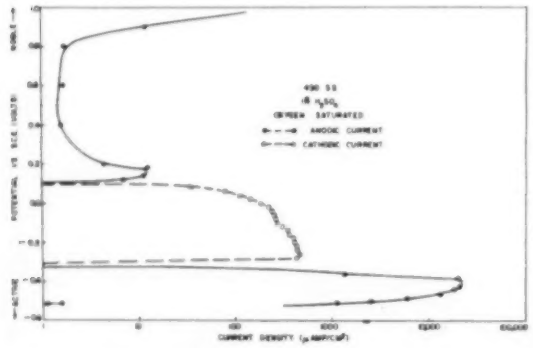

Fig. 2. Anodic polarization of Type 430 stainless steel in oxygen-saturated 1N sulfuric acid.

rated acid, this system demonstrates two stable mixed potentials as evidence by the appearance of the cathodic loop between −0.300 and 0.100 v. In this environment, Type 430 stainless alloy can exist in either the active state at −0.517 v or the passive state at 0.100 v.[7] Since both active and passive states are stable, the system does not spontaneously transform from one to the other. However, the alloy can be repeatedly transformed from one state to the other by application of suitable anodic or cathodic currents. Thus, the limiting diffusion current of oxygen in an oxygen-saturated solution is sufficient to maintain stable passivity but insufficient to cause spontaneous passivation. For descriptions of cathodic loops, spontaneous passivation, and other phenomenological features of active-passive metals, see (2, 5, 8, 14).

Similar experiments were performed in 5 and 10*N* sulfuric acid and are summarized in Table I.

[7] Although the initial passive potential of this system was 0.100 v, the time-dependency of passive dissolution (4, 7, 13) produced a slow shift in the noble direction. After 48 hr in the passive condition, this potential increased to 0.345 v.

Table I. Primary passive potentials (Epp) and critical anodic current densities (I.) of Type 430 stainless steel in sulfuric acid

Potentials = v vs. SCE; current = ma/cm²

Acid concentration	Hydrogen saturated		Oxygen saturated	
	Epp	*I.*	*Epp*	*I.*
1*N*	−0.420	17	−0.420	21
5*N*	−0.340	26	−0.340	29
10*N*	−0.260	40	−0.280	43

All oxygen-saturated solutions exhibited cathodic loops during anodic polarization. Differences between hydrogen-saturated and oxygen-saturated solutions shown in Table I are within the limits of experimental accuracy.

Discussion

Figures 1 and 2 and Table I demonstrate that oxygen, in sufficient concentration to maintain passivity of Type 430 stainless steel, does not affect anodic dissolution of this alloy. Thus, passivity cannot be attributed to the retardation of anodic dissolution by the adsorption of oxygen from solution as proposed by several investigators (9-11). Although oxygen adsorption undoubtedly occurs on stainless steel surfaces, it does not retard dissolution. The fact that stable passivity has been observed in the absence of oxygen (5) offers additional evidence that passivity is not caused by adsorbed oxygen.

The presence of oxygen does not measurably affect dissolution kinetics of Type 430 stainless steel in sulfuric acid. Therefore, for this system, the assumption that anodic and cathodic partial processes are mutually independent (4, 8) is correct. For predicting both the effectiveness of passivating agents and the relative passivating tendencies of alloys, this assumption can probably be generally applied, as shown by the success of recent studies of this nature (2, 7, 8).

Although a mechanism for passivity cannot be deduced from the measurements performed here, this study further confirms the phenomenological description of passivity proposed by Stern (8). Simply, any oxidizer capable of producing a mixed potential within the passive potential region can produce stable passivity. In this sense, oxygen demonstates no specific property; its behavior is typical of any strong oxidizing agent.

Summary

1. It is shown that the presence of oxygen has no apparent effect on the anodic dissolution kinetics of Type 430 stainless steel. The primary passive potential and the critical anodic current density are essentially the same in the presence or absence of dissolved oxygen.

2. The passivating inhibitor theory described by Stern is supported by this study.

3. Results of this study are not consistent with adsorbed oxygen theories of passivity.

Acknowledgment

The author acknowledges the capable assistance of E. A. Tomes who performed the experimental measurements presented here. Discussions with Dr. A. C. Makrides and Dr. M. Stern are greatly appreciated.

Manuscript received Jan. 20, 1960.

Any discussion of this paper will appear in a Discussion Section to be published in the December 1960 JOURNAL.

REFERENCES

1. W. A. Mueller, *Can J. Technol.*, **34**, 162 (1956).

2. C. Edeleanu, *J. Iron Steel Inst.*, **188**, 122 (1958).
3. M. Prazák and V. Cihál, *Z. Elektrochem.*, **62**, 739 (1958).
4. Y. M. Kolotyrkin, *ibid.*, **62**, 664 (1958).
5. M. Stern and H. Wissenberg, *This Journal*, **106**, 755 (1959).
6. R. Otsuka, *J. Electrochem. Soc. Japan*, (Overseas Ed.), **27**, E41 (1959).
7. N. D. Greene, To be published.
8. M. Stern, *This Journal*, **105**, 638 (1958).
9. M. G. Fontana and F. H. Beck, *Metal Progress*, **51**, 939 (1947).
10. T. P. Hoar and U. R. Evans, *This Journal*, **99**, 212 (1952).
11. H. H. Uhlig and S. S. Lord, Jr., *ibid.*, **100**, 216 (1953).
12. N. D. Greene, *Corrosion*, **15**, 369t (1959).
13. M. Stern, *This Journal*, **106**, 376 (1959).
14. G. Okamoto and M. Nagayama, *Corrosion Engineers* (Japan), **7**, 1 (1958).

A Controlled Diffusion Process for Indium in N-Type Germanium

F. Barson, M. J. Dyett, C. Karan, and W. E. Mutter

Product Development Laboratory, International Business Machines Corporation, Poughkeepsie, New York

In the fabrication of NPN diffused base transistors, one conventional process starts with N-type germanium and diffuses a P-type skin into its surface. An N-type emitter dot is then alloyed into the diffused skin to complete the NPN structure.

One complication which arises, particularly during the diffusion process, is that of thermal conversion; that is, when germanium is heated above about 500°C and cooled fairly rapidly, additional acceptor levels appear in the bulk of the crystal (1). The density of these thermal acceptors is often great enough that N-type germanium is completely converted to P-type.

The cause of this thermal conversion in germanium is associated primarily with the introduction of copper into the material. Copper is apparently usually present in trace amounts on the surface and, due to its very high diffusivity at elevated temperatures, spreads rapidly throughout the bulk of the germanium where it acts as an acceptor center (2, 3). In addition, quenches from high temperatures may introduce acceptor levels of another kind, which are apparently due to quenched-in lattice defects (4, 5). Except with very rapid cooling rates, however, this latter type of thermal acceptor is not too troublesome.

Several investigators have suggested means of minimizing thermal conversion due to copper contamination. Annealing the germanium at 500°C precipitates the copper in clusters which are electrically inactive (2, 6); however, since the copper is not actually removed from the sample by this method, further heating cycles may cause conversion to occur once more. A vacuum heat treatment, on the other hand, removes the possibility of conversion by actually evaporating the copper from the sample, maintaining its resistivity (7). Another method is to clean the germanium in potassium cyanide prior to any proposed heat treatment (8, 9). The cyanide forms soluble complexes with copper, removing it before it can diffuse in and be troublesome. Finally, it has been shown that certain molten metals in contact with germanium, due to their high solubility for copper, act as getters which extract the copper from the germanium (10-12).

It is this last method which has been employed in the present work to develop a practical process for diffusion into N-type germanium. By a proper choice of the getter metal, it has been found possible not only to retain the original resistivity of the N-type germanium wafer, but also to use this metal as a source of acceptor impurities for the diffusion itself.

Method and Results

Approximately 0.1 mil thickness of indium metal was evaporated onto one side of the N-type germanium wafers to be diffused. The wafers were then placed, indium side down, on a graphite slab and heated in a wire-wound furnace under an atmosphere of slowly flowing forming gas. The temperature used for the diffusion was 875°C. At this temperature, the molten indium film under the germanium provided enough indium vapor in the furnace so that a P-type skin formed by diffusion on the upper sides of the wafer.

In this way, the indium served both as a getter to remove copper from the sample and also as a source of the acceptor impurity for diffusion as well. The thickness of the P-type skin so formed could be controlled by the length of time that the sample was held at high temperature. Following the diffusion, the samples were cooled and the indium film, presumably now containing any copper originally present in the germanium, was removed from the bottom of the wafers by lapping.

The resistivities of the wafers were measured by the four-point probe method prior to the evaporation, and again after the diffusion (on the lapped, N-type surface). Seldom was the density of thermal acceptors introduced by the process found to exceed 1×10^{14} cm^{-3}. This means that germanium in the range of 3-6 ohm-cm suffered an increase in resistivity of less than 0.5 ohm-cm.

The junction depth X_j for a diffusion was measured by beveling a portion of the surface at a low angle and locating the junction with a thermal probe mounted on a sensitive depth gauge. To estimate C_s, the surface concentration for the indium diffusion, the familiar error function distribution was evaluated at the junction:

$$C_j = C_s \operatorname{erfc} X_j/2\sqrt{Dt}$$

Assuming a diffusion coefficient of 1.5×10^{-12} cm^2/sec at 875°C, C_s was calculated to be about 5×10^{18}

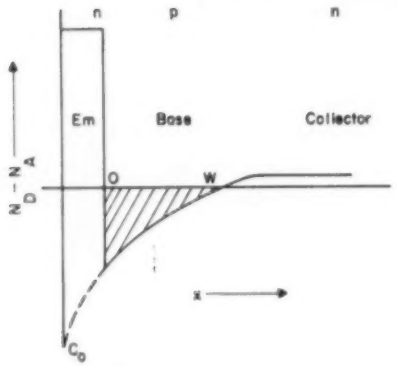

Fig. 1. Impurity distribution in a transistor made by the process described. Shaded area represents $\int_0^\infty P\,dx$.

cm^2. The assumed diffusion coefficient is in good agreement with that determined by several earlier investigators (13-15); furthermore, the resulting C_s was consistent with sheet resistance measurements made in a manner similar to that of Backenstoss (16) for silicon diffusions.

In order to point out a practical difficulty in making transistors of the indium-diffused material described above, we recall that the fabrication process is now to alloy an N-type emitter into the P-type skin. This results in an impurity distribution somewhat as shown in Fig. 1. The emitter efficiency for this structure can be shown to be (17):

$$\gamma = \frac{1}{1 + \dfrac{\mu_p}{\mu_n}\dfrac{\int_0^\infty P\,dx}{L_{p_0}N_s}}$$

Notice that the integral, which represents the shaded area in Fig. 1, should have a small value to give a high emitter efficiency. This means that if C_s is large, the emitter must be alloyed very close to the collector junction (that is, the base must be very narrow) to preserve a high emitter efficiency. This calls for very precise control of alloying; for placing the emitter junction at too shallow a depth results in low emitter efficiency, while placing it at too great a depth results in alloying completely through to the collector junction. There are several ways to lower C_s in the indium diffusion process so as to decrease the slope of the impurity distribution and thus allow more leeway in the emitter alloying process. A method which was both simple and effective was to use an evaporated film of both indium and tin together as a getter-source and then to perform the diffusion exactly as described in the original process, a single-zone furnace sufficing.

We recall that, for an ideal solution, the vapor pressure of the solute is proportional to its mole fraction in the solution (Raoult's law). Hence, we would expect that as the concentration of indium in the evaporated tin-indium film was decreased, the vapor pressure of the indium at diffusion temperatures would similarly decrease, and with it the C_s of the diffusion process. That this is actually the case is illustrated in Fig. 2 which shows the C_s for several diffusions using indium and tin-indium films on the germanium wafers. The values of C_s are based once more on junction depth measurements and an assumed diffusivity of $D = 1.5 \times 10^{-12}$ cm^2/sec at 875°C. The limits of probable error shown are largely due to uncertainty in the junction depth measurement, which was about ± 0.02-0.03 mil. The trend, however, is clear, demonstrating the variation of C_s which is possible with the method described.

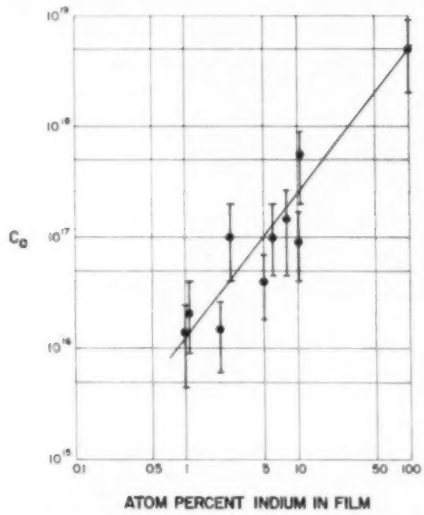

Fig. 2. Surface concentration C_s as a function of the evaporated film composition.

Tin was selected as the second metal to dilute the indium, partly because it is reportedly inert electrically in germanium (18) and partly because, due to its low vapor pressure, it did not itself evaporate appreciably during the longer diffusion runs. It should perhaps be pointed out that, although it is the atom percent of indium in the evaporated film which is plotted in Fig. 2, the actual molten film during diffusion was a ternary solution of indium, tin, and also germanium dissolved at the diffusion temperature. Thus the data presented apply only to the case described, in which the film is in physical contact with the germanium during diffusion.

Conclusion

The experimental results presented show that molten indium metal in contact with germanium can be used not only as a getter to prevent thermal conversion, but also as a simultaneous source of indium vapor for diffusion into the germanium. Furthermore, by diluting the indium with tin, the surface concentration of indium in the diffused skin can be reduced controllably. This, plus the fact that only a simple, one-zone diffusion furnace is required, makes the process an easy and practical one for producing diffused skins on germanium for diffused base transistor manufacture.

Acknowledgments

The authors are indebted to Mr. P. Ostapkovich for his advice and assistance in arranging the ex-

perimental work, and to Mr. B. Szabo for sheet resistance measurements.

Manuscript received Sept. 21, 1959. This paper was prepared for delivery before the Ottawa Meeting, Sept. 28-Oct. 2, 1958.

Any discussion of this paper will appear in a Discussion Section to be published in the December 1960 JOURNAL.

REFERENCES

1. H. C. Theuerer and J. H. Scaff, *J. Metals*, **4**, 59 (1951).
2. C. S. Fuller and J. D. Struthers, *Phys. Rev.*, **87**, 526 (1952).
3. W. P. Slichter and E. D. Kolb, *ibid.*, **87**, 527 (1952).
4. S. Mayburg, *ibid.*, **95**, 38 (1954).
5. H. Letaw, *J. Phys. and Chem. of Solids*, **1**, 100 (1956).
6. R. A. Logan, *Phys. Rev.*, **100**, 615 (1955).
7. G. Finn, *ibid.*, **91**, 754 (1953).
8. R. A. Logan, *ibid.*, **91**, 757 (1953).
9. P. Wang, *J. Phys. Chem.*, **60**, 45 (1956).
10. R. A. Logan and M. Schwartz, *J. Appl. Phys.*, **26**, 1287 (1955).
11. H. Kroemer, "Transistors I," p. 132, RCA Laboratories, Princeton, N. J. (1956).
12. C. D. Thurmond and R. A. Logan, *J. Phys. Chem.*, **60**, 591 (1956).
13. C. S. Fuller, *Phys. Rev.*, **86**, 136 (1952).
14. W. C. Dunlap, *ibid.*, **94**, 1531 (1954).
15. W. Boesenberg, *Z. Naturforsch.*, **10A**, 285 (1955).
16. G. Backenstoss, *Bell System Tech. J.*, **37**, 699 (1958).
17. J. L. Moll and I. M. Ross, *Proc. I. R. E.*, **44**, 72 (1956).
18. F. A. Trumbore, *This Journal*, **103**, 597 (1956).

Technical Feature

The Double Layer in Electrochemistry[1]

A. N. Frumkin

Institute of Electrochemistry of the Academy of Sciences of the U.S.S.R., Moscow, U.S.S.R.

In every group of phenomena there is some specific feature which leaves its mark on the science dealing with these phenomena. As it seems to me, a specific feature of this kind in the case of electrochemical processes is the existence of the electric double layer at the metal-solution interface. Perhaps I am not quite impartial in this statement, as I, if I may say so, stood at the cradle of the double layer theory, but still I think that there are many elements of truth in it.

There is nothing exceptional in the fact that when two phases come into contact there appears a double layer at the interface. The ions, as any other solute, tend to be distributed between the phases in accordance with the difference in their standard chemical potentials. But, as their large electric charges inhibit the separation of ions in considerable quantities, the distribution equilibrium is secured by attaining a certain difference of electric potentials with a simultaneous formation of a double layer at the interface, which necessitates the transfer of but small quantities of ions from one phase to the other, provided the area of the interface is not very great. The laws governing the value of this equilibrium potential difference were established long ago by Gibbs and Helmholtz; for the form of these laws which is familiar to chemists we are indebted to Nernst and Lewis. The importance of these relationships cannot be overemphasized; however, one must keep in mind that they tell us nothing about the mechanism of the establishment of the potential difference or about the structure of the double layer being formed.

[1] Palladium Medal Address delivered at the Chicago Meeting, May 3, 1960.

At the present time we get our knowledge about the structure of the double layer in the first place from a-c measurements of electrode capacities or by other similar methods. Earlier data which I had to consider when I began to study this problem (more than 40 years ago) were based on measurements of electrocapillary curves, i.e., of the relation between interfacial tension σ and potential difference ϕ. In order to determine from these data the electric properties of the interface, one must use the Lippmann-Helmholtz equation

$$\frac{\partial \sigma}{\partial \phi} = -\epsilon \qquad [1]$$

where ϵ is the charge density on the metal surface.

The application of Eq. [1] to experimental data showed in a number of cases a rather complex relationship between σ and ϕ. The majority of scientists of that time thought that the double layer should behave as a flat condenser, i.e., that ϵ should be proportional to ϕ. They explained the deviations observed by the inaccuracy of Eq. [1], although the latter is strictly deduced from the principles of thermodynamics. Even such an authority in the field of chemical thermodynamics as van Laar held this view. Only the French physicist Gouy found a better approach to the theory of electrocapillarity. But Gouy worked at a provincial university at Nancy which he left but seldom, and his works were little known to scientists interested in physicochemical problems. In any case, when I presented a paper with the experimental confirmation of the correctness of Eq. [1] and some critical remarks on the

theory of van Laar to the "Zeitschrift für physikalische Chemie," it was at first rejected by the Editor.

In this paper the electric charges were determined from the current strength necessary for charging a growing mercury drop, just in the same way as it is often done at the present time, and $\partial\sigma/\partial\phi$ was calculated from electrocapillary curves (1). There still remained a contradiction which could not be removed for a long period of time: the double layer capacities as directly measured by Krüger, Bowden and Rideal, Erdey-Gruz and Kromrey always proved to be much smaller than the capacities calculated from electrocapillary data using Eq. [1] or found from experimental values of ϵ. This discrepancy seemed to be so firmly established that even attempts to give it a theoretical explanation were made. Thus a hypothesis was suggested according to which the capacity measured by means of an alternating current must be exactly equal to one-half the capacity obtained from electrocapillary data (2). However Proskurnin and Frumkin showed in 1935 (3) that the discrepancies observed were caused by a different and much more trivial circumstance, viz., the presence of organic impurities which penetrate the capillary of the capillary electrometer slowly, but easily reach the unprotected surface of a mercury electrode used in capacity measurements. It was found that when such impurities are carefully eliminated both methods of capacity determination give identical results. Overcoming the difficulties connected with capacity measurements in dilute solutions enabled us to find a capacity minimum at the point of zero charge, which was a strong confirmation of the theory of the diffuse double layer (4).

Somewhat later Grahame adapted the a-c method to capacity measurements on a growing mercury drop (5), which permitted the requirements to be lowered in respect to solution purity and to increase the precision of the method.

The demonstration of the correctness of the Lippmann-Helmholtz equation and the development of methods of direct capacity measurements formed a sound basis for the investigation of the structure of the double layer and for the verification of the theory of the double layer on the metal-solution interface. I shall not dwell here on the well-known history of the development of this theory which is associated with the names of Helmholtz, Gouy, and Stern. Considerable advances were made in the postwar period by David Grahame, whose untimely death was a great blow to all his friends and colleagues. By introducing the concept of a difference in the distances of closest approach of anions and cations to the metal surface, Grahame succeeded in giving a satisfactory picture of the relationship between the double layer structure and the concentration of the electrolyte for the case when ions are attracted by coulombic forces only, i.e., when the phenomenon commonly called specific adsorption is absent (6).

Such an agreement between theory and experiment is somewhat surprising, as the fact that the solution side of the double layer is composed of individual ions was not taken into consideration in the development of the theory, or in other words, the ionic charges were, so to say, smeared parallel to the metal-solution interface. Indeed, the theory developed on this basis cannot account for the experimentally observed dependence of the double layer structure on the concentration in the presence of a marked specific adsorption of anions. On my suggestion Esin and his collaborators (7) and later Ershler (8) attempted to work out a theory of a discrete double layer and to remove these discrepancies. Ershler's concepts recently were developed further by Grahame (9); several papers by Parsons (10) also are concerned with this problem. However, despite the efforts exerted, in my opinion we are not yet in possession of a fairly satisfactory quantitative theory of the double layer in which this discrete structure would be taken into account. Some success in this direction was achieved recently by Levich and Kiryanov (11).

Grahame supposed, following Gouy in this, that inorganic cations, unlike anions, do not display any specific adsorbability on the metal-solution interface; in the case of cations such an adsorbability was ascribed only to large organic cations. The investigations carried out in the past years at the Moscow University showed, however, that this assumption is not quite justified (12). Thus, the adsorbability of the Tl^+ ion on the mercury surface, as seen from Fig. 1, in which the electrocapillary curves for solutions of H_2SO_4 with additions of Tl_2SO_4 are shown, can be compared with that of the Br^- ion. A certain adsorbability also is displayed by the lead ions and a very small, although a clearly detectable one, even by the ions of the alkali metal Cs^+ (13). These phenomena are much more pronounced in the case of cation adsorption on the surface of the solid metal platinum (14). Proving the existence of a specific cation adsorption is, in my opinion, important in connection with the role that the adsorbed atoms (or adions) are supposed to play in the electrodeposition of metals (15-17).

The presence of a double layer at the mercury-solution interface affects a number of its properties, for instance interfacial tension, adhesion between metal and solution, and others. I shall discuss here only one of these properties, viz., mobility in an

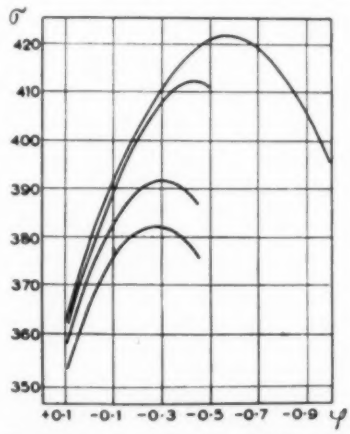

Fig. 1. Electrocapillary curves in N KNO_3 + 0.01N HNO_3 + x N $TlNO_3$ solutions. Curves from top to bottom: x = 0; 0.01; 0.1 and 0.2 (NCE).

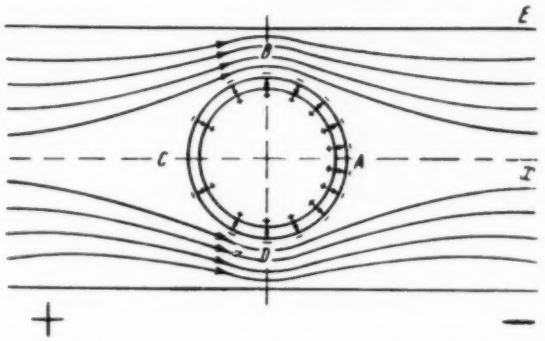

Fig. 2. Schematic picture of the double layer of an ideal polarized positively charged metal drop placed in an external electric field. The arrows show the direction of the lines of force of the field.

electric field. When an electric field is applied, the mercury drop in the electrolyte solution comes into motion. The mechanism of this motion, first observed by Christiansen (18), essentially differs from that of the well-known electrokinetic motion. Its velocity, in the case of identical field tension and solution viscosity for drops having a radius a of the order of 1 mm, may exceed that of electrokinetic motion by five orders of magnitude. The mechanism of these movements is best illustrated by the simple example of an ideal polarized positively charged drop with a Helmholtz double layer. In this case, the distribution of the lines of force of the external electric field in the vicinity of the drop (Fig. 2) is similar to their distribution in the vicinity of an insulator, in other words they are tangential to the drop. Under these conditions the electric field acts on the outer sheet of the double layer, but not on the inner one, as the field tension within the metal is equal to zero due to its high electric conductivity. Thus, the effect of the field on the outer sheet of the double layer is not compensated for (to be more precise, it is compensated by the forces applied at a considerable distance from points B and D to the poles of the drop A and C). Under the influence of these forces the mercury in the drop comes into a vortical motion, as is shown in Fig. 3, and the reactive repulsion from the surrounding medium causes the drop to move along the field lines. The mathematical theory of this motion developed by Levich and myself (19) gives the following expres-

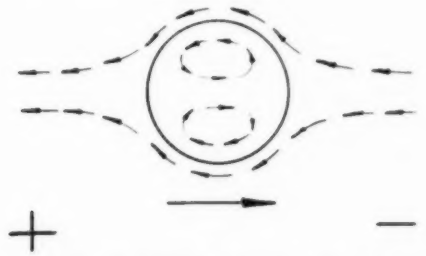

Fig. 3. Motion of a positively charged mercury drop in an electrolyte solution under the action of the electric field. The small arrows show the direction of the motion of the solution and mercury at any point, the big arrow, the direction of the motion of the drop as a whole.

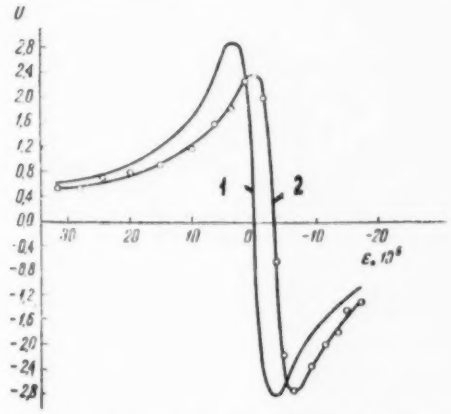

Fig. 4. Relationship between the mobility of mercury drops in a 0.02N KBr solution in glycerol and the charge density ϵ; $\kappa = 1.9 \times 10^{-5}$; $\mu = 2.8$. 1, Computed from Eq. [2]; 2, experimental data. μ in cm/sec v; ϵ in coulomb/cm^2.

sion for the drop velocity v, the field tension at a sufficient distance from the drop being equal to E

$$v = \frac{a \epsilon E}{2\mu + 3\mu^1 + \epsilon^2/\kappa} \qquad [2]$$

where μ and κ denote the viscosity and the electric conductivity of the solution and μ^1 the viscosity of mercury.

Equation [2] was verified on mercury drops falling in a viscous glycerol solution and deflected by a horizontal electric field; definite electric charges were imparted to the drops before they broke off from the capillary (20). As seen from Fig. 4, the theoretical calculations are confirmed by experiments; the slight shift of the experimental curve is caused by the presence of oxygen traces which gradually made ϵ somewhat more positive (it is very difficult to remove oxygen completely from the viscous solution). For small values of ϵ, Eq. [2] gives mobility values of the same order as those which would be found in the case of a sphere having a free charge with the density ϵ. At first sight, this seems surprising, as the charge of the metal side of the double layer is completely compensated by the charges with an opposite sign which are located in the ionic sheet of the double layer. However, as I have already mentioned, a compensation of charges does not lead to a compensation of forces. With increase of ϵ, v increases, reaching a maximum at

$$\epsilon = \kappa^{1/2}(2\mu + 3\mu^1)^{1/2} \qquad [3]$$

and then decreases. This can be accounted for by the fact that the transfer of charges by the moving mercury surface results in an electric field directed opposite to the impressed field and diminishing its effect (this has not been taken into account in plotting Fig. 4, which therefore holds true only for small values of ϵ). A similar inhibiting effect is also observed in the case of a drop moving under the action of forces of a different nature, e.g., gravity, which results in a somewhat unexpected relationship between the velocity of the falling drop and its

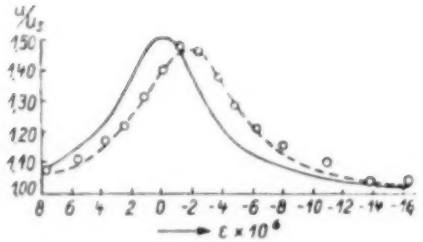

Fig. 5. Ratio of the rate of fall of a mercury drop in a glycerol solution saturated with Na_2SO_4 to that calculated by Stokes formula as a function of the charge density ϵ; $\kappa = 8.1 \times 10^{-6}$, $\mu = 7.2$. Solid curve, calculated values; circles, experimental data.

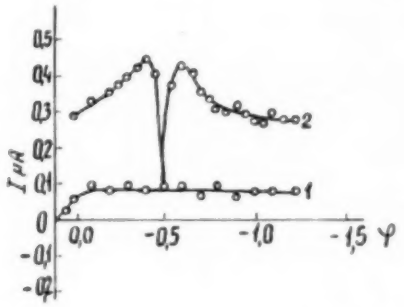

Fig. 6. C.v. curves in 0.28×10^{-4} N $Hg_2(ClO_4)_2$ + 0.002N $KClO_4$ corrected for charging current (NCE). 1, In the absence of an external field, 2, with the external field applied, E = 0.47 v/cm.

charge (21). A more detailed analysis permits us to conclude that in a viscous medium an uncharged drop must fall one and a half times faster than a charged one. The relationship between the velocity of the fall and the charge observed experimentally is compared in Fig. 5 with the theoretical dependence; the velocities of the fall are referred to that of a strongly charged drop, which is in accordance with Stokes law. The slight shift of the experimental curve with respect to the theoretical one can be accounted for quantitatively, if the depolarizing effect of the oxygen traces is taken into consideration.

The electrocapillary motion of droplets with metallic conductivity may arise in any electrolyte. A method was proposed recently to make use of this motion in extracting sulfide inclusions from molten slags (22).

Electrocapillary movements underlie the so-called polarographic maxima. The tangential movement of the drop surface calls forth an extra supply of the depolarizer which, according to Levich (23), is proportional to the square root of the tangential velocity. This fact makes it possible for currents in excess of the normal limiting diffusion current, which can be computed with the help of Ilkovic's equation, to pass through the cell. However, under the usual working conditions of a dropping electrode, the electric field causing the movement of the drop surface depends on complex geometrical conditions at the capillary tip; it is also influenced by the effect of convective diffusion of the depolarizer on the concentration polarization. Moreover the polarization curves are distorted by ohmic potential drops in the solution. Therefore the development of a quantitative theory of polarographic maxima presents great difficulties, which account for the chaotic state of this problem in modern polarographic literature. I shall not dwell here on the attempt made in this direction by myself and Levich, although, as it seems to me, we succeeded in explaining the basic features of the phenomena observed (24). I prefer to confine myself to the consideration of a case, when the polarographic maxima of the first kind may, so to say, be observed in an idealized form. To achieve this in the place of the mechanism of self-generation of motion, which is operative in the case of polarographic maxima of the first kind, we must provide a possibility to generate motion by means of an electric field which would be independent of the current on the drop. For this purpose a dropping mercury electrode was placed in an electrolyte solution and an electric field was applied to the latter by means of two subsidiary electrodes, the ratio of the supporting electrolyte and of the depolarizer concentrations being chosen in such a way that no polarographic maximum of the first kind should occur under normal conditions (25). The results obtained with $0.28N$ $Hg_2(ClO_4)_2 + 0.002N$ $KClO_4$ are given in Fig. 6. Current-voltage curve 1 was obtained without the application of an external electric field, curve 2 with the application of a field having a gradient of 0.47 v/cm. This curve, which is of an unusual shape, is in close agreement with Eq. [2]. Its left-hand branch, corresponding to positive values of ϵ, greatly resembles the positive polarographic maxima of the first kind, as they are observed when the concentration of the supporting electrolyte is not too low. Polarograms obtained under normal conditions, however, show no second maximum at negative values of ϵ. I cannot discuss here the causes of this discrepancy, which, however, may be explained on the basis of the theory mentioned above (24).

The theoretical interpretation of the so-called maxima of the second kind, which depend on the flow of mercury out of the capillary, is much simpler than the interpretation of the maxima of the first kind. In this case, it is of fundamental importance to take into consideration the same inhibition of the surface motion by the double layer charges, which results in the decrease of the velocity of a falling charged drop. The maxima of the second kind play an important role in the theory of the rotating mercury drop electrode of Kolthoff and Okinaka (26).

Of special interest is the question about the relationship between the double layer structure and the nature of the metal. The latter may have an effect on the capacity of the Helmholtz layer as well as on the potential of zero charge. At the present time we are in possession of sufficient experimental data only on the second point. Let us consider first liquid metals. The information which we can obtain on this subject from measurements in

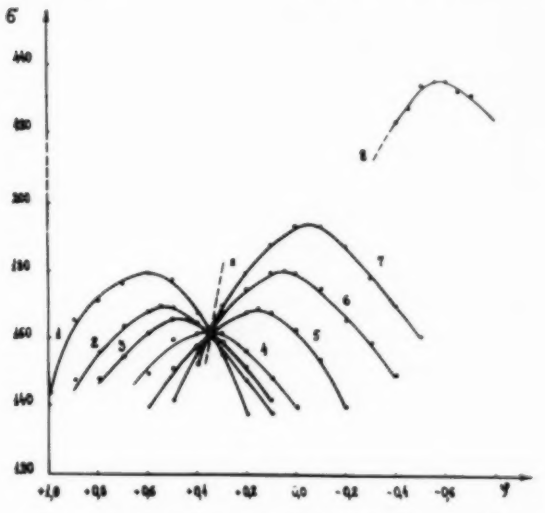

Fig. 7. Electrocapillary curves of Te-Tl alloys in LiCl + KCl. 1, Te; 2, 3.83 at. % Tl; 3, 10.9%; 4, 22.1%; 5, 42.3%; 6, 53.7%; 7, 65.2%; 8, Tl. Reference electrode Pb, LiCl + KCl, 0.1% $PbCl_2$.

aqueous solutions is naturally limited; we get more data with molten electrolytes. Electrocapillary phenomena in melts have been particularly investigated at the Sverdlovsk University (27). Electrocapillary curves for the Te-Tl system, plotted from measurements made by Kusnezov, *et al.*, are shown in Fig. 7. This system is characterized by an exceptionally great difference in the positions of the electrocapillary maxima, i.e., of the points of zero charge, which is as large as 1.25 v. The double layers at the metal-electrolyte interface at the point of zero charge being eliminated, the value given is similar in many respects to the Volta potential between the respective metals measured in vacuum (28). If the orientation of molecules of the solvent and the specific adsorption of ions are not taken into consideration, this value can be regarded as a kind of Volta potential in a material medium. I have already dealt with this problem in a paper which I presented at the 7th Annual Symposium on Colloid Chemistry at Baltimore about 30 years ago. At the present time a similar point of view is held by many electrochemists, e.g., Temkin (29), Rüetschi and Delahay (30). In my opinion, the determination of zero charge potentials gives the most direct answer to the question about the relationship between the difference of potentials between the poles of a galvanic cell with electrodes from different metals and the corresponding Volta potential, which has greatly attracted the attention of electrochemists since the beginning of the 19th century.

However, the similarity between the differences of zero charge potentials and Volta potentials does not necessarily result in a complete coincidence of these values, as the zero charge potentials may be influenced in a varying degree on the two electrodes by the preferential adsorption of one of the ions of the melt or by the orientation of the molecules of the solvent; the presence of a material medium may also have some effect on the distribution of the electronic cloud in the surface layer of the metal.

As a result of these complications the potential difference between water and mercury at the zero charge point of mercury is not equal to the sum of the galvani-potentials at the water-gas and vacuum-mercury interfaces, but exceeds it by an amount which was found by me to be equal to 0.30 v (31). Using more recent values of the Volta-potential between mercury and aqueous solutions (32), and of the zero charge potential of mercury (6) we get the value 0.26 v for this quantity. The assumption that the difference between the potentials of zero charge of two metals coincides with the Volta-potential between them is equivalent to the assumption that there exists a relationship between the zero charge potential and the electronic work function w, which can be expressed by the equation (33)

$$\phi_s - w = \text{constant} \qquad [4]$$

In accordance with the foregoing this relationship can only be approximate; it is not likely that one can make it more exact by introducing a certain coefficient before w, as has sometimes been suggested (34). The problem of the relationship between ϕ_s and w was recently discussed also in American literature (30, 35, 36). In the author's opinion, in order to verify these relationships at the present time, first it is necessary to be in possession of more exact experimental data both on the electronic work function and especially on the zero charge potentials.

The problem of investigating the double layer structure becomes more complicated when dealing with solid metals, although in the place of interfacial tension measurements, which cannot be carried out in this case, there appears an opportunity to study the effect of the double layer on such properties of metals as hardness (37-39), friction (40, 41), electrokinetic potential (42), stability of suspensions or sols. Unfortunately, the interpretation of results obtained from such measurements is not always as unambiguous as it is in the case of electrocapillary measurements. Very much was expected from capacity measurements on solid electrodes, in particular from the determination of zero charge potentials by means of the location of the capacity minimum in dilute solutions of electrolytes (43). However, the investigations carried out hitherto have only partly justified these expectations, as it is not always possible to obtain with solid metals capacity-potential (C,ϕ) curves comparable with those for mercury. Such a curve for the surface of a Zn monocrystal in 0.1N KCl (44), together with curves for Hg and liquid Ga (45) in the same electrolyte, is shown in Fig. 8. The capacity of the Zn monocrystalline surface within the frequency range of 1-10 kilocycles changes but little with frequency (by 5-8%) in contrast to what is observed in the case of polycrystalline zinc. This makes us suppose that the dispersion of the capacity, which interferes with capacity measurements on solid metals, is at least partially accounted for by the unevenness of the surface and the presence of micro-

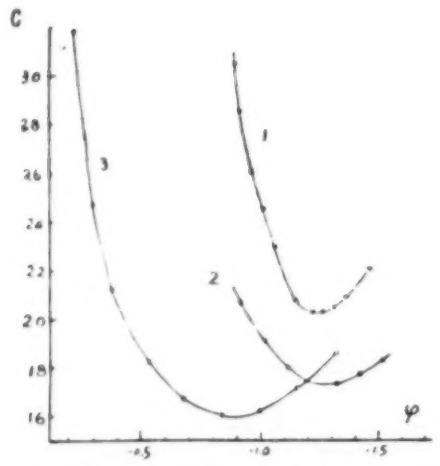

Fig. 8. Relationship between the differential capacity C and the potential ϕ in 0.1N KCl (NHE). 1, Zn monocrystal; 2, liquid Ga (according to Grahame); 3, Hg.

scopic cracks, although other explanations have been given to this phenomenon as well (46).

A curious inference can be made from determinations of zero charge potentials by means of the capacity minimum in dilute solutions (as well as from the hardness maximum) in the case of Pb and PbO_2 electrodes (47). The zero charge potential ϕ_s of PbO_2 is located at 1.8 v vs. NHE, the zero charge potential of Pb at −0.7; the difference between these two values is 2.5 v, which is even greater than the difference of potential between the poles of a lead storage cell.

With the help of capacity measurements Leikis has studied in detail the behavior of a silver electrode. As shown in Fig. 9, a pronounced minimum is observed in a dilute solution of Na_2SO_4 on the C,ϕ curve of silver; the silver wire had been subjected to cleaning with moist glass powder and boiling in an alkaline solution. This minimum disappears with an increase in solution concentration. The zero charge potential found in this way is equal to −0.7 v vs. NHE which coincides approximately with the results of electrocapillary measurments on molten silver

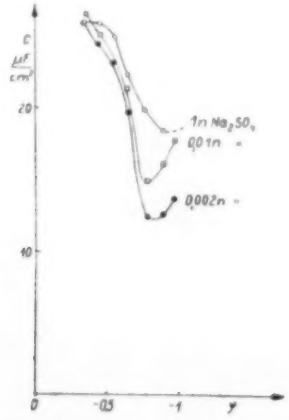

Fig. 9. Differential capacity of an Ag electrode in Na_2SO_4 solutions (NHE).

($\phi_s = -0.6$), but not with other data in the literature. The investigation of the effect of the solution concentration and of the presence of surface active anions and organic substances confirms the correctness of this ϕ_s value.

Leikis's experiments produced a noteworthy result. In electrochemical measurements wide use is made of a technique for cleaning electrode surfaces by means of vigorous cathodic polarization. But if a silver electrode is subjected to cathodic polarization in N Na_2SO_4 up to $\phi = -1.25$ v vs. NHE, the conditions of the surface, as it can be inferred from capacity measurements, change markedly, and at $\phi = -1.35$ v this change becomes irreversible. C,ϕ curves obtained with such an electrode differ widely from normal curves.

There exists still another reason why care must be exercised in interpreting the results of the measurements of C,ϕ curves when solid electrodes are used. In the presence of adsorbed hydrogen or oxygen on the electrode surface along with the double layer capacity a pseudocapacity is measured, the value of which depends on the exchange current between the adsorbed layer and the solution (48). In these cases the minima observed on C,ϕ curves may represent pseudocapacity minima and therefore tell us nothing about the zero charge potential. Apparently, such is the case with active platinum electrodes (49), and this accounts for the relationship observed between the location of the minimum on C,ϕ curves of Pt and the pH of the solution (50). While making measurements in dilute solutions at high frequencies Kabanov and Birinzeva could find no capacity minimum on platinum which could be interpreted as corresponding to the most diffuse state of the double layer at the point of zero charge (51). This is possibly due to a marked heterogeneity of the surface of an activated platinum electrode.

It is evident that in the case of an extremely heterogeneous surface the measurable potential of zero charge represents a certain mean value at which occurs the transition from a preferential anion adsorption to a preferential cation adsorption. Such a potential of zero charge does not necessarily correspond to the most diffuse structure of the double layer.

In the case of solid electrodes with a large surface, the formation of the double layer causes marked changes in the composition of the solution, which are known to produce errors in pH measurements with the help of platinized platinum electrodes if the system is insufficiently buffered. The determination of these changes in the composition can serve as a method for the investigation of the double layer structure. This method was applied successfully to such substances as platinum and activated carbon. Two results obtained recently may be mentioned in this connection. As the zero charge potential for platinum is more positive than the normal hydrogen potential, this metal is negatively charged when placed in a hydrogen atmosphere in acid solutions. The formation of the double layer, for instance in an acidified N Na_2SO_4 solution, is accompanied therefore by a transfer of hydrogen ions to the solution and by an increase in solution acidity, which can be

measured if platinized electrodes are used. However, in the presence of surface active halogen anions, the mechanism of the establishment of the equilibrium potential difference is changed; with the increase of the anion adsorbability the double layer formed by negative charges on the metal surface and cations attracted by them is replaced by a double layer with a negative sheet formed by adsorbed anions. In the case of a *N* NaI-solution acidified up to pH ~ 3, as has been found by Balashova and Kasarinov (52), the potential difference due to the adsorption of anions becomes so great that at the equilibrium hydrogen potential the sign of the charge of the platinum is reversed. Under these conditions the formation of the double layer is accompanied by a decrease in the solution acidity, and not by an increase in the latter.

A hydrogen electrode with a still better developed surface can be made by depositing some platinum on the surface of activated carbon. Such platinized carbon in a hydrogen atmosphere adsorbs from neutral solutions of salts considerable amounts of cations, which are replaced by hydrogen ions. The magnitude of the adsorption effect depends on the final pH of the solution just as would be expected from the theory outlined, if one assumes that ϕ_x for "hydrogen" carbon is equal to 0.03 v (53).

The idea according to which the electrolyte adsorption on activated carbon is a process connected with the establishment of the equilibrium potential difference was met with opposition. A number of scientists preferred to interpret these phenomena on the same lines, as is done in the case of adsorption on ion exchange resins, i.e., without taking into account the electronic conductivity of carbon. However, the "electrochemical" theory of electrolyte adsorption on carbon received recently a conclusive corroboration in the investigations carried out by Strazhesko at the Ukrainian Academy of Sciences in Kiev (54). Strazhesko found that the acidification caused by cation adsorption from solution increases markedly (2-3 times), when solutions in nonaqueous solvents, e.g., acetone, are used instead of aqueous ones. Such a phenomenon, quite inexplicable on the basis of the "chemical" theory of electrolyte adsorption on carbon, can be interpreted, if one assumes that the zero charge potential of carbon, as well as that of mercury, is shifted toward more positive values when molecules of acetone are substituted for those of water. In this case at the reversible hydrogen potential the carbon surface must really carry a more negative charge in a nonaqueous solvent.

An original method for the determination of the zero charge point of platinum was proposed recently (42, 55). The presence of the diffuse double layer causes two metallic surfaces in an electrolyte solution to repel and prevents them from drawing together. Voropaeva, Derjaguin, and Kabanov measured the force necessary for establishing at different potentials a conducting contact between two crossed platinum wires immersed in a dilute KCl solution. As seen in Fig. 10, there is a pronounced minimum on the curve showing the relationship

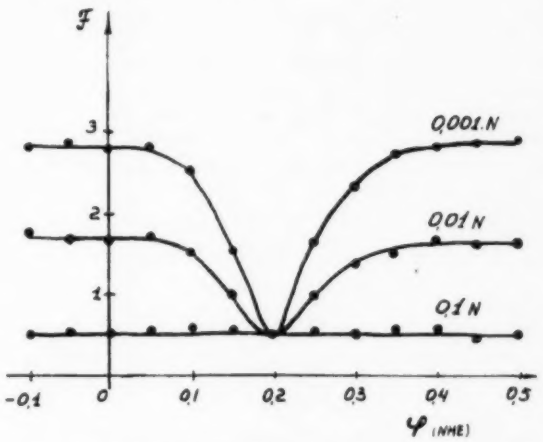

Fig. 10. Relationship between the potential and the force F, which must be applied in order to establish a contact between two platinum wires in KCl solutions.

between the force and the potential, at the zero charge potential. The value of ϕ_x found in this way is in good agreement with the results of adsorption measurements. It is not quite clear why in this case we do not meet with the difficulties, which were encountered during the attempts to determine the location of the zero charge potential of platinum from the capacity minimum in dilute solutions.

When dealing with the problem of points of zero charge, the supposed existence of an essential difference between the case of a reversible electrode and that of an ideal polarized one has been sometimes mentioned in the literature (30, 56). It seems to me however that there are no theoretical grounds for such a differentiation (39). Although the mechanism of the formation of the double layer in these two cases is, generally speaking, different, its structure and, consequently, the physical meaning of the zero charge potential must be similar. In accordance with this it was possible to show that the change in the double layer capacity with electrolyte concentration at the zero charge potential of thallium amalgams in dilute solutions of electrolytes proceeds in conformity with the same laws as those for mercury, although the equilibrium concentration of Tl^+ ions in the solution at the zero charge potential reaches in this case a measurable value (57).

The concept about the existence of the electric double layer was not made use of in the first investigations of the kinetics of electrochemical processes. This could not have been expected, since at the time the net velocity of electrochemical processes was associated with purely chemical or diffusion steps. Only after the idea of the finite velocity of electrochemical steps proper and of their dependence on the interfacial potential difference had been introduced in the theory of electrode processes (Audubert, Butler, Erdey-Gruz, and Volmer), did it become possible to combine the double layer theory and the principles of electrochemical kinetics. The first attempt in this direction was seemingly made by the author (58); it was supposed

that the reacting particles follow the Boltzmann distribution law and that only a part of the potential difference is effective in determining the rate of the process. The original conclusions referred to the case of the hydrogen ion discharge. If we generalize the expression obtained for the case when an electron is transferred to a particle carrying n charges, where n can be either positive or negative, the result assumes the following form (59)

$$i = K \exp\left[-\alpha(\phi-\phi_1) - n\phi_1\right] F/RT \qquad [5]$$

where i is the current density, c the bulk concentration of the reacting particle, if necessary corrected for concentration polarization, and α a constant satisfying the condition $0<\alpha<1$. The problem of the physical interpretation of the value α is yet open to discussion and in practical use of the equations of electrochemical kinetics α must be considered as an empirical constant. An accurate determination of the meaning of ϕ_1 is of great importance. The value ϕ_1 was regarded primarily as the potential in the center of the charge of the reacting particle at its equilibrium location in the Helmholtz layer, although the possibility to refer it to the location of the charge center in the transition state of the reaction should be considered too.[2] As was shown by the experiments of Bagozky (62) and others, Eq. [5] expresses exactly the relationship between the H_3O^+ ion discharge rate in KCl + HCl solutions and the concentrations of the components, if the value ϕ_1 is considered as the potential in the plane of the closest approach of cations to the electrode surface and this potential is computed on the basis of the classical theory of the diffuse double layer. Thus, neglecting the details of the double layer structure involves no great errors in the case when the reacting particle is an H_3O^+ cation, repelled by K^+ or H_3O^+ cations which form the ionic sheet of the double layer. However, much greater difficulties were encountered, when a different group of reactions was considered, i.e., the electroreduction processes of multivalent anions, during which the reacting particles are attracted by the ions present in the ionic sheet of the double layer. These reactions, which have been studied in detail in Moscow since 1949, are characterized by an anomalous form of c.v. curves (59, 63). Namely, the usual increase in the current, which occurs when the cathodic polarization is increased, is followed by a sharp falling off, taking place at potentials in the vicinity of the zero charge potential or more negative than the latter. When the potentials become still more negative, the current rises again. In many but not in all cases (64) these anomalies disappear with an increase in the concentration of the supporting electrolyte. As an example of these anomalous c.v. curves, a curve for the reduction of the $S_2O_8^{=}$ ion on an amalgamated rotating disk electrode in the presence of 0.01N Na_2SO_4 is shown in Fig. 11.

The pecularities of the electroreduction of multivalent anions are explained by the repulsion between the reacting particle and the negatively

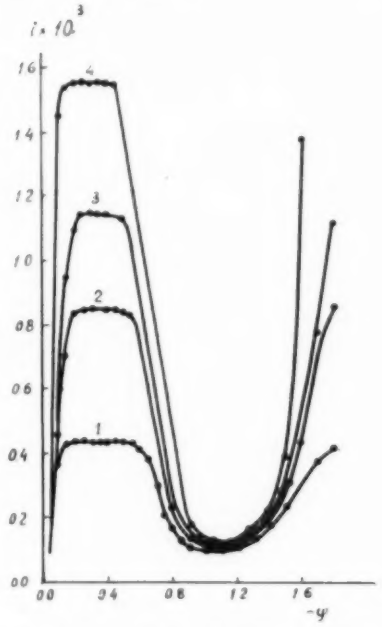

Fig. 11. C.v. curves for the reduction of 10^{-3} N $K_2S_2O_8$ in the presence of 10^{-2} N Na_2SO_4 on a rotating amalgamated disk electrode. Rates of rotation: 1, 650; 2, 2800; 3,5000; 4, 9000 rpm.

charged electrode surface. In Eq. [5] this effect is accounted for by the term containing ϕ_1; in fact, it is easy to show, that at $n = -2$ or $n = -3$ and with a reasonable value assumed for α, Eq. [4] represents a c.v. curve with a minimum in the region of potentials corresponding to negative surface charges. Although in some cases the experimental c.v. curves, corrected for concentration polarization, can be expressed even quantitatively by means of Eq. [5], a more detailed study of this problem shows that the concepts used as a basis in the derivation of this equation in this case are insufficient. As it is beyond the scope of this paper to discuss all the aspects of the problem, which, moreover, have been dealt with lately in a number of reviews (65), I intend to mention only the following point. Equation [5] is derived on the assumption that within the double layer the reacting particles follow the Boltzmann distribution law. As Levich's calculations have shown (66), this distribution cannot be realized at sufficiently high current densities in the case when the sign of the charge of a reacting multivalent particle is opposite to that of the charge of the electrode surface, if the distribution of potentials is in accordance with the classical theory of the double layer. In fact the rate of the penetration of such particles through the double layer and therefore the rate of their transfer from the bulk to the electrode surface under the conditions stated would be insufficient. Moreover the theoretical rate values obtained under these assumptions are several orders of magnitude lower than those observed.

It seems to me that the only way to overcome this difficulty is to take into consideration the discrete

[2] An equation similar to Eq. [5] and differing from the latter only in that 1/2 is substituted for α, was recently deduced on a different basis, that of a theory developed by Marcus (60, 61).

structure of the ionic sheet of the double layer and the interaction between the reacting anions and the neighboring cations. Another solution of this problem would be to assume that not those anions which are predominant in the bulk of the solution react on the cathode, but ionic pairs with a smaller charge, as, for instance, the $MeS_2O_8^-$ ions in the case of a $Me_2S_2O_8$ solution (66, 67) and $Me_2Fe(CN)_6^-$ ions in the case of a $Me_4Fe(CN)_6$ solution. But difficulties are encountered if we are to follow this hypothesis consistently, i.e., improbably low values must be ascribed to α. Furthermore the thickness of the reaction layer in the case of reactions of the type

$$Me^+ + S_2O_8^{=} \rightleftharpoons MeS_2O_8^- \qquad [6]$$

in all probability is so small that the formation of those ionic pairs which react on the electrode must take place within the double layer. Thus, if we accept this assumption, we still must make an allowance for the interaction between oppositely charged ions within the double layer.

It appears that in that range of potentials for which reliable determinations of the c.v. curves can be made, it is possible to account for the phenomena observed during the reduction of multivalent anions by means of the theory of slow discharge, taking into account the formation of cationic bridges in the double layer. But involuntarily one is led to think that at sufficiently negative potentials a different mechanism of the electrode process is possible, consisting of a transfer of electrons from the electrode to particles located at distances comparable with the thickness of the diffuse double layer. As such a transfer would remove the difficulties connected with the repulsion of anions by the electrode surface, it would seem that in the case of anion reduction the most favorable conditions for such a mechanism are realized. Gurney was the first to point out the possible role of such electronic transfers in discharge processes (68), although the example chosen by him–the hydrogen ion discharge–was undoubtedly not suitable, as the high value of the adsorption energy of the product of the reaction–the hydrogen atom–makes the discharge at a distance from the metal surface energetically unfavorable. We must admit however that the feasibility of such transfers even in the case of anion reduction has not hitherto been corroborated by experiment, although we do not have sufficient reasons to deny their reality in the case when the cations of the electrolyte, as for example Li^+ cations, have a relatively low tendency to form ionic pairs. The research work in this direction must be continued, particularly taking into account what is known about the existence of solvated electrons in many solvents. Generally speaking, it may be said that the state of our knowledge about the transfer of electrons over long distances in the case of electrode processes is about the same as in the case of redox reactions occurring in the bulk of the solution.

The idea of the importance of the structure of the double layer for the kinetics of electrode processes has gradually become firmly established in electrochemistry, as for instance is shown by the review of Breiter, Kleinerman, and Delahay (69). However, one must mention the progress made in research in another, at first sight opposite, direction. Investigations carried out after the war, in particular in Czechoslovakia, have shown that the net rate of a great number of electrode processes is determined by chemical reactions resulting in the formation of an electroactive substance from inactive components in the bulk of the solution and therefore, as it would seem, independent of the double layer structure. At present it appears, however, that such a contraposition of these two concepts would be incorrect, as in a number of cases the thickness of the reaction layer becomes comparable with that of the diffuse double layer (70). Under these conditions it is necessary to take into consideration the effect of the electric field of the double layer upon the kinetics of the process, although it is a chemical and not an electrochemical one. Unfortunately we know as yet very little how this is to be done.

I have dealt hitherto only with the direct effect of the double layer on the reactions on the electrode. But its indirect effects are perhaps of still greater importance. The adsorption of surface active ions and of neutral molecules depends on the electric field of the double layer and these ions and molecules, in their turn, may act as catalyzers or inhibitors in electrochemical processes. It would be beyond the scope of the present paper to dwell on this problem, the study of which has given us many conclusive proofs of the existence of a close connection between the structure of the interface and the kinetics of the electrode processes (71, 65). However, I want to consider at least one particular case, that of the adsorption of anions which do not take a direct part in the electrode process. I have chosen this case because its consideration brings us, in a sense, to the limits within which we may use those very elementary concepts on whose basis Eq. [5] and some other similar relationships were deduced. In accordance with Eq. [5] the specific adsorption of anions must shift the ϕ_1 — potential toward more negative values and consequently increase the velocity of the processes of cation reduction. As might be easily proved, this conclusion holds for anodic processes of cation formation as well. It was first confirmed in the work of Jofa, Kabanov, *et al.*, for the case of the discharge of hydrogen ions on a Hg cathode (72) and later for a number of other reactions, many of which are well known from polarographic literature (73). However, at present, we know that in some cases the adsorption of anions on solid electrodes results not in an acceleration, but in a retardation of reactions of discharge and of formation of cations (74, 75). Thus, the adsorption of the Br^- ion and particularly of the I^- ion greatly retards the ionization of H_2 on a Pt electrode (76, 77), as well as the ionization of the hydrogen on the β phase of the Pd-H system (78). Apparently, the bond between the adsorbed anion and the metal surface becomes so firm in these cases that it is the modification of the properties of the electrode surface by the adsorbed

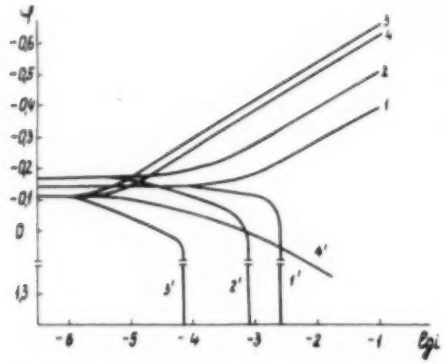

Fig. 12. Cathodic and anodic c.v. curves for stainless steel. 1, 1' 10N H_2SO_4; 2, 2' 10N H_2SO_4 + 0.01N KBr; 3, 3' 10N H_2SO_4 + 0.001N KI; 4, 4' 10N H_2SO_4 + 0.2N KI. The potentials are referred to a hydrogen electrode in 10N H_2SO_4.

anions, which results in a kind of passivity, that is of principal importance and not the change in the distribution of the potential in the double layer. This passivity probably is caused by the saturation of the free valencies of the electrode surface by chemisorbed anions and is accompanied by a decrease in the double layer capacity (79). The fact that this phenomenon is observed with solid electrodes only suggests that it is connected somehow with the presence on the electrode surface of active centers with high values of adsorption energies which strongly influence the kinetics of the process. An interesting example of this kind of action of anions is seen in the behavior of a stainless steel with 17% Cr and 9% Ni in the presence of I^- ions (80). As shown in Fig. 12, the addition of I^- ions to 10*N* H_2SO_4 increases the hydrogen overvoltage and facilitates the anodic passivation of steel. The inhibition of the cathodic and anodic processes results in a great diminution (4000 times) in the rate of the spontaneous dissolution of this steel in 10*N* H_2SO_4. The dissolution rate passes through a minimum at a I^- ion concentration of about 0.01% and increases again with further increase in the latter, not attaining, however, its original value. As it appears to me, these results show conclusively that metal passivation does not necessarily involve the covering of the surface with a protective layer forming a phase.

The investigation of the effect of anions on the kinetics of electrode processes permits us to draw the conclusion that the development of the theory of the double layer on the basis of purely electrostatic concepts must be considered as only a step in the building up of a surface chemistry of metals on a wider scale.

My address was concerned with the double layer on the metal-solution interface, but in order to understand their electrical properties it is essential to compare phenomena occurring on different kinds of interfaces. In a paper presented at the 7th Symposium on Colloid Chemistry I gave particular consideration to the comparison between the orientation of organic molecules on the metal-solution and solution-gas interfaces. It is very instructive as well to compare the results of electrocapillary measurements in solutions containing aromatic compounds (71, 81) with the results of determinations of the electron work function in the presence of adsorbed layers of molecules of this kind (82). Great attention has been paid lately to the problems of the semiconductor-vacuum and the semiconductor-electrolyte interfaces. The application of ideas developed in the investigation of the metal-electrolyte interface to the study of these interfaces has already given important results and undoubtedly will be still more fruitful in the future.

REFERENCES

1. A. Frumkin, *Z. physik. Chem.*, **103**, 43 (1923).
2. F. Krüger and G. Krumreich, *Z. Elektrochem.*, **19**, 617 (1913).
3. M. Proskurnin and A. Frumkin, *Trans. Faraday Soc.*, **31**, 110 (1935).
4. M. Vorsina and A. Frumkin, *Compt. rend. acad. sci. U.R.S.S.*, **24**, 918 (1939).
5. D. C. Grahame, *J. Am. Chem. Soc.*, **63**, 1207 (1941); **68**, 301 (1946); *Chem. Revs.*, **41**, 441 (1947).
6. D. C. Grahame, *This Journal*, **98**, 343 (1951); *J. Am. Chem. Soc.*, **76**, 4819 (1954); **79**, 2093 (1957); *Z. Elektrochem.*, **59**, 773 (1955); D. C. Grahame and B. Soderberg, *J. Chem. Phys.*, **22**, 449 (1954); D. C. Grahame, M. Poth, and J. Cummings, *J. Am. Chem. Soc.*, **74**, 4422 (1952).
7. O. Esin and B. Markov, *Acta Physiochim. U.R.S.S.*, **10**, 353 (1939); O. Esin and V. Shikov, *J. Phys. Chem.* (*U.S.S.R.*), **17**, 236 (1943).
8. B. Ershler, *J. Phys. Chem.* (*U.S.S.R.*), **20**, 679 (1946).
9. D. C. Grahame, *Z. Elektrochem.*, **62**, 264 (1958); *J. Am. Chem. Soc.*, **80**, 4201 (1958).
10. R. Parsons, *Trans. Faraday Soc.*, **51**, 1518 (1955); **55**, 999 (1959); Proc. 2nd Congr. Surface Activity, Electrical Phenomena, p. 38 (1957); Proc. of the 4th Electrochemical Meeting, Academic Press, p. 42, Moscow (1959).
11. B. Levich and V. Kirjanov, *Compt. rend acad. sci. U.R.S.S.*, In press.
12. A. Frumkin and A. Titievskaja, *J. Phys. Chem.* (*U.S.S.R.*), **31**, 485 (1957); A Frumkin and N. Poljanovskaja, *ibid.*, **32**, 157 (1958); A. Frumkin, in "Surface Phenomena in Chemistry and Biology," p. 189 (1958).
13. B. Damaskin, N. Nikolajeva-Fedorovich, and A. Frumkin, *Compt. rend. acad. sci. U.R.S.S.*, **121**, 129 (1958); F. Deane, A. Higinbotham, D. C. Grahame, Abstracts Theoretical Division, Electrochemical Society, Philadelphia Meeting, 1959, p. 39.
14. A. Obrucheva, *J. Phys. Chem.* (*U.S.S.R.*), **32**, 2155 (1958); *Compt. rend. acad. sci. U.R.S.S.*,**120**, 1072 (1958).
15. E. Mattson and J. O'M. Bockris, *Trans. Faraday Soc.*, **55**, 1586 (1959); B. E. Conway and J. O'M. Bockris, *Proc. Roy. Soc.* (*A*), **248**, 394 (1958); W. Mehl and J. O'M. Bockris, *Can. J. Chem.*, **37**, 190 (1959).
16. H. Gerischer and R. Tischer, *Z. Elektrochem.*, **61**, 1159 (1957); H. Gerischer, *ibid.*, **62**, 256 (1958).
17. W. Lorenz, *Z. physikal. Ch. N. F.*, **19**, 25 (1959).
18. Christiansen, *Ann. Phys.*, (4), **12**, 1072 (1903).
19. A. Frumkin and B. Levich, *Acta Physicochim. U.R.S.S.*, **19**, 573 (1945); A. Frumkin, *J. Colloid. Sci. I* 277 (1946); B. Levich, *J. Phys. Chem.* (*U.S.S.R.*), **21**, 689 (1947).
20. I. Bagozkaja, *J. Phys. Chem.* (*U.S.S.R.*), **23**, 123 (1949).
21. I. Bagozkaja and A. Frumkin, *Compt. rend. acad. sci. U.R.S.S.*, **55**, 135 (1947); *J. Phys. Chem.* (*U.S.S.R.*), **21**, 1033 (1947); *J. Phys. Colloid Chem.*, **52**, 1 (1948); A. Frumkin and B. Levich, *Acta Physicochim. U.R.S.S.*, **21**, 193 (1946).

22. V. Chlynov and O. Esin, *Compt. rend. acad. sci. U.R.S.S.*, **123**, 320 (1958); **120**, 134 (1958).
23. B. Levich, *J. Physic. Chem. (U.S.S.R.)*, **22**, 721 (1948); Physico-chemical hydrodynamics, 2nd ed., p. 406, Moscow (1959).
24. A. Frumkin and B. Levich, *J. Phys. Chem. (U.S.S.R.)*, **21**, 1335 (1947); A. Frumkin, *ibid.*, **29**, 1318 (1955); T. Krjukova, S. Sinjakova, and T. Arefjeva, "Polarographic Analysis," p. 94, 617, Moscow (1959); T. Krjukova, *Z. Physik. Chem.*, **212**, 247 (1959).
25. T. Popova and T. Krjukova, *J. Phys. Chem. (U.S.S.R.)*, **25**, 283 (1951).
26. J. Kolthoff and Y. Okinaka, *J. Am. Chem. Soc.*, **79**, 3326 (1957).
27. S. Karpachev and A. Stromberg, *J. Phys. Chem. (U.S.S.R.)*, **7**, 755 (1936); **10**, 739 (1937); **13**, 1831 (1939); **18**, 47 (1944); *Acta Physicochim. U.R.S.S.*, **12**, 523 (1940); V. Kusnezov, V. Kocherguin, M. Tishchenko, and E. Posdnysheva, *Compt. rend. acad. sci. U.R.S.S.*, **92**, 1197 (1953); V. Kusnezov, V. Ashpur, and G. Poroshina, *ibid.*, **101**, 301 (1955); V. Kusnezov, V. Axenov, and M. Klevzova, *ibid.*, **128**, 763 (1959); V. Kusnezov, T. Djakova, and V. Malzeva, *J. Phys. Chem. (U.S.S.R.)*, **33**, 1551 (1959).
28. A. Frumkin and A. Gorodetzkaja, *Z. physik. Chem.*, **136**, 451 (1928); A. Frumkin, *Coll. Symp. Ann.*, **7**, 89 (1930).
29. M. Temkin, *Bull. acad. sci. U.R.S.S. (Izvestiya), Chem. Ser.*, 235 (1946).
30. P. Rüetschi and P. Delahay, *J. Chem. Phys.*, **23**, 697 (1955).
31. A. Frumkin, *ibid.*, **7**, 552 (1939).
32. J. B. Randles, *Trans. Faraday Soc.*, **52**, 1573 (1956).
33. V. Novakovsky, E. Ukshe, and A. Levin, *J. Physic. Chem. (U.S.S.R.)*, **29**, 1847 (1955).
34. B. Vasenin, *ibid.*, **27**, 878 (1953); **28**, 1672, 1872 (1954).
35. B. Jakuszewski, *Bull. soc. sci. lettres Lódz*, Cl.III, N4 (1957); *J. Chem. Phys.*, **31**, 846 (1959).
36. A. de Bethune, *ibid.*, **31**, 847 (1959).
37. P. Rehbinder and E. Venstrem, *J. Phys. Chem. (U.S.S.R.)*, **19**, 1 (1945); **26**, 12 (1952); *Compt. rend. acad. sci. U.R.S.S.*, **68**, 329 (1949); P. Rehbinder and V. Lichtman, Proc. 2nd Congress Surface Activity, Electrical Phenomena, 1957, p. 563.
38. W. Klinkenberg, K. Lucke, and S. Masing, *Z. Metallkunde*, **42**, 361 (1951).
39. A. Frumkin, *Uspekhi Khim.*, **24**, 933 (1955); *Z. Elektrochem.*, **59**, 807 (1955).
40. F. Bowden and Young, *Research*, **3**, 235 (1950); F. Bowden and D. Tabor, Properties of the Metallic Surfaces, Inst. Metals, 1953.
41. J. O'M. Bockris and Parry-Jones, *Nature*, **171**, 930 (1953).
42. N. Balashova and A. Frumkin, *Compt. rend acad. sci. U.R.S.S.*, **20**, 449 (1938).
43. T. Borisova, B. Ershler, and A. Frumkin, *J. Phys. Chem. (U.S.S.R.)*, **22**, 925 (1948); T. Borisova and B. Ershler, *ibid.*, **24**, 337 (1950).
44. Tsa Chuan-sin and S. Jofa, *Compt. rend. acad. sci. U.R.S.S.*, **131**, 137 (1960).
45. D. Grahame, Proc. of the 4th Electrochemical Meeting, p. 27, Academic Press, Moscow (1959).
46. J. O'M. Bockris, W. Mehl, and B. Conway, Proc. of the 4th Electrochemical Meeting, p. 380, Academic Press, Moscow (1959); J. O'M. Bockris and B. Conway, *J. Chem. Phys.*, **28**, 707 (1958).
47. B. Kabanov, I. Kiseleva, and D. Leikis, *Compt. rend. acad. sci. U.R.S.S.*, **99**, 805 (1954); D. Leikis and B. Kabanov, *Trans. Inst. Phys. Chem.* (New Methods of Physicochemical Investigations) Moscow (1957), **6**, p. 5; D. Leikis and E. Venstrem, *Compt. rend. acad. sci. U.R.S.S.*, **112**, 97 (1957).
48. D. Leikis, *ibid.*, In press.
49. P. Dolin and B. Ershler, *J. Phys. Chem. (U.S.S.R.)*, **14**, 886 (1940); *Acta Physicochim. U.R.S.S.*, **13**, 747 (1940); P. Dolin, B. Ershler, and A. Frumkin, *J. Phys. Chem. (U.S.S.R.)*, **14**, 907 (1940); *Acta Physicochim. U.R.S.S.*, **13**, 779 (1940).
50. B. Kabanov and T. Birinzeva, *Compt. rend. acad. sci. U.R.S.S.*, **131**, 132 (1960).
51. V. Cheifetz and B. Krasikov, *ibid.*, **109**, 586 (1956).
52. N. Balashova and V. Kasarinov, *ibid.*, In press.
53. E. Kuchinsky, R. Burstein, and A. Frumkin, *J. Phys. Chem. (U.S.S.R.)*, **14**, 441 (1940); *Acta Physicochim. U.R.S.S.*, **12**, 795 (1940); B. Bruns, R. Burstein, N. Fedotov, and M. Livshitz, *ibid.*, **8**, 47 (1938).
54. D. Strazhesko, *Compt. rend. acad. sci. U.R.S.S.*, **102**, 885 (1955).
55. T. Voropajeva, B. Derjaguin, and B. Kabanov, *ibid.*, **128**, 981 (1959).
56. H. Oehl and H. Strehlov, *Z. physik. Chem. N. F.*, **1**, 241 (1954); **4**, 89 (1955); *Z. Elektrochem.*, **58**, 665 (1954); **59**, 818 (1955).
57. L. Boguslavsky, *J. Phys. Chem. (U.S.S.R.)*, In press.
58. A. Frumkin, *Z. physik. Chem. (A)*, **164**, 121 (1933).
59. A. Frumkin and G. Florianovich, *Compt. rend. acad. sci. U.R.S.S.*, **80**, 907 (1952).
60. W. Reinmuth, L. Rogers, and L. Hummelstedt, *J. Am. Chem. Soc.*, **81**, 2947 (1959).
61. R. A. Marcus, *Can. J. Chem.*, **37**, 155 (1959); *J. Chem. Phys.*, **24**, 979 (1956).
62. V. Bagozky, *Compt. rend acad. sci. U.R.S.S.*, **58**, 1387 (1947); *J. Phys. Chem. (U.S.S.R.)*, **22**, 1466 (1948); V. Bagozky and I. Jablokova, *J. Phys. Chem. (U.S.S.R.)*, **23**, 413 (1949).
63. T. Krjukova, *Compt. rend acad. sci. U.R.S.S.*, **65**, 517 (1949); T. Kalish and A. Frumkin, *J. Phys. Chem. (U.S.S.R.)*, **28**, 473 (1954); G. Florianovich and A. Frumkin, *ibid.*, **29**, 1827 (1955); A. Frumkin and N. Nikolajeva, *Chem. Phys.*, **26**, 1552 (1957); A. Frumkin, N. Nikolajeva-Fedorovich, and R. Ivanova, *Can J. Chem.*, **37**, 253 (1959); N. Nikolajeva-Fedorovich, L. Fokina, and O. Petrij, *Compt. rend. acad. sci. U.R.S.S.*, **122**, 639 (1958); N. Nikolajeva-Fedorovich and B. Damaskin, Proc. of the 4th Electrochemical Meeting, Academic Press, Moscow, 1959, p. 150; A. Frumkin, O. Petrij, and N. Nikolajeva-Fedorovich, *Compt. rend. acad. sci. U.R.S.S.*, **128**, 1006 (1959).
64. H. Laitinen and E. Onstott, *J. Am. Chem. Soc.*, **72**, 4565 (1950).
65. A. Frumkin, *Trans. Faraday Soc.*, **55**, 156 (1959); *Bull. acad. sci. U.R.S.S. (Izvestiya) Chem. Ser.*, 1429 (1957); Abstracts Theoretical Division, Philadelphia Meeting, 1959, p. 1; A. Frumkin and N. Nikolajeva-Fedorovich, *Bull. Moscow Univ. (Vestnik)*, N4, 169 (1957).
66. B. Levich, *Compt. rend. acad. sci. U.R.S.S.*, **67**, 309 (1949); **124**, 869 (1959).
67. L. Gierst, "Cinétique d'approche et réactions d'électrodes irréversibles," Bruxelles (1958).
68. R. Gurney, *Proc. Roy. Soc.*, **A134**, 137 (1932).
69. M. Breiter, M. Kleinerman, and P. Delahay, *J. Am. Chem Soc.*, **80**, 5111 (1958).
70. J. Koryta, Abstracts of Papers 2nd Int. Congr. Polarography, p. 29 (1959).
71. A. Frumkin, Proc. Sec. Int. Congr. Surface Activity, Electrical Phenomena, p. 58 (1957); *Nova Acta Leopoldina, N.F.*, **19**, N132, (1957); *Compt. rend. acad. sci. U.R.S.S.*, **85**, 373 (1940).
72. S. Jofa, B. Kabanov, E. Kuchinsky, and F. Chisjakov, *J. Phys. Chem. (U.S.S.R.)*, **13**, 1105 (1939).
73. Y. Heyrovsky, *Disc. Faraday Soc.*, **1**, 212 (1947); R. Piontelli, *Compt. rend. 2-ème Réunion CITCE, Milano*, 1951, p. 3; J. Randles and K. Somerton, *Trans. Faraday Soc.*, **48**, 937, 951 (1952); K. Schwabe, *Z. Elektrochem.*, **59**, 663 (1955); L. Antropov, *Uspekhi Khim.*, **25**, 1043 (1956).
74. J. Kolotyrkin and N. Bune, *J. Phys. Chem. (U.S.S.R.)*, **21**, 581 (1947); **29**, 435 (1955); *Compt. rend. acad. sci. U.R.S.S.*, **100**, 295 (1955); J. Kolotyrkin and L. Medvedjeva, *J. Phys. Chem. (U.S.S.R.)*, **25**, 1355 (1951); **29**, 1477 (1955); L.

Medvedjeva and J. Kolotyrkin, *ibid.*, **31**, 2668 (1957); J. Kolotyrkin, Proc. 9th Meeting CITCE, London, 1959, p. 406; *Trans. Faraday Soc.*, **55**, 455 (1959).
75. S. Jofa and L. Medvedjeva, *Compt. rend acad. sci. U.R.S.S.*, **69**, 213 (1949); S. Jofa, E. Ljachovezkaya, and K. Sharifov, **84**, 543 (1952); S. Jofa and G. Roshdestvenskaja, **91**, 1159 (1953); S. Jofa, *Bull. Moscow Univ.* (*Vestnik*), **N2**, 139 (1956).
76. E. Wicke and B. Weblus, *Z. Elektrochem.*, **56**, 169 (1952).
77. A. Frumkin and E. Ajkasjan, *Compt. rend acad. sci. U.R.S.S.*, **100**, 315 (1955); *Bull acad. sci. U.R.S.S. (Izvestiya) Chem. Ser.*, 202 (1959); E. Ajkasjan, *J. Phys. Chem.* (*U.S.S.R.*) **33**, 1016 (1959).
78. L. Shanina, *Compt. rend. acad. sci. U.R.S.S.*, In press.
79. V. Losev, *ibid.*, **88**, 499 (1953); T. Birinzeva and B. Kabanov, *J. Phys. Chem.* (*U.S.S.R.*), **33**, 844 (1959); A. Rakov, T. Borisova, and B. Ershler, *ibid.*, **22**, 1930 (1948).
80. Chua Bao-din, Shen Sin-su, S. Jofa, and E. Michailova, *Compt. rend. acad. sci. U.R.S.S.*, **130**, 129 (1960).
81. M. Gerovich *ibid.*, **86**, 543 (1954); **105**, 1278 (1955); M. Gerovich and G. Rybalchenko, *J. Phys. Chem.* (*U.S.S.R.*), **32**, 109 (1958); M. Gerovich and N. Poljanovskaja, *Nauch. Doklady Wisschei Shkoly, Chimia*, 651 (1958).
82. M. Suhrmann, *Z. Metallkunde*, **46**, 780 (1955).

Brief Communications

Preparation of Solid Electrodes for Hydrogen Overpotential Studies

A. C. Makrides and M. T. Colthorp[1]

Metals Research Laboratories, Union Carbide Metals Company, Division of Union Carbide Corporation, Niagara Falls, New York

The importance of minimizing the amount of impurities in solution in hydrogen overpotential measurements has been stressed repeatedly (1). Following the example of Frumkin and his co-workers (2), pre-electrolysis is used extensively to this end. In purified solutions, hydrogen overpotential on mercury follows the Tafel equation with closely reproducible exchange current and Tafel slope (3). Results with solid electrodes vary widely, however. Deviations from Tafel behavior and time dependence of the overpotential at any given current density have been reported frequently (4, 5).

We have measured hydrogen overpotential on nickel ("spectroscopic" purity) by the direct method. Unlike previous work with this system (6), results were time independent and coincident curves were obtained with increasing and decreasing current densities. This study will be reported in detail later. The method used to prepare electrodes, which we believe applicable to similar studies with other metals, is presented here.

Nickel electrodes were cleaned by immersion in a chromic-sulfuric acid solution ("cleaning solution"), followed by washing with boiling conductivity water. Upon immersion in alkaline (0.1*N* NaOH) test solutions, electrodes exhibited passive potentials (>0.200 v vs. hydrogen in the same solution). They were activated by cathodic polarization at 2 ma/cm^2 for about 5 min. Rest potentials were within 2-3 mv of the reversible hydrogen potential. After a run, which generally required about 100 min, the electrode was passivated by anodic polarization at about 40 μa/cm^2 and left in this condition until the next run whereupon the electrode was again activated by cathodic polarization as described above. Reproducible results were obtained over a period of about two days. For longer times, the rest potentials became increasingly positive and overpotentials became time dependent, particularly at higher current densities. It is probable that for the longer times adsorbed impurities, probably dissolved glass, were not removed by passivation (anodic polarization to 1.0 v).

The Tafel slope was 0.110 v at 30°C, not much different from that reported by Bockris and Potter in their study of hydrogen overpotential on nickel (6). However, the exchange current in 0.1*N* NaOH was 1.5 x 10^{-5} amp/cm^2, i.e., about 30 times larger than 5 x 10^{-7} amp/cm^2 given in (6).

The possibility that these results can be attributed to a film of high specific area formed by reduction of the passive layer was ruled out by runs in 0.1*N* HCl. In this solution nickel activates spontaneously, the oxide apparently dissolving. The electrode was in solution for about 4 hr. It corroded at a rate of about 4 x 10^{-5} amp/cm^2 with a rest potential of —0.014 v against hydrogen. The equivalent of about 300 surface layers (~ 180 x 10^{16} atoms) dissolved during this time. Results were entirely analogous to those in alkaline solutions, i.e., overpotentials were time independent and ascending and descending curves agreed closely. The Tafel slope, 0.100 v, was essentially that reported in (6) while the exchange current was 5 x 10^{-5} amp/cm^2, or about 40 x the value 1.2 x 10^{-6} given in reference (6)

The time dependence of the overpotential, the inability to retrace a polarization curve with the same electrode, the deviation from the Tafel relation of the steady-state curves, and the low exchange currents reported in (5) and (6) must therefore be attributed to impurities adsorbed on the electrode,

[1] Present address: Department of Chemistry, University of Texas, Austin, Texas.

probably prior to its exposure to solution. Electrodes were pretreated in (6) by heating in hydrogen at about 350°C.

Common methods of preparing solid electrodes involve either etching or heating in hydrogen at temperatures below the softening point of borosilicate glass (6). Etching does not remove all impurities, a fact demonstrated by the existence of a variety of compounds which inhibit dissolution. Heating in vacuum or in hydrogen apparently is not effective unless temperatures approaching the melting point of the metal are used ("flashing") (7). In the method presented here the electrode is exposed to highly oxidizing conditions. Impurities are probably displaced by negative ions at the large positive potentials (> 1.0 v) attained. Further, it is generally found that organic impurities are adsorbed to a smaller extent on oxides than on metals; at the same time, they are adsorbed less strongly in the oxidized than in the reduced form (8). It is expected, therefore, that on reducing or dissolving the passive layer a "clean" electrode surface is produced.

"Active," reproducible platinum electrodes have been obtained by anodic polarization (9). Recently, Walker and Adams (10) cleaned platinum electrodes for polarographic studies in a manner similar to that presented here. This method can be employed with all metals which do not dissolve markedly under highly oxidizing conditions and which can be activated by a cathodic current. The surface can be regenerated after one or more runs if the metal passivates in the test solution at small anodic current densities (for example, nickel in 0.1*N* NaOH).

Manuscript received Dec. 7, 1959.

Any discussion of this paper will appear in a Discussion Section to be published in the December 1960 JOURNAL.

REFERENCES

1. J. O'M. Bockris and E. B. Conway, *Trans. Faraday Soc.*, **45**, 989 (1949); J. O'M. Bockris, "Modern Aspects of Electrochemistry," p. 260, Butterworths, London (1954).
2. A. Frumkin, *Acta Physicochim.*, **18**, 23 (1943).
3. Jofa, *ibid.*, **10**, 903 (1939). Jofa and A. Frumkin, *ibid.*, **18**, 183 (1943); J. O'M. Bockris and A. M. Azzam, *Trans. Faraday Soc.*, **48**, 145 (1952).
4. P. Lukowzew, S. Lewina, and A. Frumkin, *Acta Physicochim.*, **11**, 21 (1939).
5. A. M. Azzam, J. O'M. Bockris, B. E. Conway, and H. Rosenberg, *Trans. Faraday Soc.*, **46**, 918 (1950).
6. J. O'M. Bockris and E. C. Potter, *J. Chem. Phys.*, **20**, 614 (1952).
7. J. K. Roberts, *Proc. Roy. Soc. (London)*, **A152**, 445 (1935).
8. E. B. Maxted, "Advances in Catalysis," Vol. III, p. 129, Academic Press, New York (1951).
9. S. Schuldiner, *This Journal*, **106**, 891 (1959).
10. D. E. Walker and R. N. Adams, 136th Meeting of Am. Chem. Soc., Atlantic City, 1959.

Periodic Phenomena at a Nickel Electrode in Sulfuric Acid

Jörg Osterwald[1] and Heinz-Gerhard Feller[2]

Corrosion Laboratory, Department of Metallurgy, Massachusetts Institute of Technology, Cambridge, Massachusetts

In connection with electrochemical investigations of nickel-copper and chromium-nickel-iron alloys we observed positively and negatively damped oscillations occurring at the nickel electrode in sulfuric acid. This type has not yet been described in the literature, although periodic phenomena at a nickel electrode are known (1, 2). Although investigations of this new type could not be completed during our stay in the United States, we should like to summarize the most important experimental results obtained so far.

The polarization curve for transpassive nickel in 1*N* sulfuric acid at 25°C obtained potentiostatically is shown in Fig. 1. If one tries to measure the same curve galvanostatically, this is only possible for current densities below A. Above A the electrode potential does not become stable, but oscillations occur. Near A these oscillations are almost sinoidal (see right part of Fig. 2b), while they become more and more deformed with higher current densities. If one increases the current density beyond B, the potential jumps to a value lying above C on the other branch of the polarization curve. This phenomenon is remarkable, because usually the other

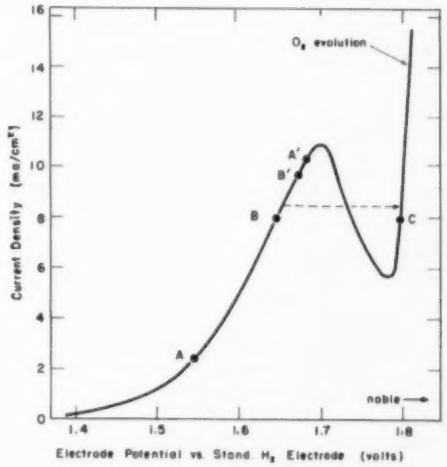

Fig. 1. Polarization curve of nickel in the transpassive region at 25°C obtained potentiostatically.

branch of a polarization curve can only be reached by applying a current density greater than the value related to the maximum.

As already mentioned, a constant potential is obtained below A under galvanostatic conditions, but

[1] Present address: Max-Planck-Institut für physikalische Chemie, Göttingen, Germany.
[2] Present address: Institut für Metallkunde der Technischen Universität, Berlin, Germany.

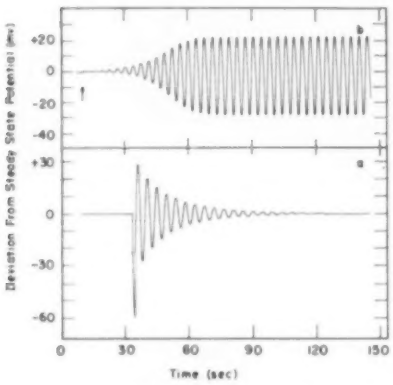

Fig. 2. Oscillations of potential under galvanostatic conditions (original oscillograms); T = 25°C. a, Damped oscillations, c.d. = 2.26 ma/cm²; b, negatively damped and steady oscillations, c.d. = 2.87 ma/cm².

a small positive or negative additional current pulse stimulates damped oscillations (Fig. 2a). With the exception of the first oscillations after the stimulating pulse the deviation ΔU from the steady-state potential may be described by the following equation:

$$\Delta U = \Delta U_0 e^{-\lambda t} \cos (2\pi\nu t + \delta)$$

ΔU_0 depends on the height of the pulse, while the damping constant λ and the frequency ν are only functions of the current density applied continuously. The phase angle δ depends on the zero point of the time scale.

In the region above A, oscillations occurring with increasing amplitude or, in other words, with negative values of λ can be observed by means of a special technique. A potential of the region above A is applied potentiostatically to the electrode. Then the galvanostatic circuit is adjusted to a current density equal to that which corresponds to the potentiostatically applied potential. If one now applies this current density to the cell immediately after having disconnected it from the potentiostatic circuit, one observes sinoidal potential oscillations, which eventually turn to steady oscillations. Figure 2b gives an example. The arrow marks the point at which the cell was switched from the potentiostatic to the galvanostatic circuit.

Using the same technique we found that above B' in Fig. 1 again steady oscillations occur under galvanostatic conditions, while above A' damped oscillations can be observed.

With decreasing acid concentration the whole region between A and A' becomes smaller, until first the region between B and B' disappears and finally at approximately 0.3*N* sulfuric acid only damped oscillations occur. The damping constant λ, however, has a minimum at a certain current density, to which a maximum of the frequency corresponds approximately.

A more quantitative description of the phenomena and an attempt at a theoretical explanation will be given after further information has been obtained, especially for the dynamic behavior of the nickel electrode under potentiostatic or other than galvanostatic conditions.

Acknowledgment

The authors are indebted to Professor H. H. Uhlig for his aid and encouragement. They wish to express their gratitude to the International Nickel Company and to the Shell Companies Foundation, Inc. for fellowship grants.

Manuscript received Jan. 19, 1960.

Any discussion of this paper will appear in a Discussion Section to be published in the December 1960 JOURNAL.

REFERENCES

1. R. Piontelli and G. Sarravalle, *Z. Elektrochem.*, **62**, 759 (1958).
2. U. F. Franck, Private communication.

Manuscripts and Abstracts for Fall 1960 Meeting

Papers are now being solicited for the Fall Meeting of the Society, to be held at the Shamrock Hotel in Houston, Texas, October 9, 10, 11, 12, and 13, 1960. Technical sessions probably will be scheduled on Batteries, Corrosion, Electrodeposition, Electronics (Semiconductors), and Electrothermics and Metallurgy.

To be considered for this meeting, triplicate copies of abstracts (*not exceeding 75 words in length*) must be received at Society Headquarters, 1860 Broadway, New York 23, N. Y., *not later than June 1, 1960. Please indicate on abstract for which Division's symposium the paper is to be scheduled, and underline the name of the author who will present the paper.* Complete manuscripts should be sent in triplicate to the Managing Editor of the JOURNAL at the same address.

Papers submitted for presentation at the meeting become the property of The Electrochemical Society and may not be published elsewhere, in whole or in part, unless permission is requested and granted by the Society. Papers already published elsewhere, or submitted for publication elsewhere, are not acceptable for oral presentation except on invitation by a Divisional program Chairman.

• • •

The Spring 1961 Meeting will be held in Indianapolis, Ind., April 30, May 1, 2, 3, and 4, 1961, at the Claypool Hotel. Sessions will be announced in a later issue.

FUTURE MEETINGS OF
The Electrochemical Society

Houston, Texas, October 9, 10, 11, 12, and 13, 1960

Headquarters at the Shamrock Hotel
Sessions probably will be scheduled on
Batteries, Corrosion, Electrodeposition,
Electronics (Semiconductors),
and Electrothermics and Metallurgy

★ ★ ★

Indianapolis, Ind., April 30, May 1, 2, 3, and 4, 1961

Headquarters at the Claypool Hotel

★ ★ ★

Detroit, Mich., October 1, 2, 3, 4, and 5, 1961

Headquarters at the Statler Hotel

Papers are now being solicited for the meeting to be held in Houston, Texas, October 9-13, 1960. Triplicate copies of each abstract *(not exceeding 75 words in length)* are due at Society Headquarters, 1860 Broadway, New York 23, N. Y., *not later than June 1, 1960* in order to be included in the program. *Please indicate on abstract for which Division's symposium the paper is to be scheduled and underline the name of the author who will present the paper.* Complete manuscripts should be sent in triplicate to the Managing Editor of the JOURNAL at 1860 Broadway, New York 23, N. Y.

Papers submitted for presentation at the meeting become the property of The Electrochemical Society and may not be published elsewhere, in whole or in part, unless permission is requested of and granted by the Society. Papers already published elsewhere, or submitted for publication elsewhere, are not acceptable for oral presentation except on invitation by a Divisional program Chairman.

Current Affairs

1960 Gordon Research Conferences

The 1960 Gordon Research Conferences on Corrosion, Physical Metallurgy-Relation of Structure and Properties, and Chemistry and Physics of Solids-Point Defects will be held from June 13 to September 2 at Colby Junior College, New London, N. H.; New Hampton School, New Hampton, N. H.; and Kimball Union Academy, Meriden, N. H.

The conferences were established to stimulate research in universities, research foundations, and industrial laboratories. This purpose is achieved by an informal type of meeting consisting of scheduled lectures and discussion groups. Sufficient time is available to stimulate informal discussions among the members of each conference. Meetings are held in the morning and in the evening, Monday through Friday, with the exception of Friday evening. The afternoons are available for recreation, reading, or participation in discussion groups.

It is hoped that each conference will extend the frontiers of science by fostering a free and informal exchange of ideas among persons actively interested in the subjects under discussion. The purpose of the program is to bring experts up to date on the latest developments, to analyze the significance of these developments, to provoke suggestions concerning the underlying theories and profitable methods of approach for making progress. It is not to review the known fields of chemistry and physics.

Attendance at the conferences is by application. Individuals interested in attending the conferences are requested to send their applications to the Director at least two months prior to the date of the conference. *All applications must be submitted on the standard application form which can be obtained by writing to the office of the Director.* This procedure is important because certain specific information is required in order that a fair and equitable decision on the application may be made. Attendance at each conference is limited to approximately 100 conferees.

Requests for attendance at the conferences, or for additional information, should be addressed to W. George Parks, Director, Dept. of Chemistry, University of Rhode Island, Kingston, R. I. From June 13 to September 2, mail should be addressed to Colby Junior College, New London, N. H.

Corrosion

July 18-22, 1960

Colby Junior College

New London, N. H.

Milton Stern, Chairman

Morris Cohen, Vice-Chairman

The Electrode Kinetics of Dissolution Processes

July 18

Discussion Leader, M. Cohen

L. H. Jenkins—Observations on Surface Structures of Copper Single Crystals Undergoing Aqueous Dissolution

M. Nagayama—The Nature of the Passive Film on Iron in Neutral Solution

F. A. Posey—Potentiostatic and Galvanostatic Studies on Passive Stainless Steel

N. D. Greene—Some Recent Studies of Corrosion and Passivity

S. Barnartt—Anodic Reactions of Stainless Steels during Stress Corrosion Cracking

July 19

Discussion Leader, M. Stern

A. C. Makrides—Cathodic Processes in Alkaline Solution

J. M. Kolotyrkin—Influence of Anions on the Dissolution Kinetics of Metals

G. H. Cartledge—Effects of Iodide Ions and Other Inhibitors in the Polarization of Iron

J. O'M. Bockris—The Mechanism of the Dissolution of Iron

T. P. Hoar—Dissolution Kinetics of the Iron Group Elements and Their Alloys—Annealed Strained and Yielding

July 20

Discussion Leader, J. F. Dewald

J. F. Dewald—Analogies and Distinctions between Semiconductor and Metal Electrodes

H. Gerischer—Corrosion Behavior of Germanium as an Example for Semiconductor Corrosion

W. W. Harvey—Chemisorption and Semiconductor Properties of Germanium Electrode Surfaces

W. Mehl—The Effect of Hydrofluoric Acid on the Mechanism of Anodic Dissolution of Germanium in Sulfuric Acid

W. H. Brattain—Observations on Electrolytic Processes at a Germanium Surface

July 21

Discussion Leader, J. V. Petrocelli

H. Kaesche—Mechanism of Anodic Pitting of Aluminum

C. Edeleanu—Anodic Polarization Effects on Aluminum

L. Young—Anodic Oxide Films on Tantalum and Zirconium

N. D. Tomashov—The Corrosion and Passivity of Titanium

J. B. Cotton—Formation and Breakdown of Anodic Films on Titanium

July 22

Discussion Leader, C. Edeleanu

E. L. Koehler—Application of Electrochemical Methods to the Corrosion of Can-Making Metals in Food-Acid Media

J. D. Sudbury—Anodic Passivation Studies

Physical Metallurgy—Relation of Structure and Properties

June 27-July 1, 1960

Kimball Union Academy

Meriden, N. H.

R. L. Fullman, Chairman

Michael Bever, Vice-Chairman

R. D. Seraphim—Effect of Impurities and Defects in Superconductors

A. W. Overhauser—Theory of Re-

sistance Minimum in Dilute Paramagnetic Alloys
W. B. Pearson—Low-Temperature Thermoelectric Behavior in Pure Metals and Dilute Alloys
P. A. Flynn—Deformation of Solid Solutions
D. A. Thomas—Influence of Grain Size on Deformation
J. Kruger—Relationship between Surface Orientation and Film Formation in Aqueous Solutions
F. W. Young—Mechanism of Dislocation Etch Pitting
D. A. Vermilyea—Electrodeposition and Defect Structure
J. E. Dorn—Shock Loading
J. W. Nutting—Dispersons and Creep
W. W. Smeltzer—Oxidation Characteristics of Zirconium, Titanium, and Hafnium
B. Wagner—Oxidation of Metals in Carbon Monoxide-Dioxide Mixtures
W. A. Backofen—Ductile Fracture
T. L. Johnston—Brittle Fracture
D. O. Smith—Origin of Anisotropy in Thin Magnetic Films
D. S. Rodbell—Ferromagnetic Resonance Studies of Whiskers and Particles
S. Chikazumi—Roll Magnetic Anisotropy
E. A. Nesbitt—Magnetic Annealing in Permalloys
A. Arrott—Ferromagnetism and Antiferromagnetism in Alloys
P. Beck—Electronic Specific Heat and Resistivity of Chromium Alloys

Chemistry and Physics of Solids—Point Defects

August 8-12, 1960

Kimball Union Academy

Meriden, N. H.

Robert L. Sproull, Chairman

Robert Maddin, Vice-Chairman

August 8

J. M. Whelan—Interactions of Holes, Electrons, and Electrically Active Impurities in GaAs
E. M. Pell—Lithium Impurity Interactions in Silicon
H. Brooks—Key Problems in the Theory of Point Defects
G . H. Vineyard—Information on Point Defects from Radiation Damage

August 9

D. Wilsdorf—Interaction of Point Defects and Dislocations
M. J. Makin—Point Defects and Mechanical Properties of Metals
R . W. Balluffi—Measurements of Equilibrium Point Defect Concentrations
T. Federighi—The Role of Point Defects in Clustering in Supersaturated Aluminum Alloys

August 10

R. M. Walker—Electrical Resistivity Changes in Metals
J. S. Koehler—The Nature of Point Defects in Metals
H. S. Sack—Review of Dielectric Relaxation and Internal Friction
R. W. Dreyfus, D. O. Thompson, B. S. Berry, and C. A. Wert—Round-table discussion on Review of Dielectric Relaxation and Internal Friction

August 11

G. D. Watkins—Study of Defects by Electron Spin Resonance
C. P. Slichter—Applications of Nuclear Magnetic Resonance
W. D. Compton—Optical Studies of Point Defects in Insulators
S. Zwerdling—Zeeman Effect of Impurity Excited States in Semiconductors

August 12

J. H. Crawford, Jr.—Defect Formation in Ionic Crystals by Ionizing Radiation

Section News

Columbus Section

In spite of rainy weather, a record number of 41 people turned out on February 10 to hear President William C. Gardiner speak to the Columbus Section of The Electrochemical Society on the subject "Developments in the Chlor-Alkali Industry."

The illustrated lecture held at Battelle Memorial Institute was followed by a lively discussion on various technical problems associated with chlor-alkali cells. Graphite anode costs, for example, tend to be excessive. It may prove feasible to design a cell, according to Dr. Gardiner, using platinized titanium anodes. Unlike graphite anodes, which need to be adjusted at regular intervals to maintain the proper spacing, the platinized titanium anodes would be fixed in position.

F. W. Fink, *Chairman*

Detroit Section

The annual joint meeting of the Detroit Sections of The Electrochemical Society and the National Association of Corrosion Engineers was held on February 18.

Following a fellowship hour at the Park-Shelton Hotel and dinner at the Engineering Society of Detroit, the group heard a talk by Howard T. Francis, of the Armour Research Foundation, describing and illustrating a technique for "Mapping of Surfaces during Corrosion and Plating." By means of a rotating electrode and oscilloscopic techniques, it is possible to obtain a visual pattern of the location of anodic and cathodic sites and to follow the course of corrosion over a period of time. He also indicated how this method may be used to identify porosity in nickel deposits and to map the intensity and direction of current lines during electrodeposition.

S. E. Beacom, *Secretary-Treasurer*

Indianapolis Section

The Indianapolis Local Section held its third technical meeting of the current season on February 9 at Butler University in Indianapolis. Dr. William C. Gardiner, Society President, was the speaker for the evening.

After a report on the current status of the Society and its varying activities, Dr. Gardiner discussed "Developments in the Chlor-Alkali Industry." He reviewed the present magnitude of the chlor-alkali industry, giving some history, fundamentals of electrolysis of brine in diaphragm and mercury cells, and a brief description of complete plants as a background. He then outlined recent developments in the industry, including semiconductor rectifiers, methods of handling salt or brine, effect of pure graphite, large capacity cells, vertical mercury cells, and changes in handling of caustic soda and chlorine. Dr. Gardiner concluded his talk with predictions of developments during the next decade.

The next technical meeting, scheduled for April 4, will be a cooperative affair with the Indianapolis Section of the American Electroplaters' Society.

T. C. O'Nan, *Secretary-Treasurer*

Pittsburgh Section

The Pittsburgh Section held a joint meeting with the Physical and Inorganic Chemistry Group of the American Chemical Society on January 25, at which Dr. G. J. Dienes, of the Brookhaven National Laboratory, talked on "Radiation Enhanced Diffusion in Solids."

He discussed the interaction of high-energy radiation with solids producing simple crystalline defects, thermal spikes, and fission spikes. For most nonfissionable metals, the most important radiation effect is

the production of simple lattice defects.

Since diffusion in metals occurs by the motion of vacancies and since high-energy radiation produces vacancies in excess of their equilibrium concentration, an enhancement of diffusion processes by radiation is expected. A simple theory presented described the dependence of this enhancement on radiation flux and on temperature under steady-state conditions. Experiments with alpha-brass were described in which diffusion was easily followed by measuring the electrical resistivity changes associated with changes in short-range order.

W. E. Haupin, *Secretary*

Personals

Robert F. Ayres has accepted a position as technical director with Dunham Chemical Co., a subsidiary of Chemetron Corp., Chicago, Ill. Previously, he was with Oakite Products, Inc., New York City.

John J. Bordeaux has joined Rheem Semiconductor Corp., Mountain View, Calif., as a member of the research and development team. He will work on the development of new types of transistors and other semiconductor devices. Formerly, Dr. Bordeaux was senior research scientist in the electrochemistry and solid-state chemistry section of the missile and space division of Lockheed Aircraft Corp. in Sunnyvale, Calif.

Currey E. Ford has been named director of marketing for National Carbon Co., Division of Union Carbide Corp., New York City. Mr. Ford will have over-all marketing responsibilities for the company's complete line of industrial carbon and graphite products. Prior to his new assignment, he was new products marketing manager.

Morton B. Prince has been appointed vice-president and general manager of the Semiconductor Division of Hoffman Electronics Corp., Los Angeles, Calif. Dr. Prince has been with Hoffman since 1956 in the capacity of vice-president, research and development, of the Semiconductor Division.

R. Raman has been named assistant foreman, Electronics Research and Development Establishment, Bangalore, India.

T. L. Rama Char, of Bangalore, has been elected a member of the

ECS Membership Statistics

The following three tables give breakdown of membership as of Apr. 1, 1960. The Secretary's Office feels that a regular accounting of membership will be very stimulating to membership committee activities. In Table I it should be noted that the totals appearing in the right-hand column are *not* the sums of the figures in that line since members belong to more than one Division and, also, because Sustaining Members are not assigned to Divisions. But the totals listed are the total membership in each Section. In Table I, Sustaining Members have been credited to the various Sections.

Table I. *ECS Membership by Sections and Divisions**

Section	Division: Battery	Corrosion	Electric Insulation	Electro-deposition	Electronics	Electro-Organic	Electrothermics & Met.	Industrial Electrolytic	Theoretical Electrochem.	No Division	Total as of 1/1/59	Total as of 1/1/60	Net Change
Boston	18	30	6	37	75	8	26	14	30	6	151	168	+17
Chicago	15	32	5	41	29	9	14	10	26	15	132	134	+ 2
Cleveland	52	29	2	53	41	8	30	33	36	13	198	198	0
Columbus, Ohio	3	17	0	15	10	2	26	2	11	4	49	62	+13
Detroit	13	20	4	52	11	6	8	6	24	18	91	97	+ 6
India	8	7	2	19	8	6	8	10	15	3	35	35	0
Indianapolis	14	9	6	12	15	6	10	3	10	2	39	53	+14
Midland	9	15	0	6	3	3	8	14	11	1	43	43	0
Mohawk-Hudson	4	17	16	7	17	2	9	1	19	5	54	70	+16
New York	96	111	31	148	170	35	74	70	108	40	517	575	+58
Niagara Falls	13	25	1	25	13	6	78	68	29	18	183	180	— 3
Ontario-Quebec	9	24	1	15	8	3	39	30	12	14	82	93	+11
Pacific Northwest	6	9	0	9	3	1	10	11	10	10	44	43	— 1
Philadelphia	32	28	4	36	78	9	26	20	47	30	185	205	+20
Pittsburgh	2	47	4	30	30	7	43	18	36	10	133	136	+ 3
San Francisco	9	13	1	20	24	4	16	20	20	4	71	78	+ 7
S. Calif.-Nevada	19	26	3	33	49	5	25	18	34	10	105	135	+30
Washington-Baltimore	39	40	7	37	25	3	11	10	34	6	129	140	+11
U. S. Non-Section	71	92	14	92	100	42	65	83	125	30	408	452	+44
Foreign Non-Section	47	67	10	68	39	33	43	61	81	92	262	285	+23
Total as of Jan. 1, 1960	479	658	117	755	748	198	569	502	718	331		+271 3182	
Total as of Jan. 1, 1959	441	638	103	723	621	190	549	486	656	329	2911		
Net Change	+38	+20	+14	+32	+127	+8	+20	+16	+62	+2			

* Figures being revised.

Table II. *ECS Membership by Grade*

	Total as of 4/1/60	Total as of 1/1/60	Net Change
Active	2582	2761	—179
Faraday (Active)	29	32	— 3
Deutsche Bunsen Gesellschaft (Active)	18	18	0
Delinquent	205	88	+117
Active Representative Patron Members	10	10	0
Active Representative Sustaining Members	111	111	0
Total Active Members	2955	3020	— 65
Life	15	17	— 2
Emeritus	45	48	— 3
Associate	20	33	— 13
Student	34	57	— 23
Honorary	7	7	0
Total	3076	3182	—106

The figures pertaining to Patron and Sustaining Member Representatives, and Faraday and Deutsche Bunsen Gesellschaft members subscribing to the JOURNAL, have been added to reflect reclassifications and changes in membership status.

Table III. *ECS Patron and Sustaining Membership*

	Total as of 4/1/60	Total as of 1/1/60	Net Change
Patron Member Companies	5	5	0
Sustaining Member Companies	159	160	— 1

British Association of Corrosion Engineers, London.

J. Sundararajan has been appointed junior research assistant, Dept. of Inorganic and Physical Chemistry, Indian Institute of Science, Bangalore.

News Items

Fifth Annual Appalachian Underground Corrosion Short Course

The 1960 Appalachian Underground Corrosion Short Course will be held at West Virginia University, Morgantown, W. Va., on June 1, 2, and 3. There will be 54 classes and a number of field demonstrations.

Subject categories included are as follows: Basic, Intermediate-Pipe, Intermediate-Cable, Advanced, Public Water Systems, Pipe Coatings, Instruments, and Special Topics.

Additional information regarding this event may be obtained from R. E. Hanna, Jr., School of Mines, West Virginia University, Morgantown.

Improved Value for the Faraday

The National Bureau of Standards, Washington, D. C., recently made a new determination of the faraday using an electrochemical method which dissolves, rather than deposits, silver in an electrolytic solution. The value thus obtained, 96,516.4 ± 2.0 coulombs (physical scale), depends on the atomic weight of silver, the standards of mass and time, and the electrical standards as maintained by the Bureau.

The recent electrochemical work was carried out by D. N. Craig and W. J. Hamer, with the assistance of Catherine Law and J. I. Hoffman.

Classification Schemes Sought

The Committee on Special Classifications of the Special Libraries Association and the Classification Committee of the Cataloging and Classification Section, Resources and Technical Services Division, American Library Association, are cooperating in a continuing project to develop and expand a Loan Collection of library classification schemes originally established by the Special Libraries Association. This Collection covers all fields of science, law, medicine, technology, the social sciences, and the humanities.

New libraries or libraries with special collections are constantly asking for classifications, in all areas of knowledge, and it is imperative that the Collection be kept up to date through the addition of new schemes or with modernized versions of existing classification schedules. Curators of special collections, special librarians, and those individuals who have developed special classification schemes for specific types of material or for special subjects are invited to contribute a copy of their work to the Collection.

Classification schemes should be sent to Dr. Jesse H. Shera, Curator, SLA Loan Collection, School of Library Science, Western Reserve University, Cleveland 6, Ohio.

University of Pennsylvania Dedicates New Chemistry Laboratory

An ingenious combination of chemical and electrical phenomena provided a dramatic spectacle for guests attending the dedication of the University of Pennsylvania's new $1,500,000 chemistry laboratory at 4:30 P.M. on Wednesday, March 9.

Participating in the dedication ceremonies were Dr. G. P. Harnwell, university president; Dr. C. C. Price, chairman of the Chemistry Dept.; Dr. W. A. LaLande, Jr., vice-president of Pennsalt Chemicals Corp.; and Dr. R. A. Connor, former chairman of the board of the American Chemical Society and chairman of the board of Rohm and Haas.

Faculty members and graduate students conducted visitors on a tour of the building following the ceremonies, to which the public was invited.

The growth of a single crystal of silver one-hundredth of an inch long caused a ribbon across the doorway of the new laboratory to burst into flame to formally open the new building. The crystal was grown within one of the chemistry laboratories and, at a certain stage of its growth, completed an electrical circuit which in turn set fire to the ribbon. Outdoor spectators had a 2000-times magnified view, by closed circuit television, of the growth of the tiny, fern-like crystal which was produced by passing an electric current through a bath of molten salts at 1000°F.

The new four-story structure, connected with the John Harrison Laboratories, was placed in use at the opening of the 1959 fall semester. Designed by Harbeson, Hough, Livingston and Larson, Philadelphia architects, it contains additional teaching and research laboratories with advanced equipment, seminar rooms, faculty offices, and a supply room. The building provides facilities for instruction in general chemistry and quantitative analysis and for graduate research in radiochemistry and inorganic and organic chemistry. Construction began in the spring of 1957, after an anonymous gift of $1,000,000 provided a substantial part of the necessary funds. The remainder is being contributed by chemical interests of the country.

Notice to Members and Subscribers
(Re Changes of Address)

To insure receipt of each issue of the JOURNAL, please be sure to give us your old address, as well as your new one, when you move. Our records are filed by states and cities, not by individual names. The Post Office does not forward magazines.

Penn-Olin Chemical Co. Formed

Penn-Olin Chemical Co. has been formed as a joint subsidiary of Pennsalt Chemicals Corp. and Olin Mathieson Chemical Corp.

The subsidiary, a $6,500,000 venture, has been organized to produce sodium chlorate and other chlorate compounds, and will be owned equally by the two corporations. Preliminary engineering was completed by February 15 and it was expected that construction would start within 90 days on a 25,000-ton-a-year plant at Calvert City, Ky.

Sylvania to Expand Production of Germanium and Silicon

A $500,000 facilities expansion program for the production and processing of single-crystal germanium and silicon for use by the semiconductor industry was announced recently by the Chemical and Metallurgical Division of Sylvania Electric Products Inc., Towanda, Pa.

The new equipment will include units for producing germanium single crystals by vertical and horizontal methods, and silicon crystals by vertical and float-zoning techniques. Auxiliary equipment will include slicing and lapping machines and electrical testing facilities for crystal evaluation.

Two Major Dow Laboratories Acquire New Names

New names have been selected for two of the Dow Chemical Co.'s major laboratories, both of which carry on fundamental and long-range research on a company-wide basis.

The Electrochemical Research Laboratory has been renamed the Electrochemical and Inorganic

Chemical Research Laboratory. The new name was selected as being more representative of work performed in the fields of electrochemistry and inorganic chemistry.

The Spectroscopy Research Laboratory will be called the Chemical Physics Research Laboratory, the latter more clearly reflecting its activities in chemical research and chemical-physical measurements.

Directors, respectively, of the two laboratories are Dr. R. D. Blue and Dr. Norman Wright.

Foote's Electrolytic Manganese Capacity Now on Stream

The Foote Mineral Co., Philadelphia, Pa., recently announced that the expansion of its electrolytic manganese facilities in Knoxville, Tenn., had been successfully completed and that the new capacity has been on stream since shortly after the first of the year. Additional cells, new rectifying equipment, and other new processing equipment have increased the capacity of the company's Loraine plant by 30%.

Carborundum's Technical Branch Announces New Laboratories

The Technical Branch of the Electro Minerals Division of the Carborundum Co., Niagara Falls, N. Y., will have new laboratories and new offices for its technical personnel when the $750,000 technical building now under construction is completed in June.

The announcement of the new technical building was made by Mr. J. S. Imirie, vice-president and general manager of Carborundum's Electro Minerals Division. The structure will provide laboratory facilities for physical measurements and quality assessments, product application, process development, and chemical analysis. It will also provide pilot plants for abrasive powders as well as abrasive grains.

Fourteenth Annual Power Sources Conference

The Fourteenth Annual Power Sources Conference, under the sponsorship of the Power Sources Division, U. S. Army Signal Research and Development Lab., Fort Monmouth, N. J., will be held on Tuesday, Wednesday, and Thursday, May 17, 18, and 19, at the Shelburne Hotel, Atlantic City, N. J.

Attendance at the conference is by invitation only. Persons who wish to attend can make the necessary arrangements by writing direct to the Power Sources Division, USASRDL.

Tentative Program

Registration—May 16-19
Thermal Energy Conversion—May 17
Solar Energy Conversion—May 17
Fuel Cell Batteries—May 18
Secondary Batteries—May 18
Comparison of Energy Conversion Systems—May 19
Energy Storage Devices—May 19
High-Rate Batteries—May 19
Primary Batteries—May 19
Cocktail Party and Banquet—May 17

Book Reviews

Modern Aspects of Electrochemistry, No. 2. Edited by J. O'M. Bockris. Published by Academic Press, Inc., New York City, 1959. IX + 407 pages; $13.00.

This book is the second volume in the series on Modern Aspects of Electrochemistry. The subjects presented in the five chapters are well in keeping with the more recent developments in the field.

Chapter 1 by H. Falkenhagen and G. Kelby, entitled "The Present State of the Theory of Electrolytic Solutions," deals with interionic attraction in solution. This field again has aroused considerable interest because of recent developments in studies on concentrated solutions. The subject is expertly handled by the authors in a well-organized presentation.

The physical chemistry of ion-exchange resins, covered in Chapter 2 by J. A. Kitchener, has been discussed in numerous other monographs. The presentation here, however, is somewhat more fundamental than in previous works. Unfortunately, such aspects as membrane phenomena and the use of resins in column electrophoresis, which are quite important in any discussion on ion-exchange resins, were considered by the author as outside the scope of the presentation.

Chapter 3 by H. Bloom and J. O'M. Bockris deals with molten electrolytes. This topic is of great interest, first, because of the tremendous industrial importance of molten electrolytes which are being used to a greater extent for the electrolytic extraction and purification of elements and more recently in nuclear reactors; second, because, since molten electrolytes do form a branch of the liquid state, their study is of importance in understanding that segment of this state in which the force field is essentially coulombic. It is unfortunate that with the excellent treatment of the structure of such systems the authors did not extend the subject matter to include some practical applications of this system.

T. P. Hoar, in his coverage of the anodic behavior of metals in Chapter 4, presents a complete and thorough discussion of the fundamentals pertaining to anodic processes at electrode surfaces. Through this the reader is able to obtain a better understanding of the corrosion process as well as the processes of electrodeposition, electrorefining, and anodic polishing.

The electrochemistry of the semiconductor-electrolyte interface, discussed in Chapter 5 by M. Green, is both timely and important especially in view of the tremendous strides made in recent years in the development of semiconducting compounds. The author handles this complex subject in a very commendable manner. He has attempted and I believe succeeded in laying down a firm foundation for future work in this field.

This book is certainly recommended as a reference book to those in the field of electrochemistry and to those looking for new horizons.

M. J. Allen

Physical Chemistry, by E. A. Moelwyn-Hughes. Published by Pergamon Press, Inc., New York City, 1957. 1295 pages; $15.00.

This text was written to supplement a course in physical chemistry for those undergraduates who in their senior year were studying for the Natural Science Trips at Cambridge University. It certainly sets a high standard for them.

The presentation makes use of thermodynamics and quantum theory wherever possible. In general, each topic is covered by presenting the experimental background, the theoretical development, and the mathematical formulation in separate chapters. All the major divisions of physical chemistry are treated in lucid style. It is possible, however, to question the author's emphasis on certain subjects and even to question his omissions. These, of course, reflect his own interests and preferences. The excellent chapters on kinetics are what one would expect from Moelwyn-Hughes.

There is little material on electrochemistry to be found in the book, less than in some of our own under-

CHEMICAL ENGINEER

ADVANCE DEVELOPMENT OF SEMICONDUCTOR DEVICES

PHD, MS or equivalent to expand and design processes and techniques to obtain stable device surfaces, surface protectants, and precise surface ambients during transistor encapsulation.

WRITE: M. D. Chilcote, Div. ES-5
Semiconductor Products Dept.
Electronics Park, Syracuse, New York

GENERAL ELECTRIC

METALLURGIST

ADVANCE DEVELOPMENT OF SEMICONDUCTOR DEVICES

PHD or MS or equivalent with background in Physical Metallurgy or solid state to assist in development of micro metallurgical techniques under protective atmospheres, vacuum deposition of high purity metals, and the study of re-crystallization of rare metals during alloying and welding operations on subminiature scale.

WRITE: M. D. Chilcote, Div. ES-5
Semiconductor Products Dept.
Electronics Park, Syracuse, New York

GENERAL ELECTRIC

PHYSICAL CHEMIST

ADVANCE DEVELOPMENT OF SEMICONDUCTOR DEVICES

PHD, MS or equivalent with a background in surface-gas reactions, diffusion, surface reaction kinetics or electrochemical phenomena to develop basic processes for the stabilization of semiconductor device surfaces.

WRITE: M. D. Chilcote, Div. ES-5
Semiconductor Products Dept.
Electronics Park, Syracuse, New York

GENERAL ELECTRIC

graduate texts. This reviewer has found it to be a useful reference, rather than a textbook as such. He has recommended it to several of his better students, and believes it should be kept available to research workers as a reference and source book.

David Lewis

New Products

Corunda®. Two new electronic-semiconductor grades of levigated alumina abrasives—Liquid Sapphire and Liquid Ruby—for ultrahigh polished surfaces are now being marketed. Production methods assure a new standard of uniform particle size, and homogeneity is certified by laboratory analysis of each batch. Data sheets detailing the properties of "Corunda" are available from Geoscience Instruments Corp., 425 Park Ave., New York 22, N. Y.

Announcements from Publishers

"Determination of Hydrogen in Solid Hydride Compounds by Use of Induction Heating," Dec. 1959. AEC Report APEX-243,* 8 pages; 50 cents.

"Organic Fluorine Compounds Prepared by the Electrochemical Method Literature Survey, 1950-July 1959," Jan. 1960. AEC Report K-1438,* 20 pages; 75 cents.

"Effect of a Thermal Gradient on the Hydrogen Distribution in a Metal: Application to the Sodium Reactor Experiment," Dec. 1959. AEC Report NAA-SR-4194,* 20 pages; 75 cents.

"Dissolution of Thorium in Mixtures of HNO_3 and HF," Sept. 1959. AEC Report DP-399,* 15 pages; 50 cents.

"Corrosion of Metals in Tropical Environments: Part 4—Wrought Iron," C. R. Southwell and others, U. S. Naval Research Lab., Oct. 1959. Report PB 151852,* 20 pages; 50 cents.

"Hydrogen-Embrittlement Susceptibility of Some Steels and Nonferrous Alloys," J. E. Scrawley, U. S. Naval Research Lab., Oct. 1959. Report PB 151937,* 28 pages; 75 cents.

* Order from Office of Technical Services, Business and Defense Services Administration, U. S. Dept. of Commerce, Washington 25, D. C.

Literature from Industry

Vitro Brochure. New brochure describes products and services of Vitro Chemical Co., a division of Vitro Corp. of America. Listed are 46 chemical and metallurgical products for use in manufacturing and research, including cobalt, nickel, vanadium, uranium, zirconium salts, rare earths, and thorium chemicals, metals, and alloys. Available from Vitro Corp. of America, 261 Madison Ave., New York 16, N. Y.

"Graphite Anodes." Illustrated brochure tells about a technical exchange program which has helped electrolytic cell operators lower production costs, and presents standard sizes and grades of square and rectangular anodes for diaphragm and mercury cells. Available from Electrode Division, Great Lakes Carbon Corp., 18 E. 48 St., New York 17, N. Y.

Nuclear-Chicago Educational Bulletin. Bulletin 131 describes a complete radioisotope laboratory, the Model 4000 Nuclear Training System, for high school and college science programs. Details and specifications on each instrument in the system are given, and a bibliography of articles related to training in radioisotope applications is included on the last page. For copies write to Nuclear-Chicago Corp., 359 E. Howard Ave., Des Plaines, Ill.

Carborundum Technical Data Folder. Twenty-six new products from the Carborundum Co.'s Research and Development Division are described in a summary technical data folder. Some of the materials are available in full commercial quantities; some are in pilot plant stages; others are available in sample quantities for experimental purposes. The products represent significant advances in materials resistant to abrasion, chemicals, corrosion, nuclear radiation, and high temperatures. The folder can be obtained from Dept. B. M. D., Carborundum Co., Niagara Falls, N. Y.

Industrial Acid-Gold Plating Process. A six-page booklet, AG-2, describes metallurgical properties, operational data, and uses of a patented acid-type industrial gold electroplating formulation, trademarked Autronex. Covered in detail is the composition of this low pH gold formulation for industrial applications. Deposit characteristics, corrosion resistance, equipment requirements, solution make-up and maintenance, gold consumption, trouble shooting, analytical procedures, and metal content chart are carefully outlined.

For copies, write to Sel-Rey Corp., Nutley, N. J.

Advertiser's Index

American Brass Company 118C
Bell Telephone Laboratories, Inc. 115C
General Electric Company 125C
General Motors Research Laboratories 114C
Great Lakes Carbon Corp., Electrode Division ..... Cover 2
National Carbon Company 126C
Sylvania Electric Products Inc. 117C

Employment Situation

Position Wanted

Chemical Engineers—M.S. Thirteen years' diversified experience in process and production control, assistant plant manager, process design, plant start-up, and trouble shooting in chloro-alkali industry. Desires responsible position in production or development. *Reply to Box 367, c/o The Electrochemical Society, 1860 Broadway, New York 23, N. Y.*

FUEL CELL RESEARCH MANAGER

National multi-plant corporation Research and Development Division located in midwest has immediate opening for an experienced (Fuel Cell) and qualified Physical or Electro-Chemist to assume leadership of laboratory and research project for development of Fuel Cells. All new laboratory facilities have been provided and further expansion of staff and equipment will be first responsibility of manager. This is a new field for the company and there will be opportunities beyond this position.

Resumé should include complete explanation and detail of Fuel Cell experience. Write Box A-283, c/o Electrochemical Society, 1860 Broadway, New York 23, N. Y.

ELECTROCHEMICAL ENGINEER

Recent graduate with B.S. or M.S. in Chemical Engineering or Chemistry for technical service and product development on electrolytic anodes. Position requires strong interest in electrochemistry as well as an outstanding scholastic background.

After an initial assignment of one or two years with our research and development staffs, permanent job location will be New York City.

Send resumes to:
W. W. Palmquist,
National Carbon Company,
Division of Union Carbide Corporation,
P.O. Box 6087, Cleveland 1, Ohio.

UNION CARBIDE

The Electrochemical Society

Patron Members

Aluminum Co. of Canada, Ltd.,
Montreal, Que., Canada

International Nickel Co., Inc.,
New York, N. Y.

Olin Mathieson Chemical Corp.,
Niagara Falls, N. Y.
Industrial Chemicals Div., Research
and Development Dept.

Union Carbide Corp.
Divisions:
Union Carbide Metals Co.,
New York, N. Y.
National Carbon Co., New York, N. Y.

Westinghouse Electric Corp., Pittsburgh, Pa.

Sustaining Members

Air Reduction Co., Inc.,
New York, N. Y.

Ajax Electro Metallurgical Corp.,
Philadelphia, Pa.

Allen-Bradley Co., Milwaukee, Wis.

Allied Chemical & Dye Corp.
General Chemical Div., Morristown, N. J.
Solvay Process Div., Syracuse, N. Y.
(3 memberships)

Allied Research Products, Inc.,
Detroit, Mich.

Alloy Steel Products Co., Inc., Linden, N. J.

Aluminum Co. of America,
New Kensington, Pa.

American Metal Climax, Inc.,
New York, N. Y.

American Potash & Chemical Corp.,
Los Angeles, Calif. (2 memberships)

American Smelting and Refining Co.,
South Plainfield, N. J.

American Zinc Co. of Illinois,
East St. Louis, Ill.

American Zinc, Lead & Smelting Co.,
St. Louis, Mo.

American Zinc Oxide Co., Columbus, Ohio

M. Ames Chemical Works, Inc.,
Glens Falls, N. Y.

Auto City Plating Company Foundation,
Detroit, Mich.

Basic Inc., Maple Grove, Ohio

Bell Telephone Laboratories, Inc.,
New York, N. Y. (2 memberships)

Bethlehem Steel Co., Bethlehem, Pa.
(2 memberships)

Boeing Airplane Co., Seattle, Wash.

Burgess Battery Co., Freeport, Ill.
(4 memberships)

Canadian Industries Ltd., Montreal, Que.,
Canada

Carborundum Co., Niagara Falls, N. Y.

Catalyst Research Corp., Baltimore, Md.

Chrysler Corp., Detroit, Mich.

Ciba Pharmaceutical Products, Inc., Summit,
N. J.

Columbian Carbon Co., Brooklyn, N. Y.

Columbia-Southern Chemical Corp.,
Pittsburgh, Pa.

Consolidated Mining & Smelting Co. of
Canada, Ltd., Trail, B. C., Canada
(2 memberships)

Continental Can Co., Inc., Chicago, Ill.

Cooper Metallurgical Associates, Cleveland,
Ohio

Corning Glass Works, Corning, N. Y.

Diamond Alkali Co., Painesville, Ohio
(2 memberships)

Dow Chemical Co., Midland, Mich.

Wilbur B. Driver Co., Newark, N. J.
(2 memberships)

E. I. du Pont de Nemours & Co., Inc.,
Wilmington, Del.

Eagle-Picher Co., Chemical Div., Joplin, Mo.

Eastman Kodak Co., Rochester, N. Y.

Thomas A. Edison Research Laboratory, Div.
of McGraw-Edison Co., West Orange, N. J.

Electric Auto-Lite Co., Toledo, Ohio
C & D Division, Conshohocken, Pa.

Electric Storage Battery Co., Yardley, Pa.

Englehard Industries, Inc., Newark, N. J.
(2 memberships)

The Eppley Laboratory, Inc., Newport, R. I.
(2 memberships)

Erie Resistor Corp., Erie, Pa.

Exmet Corp., Tuckahoe, N. Y.

Fairchild Semiconductor Corp., Palo Alto,
Calif.

Food Machinery & Chemical Corp.
Becco Chemical Div., Buffalo, N. Y.
Westvaco Chlor-Alkali Div., South
Charleston, W. Va.

Foote Mineral Co., Paoli, Pa.

Ford Motor Co., Dearborn, Mich.

General Electric Co., Schenectady, N. Y.
Chemistry & Chemical Engineering
Component, General Engineering
Laboratory
Chemistry Research Dept.
General Physics Research Dept.
Metallurgy & Ceramics Research Dept.

General Instrument Corp., Newark, N. J.

(Sustaining Members cont'd)

General Motors Corp.
Brown-Lipe-Chapin Div., Syracuse, N. Y. (2 memberships)
Guide Lamp Div., Anderson, Ind.
Research Laboratories Div., Detroit, Mich.
General Transistor Corp., Jamaica, N. Y.
Gillette Safety Razor Co., Boston, Mass.
Globe-Union, Inc., Milwaukee, Wis.
Gould-National Batteries, Inc., Minneapolis, Minn.
Grace Electronic Chemicals, Inc., Baltimore, Md.
Great Lakes Carbon Corp., New York, N. Y.
Hanson-Van Winkle-Munning Co., Matawan, N. J. (2 memberships)
Harshaw Chemical Co., Cleveland, Ohio (2 memberships)
Hercules Powder Co., Wilmington, Del.
Hill Cross Co., Inc., New York, N. Y.
Hoffman Electronics Corp., Evanston, Ill.
Hooker Chemical Corp., Niagara Falls, N. Y. (3 memberships)
Hughes Aircraft Co., Culver City, Calif.
International Business Machines Corp., Poughkeepsie, N. Y.
International Minerals & Chemical Corp., Skokie, Ill.
ITT Laboratories, Nutley, N. J.
Jones & Laughlin Steel Corp., Pittsburgh, Pa.
K. W. Battery Co., Skokie, Ill.
Kaiser Aluminum & Chemical Corp.
Div. of Chemical Research, Permanente, Calif.
Div. of Metallurgical Research, Spokane, Wash.
Kennecott Copper Corp., New York, N. Y.
Keokuk Electro-Metals Co., Keokuk, Iowa
Libbey-Owens-Ford Glass Co., Toledo, Ohio
M. & C. Nuclear, Inc., Attleboro, Mass.
Mallinckrodt Chemical Works, St. Louis, Mo.
P. R. Mallory & Co., Indianapolis, Ind.
McGean Chemical Co., Cleveland, Ohio
Merck & Co., Inc., Rahway, N. J.
Metal & Thermit Corp., Detroit, Mich.
Minnesota Mining & Manufacturing Co., St. Paul, Minn.
Monsanto Chemical Co., St. Louis, Mo.
Motorola, Inc., Chicago, Ill.
National Cash Register Co., Dayton, Ohio
National Lead Co., New York, N. Y.
National Research Corp., Cambridge, Mass.
National Steel Corp., Weirton, W. Va.
New York Air Brake Co., Kinney Vacuum Div., Boston, Mass.
Northern Electric Co., Montreal, Que., Canada
Norton Co., Worcester, Mass.
Olin Mathieson Chemical Corp., Niagara Falls, N. Y.
High Energy Fuels Organization (2 memberships)
Peerless Roll Leaf Co., Inc., Union City, N. J.
Pennsalt Chemicals Corp., Philadelphia, Pa.
Phelps Dodge Refining Corp., Maspeth, N. Y.
Philco Corp., Philadelphia, Pa.
Philips Laboratories, Inc., Irvington-on-Hudson, N. Y.
Pittsburgh Metallurgical Co., Inc., Niagara Falls, N. Y.
Poor & Co., Promat Div., Waukegan, Ill.
Potash Co. of America, Carlsbad, N. Mex.
Radio Corp. of America
Tube Div., Harrison, N. J.
RCA Victor Record Div., Indianapolis, Ind.
Ray-O-Vac Co., Madison, Wis.
Raytheon Manufacturing Co., Waltham, Mass.
Reynolds Metals Co., Richmond, Va. (2 memberships)
Rheem Semiconductor Corp., Mountain View, Calif.
Schering Corporation, Bloomfield, N. J.
Shawinigan Chemicals Ltd., Montreal, Que., Canada
Speer Carbon Co.
International Graphite & Electrode Div., St. Marys, Pa. (2 memberships)
Sprague Electric Co., North Adams, Mass.
Stackpole Carbon Co., St. Marys, Pa.
Stauffer Chemical Co., New York, N. Y.
Sumner Chemical Co., Div. of Miles Laboratories, Inc., Elkhart, Ind.
Sylvania Electric Products Inc., Bayside, N. Y. (2 memberships)
Tennessee Products & Chemical Corp., Nashville, Tenn.
Texas Instruments, Inc., Dallas, Texas
Three Point Four Corp., Yonkers, N. Y.
Titanium Metals Corp. of America, Henderson, Nev.
Tung-Sol Electric Inc., Newark, N. J.
Udylite Corp., Detroit, Mich. (4 memberships)
Universal-Cyclops Steel Corp., Bridgeville, Pa.
Upjohn Co., Kalamazoo, Mich.
Victor Chemical Works, Chicago, Ill.
Western Electric Co., Inc., Chicago, Ill.
Wyandotte Chemicals Corp., Wyandotte, Mich.
Yardney Electric Corp., New York, N. Y.